Modeling, Simulation and Prediction of Vehicle Crashworthiness in Full Frontal Impact

Gulshan Noorsumar

UiA University of Agder

Doctoral Dissertations at the University of Agder 400

Gulshan Noorsumar

Modeling, Simulation and Prediction of Vehicle Crashworthiness in Full Frontal Impact

Doctoral Dissertation for the degree *Philosophiae Doctor (PhD)* at
the Faculty of Engineering and Science, Specialisation in Mechatronics

University of Agder
Faculty of Engineering and Science
2023

Doctoral Dissertations at the University of Agder 400
ISSN: 1504-9272
ISBN: 978-82-8427-113-2

Printed by Aksell
Kristiansand

Preface

The work presented in this doctoral thesis has been carried out in the period starting in May 2019 and ending in May 2022 in the Department of Engineering Sciences, University of Agder. It is organized as an article-based thesis that consists of eight appended papers prepared by the author and co-workers, which are currently published or in the process of being published. In addition, synopsis chapters are referenced to outline how the research was conducted to provide a continuous and coherent description of the entire process. Associate Professor Svitlana Rogovchenko has been the main supervisor; Professor Kjell G. Robbersmyr and Associate Professor Dmitry Vysochinskiy have been the co-supervisors during this period, all from the Department of Engineering Sciences at the University of Agder. The project has received funding from the Ministry of Education in Norway.

Acknowledgments

First and foremost I would like to thank my supervisors Associate Professor Svitlana Rogovchenko, Professor Kjell G. Robbersmyr and Associate Professor Dmitry Vysochinskiy for supporting and guiding me during my research. Thank you Svitlana for being so calm and patient over my stupid questions and silly grammatical mistakes. To Kjell - cannot thank enough for answering all the door knocks and random demands for equipment and support; Dmitry for your constructive criticism of my decisions and showing the right way always.

I would also thank all my co-authors, researchers and engineers in the Mechatronics Laboratory at University of Agder, my deepest gratitude for your constant support in developing the test setups and the crash test for my research. This project is incomplete without the support of highly skilled engineers in the laboratories working hard to help me complete my research. A special mention to Halvor-Dag Settendal from Mechatronics Innovation Laboratory (MIL). Thank you to Bjarne Hæstad for your support and advice during this project. A special thanks to Thomas Gjesteland for your guidance and financial support; and to Morten Kjeld Ebbesen, Michael Rygaard Hansen and Mohammad Poursina for our fruitful discussions and your technical advice. I would also extend my deepest gratitude to Emma Elisabeth Horneman, Senior Advisor at UiA for always having an open-door policy for any professional and personal guidance.

I would also thank Saga Pardede for inspiring me always and supporting me along the way and for all the fun times and dinner discussions. While I am very grateful for having had the opportunity to pursue a PhD in the first place, it would not have been the same without the many colleagues and friends I made during this time. A special thanks to Shaun, Alfredo, Emilio, Atle, Yvonne, Manuel, Sveinung, Jose, Hareesh, Shashank, Siri, Jayant, Dipendra, Emil, Jon, Sarang, Arild, Wei, Mareike and Bilal for making this journey memorable.

This journey has been memorable and tough at the same time, but friends like Vijai, Sai and Gayatri have kept my spirits high throughout this process. I also cannot forget the coffee sessions and long video call discussions with Jayaraj, we began this journey together from different parts of the globe and hope to finish it soon. A special mention to Alokesh, Sourav, Swaroop and Dheeraj for your encouraging

words whenever I felt low on confidence.

This journey would be incomplete without the love and support of Martin. I would finally, thank my parents for their patience and constant support; my siblings Shabnam and Shamir. To my mom and little brother; you have always been very proud of my achievements and have been my pillar of strength in tough times - thank you for your unconditional love.

Gulshan Noorsumar
Grimstad, Norway
May 2022

Abstract

Vehicle crashworthiness assessment is critical to help reduce road accident fatalities and ensure safer vehicles for road users. Techniques to assess crashworthiness include physical tests and mathematical modeling and simulation of crash events, the latter is preferred as mathematical modeling is generally cheaper to perform in comparison with physical testing. The most common mathematical modeling technique used for crashworthiness assessment is nonlinear Finite Element (FE) modeling. However, a problem with the use of Finite Element Model (FEM) for crashworthiness assessment is inaccessibility to individual researchers, public bodies, small universities and engineering companies due to need for detailed CAD data, software licence costs along with high computational demands. This thesis investigates modeling strategies which are affordable, computationally and labour inexpensive, and could be used by the above-mentioned groups. Use of Lumped Parameter Models (LPM) capable of capturing vehicle parameters contributing to vehicle crashworthiness has been proposed as an alternative to adopting FEM, while the later have been used to validate LPMs developed in this thesis.

The main crash scenario analysed is a full frontal impact against a rigid barrier. Front-end deformation which can be used to measure crash energy absorption and pitching which could lead to occupant injuries in a frontal crash event are parameters focused on. The thesis investigates two types of vehicles; vehicle with initial structure intact is defined as baseline vehicle, while a vehicle that underwent unprofessional repairs on its structural members made of Ultra High Strength Steel (UHSS) is defined as a modified vehicle.

The proposed novel LPM for a baseline vehicle impact is inspired by pendulum motion and expresses the system using Lagrangian formulation to predict the two phases of impact: front-end deformation and vehicle pitching.

Changes in crashworthiness performance of a modified vehicle were investigated with a FEM; tensile tests on UHSS coupons were conducted to generate material inputs for this FEM. Further, a full scale crash test was conducted to validate the FE simulations. An LPM to conduct crashworthiness assessment of a modified vehicle has been proposed, it is based on a double pendulum with a torsional spring representing the vehicle undergoing a full frontal impact.

Sammendrag

Kjøretøyets kollisjonssikkerhet er avgjørende for å redusere antall dødsulykker i trafikken og sikre tryggere kjøretøy for trafikantene. Teknikker for å vurdere sikkerheten inkluderer fysiske tester og matematisk modellering og simulering av krasjhendelser. Sistnevnte foretrekkes da matematisk modellering generelt er rimeligere å utføre enn fysisk testing. Den vanligste matematiske modelleringsteknikken for vurdering av kollisjonssikkerhet er ikke-lineær FE-modellering. Et problem med bruken av FEM er imidlertid tilgjengelighet for individuelle forskere, offentlige organer, små universiteter og ingeniørfirmaer på grunn av behov for detaljerte CAD-modeller og høye programvarekostnader samt høye beregningskrav.

Denne oppgaven undersøker modelleringsstrategier som er rimelige både når det gjelder beregningsmessig og arbeidskraft, og som enkelt kan benyttes av de ovennevnte gruppene. Bruk av LPM for å registrere parametere som kan bidra til kjøretøyets kollisjonssikkerhet har blitt foreslått som et alternativ til bruk av FEM. Sistnevnte har blitt brukt til å validere LPM utviklet i denne oppgaven. Det analyserte kollisjonsscenarioet er en frontkollisjon mot en stiv barriere. Fokus er rettet mot frontdeformasjonen som kan brukes til å måle energiabsorbering og vipping og kan føre til passasjerskader i en frontkollisjon. Oppgaven undersøker to typer kjøretøy; et kjøretøy med den opprinnelige strukturen intakt er definert som basiskjøretøy, mens et kjøretøy som har gjennomgått en ikke forskriftsmessig reparasjon på strukturelle deler, er definert som et modifisert kjøretøy.

Den ny foreslåtte LPM for en basis-kollisjon er inspirert av pendelbevegelse og uttrykker et system som benytter Lagrangian formulering for å forutsi de to fasene i et sammenstøt: frontdeformasjon og kjøretøyets vipping. Endringer i kollisjonsevnen til et modifisert kjøretøy ble undersøkt med FEM. Strekktester på UHSS-kuponger ble utført for å generere materialdata for FEM. Videre ble det utført en fullskala kollisjonstest for å validere FE-simuleringene. En LPM for å vurdere kollisjonssikkerhet av et modifisert kjøretøy har blitt foreslått, den er basert på en dobbel pendel med en torsjonsfjær som representerer kjøretøyet som gjennomgår en full-frontal kollisjon.

Publications

Included Works

The following papers are included as a part of this thesis. They have been published in peer-reviewed conference proceedings and journals. The included versions in this dissertation differ only in formatting compared to the original published versions.

Paper A Gulshan Noorsumar, Kjell G. Robbersmyr, Svitlana Rogovchenko and Dmitry Vysochinskiy. Mathematical Models for Assessment of Vehicle Crashworthiness: A Review. *International Journal of Crashworthiness*, 1-15, 2021. doi: 10.1080/13588265.2021.1929760.

Paper B Gulshan Noorsumar, Svitlana Rogovchenko, Kjell G. Robbersmyr, Dmitry Vysochinskiy and Andreas Klausen. A novel technique for modeling vehicle crash using lumped parameter models. *Proceedings of the 11th International Conference on Simulation and Modeling Methodologies, Technologies and Applications - SIMULTECH,*, ISBN 978-989-758-528-9; ISSN 2184-2841, pages 62-70, 2021. doi: 10.5220/0010529200620070.

Paper C Gulshan Noorsumar, Svitlana Rogovchenko, Kjell G. Robbersmyr, Dmitry Vysochinskiy and Andreas Klausen. Development and extended validation of a lumped parameter prediction model for analysing injury parameters in a vehicle crash. Submitted to *Lecture Notes in Networks and Systems - Springer*.

Paper D Gulshan Noorsumar, Svitlana Rogovchenko, Kjell G. Robbersmyr and Dmitry Vysochinskiy. Vehicle crashworthiness performance in frontal impact: mathematical model using elastic pendulum. *Mechanics Research Communications*; ISSN 0093-6413, pages 103954, volume 124, 2022. doi: 10.1016/j.mechrescom.2022.103954..

Paper E Gulshan Noorsumar, Kjell G. Robbersmyr, Svitlana Rogovchenko and Dmitry Vysochinskiy. Crash Response of a Repaired Vehicle - Influence of Welding UHSS Members. *SAE Technical Paper* 2020-01-0197, 2020, doi: 10.4271/2020-01-0197, ISSN: 0148-7191, e-ISSN: 2688-3627.

Paper F Gulshan Noorsumar, Dmitry Vysochinskiy, Even Englund, Kjell G. Robbersmyr and Svitlana Rogovchenko. Effect of welding and heat treatment on the properties of UHSS used in automotive industry. *EPJ Web of Conferences*, 250, 05015 (2021),ISSN: 2101-6275 doi: 10.1051/epjconf/202125005015.

Paper G Gulshan Noorsumar, Kjell G. Robbersmyr, Kristian Muri Knausgård, Roy Werner Folgerø, Karl Berge Rød, Jan Christian Bjerke Strandene, Harald Sauvik, Bjarne Hæstad, Tore Helleland Næss, Dmitry Vysochinskiy and Svitlana Rogovchenko. An experimental and numerical investigation into the dynamic crash testing of welded and heat treated TRIP steel members on a modern vehicle. Submitted to *International Journal of Impact Engineering-Elsevier*.

Paper H Gulshan Noorsumar, Svitlana Rogovchenko, Dmitry Vyscochinskiy and Kjell G. Robbersmyr. Modeling of modified vehicle crashworthiness using a double compound pendulum. *12th International Conference on Simulation and Modeling Methodologies, Technologies and Applications - SIMULTECH 2022*, ISBN 978-989-758-578-4; ISSN 2184-2841, pages 102-111, doi: 10.5220/0011306100003274.

Additional Contributions

In addition to the papers included in this thesis, the author has also contributed to the following papers as part of the research done in the Top Research Center Mechatronics.

Paper I Gulshan Noorsumar, Kjell G. Robbersmyr, Svitlana Rogovchenko and Dmitry Vysochinskiy. An overview of Data Based Predictive Modeling Techniques used in Analysis of Vehicle Crash Severity. In: Sanfilippo, F., Granmo, OC., Yayilgan, S.Y., Bajwa, I.S. (eds) *Intelligent Technologies and Applications. INTAP 2021, Communications in Computer and Information Science,* vol 1616. Springer, Cham. doi: 10.1007/978-3-031-10525-8_28

Contents

List of Figures

List of Tables

Abbreviations

CAD Computer Aided Design. 3, 6

CFC Channel Frequency Class. 45, 46

CG Center of Gravity. xvii, 2, 25, 44, 45, 48, 49, 59

DAS Data Acquisition System. 44, 45

DIC Digital Image Correlation. 37, 38

DoF degrees of freedom. 60

EURONCAP European New Car Assessment Programme. 41

FE Finite Element. viii, ix, 10, 11, 14, 17, 18, 25, 26, 30, 35, 36, 40, 47–49, 54, 56, 58–61

FEA Finite Element Analysis. 5, 16, 18

FEM Finite Element Model. viii, ix, xvi, 4–6, 8, 9, 13, 15–17, 22, 25, 44, 54, 57, 60

FEMe Finite Element Method. 5, 16

FMVSS Federal Motor Vehicle Safety Standards. 7

HAZ Heat Affected Zone. 51

IIHS Insurance Institute for Highway Safety. 35

LPM Lumped Parameter Models. viii, ix, xvi, 4, 6–15, 17, 20, 21, 25, 30–33, 36, 38, 40, 47, 48, 50, 51, 54, 57–61

ML Machine Learning. 61

NCAP New Car Assessment Programme. 2

NHTSA National Highway Transport and Safety Administration. 5, 18

ODE Ordinary Differential Equations. 8

PDE Partial Differential Equation. 5, 8, 16

SDS Spatially Distributed Systems. 6

TRIP Transformation Induced Plasticity. 9

UHSS Ultra High Strength Steel. viii, xiii, xvii, 8–10, 13, 14, 32–38, 40, 42, 47, 50, 55, 56, 58, 59

UTM Universal Testing Machine. 38

VRU Vulnerable Road Users. 2, 5, 41

WP Work Package. xvi, 10, 14, 20, 21, 25, 33, 34, 50, 58, 59

Chapter 1

Introduction

Sometimes I lie awake at night, and ask, "Where have I gone wrong?" Then a voice says to me, "This is going to take more than one night."- Charles M. Schulz

1.1 Background and Motivation

Vehicle collisions are the one of the leading cause of deaths in the world with approximately 1.3 million people dying every year as a result of road accidents [2]. Consequently, vehicle safety is becoming a more crucial aspect of prevention of crashes, contributing to substantial reductions in the number of fatalities and serious injuries. Features like electronic stability control and autonomous emergency braking are vehicle safety features which are responsible to prevent vehicle collisions; despite these, vehicle crashworthiness assessment is an important aspect of vehicle safety design. Crashworthiness is the ability of a given structure to protect its occupants from getting injured during an impact or collision. Vehicle crashworthiness response requirements include [3]:

- Structure on the front that bends and crumples, yet is stiff to absorb impact energy from frontal collisions through plastic deformation and protect the occupant compartment during offset collisions and crashes into narrow objects like trees
- A deformable rear structure without compromising safety of the rear passengers
- A properly designed side structure and door system to minimize intrusion from the side collisions and prevent doors from opening during the crash; a strong roof structure
- Restraint systems which work in harmony with the vehicle structure to protect occupants in a crash event

- A deformable front end design to protect Vulnerable Road Users (VRUs) in a vehicle collision

During a collision, metal is crushed, which reduces the speed of the vehicle until it is stopped or disengages from the vehicle or object. The soft crush of sheet metal produces low deceleration pulses in the vehicle. A hard metal (like structural members of the vehicle frame) produces more resistance, more deceleration, and more energy transfer. The engine produces a spike of high amplitude deceleration that is transferred to the vehicle when engaged.

The deceleration of a crash lasting more than a hundred milliseconds may be characterized by series of decelerations called a crash pulse or deceleration curve. In order to minimize occupant injuries, vehicle manufacturers and designers aim to minimize deceleration. Controlling crash deceleration pulses and managing energy are the essence of crashworthiness. The vehicle is roughly divided into 2 zones; a crumple zone to absorb the impact energy and a compartment zone which is non-deformable to safeguard the occupants in a collision. Figure 1.1 shows the structural steel members on a vehicle with commonly used material grades (coloured in red in the figure). The crashworthy vehicle structure should be able to absorb the kinetic energy from a sudden crash event while the body-in-white members should be able to distribute the load over the structure to ensure fewer injuries to occupants. If the energy is not completely absorbed by the crumple zone, it leads to an imbalance of forces and a moment about the CG which could result in vehicle rotating about the point of impact. These rotations commonly referred to as pitching, rolling and yawing depending upon the axis of rotation are one of the leading causes of head and neck deflections to occupants in a crash (Figure 1.2). It is therefore crucial to measure and accurately predict deceleration curve and vehicle rotations in a crash event to mitigate injury to occupants

Assessment of vehicle crashes is crucial to ensure safety of occupants and road users; stringent safety assessment regulations have been imposed by regulatory agencies to ensure traffic safety for road users. New Car Assessment Programme (NCAP) is one of the regulatory agencies which regulates and conducts safety assessment of new vehicles for structural integrity, occupant protection and Vulnerable Road Users (VRU) protection. Traditionally, vehicle crashworthiness was assessed by conducting full vehicle crash tests in different impact scenarios and determining the structural response to impact using instrumentation mounted on the vehicle; occupant behaviour in a test was also studied using biofidelic dummies replicating human responses to measure injuries. This entire process of physical testing has been replicated by mathematical models in the past few decades. With the advent of computational capabilities, computer simulations aided crashworthiness assessment to determine structural integrity and occupant protection. Mathematical models

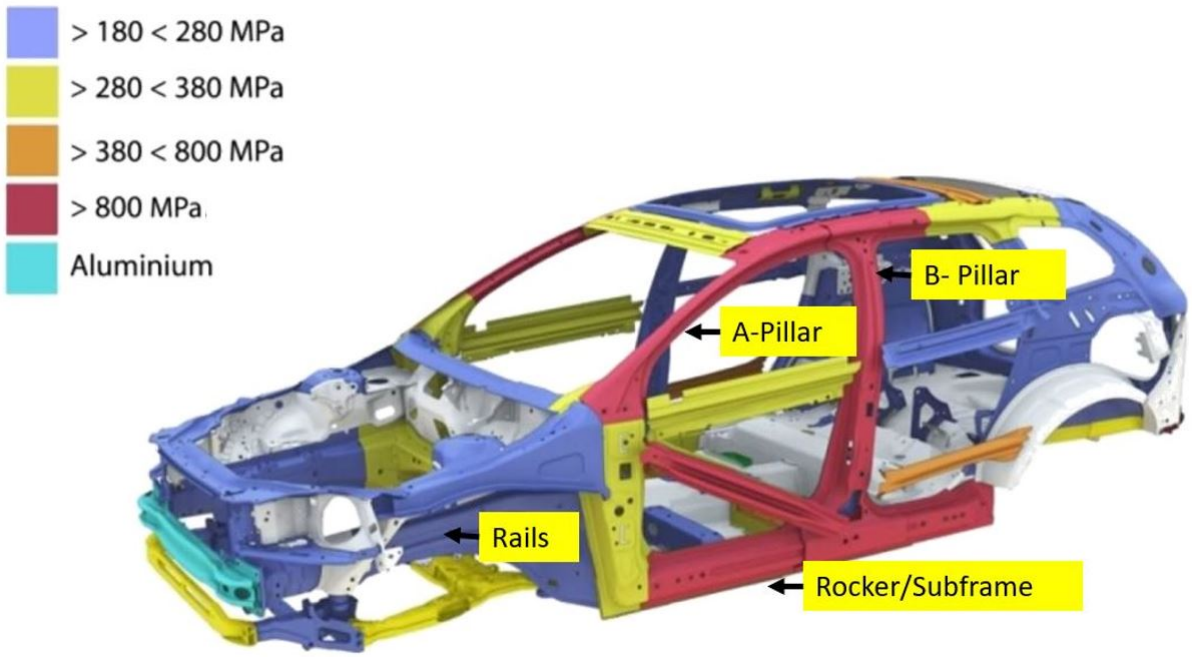

Figure 1.1: Structural parts on a modern vehicle along with their yield strengths for steel parts

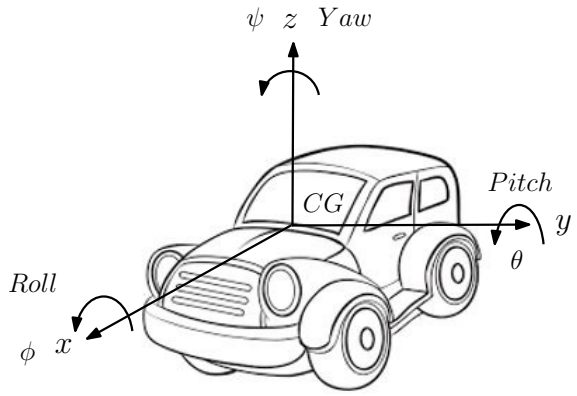

Figure 1.2: Vehicle Rotations in different axes; rolling, yawing and pitching

were inexpensive to conduct allowing multiple iterations in different impact scenarios and were expected to partially/completely replace physical testing.

Inaccessibility to complex and expensive commercial solvers and Computer Aided Design (CAD) models for developing mathematical simulations; requirement of huge computational capabilities to solve detailed models are few of the limitations to using mathematical models in vehicle crash assessment for academic and small institutions. This has led to a knowledge gap between the industry and academia. There is a need to explore a mathematical modeling strategy which encompasses the advantages and limitations of each technique allowing users to develop inexpensive yet accurate models to replicate a crash event. Often alternative modeling strategies are limited by their capability to represent impact kinematics due to lack of accurate material behaviour and geometrical non-linearities; defining the failure of structural members

in a vehicle crash with a reliable and robust modeling strategy would address the gap in application.

The motivation behind conducting this research is developing a modeling strategy which is capable of estimating important vehicle parameters contributing to vehicle crashworthiness assessment like maximum deformation, velocity of the vehicle during the impact event and rotation of the vehicle in different axes. These models can be maintained alongside FE simulations as a means of better understanding the principle dynamics of impacts along with supporting accident reconstruction methodology. FEM have been widely used in the industry to develop models replicating a vehicle crash event; however the inaccessibility of these softwares to academicians along with higher computational time warrants for models which don't require commercial solvers or complex models. One of the motivations of this work also includes using a methodology to develop mathematical models which are computationally inexpensive and open access which means it is accessible and affordable to all user groups and academicians.

1.2 State of the Art

An extensive review of mathematical modeling techniques for vehicle crash assessment was conducted in Paper A; Figure 1.3 shows the common mathematical models used for replicating a crash event listed as follows.

1. Lumped Parameter Models
2. Multi-Body Models
3. Finite Element Models
4. Crash Pulse Models
5. Response Surface Models

Paper A details each of these modeling techniques along with their advantages and limitations. One of the key takeaways from the extensive review was that the technological advances in the area of computational powers fueled the rapid growth in application of a few of these methodologies in the automotive industry.
During this project application of LPMs and FEM only have been emphasized; these methodologies are capable of assessing crashworthiness independently instead of relying on crash test data for their prediction like crash pulse models or response surface models. Multi-body models are also capable of replicating the impact dynamics; however model development is simpler with LPMs leading to the choice of this methodology for the research. FEM and LPM also require physical test data but only for validating the model and can be used for developing prediction models.

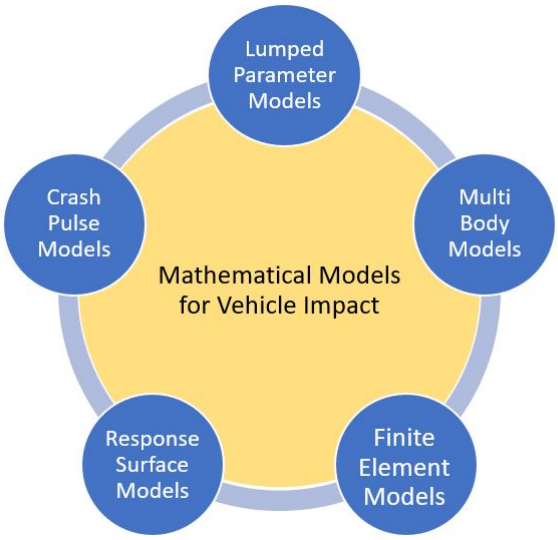

Figure 1.3: Common used models for vehicle crash

1.2.1 Application of Finite Element Models in Vehicle Crash Assessment

Of the several numerical approaches to find the solution to a Partial Differential Equation (PDE), FEM is used to discretize the space (geometry) and find an approximate solution; this solution converges to the exact solution as the number of elements are increased [4]. The variables in this system are both a function of time and space producing accurate results; however the computational time and resources required to arrive at a solution along with convergence issues are the limitations to the approach. Finite Element Analysis (FEA) is based on this methodology and has been used extensively to measure physical parameters like stress, strain, contact forces etc. for dynamic systems. FEAs are also widely used in the domain of vehicle safety. The Finite Element Method (FEMe) approach, first developed in the 1940s when Hrennikov [5] and Courant [6] used mesh discretization for elasticity and structural analysis problems. One of the first works published by Clough [7] in 1960 laid the foundation to numerous studies applying FEM to academic and industry applications. With the emergence of fast computational resources, the last two decades have witnessed FEM not just partially replacing physical testing during vehicle development stages but also solving problems previously not possible to solve. Böttcher et al. [8] discuss the steep growth of FE modeling over 20 years; the approach has been applied to determine structural integrity; occupant injuries predictions as well as injury to VRU during road collisions [9], [10], [11]. FEM was used in accident reconstruction studies allowing researchers to establish factors contributing to vehicle crash events [12], [13], [14]. Figure 1.4 shows a full vehicle model in FEM developed by National Highway Transport and Safety Administration

(NHTSA) to replicate the impact kinematics. One of the limitations to development and use of these models is the dependence on strong computational powers and a well-defined CAD to replicate the geometry of the parts. These requirements pose constraints to use the approach by academicians or research organizations not having access to these facilities.

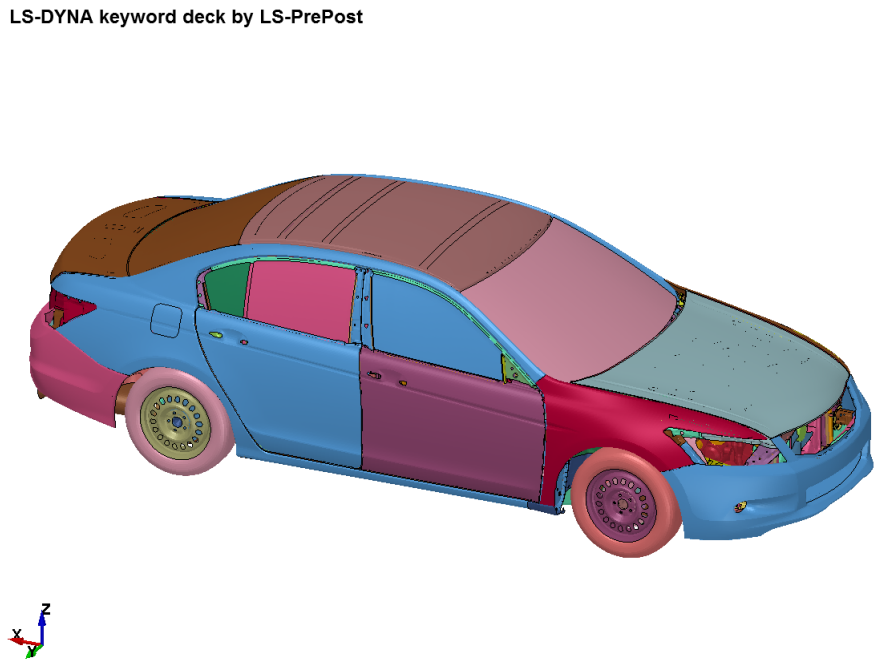

Figure 1.4: FEM for Honda Accord

1.2.2 Application of Lumped Parameter Models in Vehicle Crashworthiness Assessment

LPMs are a type of reduced order models, LPMs offer a simplification to the behaviour of Spatially Distributed Systems (SDS) in many engineering problems. The variables in these systems, as opposed to the SDS are only a function of time; while distributed-parameter systems are characterized by independent temporal and spatial dynamics, which means that all involved signals are functions of time and space [4]. This simplification reduces the state space of the physical system to a finite dimension by simplifying the partial differential equations (PDEs) of the continuous (infinite-dimensional) model. These PDEs are transformed into ordinary differential equations (ODEs) with a finite number of parameters. There are also disadvantages to LPM because it ignores the geometrical and material non-linearity of the system making it a crude representation of the dynamics of the system. LPMs have been utilized in crashworthiness analysis since the early 1970s. These models are extensively used in the field of vehicle crashworthiness due to the advantage of reducing computational

burdens of FEM. The study conducted by Kamal [15] was one of the pioneering works in the area of modeling vehicle crashes in an LPM. The study paved the way for several researchers including LPM to replicate the impact scenario ([16], [17]).

In the last two decades, LPMs have found applications in discrete time domain simulations where the vehicle deformation, velocity and rotation can be predicted using an LPM. The studies from Elkady et al. ([18], [1]) and Elmarakbi [19] present an LPM for predicting the response due to Vehicle Dynamics Control Systems (VDCS) for an offset impact; the model also establishes the injury parameters for a 3 DOF dummy. The front-end spring deformation curves are approximated using a piecewise linear curve; these studies show good correlation in predicting the pitching, rolling and yawing of the vehicle in an offset impact along with a vehicle-vehicle impact. Parameter identification is an important area to predict the injury values for occupants in a crash and factors contributing to vehicle crashworthiness; researchers have used LPMs to predict the front-end deformation in several instances [20], [21], [22]. More recently, LPMs have found applications in accident reconstruction and replacing Finite Element models and Multi-Body models for faster, low-cost simulation models [23], [24], [25].

Occupant modeling for predicting impact injury is a crucial field of research; LPMs have found applications in this area [26], [27]. Head, neck and spinal injuries are the most common injuries to occupants in vehicle crashes [28], [29]. As a result of the increased attention on unbelted occupants to meet Federal Motor Vehicle Safety Standards (FMVSS) 208, researchers have realized that vehicle pitch and drop have contributed to higher head and neck injuries during crashes [30], [31], [32]. The goal of the vehicle structure is not limited to energy absorption during the event, it is also expected to reduce the vehicle rotations and prevent higher injuries to occupants. Chang et al. [31], [33] have also concluded that vehicle rotations (pitch and drop) have been contributing factors for injuries in un-belted occupants. The studies from Chang et al. also highlighted the contribution of vehicle rails in distributing the impact loads for a body-on-frame vehicle. More recently, Elkady et al. [18] and Elmarakbi et al. [19] have also presented an LPM emphasizing on the role of vehicle rotations (especially pitching) during impact on the head and neck deflections of occupants, the model predicts the vehicle rotations to determine the influence of collision mitigation features on modern vehicles and are validated against reduced order MSC-ADAMS (Automated Dynamic Analysis of Mechanical Systems) multi-body model. It was realized that most applications of LPM in assessing vehicle crashworthiness were limited to determining the maximum crush and the impact acceleration. There was a need to investigate the behaviour of the vehicle after the maximum deformation phase; developing a model which also predicts vehicle rotations in different axes is critical to understanding impact mechanics to improve

occupant safety in vehicles.

Another aspect which was focused during this review is the technological growth in different modeling approaches. FEM received a technological push in 1990s resulting in faster computation capabilities with commercial solvers leading to more accurate assessments. LPM was used to assess crashworthiness prior to these technological advancements; these models which are outlined by the fundamental processes in dynamical systems were slowly replaced due to limitations of solving complex equations and lack of mathematical tools supporting their applications in industry and academia. However with the emergence of commercial and open source solvers like MATLAB - Simulink, Simscape, FEniCS, Python etc. it has been possible to quickly solve PDE and ODE; allowing researchers to try alternative modeling and simulation strategies for engineering problems. One of the limitations associated with LPM being its inability to represent non-linearity in dynamic systems was also highlighted during the review; it is noteworthy how researchers have used methodologies to use approximations to overcome this issue. With these advancements I believe that this existing methodology can be given a chance to find new applications in solving engineering problems.

The state-of-the-art also highlights the focus of researchers in predicting front-end energy absorption accurately; attention needs to be given to the second part of the event leading to vehicle rotations.

1.2.3 Crashworthiness Assessment of a Modified Vehicle

During the literature review it was realized that material failures were not represented in LPMs due to the limitations associated with incorporating geometry and material behaviour within these simple models; one of the cases highlighted in this thesis is the effect of unprofessional repairs on vehicle crashworthiness.
Vehicle manufacturers recommend to follow the collision repair manual in modern vehicles to avoid unprofessional repairs; especially on structural members which contribute on the load distribution during the impact. Modifying a vehicle with unprofessional repairs introduces a new load path capability into the vehicle's joints, while weakening or strengthening the joint beyond its original strength, thus diverting the original load path. Repair joints require replacement of the whole component and spot welding at appropriate locations to maintain their structural capabilities. Such a vehicle with modifications in the structural members made of UHSS is referred to as a *modified vehicle* in the context of this research; in contrast a vehicle with no structural modifications is hereafter referred to as a *baseline* vehicle. Unprofessional repairs could occur due to the following reasons [34]:
-Insufficient knowledge of repairing the parts leading to wrong assembly or processes

-Incorrect process to repair the parts and absence of special tools
-Repair of parts when replacement is necessary or recommended
-Use of poor/low quality spares and components; incorrect connections and wiring of electrical harnesses or subsystems

Different definitions exist in the literature for UHSS; the definition adopted for this thesis is as follows: UHSS have yield strengths higher than 800 MPa. Transformation Induced Plasticity (TRIP) steels are a type of UHSS. TRIP steels contains a mixture of ferrite, with retained austenite, martensite and bainite in varying amounts. These have been shown to benefit from the austenite-martensite transformation during straining and this results in a better balance between strength and ductility. The mechanical properties of TRIP steels are superior in terms of strength and elongation compared to other types of steels [35]. Modern vehicles use TRIP steels for their structural members to improve their vehicle crashworthiness performance. Figure 1.1 presents the structural members along with their tensile strength for a modern car; the grades of steel with yield strength above 800 MPa is commonly referred to as UHSS and are used on structural members like A-Pillar and Rocker to prevent intrusions in the driver compartment during an impact. The process of welding and heat treatment on Transformation Induced Plasticity TRIP steels may lead to micro-structural changes in the material, thereby deteriorating the mechanical properties of the weld region. There are studies investigating the weldability and heat treatment of TRIP steels in the literature, for example Amirthalingam [36], [37]. Uwe [34] concluded that unprofessional repairs on a vehicle resulted in negative influences on the crashworthiness performance of the vehicle in side impact. The study concluded that there was noticeably higher intrusion in the side compartment and the passenger side curtain airbag failed to operate due to higher intrusions in the compartment. FEM has been employed to develop constitutive material models of UHSS in welded and heat treated samples [38], [39]; however there are lack of reduced order models for the same using LPM which is a gap intended to be filled with research in this thesis. The development of an LPM capturing the kinematics of a modified vehicle is part of this research contributing to the improvement of LPM in modeling vehicle crashworthiness.

1.3 Research Objective

The overarching goal of this thesis is exploring accessible and affordable crash assessment techniques for the industry and the academia; these models should capture the different vehicle parameters contributing to increased risk of injury to road users in a crash. Along with this, the crashworthiness assessment of a modified vehicle and its consecutive representation in an LPM is another critical element of

this research. The extensive review helped to streamline the motivation into the following research objectives for this project.

- Develop an LPM for a baseline vehicle undergoing a full frontal crash which captures the front-end deformation and the pitching angle to assess crashworthiness.
- Conduct vehicle crashworthiness assessment of a modified vehicle in a full frontal crash.
- Propose and verify an LPM capable of capturing the impact kinematics in a full frontal impact for a modified vehicle.

1.4 Methodology and Contributions

Figure 1.5 presents the research workflow and the methodology adopted in this thesis with different colours in the figure representing a WP and the arrows in blue indicate the research progress. The dissertation provides context to the contributions of the following papers as presented in Figure 1.5 and an overview of individual paper objectives and contributions presented in Figure 1.6. This research was divided into 3 work packages to present an improved mathematical model replicating a vehicle crash event.

- **WORK PACKAGE - 1** (Paper A - D) predominantly addresses the question around mathematical modeling of baseline vehicle impacting a rigid barrier (green zone in the figures)
  - One of the challenges in assessing crashworthiness is the inaccessibility to complex finite element based solvers and computational resources for academic institutions. The methodology in this research has been focused on developing a LPM which replicates a full frontal vehicle crash event and validating it against FE simulations. They have been defined and published as Papers B - D
- **WORK PACKAGE - 2** (Paper E - G) In this WP experimental data is collected to address one of the shortcomings of LPM with a special case of modified vehicles using welded and heat treated structural members. Literature documents the micro-structural changes in the welded UHSS samples; however the effect on crashworthiness performance was not evaluated along with insufficient data available to develop an LPM. The methodology in this WP was focused on the research problem outlined around modified cars (grey zone in the figures).

– Simulating the behaviour of the modified vehicle with welds in FE simulation to check the hypothesis about reduced crashworthiness performance during an impact; presented in Paper E

– Conducting coupon level testing on welded and heat treated samples to characterize the material and generating first hand data for LS Dyna material card; the results are presented in Paper F

– Conducting full vehicle impact test with welding and heat treatment in its structural members to generate real-time data for LPM development and validation. The results are correlated with an FE model of a Toyota Yaris modified to replicate the repairs on the physical test vehicle.

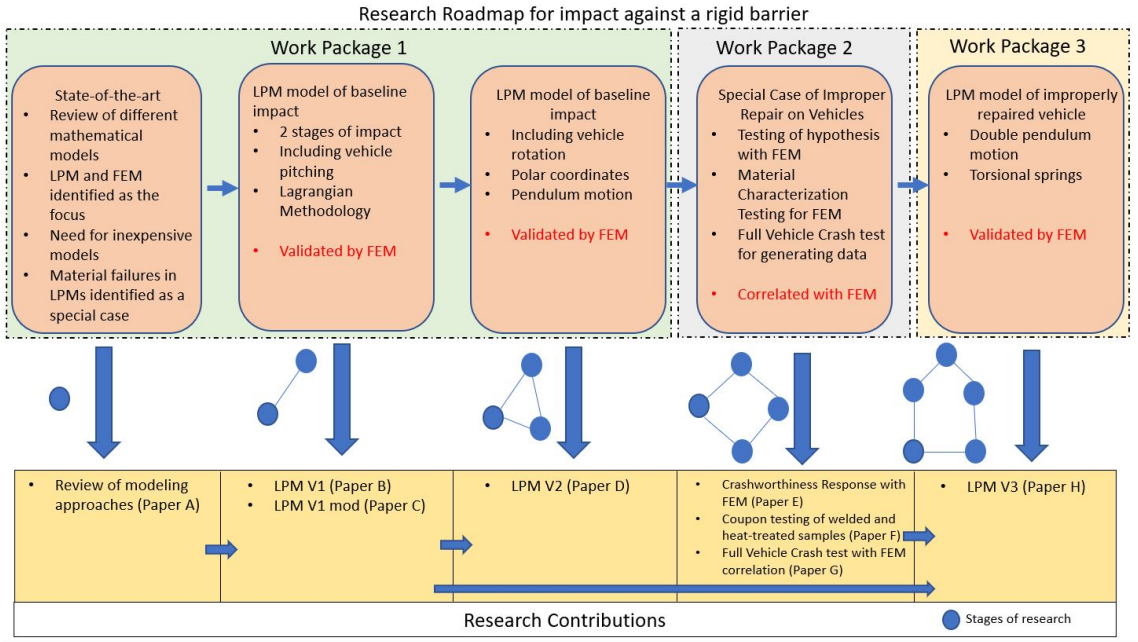

Figure 1.5: Research Workflow

- **WORK PACKAGE - 3** (Paper H) Using the LPM developed in WP 1 and data generated in WP 2 along with the correlated FE model ; develop and validate an LPM which can predict the crashworthiness response of the modified vehicle (yellow zone in the figures).

The two work packages support in generating the framework for developing an LPM for a modified vehicle; the research conducted in the two packages leading to a novel approach to model a modified vehicle undergoing full-frontal impact.

		Paper	Objective	Contribution
WORK PACKAGE-1 (Baseline Vehicle Impact Model)	Paper A-D	A	Mathematical Modeling Review	Identify the knowledge gaps in the research.
		B	LPM V1 with baseline vehicle impacting against a rigid barrier.	The event is divided into 2-phases; Phase I- front-end deformation, Phase II - vehicle rotation about impact point.
		C	Extend the LPM V1 to validate with another vehicle platform; conduct parameter variation study.	Robustness check on the model; increased prediction and reliabilty on the model. LPM shows good prediction for trucks and small vehicles.
		D	LPM V2 represents the vehicle as a compound elastic pendulum swinging about the point of impact.	The methodology is novel; the correlation is good for maximum crush prediction and improves for vehicle pitching angles. Reliable model for baseline vehicle.
WORK PACKAGE-2 (Modified Vehicle Impact Model)	Paper E-G	E	Crash reponse of a vehicle undergoing unprofessional repairs: FE simulations conducted to show the reduced crashworthiness performance.	Proves the initial hypothesis of reduced performance for welded and heat treated UHSS members; FE model lacks the constitutive material model for UHSS.
		F	Coupon testing conducted to determine the material properties of welded and heat treated UHSS- tensile tests run on samples cut from vehicle.	Constitutive material model developed for LS Dyna simulation and further verifies the hypothesis of reduced strength properties in UHSS.
		G	Full vehicle crash test conducted to verify the hypothesis and provide data for mathematical models; FEM simulations conducted to correlate with test.	Test data available to fill knowledge gaps; preparation of test described including instrumentation and results.Good correlation with FEM simulations. Data for LPM representing the scenario.
WORK PACKAGE -3	Paper H	H	LPM V3 with material failure using a double pendulum and torsional spring representing material failure	New methodology to represent material failure; double pendulum represents the scenario. Validation with FEM shows promising correlation. The model has scope to be improved.

Figure 1.6: Detailed objective and individual contributions from published papers

The LPMs developed improve the confidence of researchers in using these models for assessment, prediction and accident reconstruction of crash events; a few limitations of LPM have been addressed with a special case of repaired vehicles which has been successfully represented with a novel methodology. The contributions have been divided into three pillars and presented below which comprises of technical contributions along with open-source data generated and social impact of the thesis.

- **Modeling and Simulation:** The main contribution of this thesis is the development and implementation of mathematical modeling methodologies in the study of interactions and collisions between different mechanical systems modeled with the lumped parameter approach. The modeling and simulation of a vehicle impact replicating a physical test using methodology which is computationally inexpensive yet predicting the vehicle deformation and rotation is the backbone of this work. The project addresses the knowledge gaps in the development of models predicting vehicle rotations (pitching in this case); the novel methodology of using a pendulum to define the kinematics of the impact is one of the crucial contributions of this project. One of the limitations

to using LPM is the representation of material failures in the structure; their implementation to replicate vehicle crash events has been extended to include a special case of improper repairs on vehicles.

- **Crashworthiness response of a modified vehicle**: The crashworthiness response of a vehicle undergoing unprofessional repairs including welding and heat treatment of UHSS structural members has been investigated; corresponding FEM data presented in this project supports the literature data suggesting reduced crashworthiness response in a collision. The physical test conducted further supports this along with valuable data from sensors installed on the test vehicle to capture the acceleration, intrusions and impact kinematics. The test data contributes to the investigation of crashworthiness assessment of modified vehicles and the academic community would be benefited by the open-source videos and instrumentation data generated during this project. The tensile tests conducted on welded and heat treated UHSS coupon samples provides the data needed to construct a constitutive model and perform a finite-element analysis of improperly repaired UHSS parts

- **Social and Educational:** Alternative modeling approaches to assess vehicle crashworthiness identified during this work will improve road safety along with providing open source models bridging the gap between industry and academia. Developing models to predict vehicle crashworthiness performance thereby reducing the dependence on computationally intensive softwares or physical tests, sometimes not available to educational institutions or small organizations.

The thesis is divided into four main chapters, which are followed by the appended articles published or submitted in peer-reviewed conference proceedings and journals. The content of each chapter is summarized as follows:

Chapter 1 – Introduction

The background and motivation for the research along with the state-of-the-art in vehicle crashworthiness assessment has been presented. Further, the research problem and the thesis outline with contributions has been described briefly.

Chapter 2 – Baseline Vehicle Impact Model Development

In this chapter I discuss the modeling techniques used in this project and the models developed have been briefly described along with the results.

Chapter 3 – Modified Vehicle Impact Model Development

FEM used for conducting crashworthiness assessment of a modified vehicle is described along with the shortcomings of this model. The methodology used

in WP 2 to develop a constitutive model for welded and heat treated samples of structural UHSS members is detailed in this chapter. The coupon tests with tensile testing have been described with observations.

The experimental setup used to conduct physical test for a full-scale crash against a rigid barrier is also presented; the instrumentation and preliminary results have also been outlined. I also discuss the FE model developed to conduct correlations. Finally, the LPM for a modified vehicle is presented along with results overlayed against correlated FE model.

Chapter 4 – Concluding Remarks and Next Steps

This final chapter highlights the major conclusions and the next steps in this research. A few assumptions have also been outlined in this chapter.

Appended Papers

The articles published in peer-reviewed conference proceedings and journals are appended after the final chapter and bibliography.

Chapter 2

Baseline Vehicle Impact Model Development

A complex system that works is invariably found to have evolved from a simple system that works. - John Gaule

A "model" is something that mimics relevant features of a situation, thus providing the theoretical and scientific basis for study. *A mathematical model is an abstract, simplified, mathematical construct related to a part of reality and created for a particular purpose* [40]. Physical phenomena are often represented mathematically by models based on simple scientific laws, such as the principle of conservation of mass, the principle of balance between linear and angular momentum, and the principle of balance between energy and matter [41]. These equations are supplemented by equations that describe either the boundary conditions or initial conditions along with the constitutive behaviour of the system. Their solution by exact methods of analysis is often challenging due to material and geometrical complexities.

The literature review presented in Chapter 1 outlines the different mathematical modeling strategies applied in the industry and academia to define the non-linear impact kinematics along with their technological advancements over time. This thesis lays emphasis on the applications of FEM and LPM for modeling vehicle crash events and improving the existing state-of-the-art methodology. As discussed in the previous chapter, the review provided an opportunity to identify modeling methodologies which were not dependent on crash test data along with capturing the impact mechanics accurately; the decision to use LPM for this research was based on these considerations. The next section provides a summary of the theoretical background of these two methods.

2.1 Finite Element Methods (FEMe)

A PDE is a function of multiple variables and their partial derivatives that governs the dynamics of multidimensional systems. Exact solution to complex PDEs is difficult or even impossible to obtain; bringing the need for numerical approaches to solve engineering problems. Several numerical techniques focus on solving the PDE at discretized spatial locations (meshing the surface) giving a finite approximation to a set of indefinite continuous solutions.

In FEMe, a given domain is viewed as a collection of sub-domains, some of the traditional variational methods are used to approximate the governing equation at every sub-domain. At each of the connecting points, each segment of the solution should fit with its neighbor, so that the derivatives and the function are continuous (i.e. single valued) at the connecting points [41].
A geometrically complex domain which is represented as a collection called as *mesh* with sub-domains as *finite elements*. The algebraic relations between the values of the duality pairs of the problem at element nodes in a finite element is derived using governing equations and an approximation method. The resulting equations among the nodal values of the duality pairs is termed a *finite element model*. The equations from all elements, are assembled using continuity of the primary variables and balance of secondary variables. Here it is important to note that the size of the model increases incrementally with a smaller mesh size (subdomains); capturing the geometrical features in a vehicle leads to millions of elements thereby increasing the volume of equations to solve in the FEM. This is a task impossible to solve with manual calculations and requires commercial solvers to provide accurate results. With advancements in the field of computer simulations, solvers like LS Dyna, Radioss etc. have made it easier to develop and simulate full vehicle impact scenarios.

There are several stages in model development when approximations are introduced leading to errors. Firstly, while dividing the domain in sub-domains (finite elements) which may not be exact introducing an error. Secondly, the dependent unknown in the problem are approximated with the idea that any continuous function can be represented by a linear combination of known functions, and undetermined coefficients. Approximating while evaluating the integrals along with representing the solution could introduce errors in the model. The final stage of solving the assembled equations described above could also lead to errors; if all errors are equal to zero, the solution is exact which is tough to achieve in two dimensional and three dimensional problems.

FEA in structural analysis is performed to predict the response (distribution of displacement, strain and stress) of a structure subject to some external actions such as force or temperature loading, or displacement.

2.2 Lumped Parameter Models

The term *lumped* comes from electrical engineering, and refers to the description of the behaviour of spatially distributed physical systems such as electrical circuits, into a topology consisting of discrete entities that approximate the behaviour of the distributed system under certain assumptions. Modeling with reduced complexity aims to capture this behaviour of complex systems while saving computational resources. It is possible to develop reduced order models for parameter-dependent systems using the results of sample 'training' simulations. Selected parameter values can be employed in order to simulate the system using a more affordable model for numerous other parameters.

The lumped mass models describe the model behaviour by schematizing it into one or more rigid masses. These are connected by load paths consisting of zero mass elements. A basic LPM consisting of energy absorbing elements is the *Kelvin model* [42]; it is represented by a purely viscous damper and purely elastic spring connected in parallel as shown in the Figure 2.1. In this model, a system with a mass element and a spring damper system represents a vehicle undergoing front-end deformation and the non-deformable mass represents the occupant compartment. This approach has been employed to model vehicle crash models by researchers because it is an inexpensive and simple approach for developing models when accuracy can be compromised to some extent.

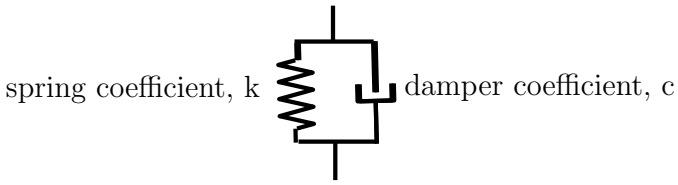

Figure 2.1: Kelvin model

2.3 Approaches to replicate the vehicle crash event

With a bunch of available methodologies to simulate the impact, the option to select the methodology which was least computationally intensive giving reliable results was adopted. The idea behind selecting LPM boils down to these considerations. One of the challenges to developing a mathematical model is the accuracy of the model in replicating the real-time results; however the compromise between computationally expensive modeling and accuracy led to developing a model which strikes a balance between these requirements. Lack of physical test data was another constraint in the modeling phase which was resolved with FE models for validating the parameters like pitching and impact forces. The vehicle impact has been modeled with FEM using

the NHTSA crash database as a baseline [43]. These models replicate the vehicle geometry, material properties of different members and thickness of each part in the model. The FE models are modified to include welds in the structural members and simulate the crashworthiness response of the vehicle us LS Dyna simulations.

During this project the following FE vehicle models have been assessed for crashworthiness:
-2014 Chevrolet Silverado (Paper B, C)
-2010 Honda Accord (Paper E)
-2010 Toyota Yaris (Paper C, D, G)

LS Dyna is a leading software used to model and analyze non-linear implicit and explicit multiphysics. It is a general purpose FEA code for analyzing the static and dynamics response of structures [44]. LS Dyna has been used to conduct FE simulations during this research.

2.4 Methods of deriving equations of motion

There are several methods to derive the equations of motion for a dynamic system; however the Newton Euler and the Lagrange are the most commonly used methods in the literature. The two methods were compared to select a suitable methodology for this research.

2.4.1 Newton Euler Equation

Newtonian mechanics is based on three laws stated for the first time in 1967 by Sir Isaac Newton in his Philosophiae Naturalis Principia Mathematica [45].
First Law: *If there are no forces acting upon a particle, the particle will move in a straight line with constant velocity.*
Second Law: *A particle acted upon by a force moves so that the force vector is equal to the time rate of change of linear momentum vector.*
Third Law: *When two particles exert forces upon one another, the forces lie along the line joining the particles and the corresponding force vectors are the negative of each other* [46].

The Newton–Euler equations of motion for a rigid body with mass m in plane motion are [47]:

$$m\ddot{r_c} = \sum F \tag{2.1a}$$

$$I_{zz}\alpha = \sum M_c \tag{2.1b}$$

or, using cartesian coordinates

$$m\ddot{x_c} = \sum F_x \tag{2.2a}$$

$$m\ddot{y_c} = \sum F_y \tag{2.2b}$$

$$I_{zz}\ddot{\Theta} = \sum M_c \tag{2.2c}$$

where, F is the forces experienced by the system; I_{zz} is the moment of inertia, M_c is the rotational moment. Some of the advantages of this method include that the equations of motion will always have the same fundamental form independent of the geometry, inertia or constraints of motion of a rigid body. The inverse dynamics is in real-time because the equations are evaluated in a numeric and recursive way [48],[49].

2.4.2 Lagrange's Equations

Lagrange's Equations are based on the stationary-action principle (also known as the principle of least action) and is a formulation of classical mechanics. Originally, it was introduced in the 1788 work Mécanique analytique by the French-Italian mathematician and astronomer Joseph-Louis Lagrange.
The equation for a conservative system is presented below where L represents the Lagrangian function

$$\frac{d}{dt}\frac{\partial L}{\partial \dot{q_k}} - \frac{\partial L}{\partial q_k} = 0, \tag{2.3}$$

Equation 2.3 presents Lagrange's equations; where, in general case, $L = T - V$, T is the total kinetic energy of the system equal to the sum of the kinetic energies of the particles, $q_k, k = 1, ..., n$ are generalized coordinates and V is the potential energy of the system.

In case of virtual work and external forces acting on the system,

$$\delta U = \sum_{j=1}^{p} F_j \cdot \delta r_j \tag{2.4}$$

There are p forces acting on the system, virtual displacement δr_j for $j = 1, 2, ..., p$ can be expressed as:

$$\delta r_j = \sum_{k=1}^{n} \frac{\partial r_j}{\partial q_k} \delta q_k \tag{2.5}$$

Substituting (2.5) into (2.4) we obtain virtual work. The virtual work can be expressed as a product of n generalized forces Q_k acting over the virtual generalized

displacements δq_k

$$\delta U = \sum_{k=1}^{n} Q_k \delta q_k \tag{2.6}$$

The Lagrangian equations can be written as below for a non-conservative system [50]:

$$\frac{d}{dt}\frac{\partial L}{\partial \dot{q}_i} - \frac{\partial L}{\partial q_i} = Q_i^{ext}, \tag{2.7}$$

Here Q_i^{ext} is the external force acting on the system; in this case it is the vertical component of the force experienced by the vehicle at the time of maximum dynamic crush [50].

Some of the advantages and limitations of using this methodology includes elimination of workless constraints to obtain constraint-free differential equations. A workless constraint is any constraint such that the virtual work (work done in a virtual displacement) of the constraint forces acting on the system is zero for any reversible virtual displacement. In order to determine the equations of motion for systems subject to constraints, it is necessary to include all the unknown constraint forces (workless constraints) explicitly with the active forces.

With Lagrangian mechanics, these difficulties are avoided by selecting independent generalized coordinates that incorporate the correlated motions induced by constraint forces. In this way, constraint forces on the system can be ignored by reducing the system to a minimum set of generalized coordinates. Using the Lagrange multiplier approach, or by including all constraint forces as generalized forces, holonomic constraint forces can be determined. The Lagranges's system is computationally efficient with $O(n^3)$ (order n to the third power); however the requirement of generalized constraints is one of the challenges associated with this method.

Methods	Computational Complexity	Generalized coordinates	Workless Constraint	Complexity of formulation
Newton Euler	$O(n^4)$	No	Yes	low
Lagrange	$O(n^3)$	Yes	Eliminated	high

Table 2.1: Comparison between Newton Euler and Lagrange Method for modeling

Table 2.1 presents the comparison between the approaches for developing the governing equations of motion; during this project the Lagrangian formulation was adopted to reduce the computational complexity being one of the motivations of the work along with presenting an alternative modeling strategy.

WP - 1 deals with developing LPM for a baseline vehicle crash impact against a rigid barrier as shown in Figure 2.2. This section defines the models and the methodology used during this WP.

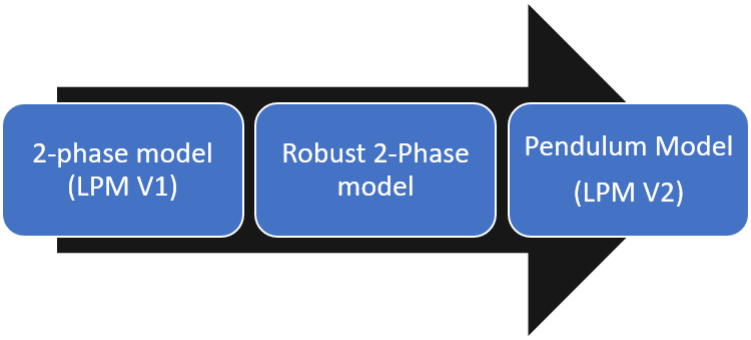

Figure 2.2: The stages in developing LPM in WP-1

2.5 Developing the Baseline Vehicle Impact Model

2.5.1 LPM V1 - 2 Phase Model

The modeling of the crash impact has been restricted to full frontal impact against a rigid barrier. The models 2 Phase and robust 2 Phase described in Paper B and Paper C are composed of the mass-spring-damper system as shown in Figure 2.4. One of the earliest and most important observations in this research was the division of the crash event into 2 distinct phases as described below (Figure 2.3):

- Phase I: time till maximum deformation and minimum vehicle velocity after start of crash event t_1, and
- Phase II: time after maximum deformation to the end of the crash event t_2.

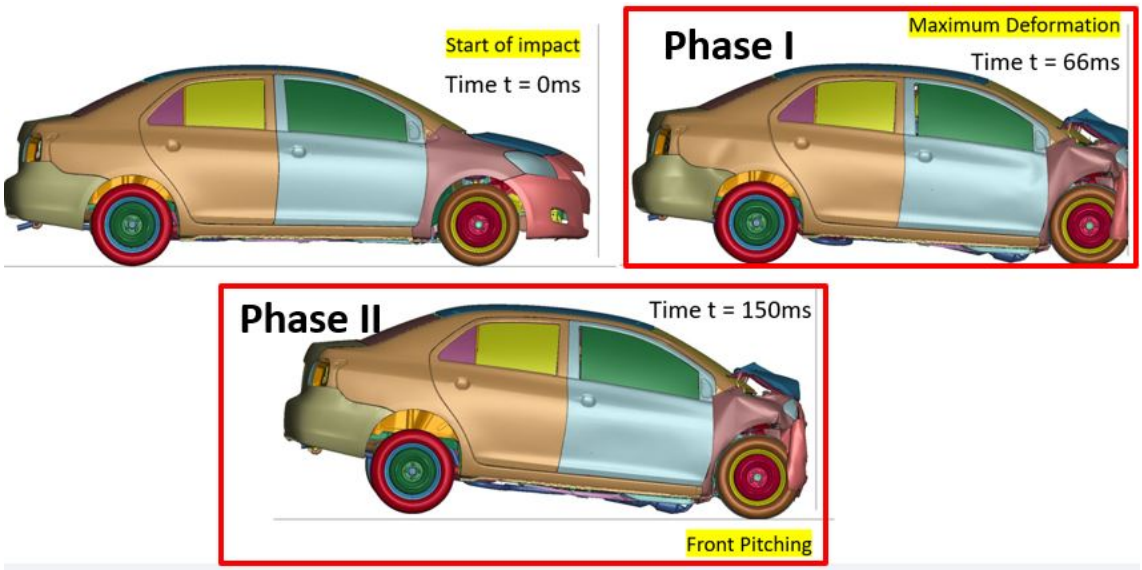

Figure 2.3: 2 Phases of impact - Deformation and Pitching

The LPM V1 was developed to demonstrate a baseline model of impact incorporating the 2 phases outlined above. The horizontal translational motion and the vertical

motion during the impact event have been separated. The vehicle is observed to pitch forward during a full frontal collision, but the rolling and yawing effects have been neglected.

FE simulation for a 2014 Chevrolet Silverado [43] running at 56 kmph and hitting a frontal barrier at 0% offset was conducted to validate the LPM. The details of the FEM have been outlined in Paper B.

Phase I: The impact leads to front-end deformation defined by the following equation of motion in Equation 2.8. In this phase the motion is restricted in all other axes except the horizontal motion in x axis.

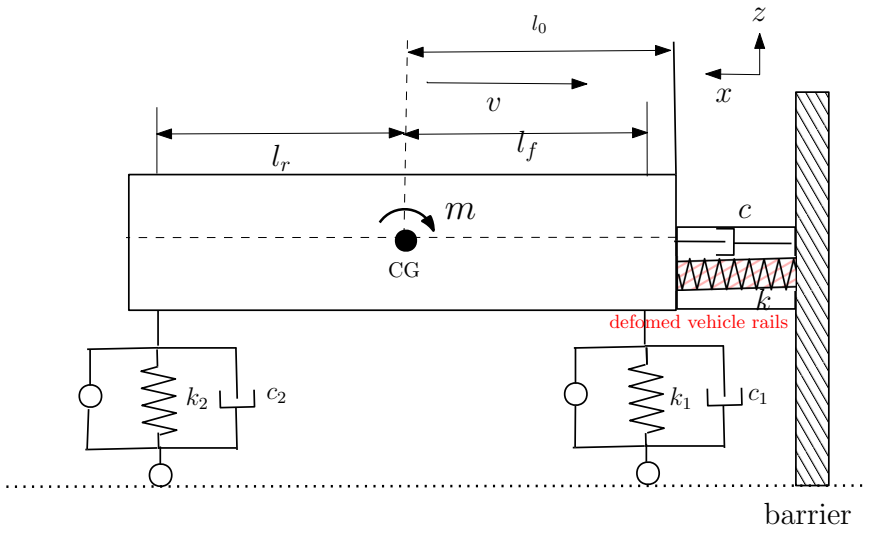

Figure 2.4: Phase I of the impact represented in LPM V1 with front end deformation

Equation of motion:

$$m\ddot{x} + c\dot{x} + kx = Q_x^{ext} \tag{2.8}$$

The front-end non-linear spring-damper system is approximated by a piecewise-linear curve [1], the forces on the spring are calculated using the general relationship between the force and deformation for a spring-damper system as shown in Figure 2.5. The spring and damper coefficient is parameterized using a gradient-descent optimization algorithm for a single mass-spring-damper system. The code searches for a global minima by performing 100 re-runs of gradient descent optimization, each with randomly generated initial parameter values. The spring characteristics are defined as follows:

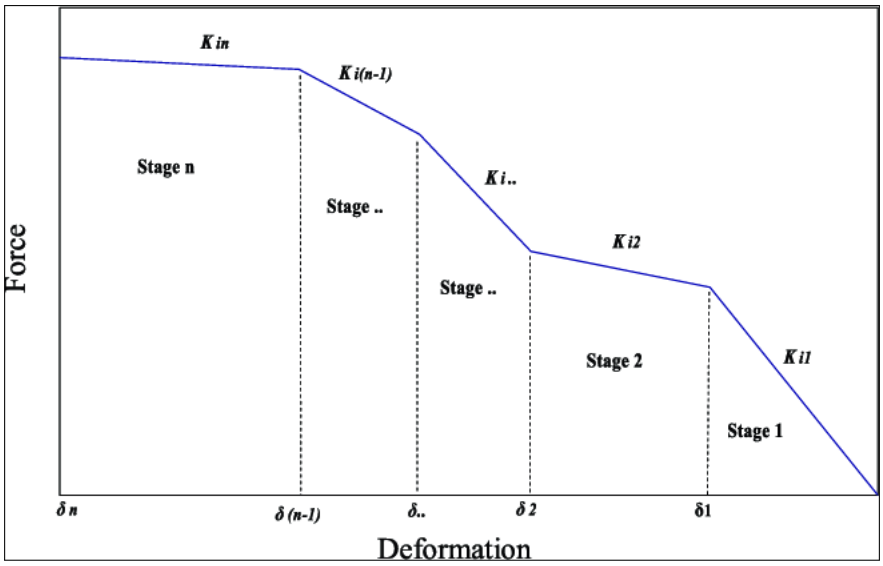

Figure 2.5: General piecewise force-deformation characteristics [1]

$$k(x) = \begin{cases} \frac{(k_2-k_1)\cdot|\hat{x}|}{x_1} + k_1 & \text{for, } |\hat{x}| \leq x_1, \\ \frac{(k_3-k_2)\cdot(|\hat{x}|-x_1)}{(x_2-x_1)} + k_2 & \text{for } x_1 \leq |\hat{x}| \leq x_2, \\ \frac{(k_4-k_3)\cdot(|\hat{x}|-x_2)}{(x_3-x_2)} + k_3 & \text{for } x_2 \leq |\hat{x}| \leq x_3, \\ \frac{(k_5-k_4)\cdot(|\hat{x}|-x_3)}{(x_4-x_3)} + k_4 & \text{for } x_3 \leq |\hat{x}| \leq x_4, \\ \frac{(k_6-k_5)\cdot(|\hat{x}|-x_4)}{(x_5-x_4)} + k_5 & \text{for } x_4 \leq |\hat{x}| \leq x_5, \\ \frac{(k_7-k_6)\cdot(|\hat{x}|-x_5)}{(C-x_5)} + k_6 & \text{for } x_5 \leq |\hat{x}| \leq C. \end{cases}$$

The damper characteristics are defined similar to the spring characteristics in the

model

$$c(\dot{x}) = \begin{cases} \frac{(c_2-c_1)\cdot|\hat{\dot{x}}|}{\dot{x}_1} + c_1 & \text{for } |\hat{\dot{x}}| \leq \dot{x}_1, \\ \frac{(c_3-c_2)\cdot(|\hat{\dot{x}}|-\dot{x}_1)}{(\dot{x}_2-\dot{x}_1)} + c_2 & \text{for } \dot{x}_1 \leq |\hat{\dot{x}}| \leq \dot{x}_2, \\ \frac{(c_4-c_3)\cdot(|\hat{\dot{x}}|-\dot{x}_2)}{(\dot{x}_3-\dot{x}_2)} + c_3 & \text{for } \dot{x}_2 \leq |\hat{\dot{x}}| \leq \dot{x}_3, \\ \frac{(c_5-c_4)\cdot(|\hat{\dot{x}}|-\dot{x}_3)}{(\dot{x}_4-\dot{x}_3)} + c_4 & \text{for } \dot{x}_3 \leq |\hat{\dot{x}}| \leq \dot{x}_4, \\ \frac{(c_6-c_5)\cdot(|\hat{\dot{x}}|-\dot{x}_4)}{(\dot{x}_5-\dot{x}_4)} + c_5 & \text{for } \dot{x}_4 \leq |\hat{\dot{x}}| \leq \dot{x}_5, \\ \frac{(c_7-c_6)\cdot(|\hat{\dot{x}}|-\dot{x}_5)}{(v_0-\dot{x}_5)} + c_6 & \text{for } \dot{x}_5 \leq |\hat{\dot{x}}| \leq v_0, \end{cases}$$

where x is the vehicle deformation; k is the spring coefficient; c is the damper coefficient; $\hat{x}$ is the computed vehicle deformation; $\dot{x}$ is the vehicle velocity; $\hat{\dot{x}}$ is the computed vehicle velocity; v_0 is the velocity at the time of maximum dynamic crush; C is the maximum dynamic crush.

The proposed algorithm uses an optimization approach to minimize an objective function. The objective function to be minimized is the error function $E(\Theta, t)$ where Θ denotes the unknown variables in the mode. The error function is defined as follows:

$$E(\Theta, t) = E_1(\Theta, t) + E_2(\Theta, t) + E_3(\Theta, t), \tag{2.9a}$$

where

$$E_1(\Theta, t) = |(a_{FE} - a_{LPM})|, \tag{2.10a}$$
$$E_2(\Theta, t) = |(v_{FE} - v_{LPM})|, \tag{2.10b}$$
$$E_3(\Theta, t) = |(x_{FE} - x_{LPM})|, \tag{2.10c}$$

where a is the acceleration; v is the vehicle velocity; and x is the displacement.

Phase II: This phase of impact (shown in Figure 2.6) starts after the front-end has deformed absorbing all the energy and the vehicle pitches forward. In the LPM developed for Paper B, the phase II of the impact assumes motion only in the vertical axis (z) along with a rotation of the vehicle in the y axis (pitching); the motion is restricted in all other axes. The governing equations of motion were defined using Lagrangian mechanics and presented below:

$$Q^{ext}_{theta} = J\ddot{\theta} + (k_1 l_f^2 + k_2 l_r^2)\theta + (c_1 l_f^2 + c_2 l_r^2)\dot{\theta} + (k_2 l_r - k_1 l_f)x + (c_2 l_r - c_1 l_f)\dot{x}, \quad (2.11)$$

$$Q^{ext}_{x} = m\ddot{x} + (k_1 + k_2)x + (c_1 l_f + c_2 l_r)\dot{\theta} + (k_2 l_r - k_1 l_f)\theta + (c_1 + c_2)\dot{x}. \quad (2.12)$$

The value of the vehicle mass m and the moment of inertia J for the lumped mass system has been calculated from the FE model of the vehicle. The vehicle starts to pitch forward at this instant. A number of studies have been conducted to understand the reason for the vehicle pitching forward, suggesting that for body-on-frame vehicles, one of the reasons is the downward plastic buckling of the frame rails [31]. Due to an imbalance of loading caused by buckling added to gravity force acting downwards, the vehicle pitches. Figure 2.8 shows this force component leading to pitching in the vehicle. The value for these forces has not been defined separately in the equations; but this force component was measured from the FE results and added to Q^{ext}_{theta} in Equation 2.11. One of the assumptions of this model is that the vehicle rails are in-line with the CG; thereby ignoring any rotational effects from an offset between the rails and the vehicle CG. Figures 2.7 and 2.8 represent the deformation and pitching angle from the simulation overlayed against the results of FE data. The maximum crush and velocity of impact in the LPM were closely predicted; the overlay of curves indicates good correlation in the model. The pitching curves, however are underpredicted and the trend of the first part of the impact is not captured in the LPM V1. The maximum value of pitching is close to the FE data but the curve trend needs to be improved.

The LPM performance has been presented in Paper B indicating the need to improve the vehicle pitching prediction. Paper C defines the Robust 2-Phase model in WP-1 which reinforces the observations and further supports the robustness of the model using parameter variation and validation with a different vehicle platforms. The 2 phase LPM was validated against two different vehicle platforms; a full size truck (2015 Chevrolet Silverado)and a hatchback (2010 Toyota Yaris). The prediction for the front-end deformation was acceptable in both cases indicating high confidence on the model. The second phase of the model (vehicle pitching) showed areas for improvement which will be discussed further in the next sections. Further, robustness check was conducted on the LPM by varying the thickness of the steel parts by 10% and 20% in the FEM. The corresponding correlation of LPM and FE simulations indicated a high level of confidence with parameter variation and robustness check on the model; consistent with the earlier observations, pitching angles showed deviation

from the test validation (FE) and needed improvements in the model.

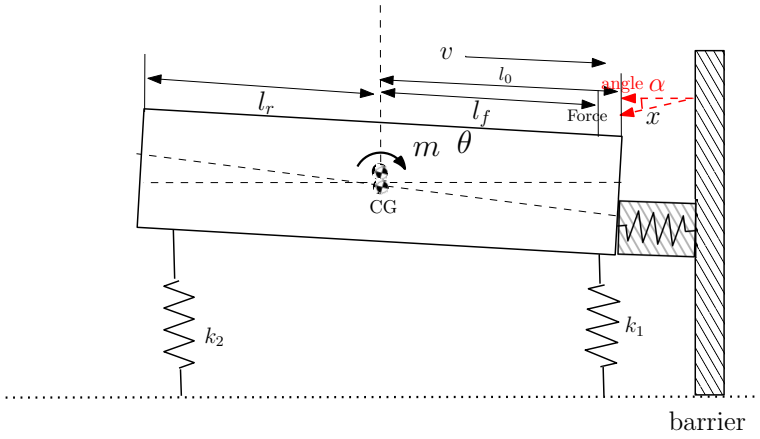

Figure 2.6: Phase II of impact with forward pitching in the vehicle - LPM V1, dampers have not been shown in the image

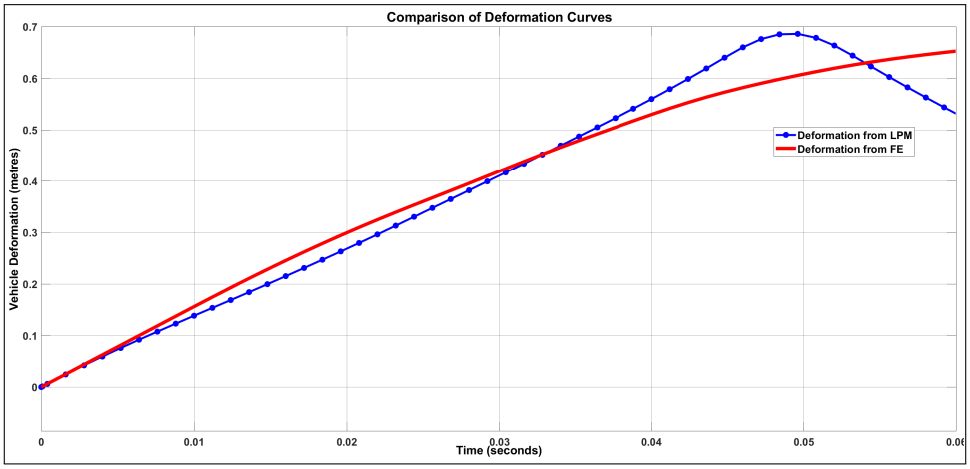

Figure 2.7: LPM V1 simulation - vehicle deformation curves compared with FE simulation data

2.5.2 LPM V2 - Pendulum Model

The LPM V1 in Subsection 2.5.1 established that the front-end spring damper model gave reliable results; however the second phase of impact which also contributes to occupant injuries (pitching) shows poor prediction bringing in the need to improve this model. The knowledge from this study also underpinned the concept for LPM V2 where the front-end deformation prediction algorithm described in the previous section is unaltered but the model addresses the shortcoming from LPM V2 and the 2-Phase robust model . Figure 2.9 illustrates a periodic pendulum motion that is used for this model. The pendulum swings back and forth from its rest position. Taking inspiration from pendulum motion; the vehicle is depicted as a pendulum combining the 2 phases in a single model. In an impact, the occupant compartment

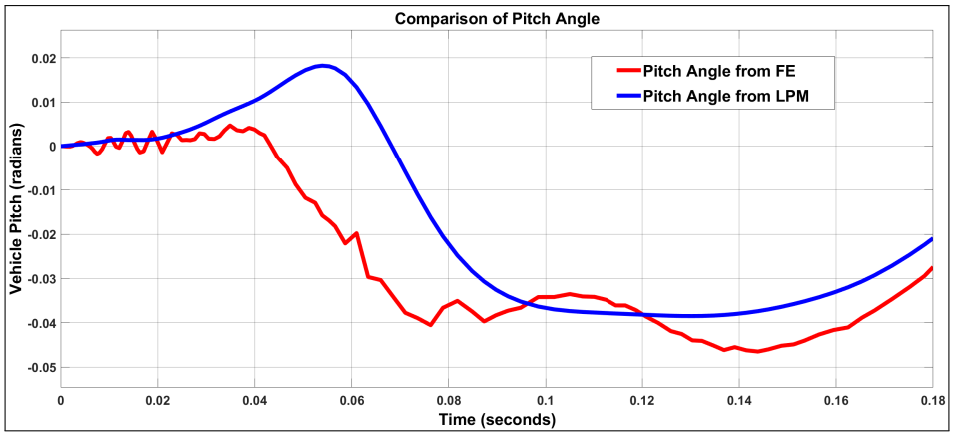

Figure 2.8: LPM V1 simulation - vehicle pitching curves compared with FE simulation data

rotates around the pivot point, causing the vehicle to pitch forward. Due to the ground acting as a constraint, the vehicle cannot swivel. Additionally, the vehicle suspension system serves as a constraint to prevent the pendulum from swinging too far. The model in undeformed state presented in Figure 2.9 at time $t = 0$ is the same as Figure 2.4. In this case the front end deformation is defined similar to LPM V1. The spring and damper coefficients were approximated by the piece-wise linear curve and defined by the same equations as explained in LPM V1. The elastic pendulum deforms to absorb energy in the first phase of the impact; during the second phase the vehicle rotates about the impact point acting as a pendulum. The governing equations explaining the system are derived using pendulum motion; the generalized Lagrangian formulation (polar coordinates) has been adopted to simplify the system. The vehicle during forward pitching is shown in Figure 2.11. The

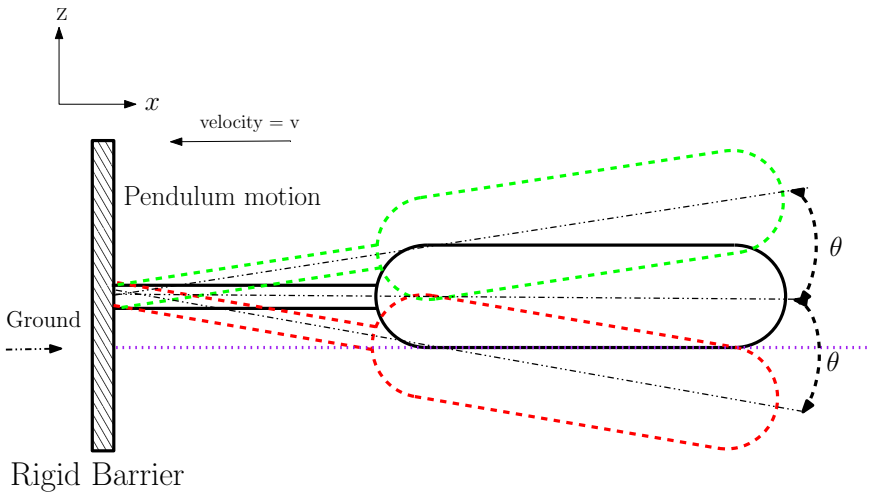

Figure 2.9: Vehicle body rotating about the point of impact like a pendulum

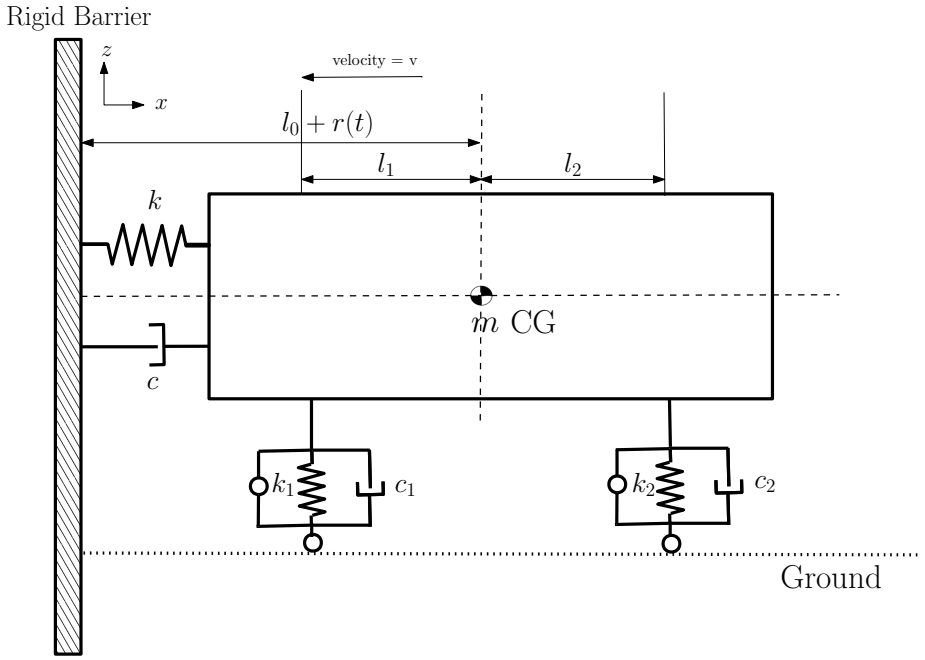

Figure 2.10: A single-mass spring damper system representing a vehicle impact at t= 0

governing equations of motion are:

$$\begin{aligned} Q_r^{ext} =& m\ddot{r} - mr\dot{\theta}^2 - ml_0\dot{\theta}^2 + mg\sin\theta \\ &+ kr + \frac{1}{2}k_1(2r - l_0r - l_1)\theta^2 \\ &+ \frac{1}{2}k_2\theta^2(2r + l_0r + 2l_2), \end{aligned} \tag{2.13}$$

$$\begin{aligned} Q_\theta^{ext} =& m(l_0 + r)^2\ddot{\theta} + mg(l_0 + r)cos\theta \\ &+ k_1(l_0 + r - l_1)^2\theta + k_2(l_0 + r + l_2)^2\theta, \end{aligned} \tag{2.14}$$

where Q_r^{ext} and Q_θ^{ext} are the external forces experienced by the vehicle. The non-conservative forces experienced by the system are included in the Lagrange's equation of motion in the form of generalized forces expressed with the formulation of virtual work δU [51]:

$$\delta U = \sum_{j=1}^{m} F_j \cdot \delta r_j, \tag{2.15}$$

where F_j are the force components, δr_j are the virtual displacements given by

$$\delta r_j = \sum_{i=1}^{N} \frac{\partial r_j}{\partial q_i}\delta q_i \tag{2.16}$$

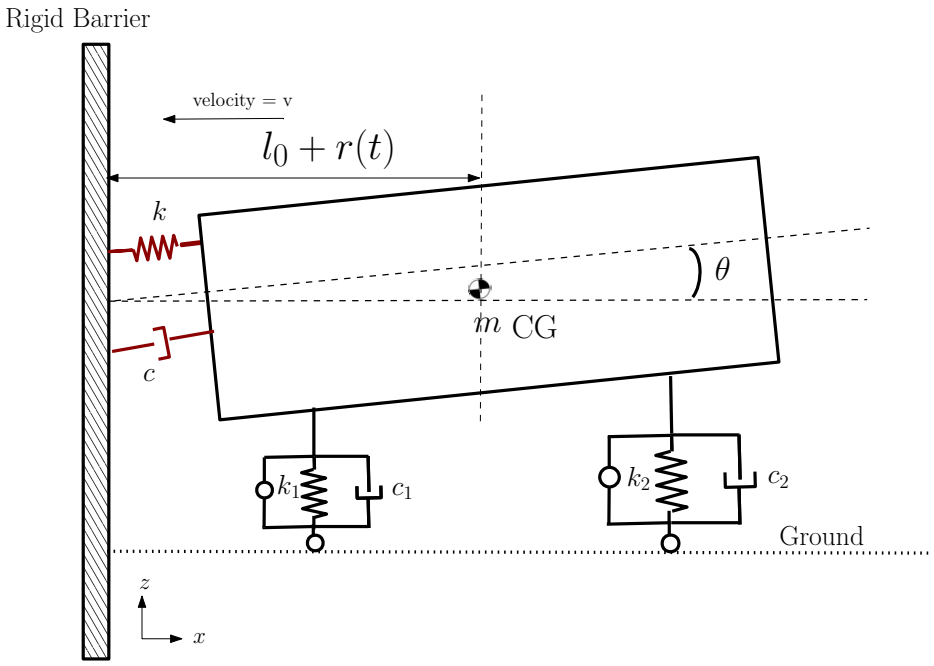

Figure 2.11: LPM representation of vehicle pitching forward in the crash event

for $j = 1, 2, 3, \ldots, m$. This yields the following equation for virtual work as:

$$\begin{aligned} \delta U = F_1 \cdot \sum_{i=1}^{N} \frac{\partial r_j}{\partial q_i} \delta q_i + F_2 \cdot \sum_{i=1}^{N} \frac{\partial r_j}{\partial q_i} \delta q_i + \cdots \\ + F_m \cdot \sum_{i=1}^{N} \frac{\partial r_j}{\partial q_i} \delta q_i. \end{aligned} \tag{2.17}$$

Using equation (2.17), we compute the generalized forces experienced by the system.

$$\begin{aligned} \delta U = F_x \cdot \left(\frac{\partial x}{\partial r} \cdot \delta r + \frac{\partial x}{\partial \theta} \cdot \delta \theta \right) \\ + F_z \cdot \left(\frac{\partial z}{\partial r} \cdot \delta r + \frac{\partial z}{\partial \theta} \cdot \delta \theta \right). \end{aligned} \tag{2.18}$$

where,

$$x = [l_0 + r(t)] \cos \theta(t), \tag{2.19}$$

$$z = [l_0 + r(t)] \sin \theta(t), \tag{2.20}$$

Substituting equations (2.19) and (2.20) in equation (2.18), we get

$$\begin{aligned} dU = F_x \cdot [(\cos(\theta) \delta r - (l_0 + r) \sin(\theta) \delta \theta] \\ + F_z \cdot [(\sin(\theta) \delta r + (l_0 + r) \cos(\theta) \delta \theta]. \end{aligned} \tag{2.21}$$

The external forces included in this LPM are barrier forces, damper forces

including front end spring damper system and suspension damper system forces. The corresponding equations are:

$$Q_r^{ext} = Q_r^{bar} + Q_r^{damp}, \tag{2.22}$$

$$Q_\theta^{ext} = Q_\theta^{bar} + Q_\theta^{damp}. \tag{2.23}$$

Detailed expression for the forces derived for this system has been presented in Paper D.

The front-end deformation is presented in Figure 2.12 indicating a close correlation between the LPM and test FE values. The maximum deformation experienced by the vehicle is very closely predicted in the LPM. On the other hand, Figure 2.13 shows the pitching angle in radians for the pendulum model; the trend of the curves is similar indicating the model captures the kinematics of the vehicle. The maximum pitching is predicted; however the pitching in the LPM continues increasing in the simulation indicating need for future work. This model was a reliable baseline model to include welds and material failures in the LPM; the maximum crush (displacement) and pitching are important factors contributing to occupant injuries in a crash. The LPM developed is not computationally intensive; needs little manual labour to determine parameters responsible for safer vehicles and requires few dimensions of the new vehicle.

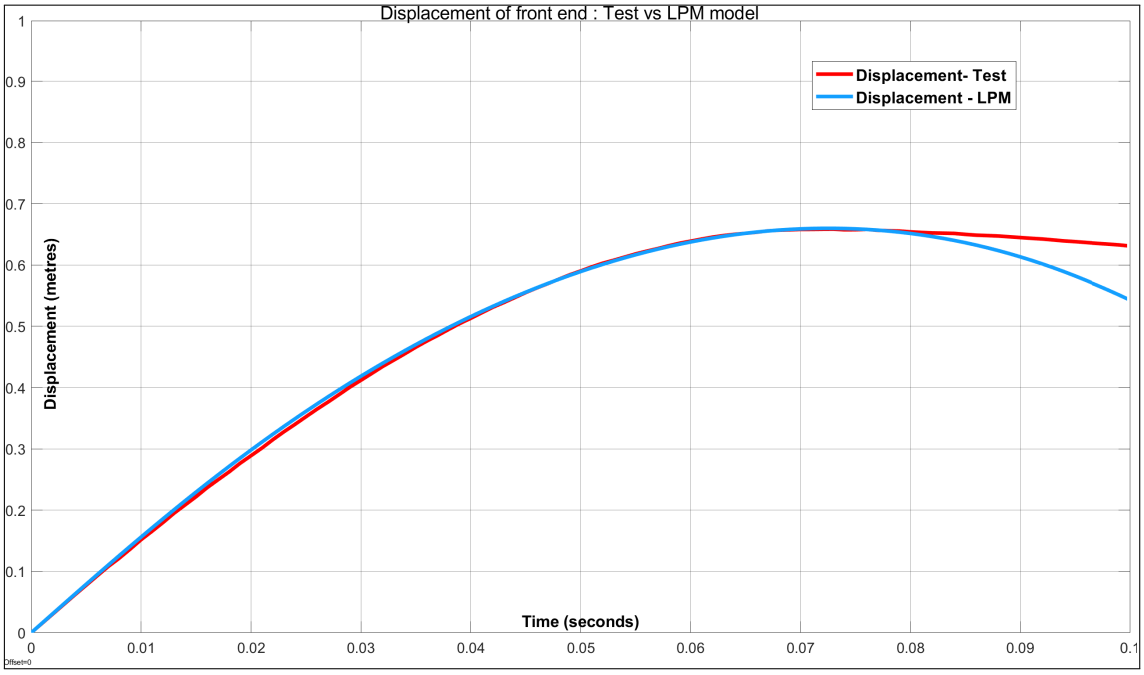

Figure 2.12: LPM V2 simulation - vehicle deformation curves compared with FE simulation data

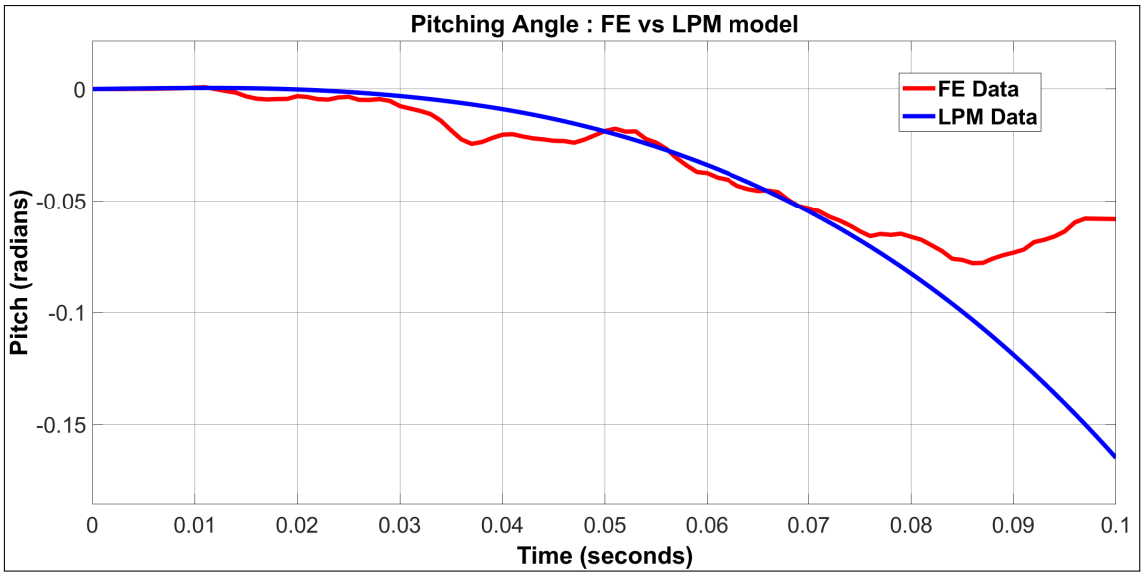

Figure 2.13: LPM V2 simulation- vehicle pitching curves compared with FE simulation data

2.6 Summary

The baseline model for vehicle impact was developed with LPM V1 and V2. The crash event was divided into two phases and presented in LPM V1 showing good correlation against the test data for the front-end deformation absorbing the impact energy. The model also predicts the vehicle rotation (pitching); in this case it was observed that the pitching angle over-predicts the validation data. The LPM was robust and capable of predicting the parameter variations based on the extended study conducted for a hatchback. However the model lacked good prediction for vehicle pitching which is a contributes to head and neck deflections in occupants during an impact. A new model was represented by a pendulum swinging about the point of impact in LPM V2. The to-and-fro movement of the pendulum describes the vehicle pitching forward after the first phase of the impact. Improved prediction of the pitching angle was achieved with this methodology; the gaps in correlation could be attributed to the limitations discussed in the Paper D, such as approximation of model parameters like suspension spring and damper coefficient values. The model also ignores energy losses in the form of heat and other forms during the impact. The LPM was extended to include material failures in a modified vehicle; the next chapter explains the experimental data collected for this model along with the model presented as LPM V3.

Chapter 3

Modified Vehicle Impact Model Development

Most advances in science come when a person for one reason or another is forced to change fields. -Peter Borden

In the previous chapter the development of a baseline impact model was discussed; the pendulum model LPM V2 was proposed to replicate both stages (deformation and pitching) of impact successfully.

Automakers strictly recommend using the collision repair manual for vehicle collision repairs. It implies that repairing vehicles after a collision is permitted if the process adopted follows a repair manual from the automaker to avoid unprofessional repairs on vehicles. An example of an unprofessional repair is cutting and welding two halves of different vehicles to repair large damages in the front or rear of the vehicle. This chapter investigates the crashworthiness performance assessment of a modified vehicle (vehicle with unprofessional repairs on its structural members) followed by replicating the impact behaviour of this modified vehicle in an LPM. Figure 3.1 shows the front-end structural members and the load paths in the event of a frontal impact. The front end members namely A-Pillar, rocker and upper rails contribute to the load distribution to prevent intrusions in the occupant compartment. In modern vehicles, these members use UHSS to improve vehicle crashworthiness along with balancing weight requirements for ride and handling; welding and heat treatment of these structural members would lead to a change in the crashworthiness performance.

To develop the LPM using a pendulum further, knowledge and data regarding the behavior of the UHSS and the behavior of the modified (unprofessional repair) vehicle is needed. Therefore, coupon samples from a relatively new vehicle were tested in a tensile testing machine. This was followed by a 5-door hatchback vehicle which was prepared and instrumented for a full scale crash test to get more information of the

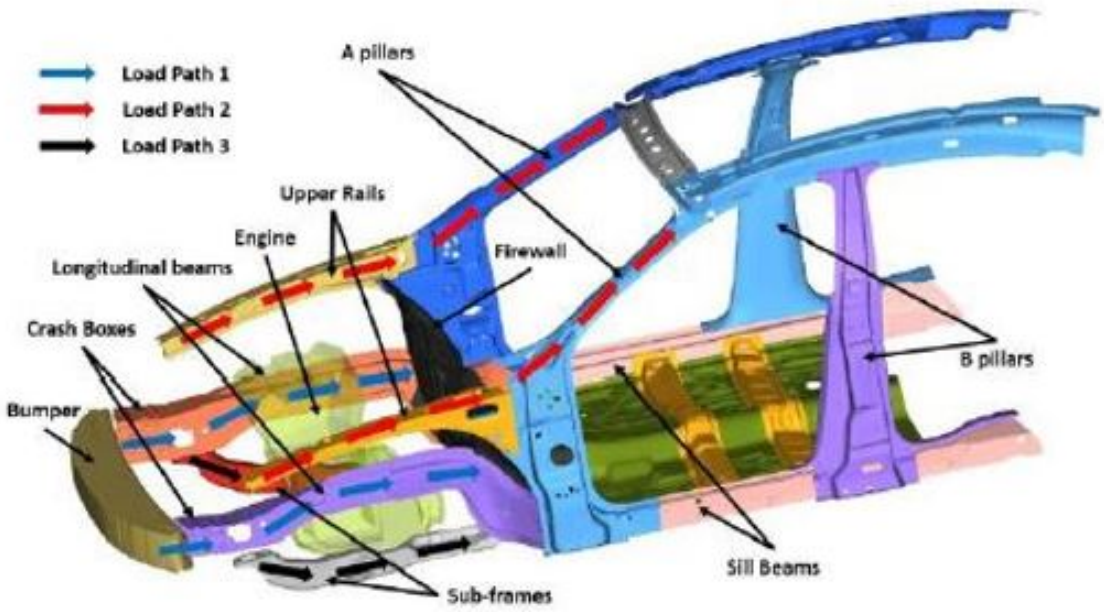

Figure 3.1: Modern vehicle structure with load paths for full frontal impact

vehicle in the crash and also measure the front-end deformation and the pitching of the vehicle. The idea is to measure the pitching of the test vehicle and get data for validating the FEM simulations. Welding and heat treatment of UHSS will entail loss of strength in the material. Hopefully there will be bending in the welded zone (rear part of the vehicle compared to the front part). Mounting sensors (accelerometers) at different locations on the vehicle will give needed information.

WP-2 (Figure 3.2) is divided into three major sections; FE model of the crash response; coupon testing of UHSS samples to determine the material response followed by full vehicle crash testing of a modified (improperly repaired) vehicle to generate physical data. The full vehicle test also serves as a dataset for future work in the area along with LPM improvements discussed further in the next chapter. The FE model developed using the material card from the coupon tests is correlated with the physical test data.

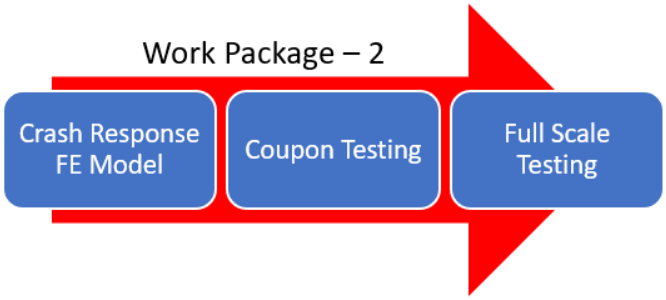

Figure 3.2: Flowchart of Thesis WP-2 from FE model to Physical Testing

3.1 Crash Response of Modified Vehicle using FEM

As discussed before, literature documents the challenges in the weldability of UHSS used in automotive applications leading to the likelihood of a reduced crashworthiness performance for a modified vehicle. There are however, no available open source FE models of a modified vehicle to determine the impact performance of such a vehicle. Paper E investigates the crash response of a modified vehicle with an FE model; the LS Dyna model based on a 2011 Honda Accord demonstrates a weld on the A-Pillar replicating a modified vehicle. The open-source FE model adopted for this study was developed by a NHTSA-led research team. The research project at NHTSA updated the FE model of the Accord (4-door mid-size sedan from 2011) to include structural members with high yield strength (1250-1500 MPa) using UHSS to improve crash performance [43]. This updated FE model was used to represent the modified vehicle in this thesis and was simulated to investigate different crash test scenarios. To represent the modified vehicle (unprofessional repairs on the structural members) welds were added on the A-Pillar and a weakened structure around the weld zone. The modeling methodology which includes using beam elements to model the weld and assigning $MAT - Spotweld$ LS Dyna material card to the welds; it

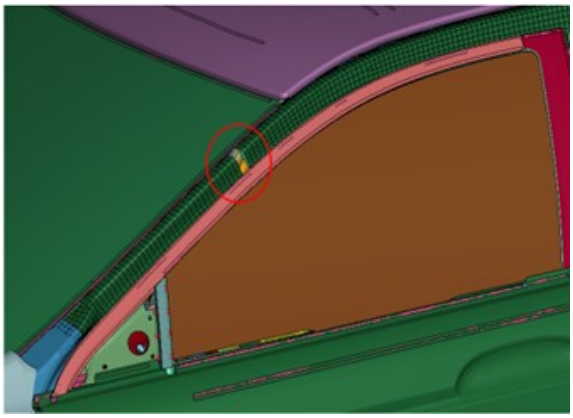

Figure 3.3: Results of crashworthiness performance for Honda Accord model with welds added on the model

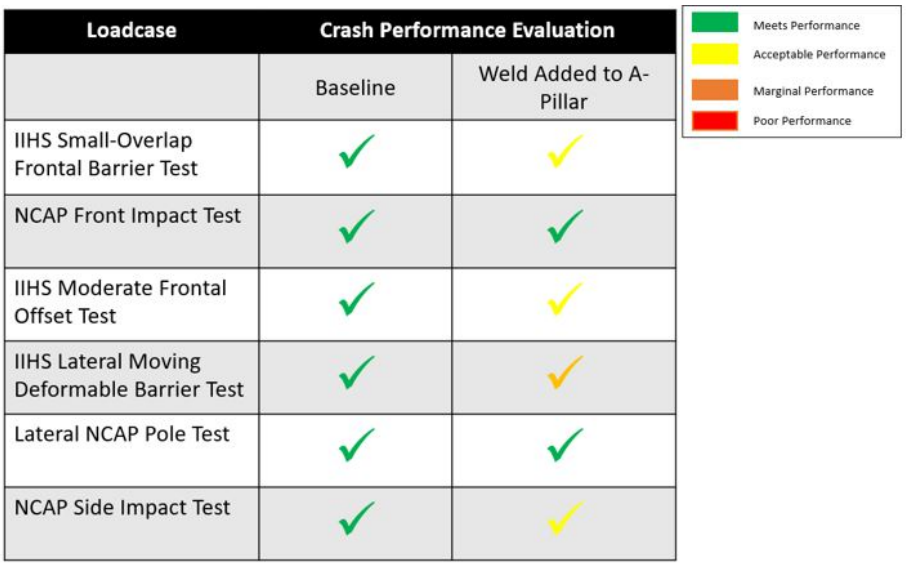

Figure 3.4: Results of crashworthiness performance for Honda Accord model with welds added on the model

was concluded that this was a realistic representation of a butt weld on the model. The FE model was used to run simulations for different crash scenarios to study the behavior of a modified vehicle in impact. The detailed input values to the material card used for representing spotwelds in the FE model is presented in Paper E. The location of the weld on the A-Pillar is shown in Figure 3.3. This vehicle uses UHSS only on the A-Pillar, so only this member was selected for representing unprofessional repairs.

The simulations highlighted a change in the crashworthiness performance of the modified vehicle due to the addition of welds on the A-Pillar (shown in Figure 3.4); the results are compared against a baseline performance of the vehicle for the different impact scenarios. As shown in Figure 3.4, the results are based on Insurance Institute for Highway Safety (IIHS) Rating Calculator for every loadcase. This rating calculator helps evaluate the safety performance of the modified vehicle in different loadcases based on the structural integrity of the vehicle [52]. The different colors indicate good, marginal, acceptable or poor performance of the vehicle in different test scenarios. The results indicate the deterioration in performance of few loadcases due to the addition of welds in the A-Pillar. It was also observed that few loadcases were more sensitive in terms of the performance as opposed to others indicating that the position of the weld was also a contributing factor; IIHS Lateral Moving Deformable test showed maximum change in performance for the modified vehicle. The baseline performance was green which turned to orange for the modified vehicle making the vehicle marginally meeting the performance. Another aspect of this work included running simulations for the same loadcase (IIHS Small Overlap Frontal Barrier test) by changing the weld positions and the number of

welds in the model; this produced interesting results highlighting the contribution of weld position and number of welds on the model. However the non-calibrated LS Dyna material model used in this work lacked experimental data to represent the UHSS structural members undergoing welding and heat treatment bringing the need to generate test data for the material model. Another shortcoming of the FE model is the lack of physical test data on a modified vehicle, so these results needed experimental data for validation. The loadcase performance of the vehicle in full frontal impact against a rigid barrier remains unchanged on the modified vehicle as per the Figure 3.4; however the LPM development for a full frontal impact in baseline and modified vehicle is the scope of this work; along with restricted resources to run a full scale test, this test scenario was selected to continue the investigation for a modified vehicle crashworthiness response. The FE model provided a scientific conjecture to first conduct experimental tests to generate data for a coupon test on UHSS samples with welding and heat treatment followed by a full scale crash test to improve the FE model in this part of the research.

3.2 Coupon Testing of UHSS Samples for Generating Data for FEM

The FE simulation described in the previous section showed the reduction in the crashworthiness performance of the vehicle for a few test scenarios; however the input to the LS Dyna material cards used for the simulations lacked real data from tests triggering the need to run coupon tests to generate test data for the FE models. Tensile Testing is a form of destructive engineering and materials science test whereby controlled tension is applied to a sample until it fully fails. It is one of the most common mechanical testing techniques used to find how strong a material is and how far it stretches before failure. During the test, the specimen is subjected to tension load and the extension caused in the steel rod is noted against the load within the elastic limit. The load values at yield point, breaking point, and ultimate point are carefully registered. With the obtained values, the stress and strain are calculated and plotted in a graph; stress strain curve of mild steel is presented in Figure 3.5.

Tensile strength and yield strength are the most common properties determined in a tensile test. *According to ASTM E6, tensile strength is calculated from the maximum force during a tension test that is carried to rupture, divided by the original cross-sectional area of the test piece* [53].

The yield strength refers to the stress at which a small, but measurable, amount of inelastic or plastic deformation occurs [53]. Toughness is defined as the resistance of a metal to fracture or its ability to absorb energy and deform plastically before

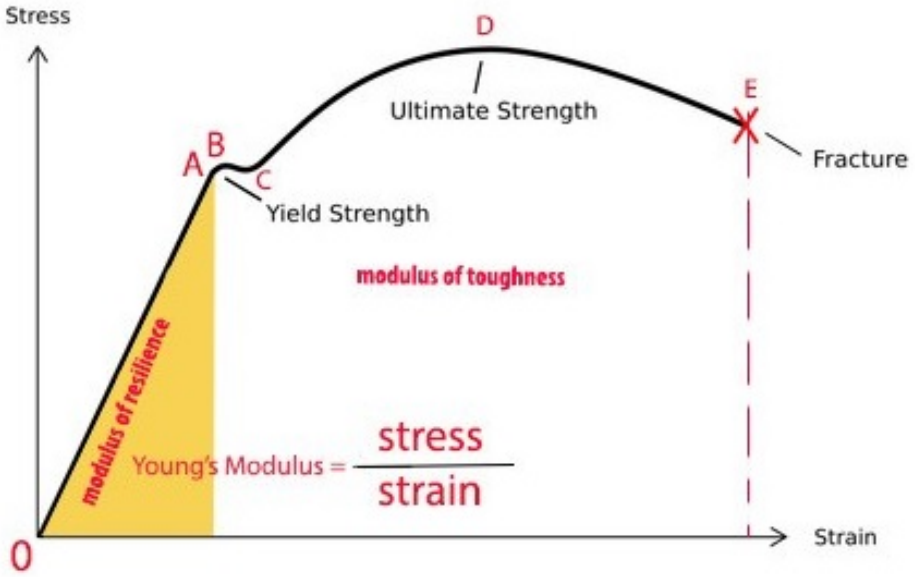

Figure 3.5: Stress Strain diagram of mild steel

fracture. A rough measure of toughness is the area under the stress–strain curve up to fracture. This area determines the amount of plastic work per unit volume at fracture and it is very important in energy-absorbing applications. For a metal to be tough, both strength and ductility must be high. Several researchers have investigated the behaviour of UHSS in tension and characterized the material properties for use in FE models and other mathematical models but there is insufficient data for developing a material card to conduct FE simulations for an improperly heat-treated vehicle member.

3.2.1 Test Description

As highlighted before, the focus of the research is restricted to frontal impacts only; based on Figure 3.1 the front-end structural members support in the load path for a frontal impact. These members like the A-Pillar and rocker, in modern vehicles use UHSS for meeting crashworthiness and vehicle dynamics requirements. The coupon test samples were generated from parts cut out from these structural parts.

The following pre-testing procedure was adopted to generate the test samples from vehicle structural parts.

-Cutting the samples from the vehicle as shown in Figure 3.6

-Water jet cutting of the samples into coupon samples

-Speckling process for DIC producing samples as shown in Figure 3.7

The samples were further divided into 4 types as explained in Table 3.1 and 4 tests conducted on every sample type to generate force-elongation curves using SI

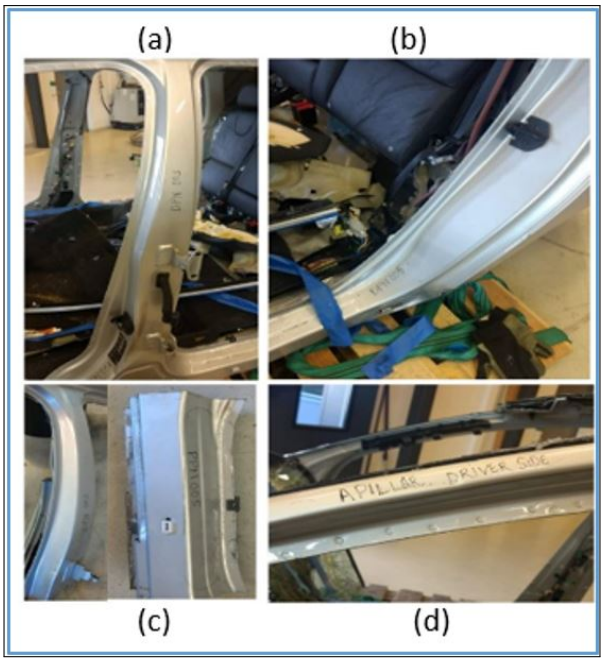

Figure 3.6: Structural parts on the vehicle cut to generate UHSS samples: (a) B-Pillar, (b) C-Pillar, (c) Rocker, (d) A-Pillar

SI No.	Sample Type	Total No. of Samples
1	Baseline	4
2	Welded	4
3	Heat Treated - 800°C	4
4	Heat Treated - 1250°C	4

Table 3.1: Specimen types used for the material test

Plan Universal Testing Machine (UTM) with 25kN capacity in University of Agder.

3.2.2 Experimental Results

The results from the Digital Image Correlation (DIC) and the extensometers was processed to determine the yield strength, ultimate strength and ultimate strain in the samples. The stress strain curves are presented in Figure 3.8. The yield strength of the baseline samples was higher than 1100 MPa as expected, however the welded and heat treated samples were observed to have lower yield strength indicating reduced structural integrity in the occupant cage. The Table 3.2 presents the experimental results for all coupons. The material properties defined in Paper F were used to develop an LS Dyna material card for running the correlation model of the full vehicle crash test. This material model is used for developing the FE model which serves as validation to the LPM V3 defined in the previous chapter.

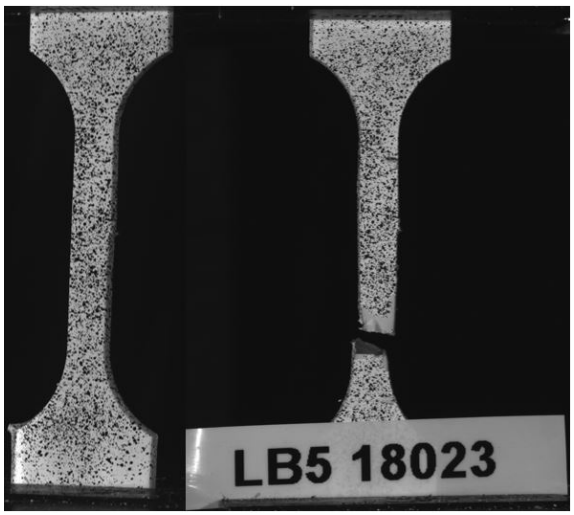

Figure 3.7: Baseline sample before and after tensile test showing fracture

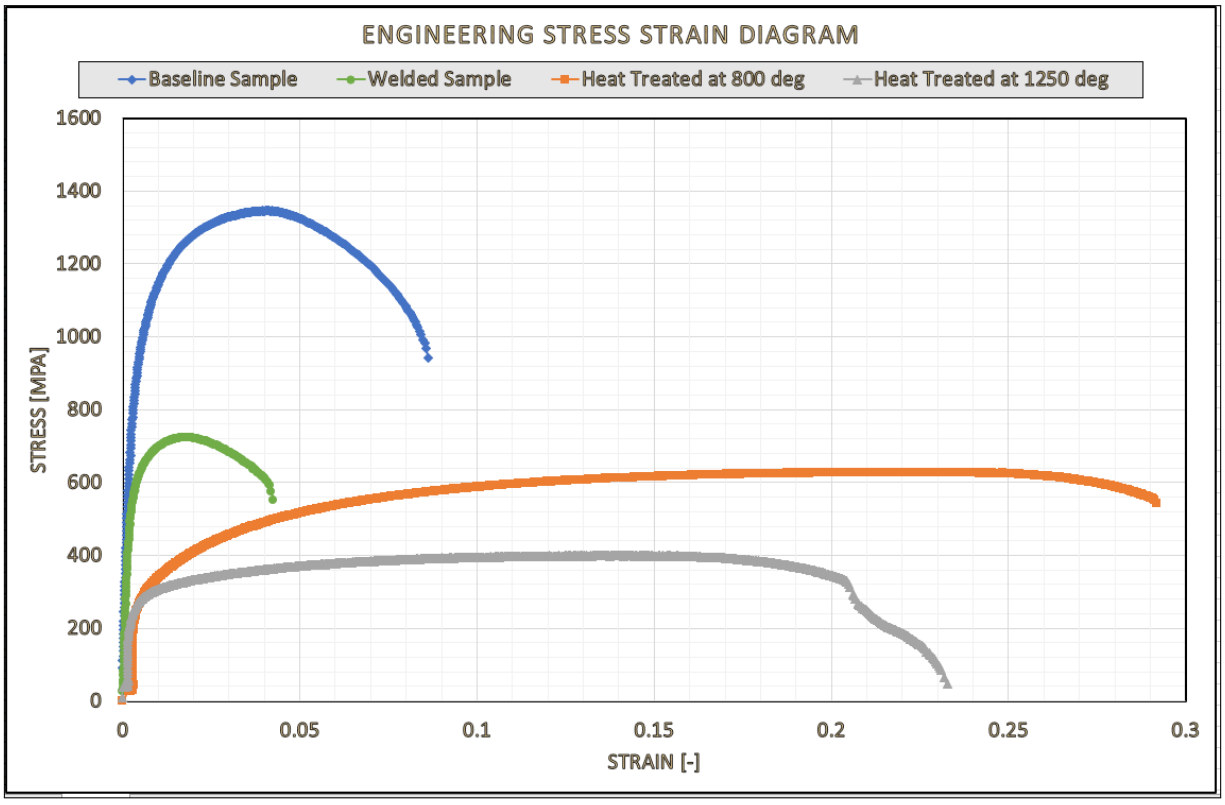

Figure 3.8: Engineering stress strain diagram for all 4 sample types

SI No.	Sample Type	Yield Strength (MPa)	Ultimate Tensile Strength (MPa)	Strain at maximum force
1	Baseline	1188	1325	0.043
2	Welded	730	758	0.016
3	Heat Treated - 800°C	386	582	0.191
4	Heat Treated - 1250°C	311	383	0.150

Table 3.2: Material properties derived from the tensile test results - average values of 4 test samples

The material properties described in this project were based on some assumptions and observations outlined in detail in Paper F. The type of welding and heat treatment parameters plays a huge role in the performance of the material under loading conditions.

The previous section explains the material behaviour of UHSS in welding and heat treatment; it concludes that the material drastically loses strength leading to unexpected material failure in the specimen. However, if this behaviour affects vehicle crashworthiness response during a crash event is yet to be answered. The hypothesis that the vehicle crashworthiness is reduced due to material failure is emphasized in Paper E and F but the real-time data required to develop and validate a simulation model was one of the gaps recognized during the literature study.

3.3 Full Scale Test for Model Validation

The lack of physical data to validate the FE model highlighted the need to run physical tests during the research. There is no physical data on behaviour of modified vehicle; although FE simulations provide some validation point it is beneficial to obtain full-scale crash test data. Full frontal rigid barrier test was conducted to generate the data required to define the LPM described as LPM V3 in Subsection 3.4.

An important step in the history of car safety is the beginning of safety tests; the first barrier crash test was performed by General Motors in 1934. The full scale crash tests paved the way for crash tests conducted with different testing scenarios

and development of new barrier types representing real-time road conditions. With the technological advancements in modern vehicles, crash tests have become more stringent in terms of barrier designs and instrumentation requirements. European New Car Assessment Programme (EURONCAP) [54] is one of the organizations assessing the safety of new vehicles; it also develops the vehicle safety standards which are compulsory to meet for all new vehicles. These standards outline the tests conducted to ensure structural integrity of the vehicle, occupant protection including child safety and VRU safety.

3.3.1 Test Requirements and Planning

EURONCAP front impact test is a full-width impact on the vehicle front. The test is run with a rigid barrier and the vehicle meeting a head-on collision at 56 kmph [55]. The test conducted in this project draws inspiration from this regulation; however the requirements of the model (LPM V3 in Subsection 3.4) were kept in mind while determining the instrumentation and measurements leading to deviations in the test setup from EURONCAP standard requirements. From the EURONCAP Front Impact Test the following requirements have been adopted for this test.

- full frontal impact against a rigid barrier
- test is run with a rigid barrier with specific dimensions
- test speed 56 kmph +/- 3 kmph

A full vehicle test is tough to conduct due to the preparation involved in the experiment along with the facilities and infrastructure required for running the test. A decommissioned outdoors test site at Farsund Airport Lista was prepared for the test. Conducting such tests outdoors also poses challenges with weather conditions.

It is important that the test vehicle hits the barrier with 0% offset and with the desired speed. At the test site there is a rail in the concrete road surface used for steering the vehicle. A steering bolt fitting the rail and connected to the vehicle was used, and the bolt was released from the vehicle 6 m before the vehicle hitting the barrier.The test was conducted by pushing the test vehicle with a fire truck till the vehicle attains the test velocity after which the fire truck disengaged with the test vehicle allowing it to hit the concrete barrier.

For the concrete barrier, 20 concrete blocks were stacked in three rows with 8-8-4 blocks to generate a large reactive force. Dimensionally, each block is 1.8 x 0.8 x 0.8 metres, and it weighs $\approx$ 2.4 tonnes. A concrete structure weighing approximately 48 tons, with dimensions of 3.2 by 3.2 metres in length and width, and an estimated height of 2.4 metres. The impact load was distributed across the structure with the help of a 200 kg steel plate placed in front of the concrete barrier. The schematic diagram presented in Figure 3.9 shows the dimensions of the barrier on the test

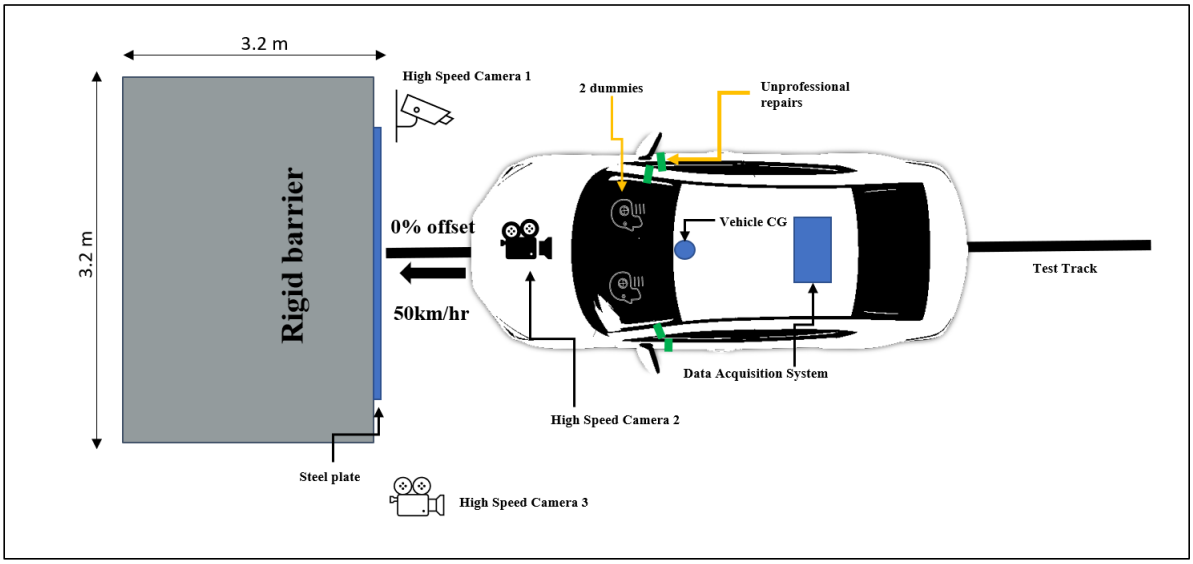

Figure 3.9: Vehicle crash test schematic with concrete barrier

track.

3.3.2 Modifications on the test vehicle

The test vehicle used in the experiment is a 5 door hatchback (2015) as shown in Figure 3.10. The basic specifications of the vehicle are outlined in Table 3.3:

Total Weight	1450 kg
Width	1700 mm
Length	3950 mm
Height	1510 mm
Wheelbase	2510 mm
Track width	1485 mm

Table 3.3: Test vehicle parameters.

The weldability and heat treatment of UHSS members has been a challenge; the same was also demonstrated by the coupon tests. With that understanding, parts needed to be identified on the full vehicle to conduct unprofessional repairs for the full scale test which could contribute to the change in the crashworthiness performance of the vehicle. Based on Figure 3.1 the A-Pillar and rocker (subframes) were modified on the test vehicle to replicate unprofessional repairs because these members contribute to the crashworthiness performance in frontal impact; collision repair manuals suggest to replace these parts or repair them by strictly following the instructions. The repair procedure adopted for this thesis included cutting the vehicle at four points: both the A-pillars as well as the Rocker panels. All the panels were cut through, including the UHSS material on the parts. In this case, the team

Figure 3.10: Test Vehicle: A 5 door hatchback

did not follow the collision manual's repair steps and the parts were welded without following the welding parameters as outlined in the manual. In order to remove excess filler material, the weld zone was ground after welding. Figure 3.11 shows the different steps in cutting, welding and grinding of the vehicle.

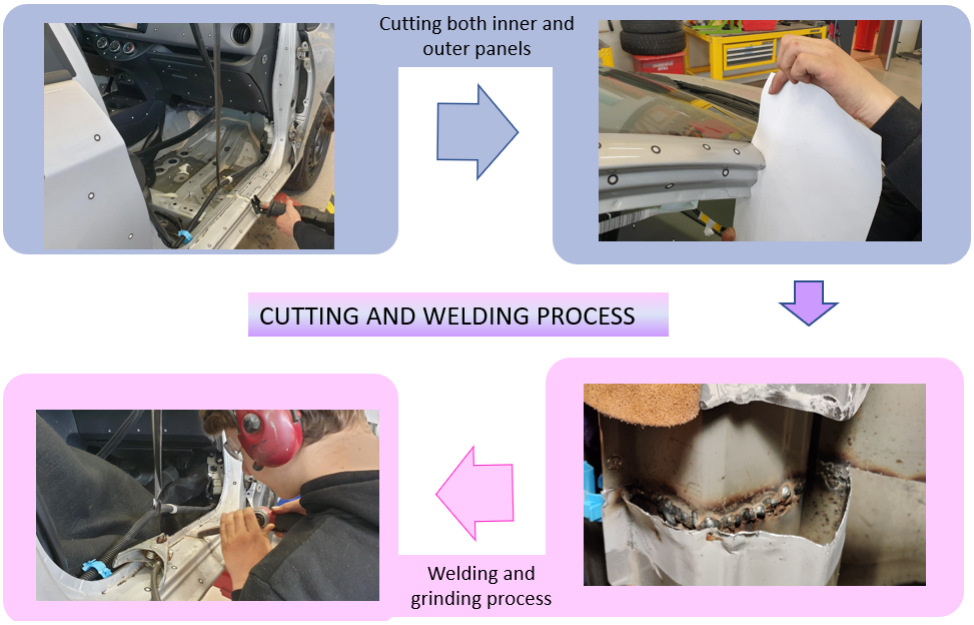

Figure 3.11: Cutting and welding process followed for preparing the test car

3.3.3 Data Acquisition and Instrumentation

The values of deformation, pitching angle and bending angle of the vehicle were important parameters planned to be measured from this test. One of the most important parts of planning a test is selecting the right instrumentation which collects data; another element of this is the safe mounting of different sensors to

ensure reliable data is captured. Dewesoft SIRIUS Waterproof Rugged IP67 was the Data Acquisition System (DAS) used for this test. The shock rating of the logger is 100 g; it has 8x2 channels; each one is capable of 3x digital inputs, 1x event counter, encoder, period, pulse-width and duty-cycle. The DAS was placed in a box with power input from a 12V battery, to avoid impact during the test it was placed in the rear passenger seat [56]. To ensure ruggedness, high output, high accuracy, and high resonant frequency, the test vehicle was equipped with three triaxial micro machined, full bridge sensors with gas damping and integral mechanical stops. In addition, 4 uniaxial accelerometers were fitted to the vehicle to get more data.

Table 3.4 shows some of the specifications relevant to accelerometers used in this study and Figure 3.12 shows the sensor mounting locations on the vehicle.

Parameter	Uniaxial	Triaxial
Sensitivity(100Hz and 10 **g**)	0.30 mV/**g**	0.30 mV/**g**
Range	1000 **g**	2000 **g**
Excitation voltage	2 to 10 V	2 to 10 V
Frequency Response	20 to 1500 Hz	20 to 1500 Hz
Number of units	4	3

Table 3.4: Uniaxial and triaxial accelerometer specifications.

The 3D accelerometers were critical to measure the vehicle pitching as well as bending angles caused by anticipated material failures; the accelerometers were mounted on a single line, one accelerometer in the vehicle CG, one before weld zone and one in the rear of the vehicle. This allows to measure both the pitching and the bending angles. The distance between the 3D accelerometers and their mounting is defined in Table 3.5.

The mounting locations are measured accurately to support in the test and FE model correlation process along with determining the vehicle pitching and bending due to the material failures around the weld.

The 1D accelerometers were mounted on vehicle parts which were identified from simulations to ensure the parts were not expected to undergo deformation in the test; rigid mounting locations would provide reliable data from the test. The eigen frequencies of each of these mounting locations was calculated and has been presented in Paper G. The mounting locations for all the 7 accelerometers along with the description of the process to determine the CG of the vehicle is presented in Paper G. The planned test speed was 56 kmph with a deviation of $+/-3$ kmph; the speed of the vehicle was measured with an encoder based speed sensor developed for the test and a GPS speed sensor installed in the DAS. Besides these, three high speed cameras (640 fps) along with a hand held camera following the vehicle were used to capture the test videos; these videos support in the correlation phase for FEM to

Accelerometer Type	Mounting	Measurement
Triaxial - 1	Vehicle Center of Gravity (CG)	Vehicle CG on a steel bracket designed for the purpose
Triaxial - 2	In front of the vehicle CG	Mounted on a steel bracket 254 mm in front of the vehicle CG and before the welded zone to capture the accelerations
Triaxial - 3	Rear of the vehicle CG	Mounted on a steel bracket- rear of the vehicle 1812 mm from the vehicle CG

Table 3.5: Accelerometer mounting locations.

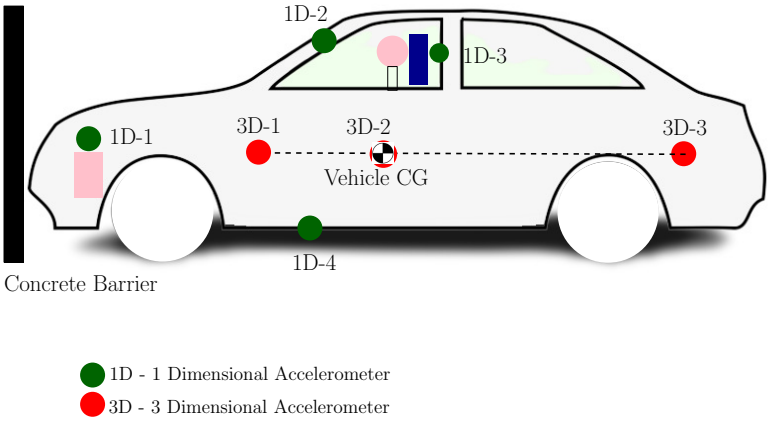

Figure 3.12: Mounting positions of the accelerometers on the test vehicle

investigate the behaviour of the test vehicle. To initiate a signal during the impact, a contact type trigger was mounted on the car front (outside of the car) to initiate a signal to the DAS. Two test dummies representing the anthropometry of a 50^{th} percentile male human were also used during the test, however these dummies are not instrumented to capture the head and neck deflections during the impact.

3.3.4 Results from the Full Scale Crash Test

The test vehicle before and after impact is presented in Figure 3.13 (side view), Figure 3.14 (front view).

The values of deformation for the front end were calculated from the accelerometer placed at the CG and filtered using a filter Channel Frequency Class (CFC)-60 (100 Hz limiting frequency) [57]. The front-end deformation was measured after the test at six points on the front end and the maximum value of deformation was determined based on the initial and final length of the vehicle, the maximum deformation was measured as 637 mm with a margin of error of 1%. The three 3D accelerometers also supported calculation of the vehicle pitching angle which was measured as a maximum of 6.58 degrees. The motion of the vehicle in the vertical axis (z axis in this

Figure 3.13: Test vehicle in side view pre and post impact.

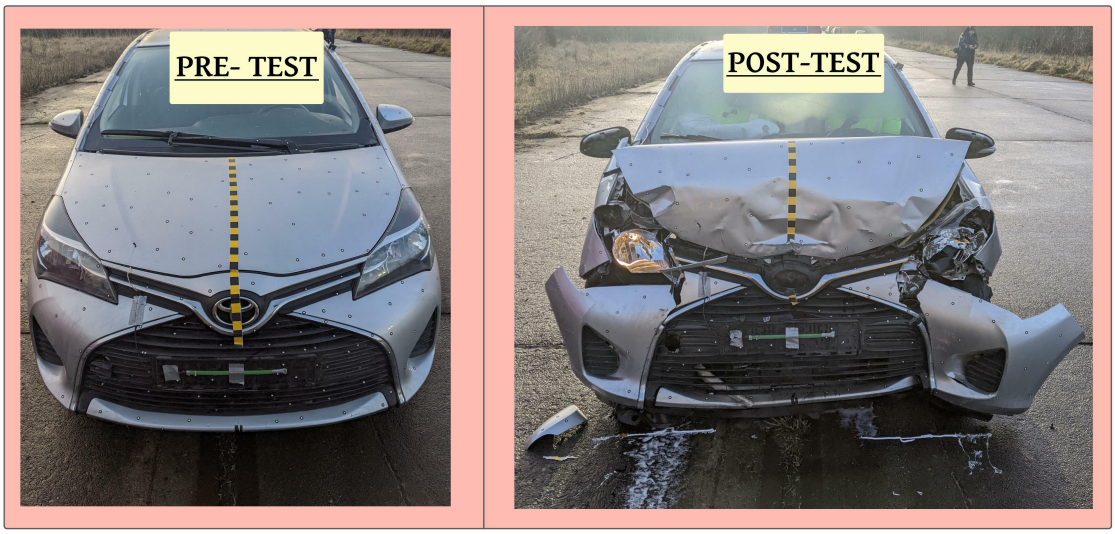

Figure 3.14: Test vehicle in front view pre and post impact.

case) was measured from the accelerometer at the vehicle CG and the accelerometer at the front; the difference between the maximum z co-ordinates was calculated and used to find the angle of rotation (pitching).

The bending angle was measured similarly using the accelerometer data from the vehicle CG and the rear of the vehicle; the maximum value measured is 0.62 degree. The data from the accelerometer presented in Paper G is validated against FEM developed for the baseline model and indicates higher acceleration at the vehicle CG. The test data curves are plotted with a filter CFC-180 (300 Hz limiting frequency) to determine the maximum values of acceleration; CFC-60 is used as a filter for test correlation and reporting the results.

Figure 3.15: Physical Test vs FE comparison for full scale test in side view..

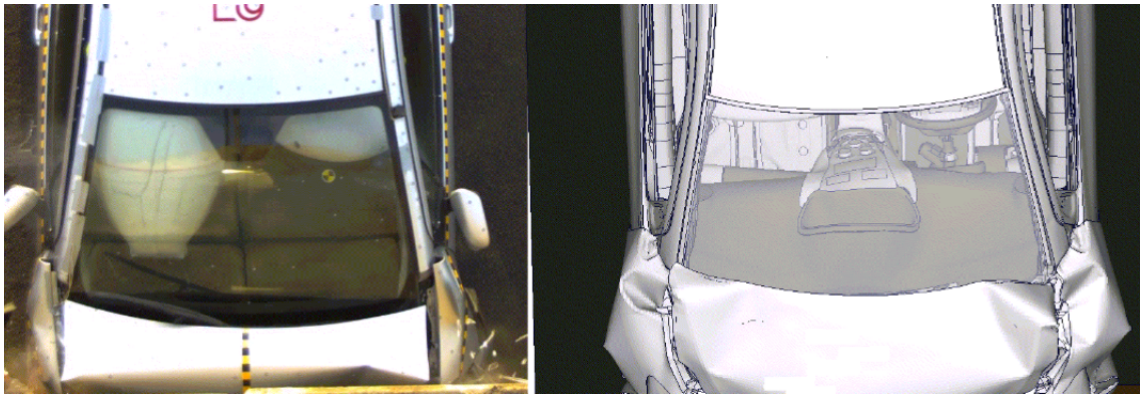

Figure 3.16: Physical Test vs FE comparison for full scale test in top view

3.3.5 Correlation of Full Scale Tests with FE model

The FE methodology defined in Paper E was adopted to model welds in a 2010 Toyota Yaris FE model. The open source FE model was adopted from the NHTSA crash test database and the model was updated to replicate a 2015 Toyota Yaris vehicle with relevant changes to the vehicle geometry and dimensions [43]. This updated FE model was used to correlate with the full vehicle crash test experimental setup . The addition of welds on the A-Pillar and rocker were consistent with the physical test to represent a modified vehicle. The UHSS parts used the material data from the coupon tests (tensile tests) for the welded and heat-treated zones along with the un-modified structural parts. This correlated FE model is used for the validation of the LPM of a modified vehicle described in the next section; the LPM defines the kinematic behaviour of the modified vehicle. Figure 3.15 and 3.16 represents the correlation with simulation in side and top view respectively;

Based on the FE model, the maximum deformation measured in the vehicle is 680 mm and the maximum pitching angle is 3.51 degrees. The maximum bending angle measured from the FE simulation is 1.2 degrees (FE curves presented in Figure 3.17). The acceleration from the 3 triaxial accelerometers is critical to correlate with the FE model because the displacement values at these locations support in the

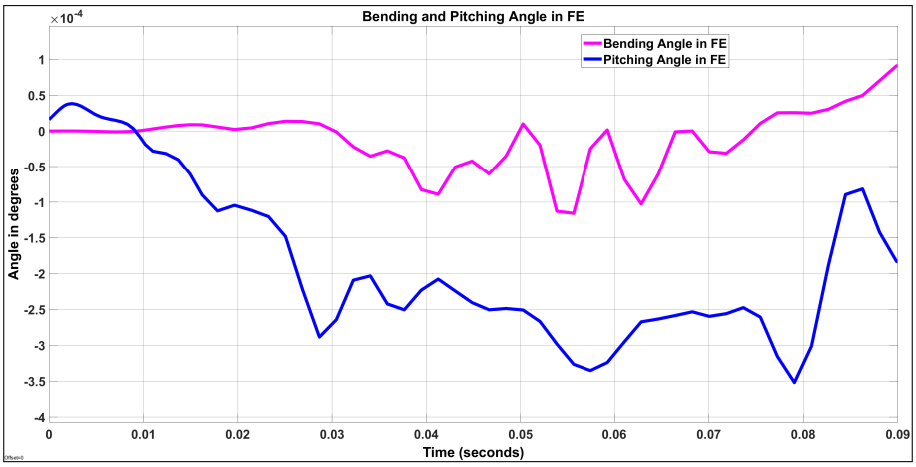

Figure 3.17: Pitching angle and bending angle from correlated FE model

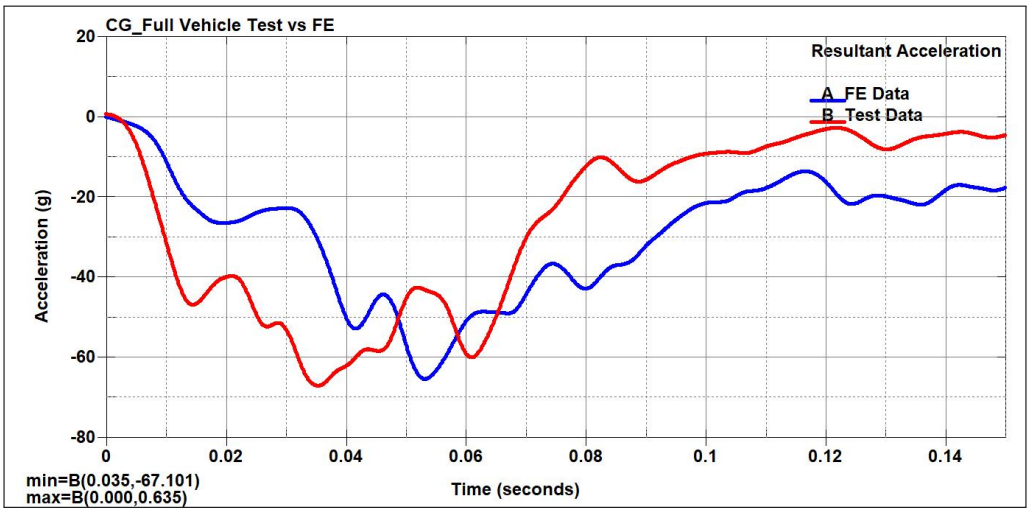

Figure 3.18: Comparison of FE vs Test curves - triaxial accelerometer placed at the CG nodes

calculation of pitching of the modified vehicle. Figures 3.18 and 3.19 present the correlation curves for the sensors mounted on the front and the vehicle CG. The curves show a deviation in the correlation; this can be attributed to the mounting brackets for the accelerometers which has been ignored in the FE model. Figure 3.20 presents the curve comparison for accelerometer placed at the rear of the vehicle. The accelerometers were mounted on the x, y, z coordinates same as the physical test; in the absence of mounting brackets nodal coordinates of these positions were used to determine the accelerometer curves. The maximum acceleration is close to the test values along with the curve trend; however the correlation can be improved with modeling the steel brackets in the FE model. The determination of test results for 1D accelerometers do not contribute to the development of the LPM defined in this thesis; these results are presented in detail in Paper G and would serve as valuable data for further research in this area.

Figure 3.21 shows the test velocity curves overlayed with the FE simulation data;

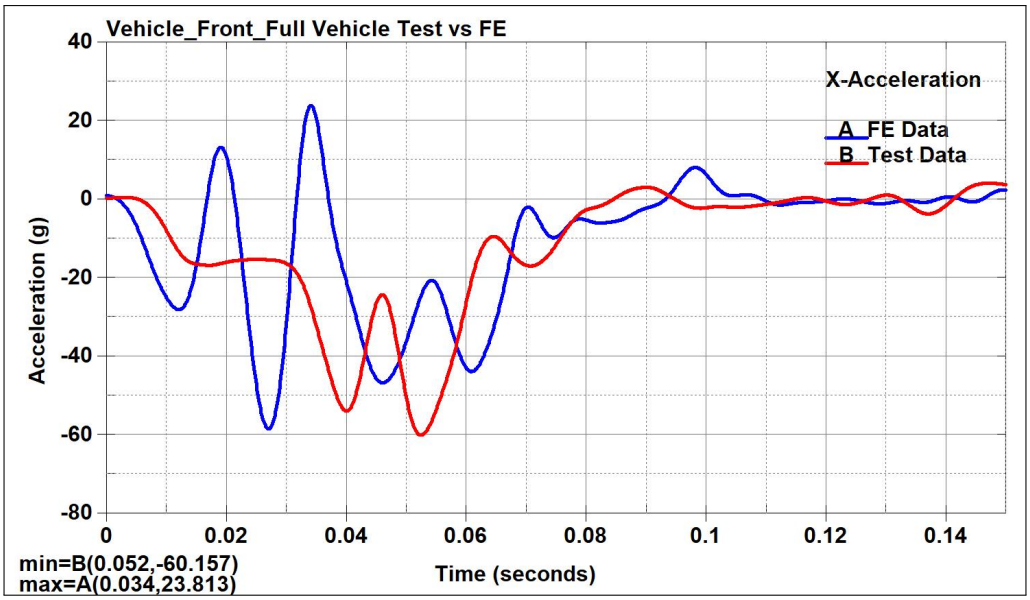

Figure 3.19: Comparison of FE vs Test curves - triaxial accelerometer placed before the welds using nodal coordinates

there is good correlation in terms of the curve trend and the time when the velocity of the vehicle becomes zero is closely predicted by the FE simulation.

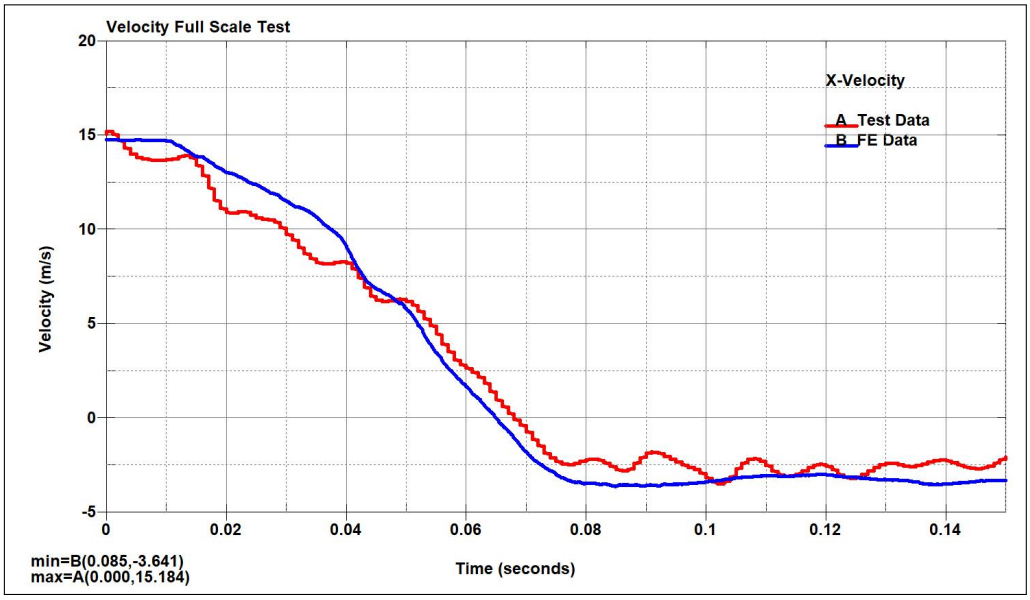

Figure 3.21: Comparison of FE vs Test curves - Velocity (using nodal coordinates)

The full scale physical test was conducted to determine vehicle parameters like the deformation of the vehicle, pitching angle, bending angle, acceleration at the vehicle CG and the test velocity. An FE model of a modified Toyota Yaris model replicating the test scenario was presented; the correlation of these simulations with the physical test data was also conducted. The test velocity and the acceleration

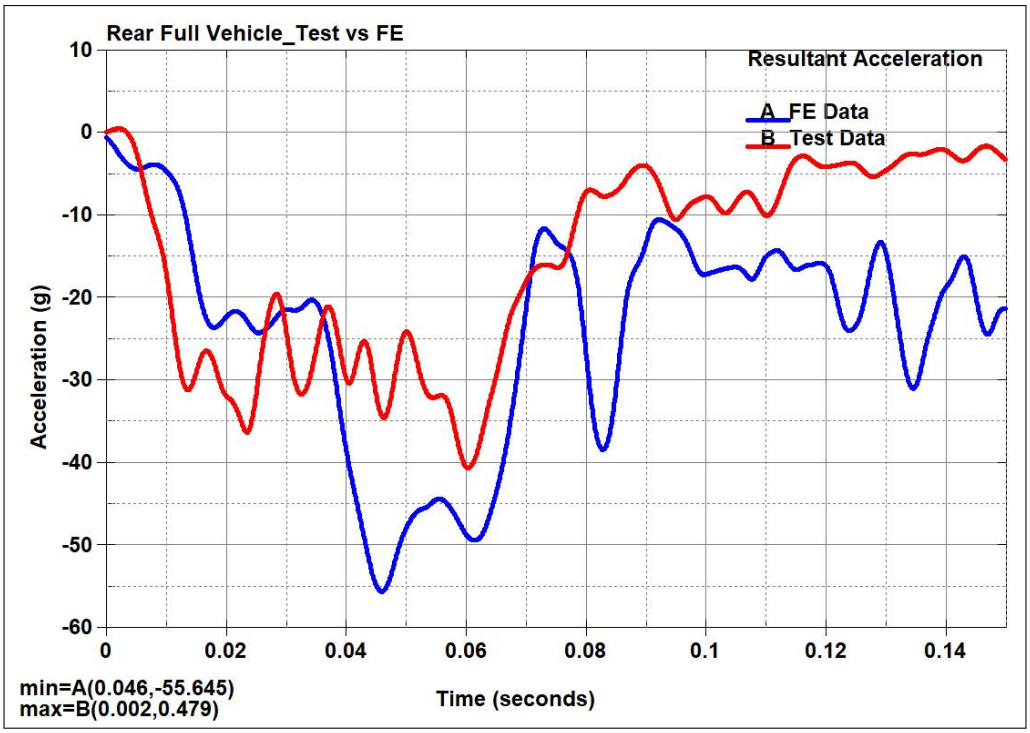

Figure 3.20: Comparison of FE vs Test curves - triaxial accelerometer placed at the rear of the vehicle-using nodal coordinates

plots at different 3D accelerometer mounting locations was overlayed for the FE simulations against the full scale test. These indicate satisfactory correlation between the test and FE values thereby increasing the confidence on the FE model. It was concluded that this FE model can be used for generating vehicle parameters as input to the LPM of a modified vehicle along with being used as validation for the LPM.

The full scale test included data from several 1D accelerometers and other sensors; however due to time constraints post-processing of all other test data has been kept out of the scope of this thesis and will be evaluated in future research.

3.4 LPM V3 - Double Pendulum Model

Figure 3.22 shows the two WP outlined in this thesis working in parallel to define the mathematical models described in the previous chapters leading to the LPM in WP-3.

The baseline model explained in the previous chapter laid the ground to extend the LPM V2 with material failure in UHSS steels; the material properties and the experimental results have been detailed in the previous section. The coupon tests and the full scale test defined above was used to generate a correlated FE model of a modified vehicle (with unprofessional repairs); this FE model was used to validate LPM V3. As welding in the structural members could lead to failure; it is anticipated

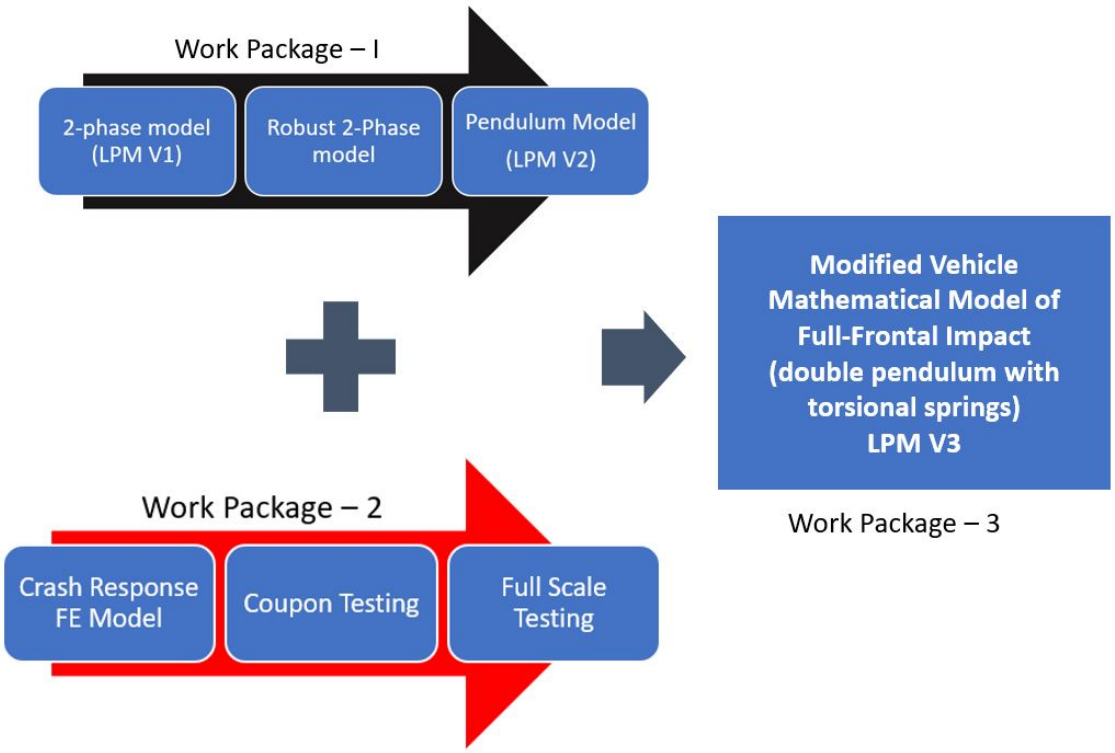

Figure 3.22: Flowchart of research

that the members could fail in a crash leading to a small bending angle. This bending angle could cause higher intrusions in the passenger compartment in the vehicle; to recreate the kinematic behavior of this modified vehicle under an impact the proposed LPM has been presented. LPM V3 replicates the effect of structural failures due to Heat Affected Zone (HAZ) and welds during a full frontal impact. To simulate the welded zone, two mass components have been used; one represents the compartment before the welded zone while the other indicates the compartment after it. Welds are represented in the model as a torsional spring that allows the body to rotate about the joint at a small angle as shown in Figure 3.23; this spring captures the bending of the vehicle due to material failures during a crash. The pendulum model defined in Subsection 2.5.2 was updated to include a dimensionless torsional spring and representing the modified vehicle as a double pendulum; the small bending angle contributing to the pitching due to the weld failure is explained by the motion of the double pendulum. The model works with similar assumptions as in Subsection 2.5.1 and 2.5.2. Figure 3.24 shows the LPM V3 with a front-end spring damper system; suspension springs acting as constraints for the double pendulum. The elastic double pendulum swings about the point of impact with pitching angle represented as θ_1 and the bending angle is represented as θ_2 as presented in Figure 3.25

The front-end spring damper system is predicted using the same optimization algorithm presented in Subsection 2.5.1 with the governing equations defined by

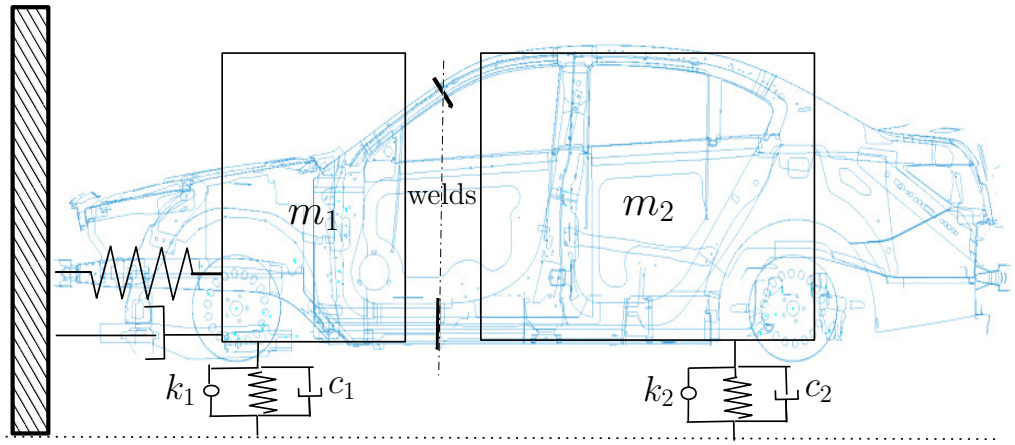

Figure 3.23: Representation of welds on A-Pillar and Rocker with lumped masses and constraints

Lagrangian formulation in polar coordinates (Paper G). The governing equations of motion derived using Lagrangian formulation are:

$$\begin{aligned} Q_r^{ext} =& m_1\ddot{r} + m_2\ddot{r} - m_2 l_1(\ddot{\theta_1}\theta_1 + 2\dot{\theta_1}) \\ & - m_2 l_2(\ddot{\theta_2}\theta_2 + 2\dot{\theta_2}) - m_1(l_0 + r)\dot{\theta_1}^2 \\ & + m_2(l_0 + r)\dot{\theta_1}^2 + m_2 l_1\dot{\theta_1}^2\theta_1^2 + m_2 l_2\dot{\theta_1}\dot{\theta_2}\theta_1\theta_2 \\ & + m_1 g\theta_1 + m_2 g\theta_2 + k_1(l_0 + r - l_3)\theta_1^2 \\ & + k_2[(l_0 + r + l_1)\theta_1^2 + l_2\theta_1\theta_2] + k_{comp}r, \end{aligned} \tag{3.1}$$

$$\begin{aligned} Q_{\theta_1}^{ext} =& m_1(l_0 + r)^2\ddot{\theta_1} + 2m_1(l_0 + r)\dot{r}\dot{\theta_1} \\ & + 2m_2(l_0 + r)\dot{r}\dot{\theta_1} + m_2 l_1^2\ddot{\theta_1} - m_2 l_1\dot{\theta_1}\dot{r} \\ & - m_2 l_1\dot{\theta_1}\ddot{r} + 2m_2 l_1[\dot{r}\dot{\theta_1}\theta_1^2 + (l_0 + r)\theta_1^2\ddot{\theta_1}] \\ & + 2(l_0 + r)l_1\dot{\theta_1}^2\theta_1 + m_2 l_1 l_2[\ddot{\theta_2}\ddot{\theta_1}\theta_2 + \dot{\theta_2}\dot{\theta_1}\theta_2] \\ & + m_2 l_2[\dot{r}\dot{\theta_2}\theta_1\theta_2 + (l_0 + r)\ddot{\theta_2}\theta_1\theta_2 \\ & + (l_0 + r)\dot{\theta_2}\dot{\theta_1}\theta_2] + m_2\dot{r}\dot{\theta_1}l_1 - 2m_2(l_0 + r)l_2\dot{\theta_1}^2\theta_1 \\ & - m_2 l_1 l_2\dot{\theta_2}\theta_1\theta_2 + m_2 l_2(l_0 + r)\dot{\theta_2}\theta_1\theta_2 \\ & + m_1 g(l_0 + r) + m_2 g[(l_0 + r) + l_1] \\ & - k_1[l_0 + r - l_3]^2\theta_1 - k_2[l_0 + r + l_1]^2\theta_1 \\ & - k_2[l_0 + r + l_1]l_2\theta_2, \end{aligned} \tag{3.2}$$

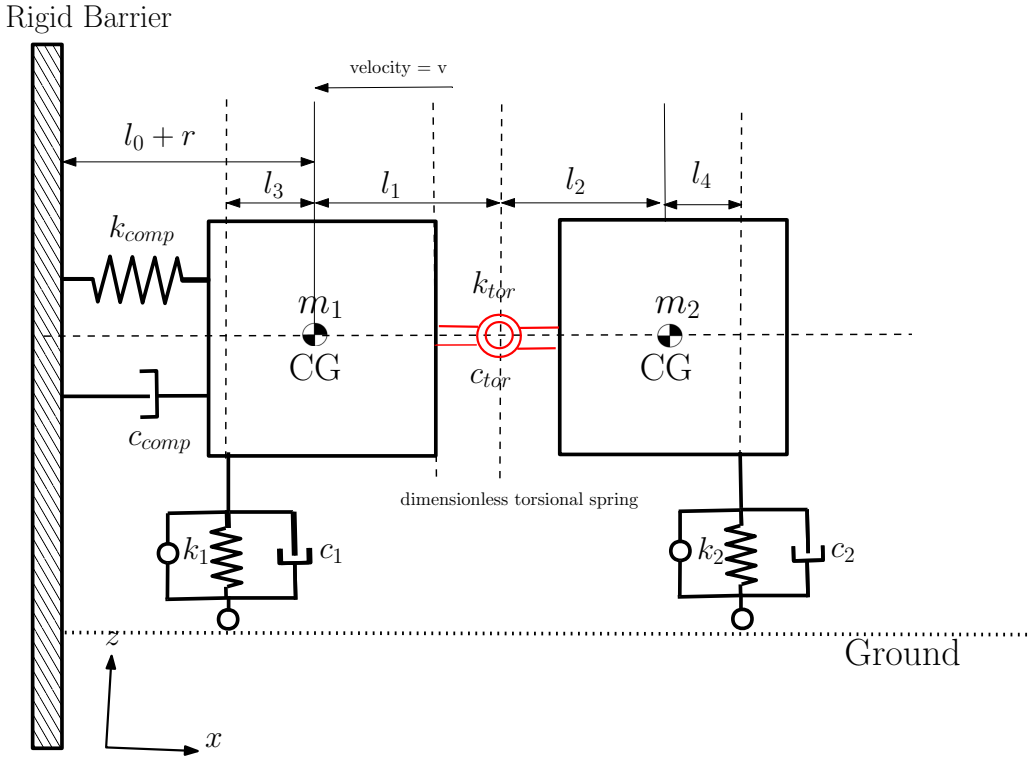

Figure 3.24: LPM V3 presented with a dimensionless torsional spring and 2 mass components impacting a rigid barrier

$$\begin{aligned} Q_{\theta_2}^{ext} =& m_2 l_2^2 \ddot{\theta}_2 + m_2 l_1 l_2 [\ddot{\theta}_1 \theta_1 \theta_2 + \dot{\theta_1}^2 \theta_2 + \dot{\theta}_1 \theta_1 \dot{\theta}_2] \\ & - m_2 l_2 [\dot{r}\dot{\theta}_1 \theta_1 \theta_2 + (l_0 + r)\ddot{\theta}_1 \theta_1 \theta_2 + (l_0 + r)\dot{\theta_1}^2 \theta_2] \\ & - m_2 l_1 l_2 \dot{\theta}_1 \dot{\theta}_2 \theta_1 + m_2 \dot{r}\dot{\theta}_2 l_2 - m_2 l_2 (l_0 + r)\dot{\theta}_1 \dot{\theta}_2 \theta_1 \\ & + m_2 g l_2 + k_2 [(l_0 + r + l_1) l_2 \theta_1 + l_2^2 \theta_2] \\ & + k_{tor} \theta_2 \end{aligned} \tag{3.3}$$

where Q_r^{ext}, $Q_{\theta_2}^{ext}$ and $Q_{\theta_2}^{ext}$ are the external forces acting on the vehicle. The non-conservative forces in the system are included in the Lagrange's equation of motion in the form of generalized forces expressed with the formulation of virtual work δU [51] as defined in Chapter 2, Equation 2.17. The external forces included in this LPM are barrier forces, damper forces including front end spring damper system and suspension damper system forces. The corresponding equations are:

$$Q_r^{ext} = Q_r^{bar} + Q_r^{damp}, \tag{3.4}$$

$$Q_{\theta_1}^{ext} = Q_{\theta_1}^{bar} + Q_{\theta_1}^{damp}, \tag{3.5}$$

$$Q_{\theta_2}^{ext} = Q_{\theta_2}^{bar} + Q_{\theta_2}^{damp}. \tag{3.6}$$

The expressions for barrier and damper forces have been detailed in Paper H.

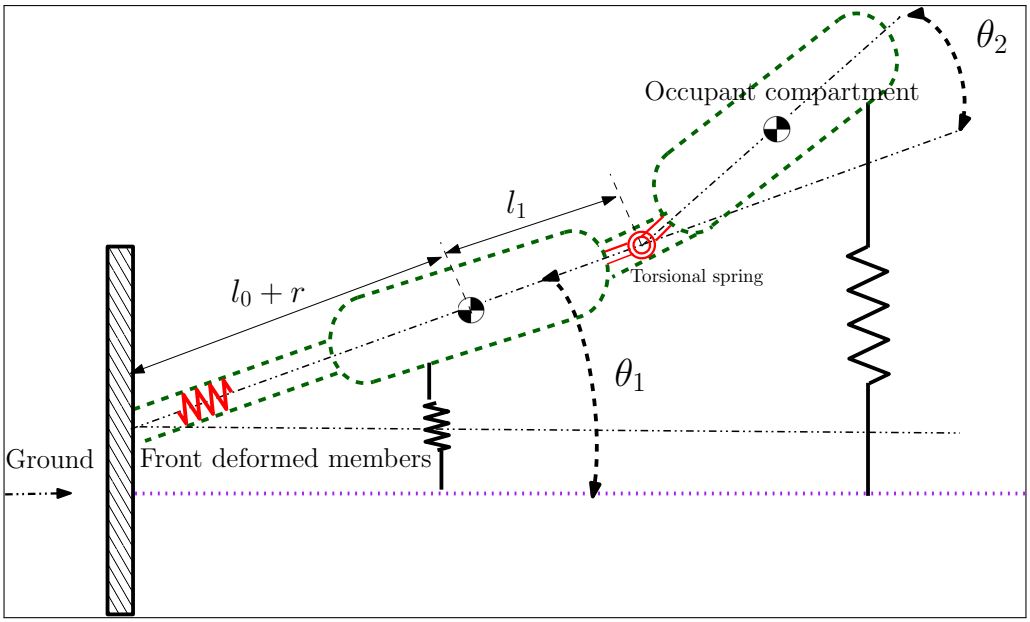

Figure 3.25: Vehicle body rotating about the impact point after front-end deformation like a double compound pendulum.

The Simulink model developed in Paper G is validated against an FE model representing welds on UHSS structural members presented in Subsection 3.3.5. The values of pitching angle (θ_1) and bending angle (θ_2) derived from FEM is compared to the LPM and presented in Figure 3.26 and Figure 3.27. An FE model of a modified 2010 Toyota Yaris was updated with welds and a HAZ was defined in the A-Pillar and rocker sections to replicate the LPM. The pitching angle curve does not follow the trend of the FE curve, however the peak value in the FE model is captured by the LPM. The LPM bending angle (θ_2) shown in Figure 3.27 in the blue curve is capable of capturing the maximum bending angle but it is clear from the curve overlay that the model needs changes to improve the LPM prediction. These deviations in the

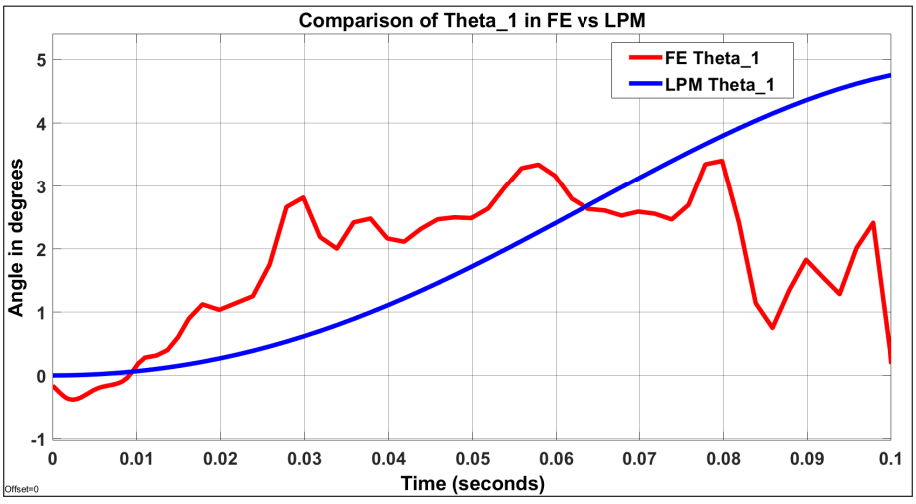

Figure 3.26: Pitching Angle θ_1 curve comparison for LPM V3 vs FE model

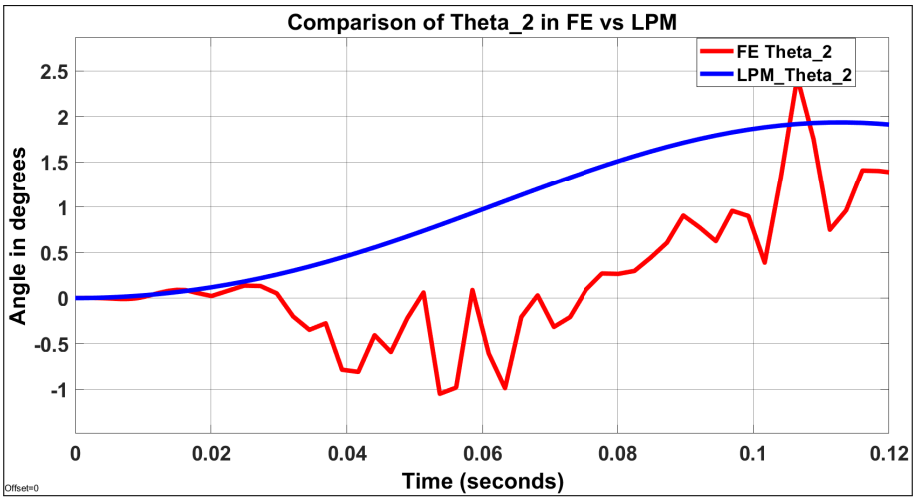

Figure 3.27: Bending Angle θ_2 curve comparison for LPM V3 vs FE model

LPM model from the FE simulations can be attributed to the assumptions made during the model development process along with several limitations to this model. These have been discussed and presented in Paper H. Incorporating these changes to the model is however out of the scope of this project and would be covered in future research.

3.5 Summary

FE simulations on the Honda Accord model investigated the crash response of modified vehicles with UHSS structural members. The different crash scenarios simulated in the study E with the welded A-Pillar highlighted the fact that the welding representation in the study was capable of determining the behaviour of the modified vehicle; also showing the reduced crashworthiness performance of the vehicle in few regulatory loadcases. This work laid the foundation for a need to generate physical test data to correlate FE models replicating the non-linear impact mechanics.

The welded and heat treated coupon test samples were observed to have reduced yield strength and ultimate strength indicating a likelihood of reduced safety in crashes for the unprofessionally repaired vehicles. The study provides data for a constitutive model to replicate the material behaviour in a simulation. It also highlights challenges in regards to sample preparation from vehicle structures; there may be internal stresses from manufacturing processes the part have undergone. The size of all samples was also a challenge during this project which can be addressed in future research. The study is also restricted to tensile testing; compressive testing along with conducting investigation of the microstructural changes due to welding and heat treatment would be a possible next study on the material characterization

aspect of this thesis.

In the absence of real-time data for modified vehicles, the full scale crash test was conducted to correlate the FE model of the modified vehicle. The full scale test helped to assess vehicle crashworthiness for the vehicle, data from the test was used to correlate an FE model replicating the physical test. This test also helped generate a database for future research in this area. The pendulum model LPM V2 was extended to incorporate the weld failures with a torsional spring to replicate the impact kinematics in LPM V3. The model representing the vehicle was defined as an elastic double compound pendulum with a torsional spring and validated with FE data. The LPM predicts the small bending angle anticipated to occur due to material failures in welded UHSS samples; the correlation between the LPM and the validation data indicates need for a an extended study to improve the prediction.

Chapter 4

Concluding Remarks and Next Steps

We are at the very beginning of time for the human race. It is not unreasonable that we grapple with problems. But there are tens of thousands of years in the future. Our responsibility is to do what we can, learn what we can, improve the solutions, and pass them on. - Richard Feynman

4.1 Conclusions

Vehicle accident prediction has evolved over the years from complete dependence on full scale crash testing to virtual models replicating the impact kinematics. The numerical simulations have in turn progressed with the emergence of strong computational power allowing researchers to capture geometry of every part of the vehicle. However, these simulation approaches are limited by their need to model the system accurately sometimes taking months of manual labour in capturing the system behaviour. The access to some of these computationally intensive techniques and softwares are also a hindrance to their application in academia bringing a gap between the industry and the academic community. Besides, one of the challenges to mathematical modeling of vehicle crash assessment lies in capturing the impact mechanics (front-end deformation and pitching) to ensure safety of occupants and road users. This research is focused on addressing these challenges to improve modeling for vehicle crashworthiness assessment.

The advantages and limitations to using LPM for modeling vehicle crash impacts was presented during the literature review; this methodology is inexpensive and less computationally intensive along with the capabilities to represent the impact kinematics making it attractive to researchers and academia. Hence, LPM was used to develop a baseline and modified vehicle crash impact model replicating a full frontal impact; all models were validated against FEM simulations.

There were three research objectives outlined in this thesis; the LPM representation of a baseline vehicle under full vehicle impact and consecutive crashworthiness assessment of the model was the first objective. Existing LPMs have focused on estimating the front-end deformation ignoring the second phase of the crash event (pitching); capturing the maximum pitching angle for vehicle crash assessment for a baseline vehicle has been emphasized in the research in this thesis. The proposed LPM for representing a baseline full frontal vehicle crash event using a 2-Phase and 2-Phase robust model was discussed to conduct the crashworthiness assessment. This model showed promising prediction for the front-end deformation; the second phase of pitching needed improvements. This conclusion underpinned the proposal of a simple pendulum model defining the impact kinematics appropriately; both phases of impact: front-end deformation along with vehicle pitching forward were modeled to achieve close correlation with FE simulations used for validation. The Lagrangian formulation used for developing these LPM models also helped to reduce the model complexity. The baseline LPM representation of a vehicle provides an estimate of the maximum deformation and pitching angles to the user along with being an open source model. It is critical to mention that these models require few vehicle parameters like length of the vehicle, mass, stiffness and damping coefficients etc. to estimate the crashworthiness performance which is one of the contributions of the work. One of the possible applications in the industry and academia for the proposed LPMs is early in the vehicle development process to determine the crashworthiness parameters while also being used in the accident reconstruction phase. This methodology (presented in Papers B - D) concluded the first research objective; improved modeling for vehicle crash assessment was achieved with LPM technique.

Based on the literature review, there was lack of physical test results and open source FE models for a modified vehicle. The research objective around the crashworthiness assessment of modified vehicles (unprofessional repairs on UHSS structural members) in a full frontal crash was addressed with WP-2. Two FE models (Honda Accord and Toyota Yaris) representing welds on a modified vehicle with beam elements were used to investigate the behavior of modified vehicles in a crash event. The results showed that the crashworthiness performance deteriorated with welding and heat treatment of UHSS members; however the change in performance is also dependent on the type of impact; as outlined in Paper E of this thesis. The FE model was updated with material data from tensile tests on welded and heat treated coupon samples and correlated against full scale crash test data. The coupon tests confirm that the material becomes weaker after welding and heat treatment while the physical tests support the correlation for the Toyota Yaris FE model. This open source FE model of a modified vehicle can be used for future research in this area.

The third research objective focuses on capturing the impact kinematics in a full frontal impact of a modified vehicle with an LPM. It was identified that welding and heat treatment of UHSS members leads to weaker sections in the structural members; this could lead to a bending angle due to material failures in a crash event. Representing the bending angle due to material failures and capturing this kinematic behavior of a modified vehicle was achieved with an LPM V3 proposed in this thesis. A double pendulum based LPM presented in Subsection 3.4 was proposed to predict the pitching along with a small angle θ_2 resulting from bending in the vehicle structure due to material failures. This novel methodology using a torsional spring in the LPM shows good correlation in estimating the vehicle parameters like maximum deformation and pitching; the bending angle prediction is promising but needs more work in this area. The vehicle parameter data required for this model was generated from the correlated FE model of a Toyota Yaris developed in WP-2. The bending angle values are not reliable but this model is a good starting point for explaining the impact kinematics in a modified vehicle.

The next section brings out the limitations associated with the project and the next steps for this work.

4.2 Limitations and Future Work

- The thesis is aimed at developing LPM to represent a vehicle crash event for a baseline and modified vehicle. One of the key limitations to these methods is the exclusion of geometrical features of the system; only considering the time domain in the system. There are however, few parameters included in the system like vehicle length; mass of the vehicle at CG etc.

- The models defined in the thesis represent a full frontal crash (0% offset), the methodology can be translated to other impact scenarios to develop prediction models; however the validation for other impact scenarios would require test data from physical tests/simulations.

- The validation of the LPMs developed in this thesis is conducted with FE simulations due to lack of physical test data for different test scenarios. The front-end spring damper system is assumed to be piecewise-linear to represent the model non-linearities.

- The thesis also outlines a methodology to model weld failure in an LPM; however the model has some limitations in terms of its prediction. Subsection 3.4 outlines the system and also discusses that the relative rotation of the

vehicle (angle θ_2); however the model can be improved to correlate with the test data; this is further discussed in future outlook for the work.

- The full scale crash test conducted as part of this thesis has been used to understand the behaviour of the modified vehicle under impact; however post-processing of all generated data from this test has been avoided due to time constraints. Nonetheless this data is valuable to the research community and the next steps in the project outlines the plans to use this test data for future projects.

In spite of these limitations; the thesis provides a framework to improve vehicle crashworthiness assessment methods along with a general understanding of impact mechanics using LPM and FEM; the alternative modeling strategy explored presents inexpensive and accessible options to the research community thereby reducing dependence on complex softwares. One of the key contributions to the research being the prediction of vehicle rotations about the point of impact; the project also includes the methodology to represent material failures in an LPM which addresses one of the limitations to the use of LPMs in vehicle crashworthiness assessment. Aspects that should be taken into consideration in future research are summarized as follows:

- During this project a modeling strategy inspired by a single and double pendulum model has been adopted to represent the system. The LPM V3 defined in this project; to my knowledge is one of the first models developed to represent a modified vehicle undergoing impact. In Paper E we developed FE models for a modified vehicle and it was observed that an offset impact would be one of the worst case scenarios for this vehicle. It would be interesting to translate the methodology to an offset impact and consider vehicle rotations in 3 dimensions and improve the system representation. The novel use of torsional springs to define the bending behaviour of the vehicle in LPM V3 gave a direction to this work; however the model prediction could be improved with defining non-linear spring and damper coefficients.

- This thesis also adopts Lagrangian mechanics as a method to develop the equations of motion; however with higher dimensions and more DoF it would be interesting to use Kane's method to compare the system behaviour. This could possibly improve the LPM prediction of bending angle in LPM V3. Kane uses vector cross products and dot products. Generalized speed, partial velocity, partial angular velocity, generalized active forces, and generalized inertial forces are introduced in this method; angular velocity and angular acceleration of rigid bodies is determined to generate the kinematic equations [58].

- The crash test conducted as part of this research has been used to partially answer one of the research questions and develop the LPM described in this thesis. Nevertheless, the data generated from the different sensors and instrumentation mounted on the test vehicle would be used for future research on assessing vehicle crashworthiness on welded UHSS steel structural members. The welded samples from the car can be investigated further for micro-structural changes in the material. The vehicle was also scanned to generate pre and post test deformation plots which can be further used to improve FE model correlations.

- Machine Learning (ML) is a growing field and has gained impetus in the last decade in most research areas; this technique has also found applications in predicting vehicle crash severity and crashworthiness performance evaluations. The data generated from FE models and physical tests conducted during this research is a valuable database to develop improved prediction models. The front-end deformation estimation for the LPMs uses an optimization algorithm which can be improved with ML models.

- Modeling of occupants with LPM in vehicle impact has been kept out of scope for this thesis. This being an interesting area to model the anthropometry of the human and replicate the kinematics of a human in simple models is potential next steps on the work.

We can only see a short distance ahead, but we can see plenty there that needs to be done - Alan Turing

Bibliography

[1] Mustafa Elkady, Ahmed Elmarakbi, and John MacIntyre. The influence of a vehicle dynamics control system on the occupant's dynamic response during a vehicle collision. *Proceedings of the Institution of Mechanical Engineers, Part D: Journal of automobile engineering*, 226(11):1454–1471, 2012.

[2] World Health Organization. GLOBAL STATUS REPORT ON ROAD SAFETY 2018 SUMMARY. Technical report, 2018.

[3] Paul Du Bois, Clifford C Chou, Bahig B Fileta, Tawfik B Khalil, Albert I King, Hikmat F Mahmood, Harold J Mertz, Jac Wismans, Priya Prasad, and Jamel E Belwafa. *Vehicle crashworthiness and occupant protection*. Citeseer, 2004.

[4] Qin Liu. *Modelling, distributed identification and control of spatially-distributed systems with application to an actuated beam*. Doctoral thesis, Technische Universität Hamburg, 2015.

[5] Alexander Hrennikov. Solution of Problems in Elasticity by the Framework Method. *Journal of Applied Mechanics*, 8:169–175, 1941.

[6] Richard Courant. Variational method for the solution of problems of equilibrium and vibrations. *Bulletin of American Mathematical Society*, 49:1–23, 1943.

[7] Ray W Clough. The Finite Element Method in Plane Stress Analysis. *Proceedings 2nd ASCE Conference On Electronic Computation*, 1960.

[8] Curd-Sigmund Böttcher, Steffen Frik, and Bernd Gosolits. 20 years of crash simulation at Opel-experiences for future challenges. *Bamberg (Germany): LS-Dyna Anwenderforum*, 2005.

[9] Steven W Kirkpatrick, Robert MacNeill, and Robert T Bocchieri. Development of an LS-DYNA occupant model for use in crash analyses of roadside safety features. In *Transportation Research Board 82nd Annual Meeting, Washington, DC, Jan*, pages 12–16, 2003.

[10] Yunzhu Meng, Wansoo Pak, Berkan Guleyupoglu, Bharath Koya, F Scott Gayzik, and Costin D Untaroiu. A finite element model of a six-year-old child for simulating pedestrian accidents. *Accident Analysis & Prevention*, 98:206–213, 2017.

[11] Ferhat Ozcan and Sezgin Ersoy. Analysis of the vehicle: applying finite element method of 3D data. *Mathematical Models in Engineering*, 7(4):63–69, 12 2021. ISSN 2351-5279. doi: 10.21595/MME.2021.22328.

[12] Yadong Zhang, Jiuqiang Wang, and Chenbin Ma. Research on Reconstruction of Frontal Collision Accidents of Two Cars Based on the Combination of PC-crash and Finite Element Method. 2021(7), 2021. ISSN 0010-8189.

[13] Sergei Evtiukov, Egor Golov, and Grigory Ginzburg. Finite element method for reconstruction of road traffic accidents. *Transportation Research Procedia*, 36: 157–165, 2018. ISSN 23521465. doi: 10.1016/J.TRPRO.2018.12.058.

[14] Shusuke Numata, Koji Mizuno, Daisuke Ito, Dai Okumura, and Hisashi Kinoshita. Validation of crush energy calculation methods for use in accident reconstructions by finite element analysis. *SAE International journal of transportation safety*, 6(2):133–146, 2018.

[15] Mounir M Kamal. Analysis and simulation of vehicle to barrier impact. *SAE Transactions*, pages 1498–1503, 1970.

[16] D J Benson and J O Hallquist. The Application of DYNA3D in Large Scale Crashworthiness Calculations, Lawrence Livermore National Laboratory. *Report No. UCRL*, 94028, 1986.

[17] Wichai Cheva, Tsuyoshi Yasuki, Vikas Gupta, and Kolita Mendis. Vehicle development for frontal/offset crash using lumped parameter modeling. Technical report, SAE Technical Paper, 1996.

[18] Mustafa Elkady, Ahmed Elmarakbi, and John MacIntyre. Enhancement of vehicle safety and improving vehicle yaw behaviour due to offset collisions using vehicle dynamics. *International journal of vehicle safety*, 6(2):110–133, 2012.

[19] Ahmed Elmarakbi, Mustafa Elkady, and John MacIntyre. Numerical analysis of vehicle-to-vehicle impact using vehicle dynamics control systems for collision mitigation. *International Journal of Dynamics and Control*, 1(2):172–191, 2013.

[20] Stuart G Mentzer, Randa A Radwan, and William T Hollowell. The SISAME methodology for extraction of optimal lumped parameter structural crash models. Technical report, SAE Technical Paper, 1992.

[21] Bernard B Mnyazikwiye, Hamid R Karimi, and Kjell Gunnar Robbersmyr. Mathematical modeling of vehicle frontal crash by a double spring-mass-damper model. In *2013 XXIV International Conference on Information, Communication and Automation Technologies (ICAT)*, pages 1–6, 2013.

[22] Bernard B. Munyazikwiye, Hamid Reza Karimi, and Kjell Gunnar Robbersmyr. Mathematical modeling and parameters estimation of car crash using eigensystem realization algorithm and curve-fitting approaches. *Mathematical Problems in Engineering*, 2013, 2013. ISSN 1024123X. doi: 10.1155/2013/262196.

[23] Dario Vangi, Filippo Begani, Michelangelo Santo Gulino, and Florian Spitzhüttl. A vehicle model for crash stage simulation. *IFAC-PapersOnLine*, 51(2):837–842, 1 2018. ISSN 2405-8963. doi: 10.1016/J.IFACOL.2018.04.018.

[24] Mostafa Pahlavani and Javad Marzbanrad. Crashworthiness study of a full vehicle-lumped model using parameters optimisation. *International Journal of Crashworthiness*, 20(6):573–591, 2015. ISSN 17542111. doi: 10.1080/13588265.2015.1068910.

[25] Javad Marzbanrad and Mostafa Pahlavani. Presenting a 5-DOF Lumped Parameter Model of Vehicle in Frontal Crash with Linear Spring and Damper. *2nd International Conference on Mechanical, Industrial, and Manufacturing Technologies*, (January 2015):223–228, 2011. doi: 10.13140/2.1.4763.6803.

[26] Mohannad Murad, Manohar Das, and Ka C. Cheok. Modeling and simulation of an advanced intelligent restraint system. In *2009 IEEE International Systems Conference Proceedings*, pages 333–337, 2009. ISBN 9781424434633. doi: 10.1109/SYSTEMS.2009.4815822.

[27] Xian Xu Bai, Shi Xu Xu, Wei Cheng, and Li Jun Qian. On 4-degree-of-freedom biodynamic models of seated occupants: Lumped-parameter modeling. *Journal of Sound and Vibration*, 402:122–141, 8 2017. ISSN 10958568. doi: 10.1016/j.jsv.2017.05.018.

[28] Paul C. Ivancic. Mechanisms and mitigation of head and spinal injuries due to motor vehicle crashes. *Journal of Orthopaedic and Sports Physical Therapy*, 46 (10):826–833, 10 2016. ISSN 01906011. doi: 10.2519/jospt.2016.6716.

[29] David C. Viano and Chantal S. Parenteau. Concussion, Diffuse Axonal Injury, and AIS4+ Head Injury in Motor Vehicle Crashes. *Traffic Injury Prevention*, 16 (8):747–753, 11 2015. ISSN 1538957X. doi: 10.1080/15389588.2015.1013188.

[30] Gulshan Noorsumar, Svitlana Rogovchenko, Kjell G. Robbersmyr, Dmitry Vysochinskiy, and Andreas Klausen. A novel technique for modeling vehicle crash using lumped parameter models. *Proceedings of the 11th International Conference on Simulation and Modeling Methodologies, Technologies and Applications, SIMULTECH 2021*, pages 62–70, 2021. doi: 10.5220/0010529200620070.

[31] J. Michael Chang, Miinshiou Huang, Tau Tyan, G. Li, and L. Gu. Structural optimization for vehicle pitch and drop. In *SAE Technical Papers*. SAE International, 4 2006. doi: 10.4271/2006-01-0316. URL `https://www.sae.org/publications/technical-papers/content/2006-01-0316/`.

[32] Gernot Woitsch and Wolfgang Sinz. Influence of pitching and yawing during frontal passenger vehicle crash tests on driver occupant's kinematics and injury. *International Journal of Crashworthiness*, 18(4):356–370, 2013. ISSN 13588265. doi: 10.1080/13588265.2013.801290.

[33] J. Michael Chang, Mohammad Ali, Ryan Craig, Tau Tyan, Marwan El-Bkaily, and James Cheng. Important modeling practices in CAE simulation for vehicle pitch and drop. In *SAE Technical Papers*. SAE International, 4 2006. doi: 10.4271/2006-01-0124.

[34] Schmortte Uwe. Crash-Test Results to Analyse the Impact of Non-Professional Repair on the Performance of Side Structure of a Car. In *22nd International Technical Conference on the Enhanced Safety of Vehicles (ESV)*, 2011. URL `https://trid.trb.org/view/1366472`.

[35] Gulshan Noorsumar, Dmitry Vysochinskiy, Even Englund, Kjell G. Robbersmyr, and Svitlana Rogovchenko. Effect of welding and heat treatment on the properties of UHSS used in automotive industry. *EPJ Web of Conferences*, 250:05015, 2021. ISSN 2100-014X. doi: 10.1051/EPJCONF/202125005015.

[36] M. Amirthalingam, M. Hermans, and I. Richardson. Microstructural development during welding of siliconand aluminum-based transformation-induced plasticity steels-inclusion and elemental partitioning analysis. *Metallurgical and Materials Transactions A: Physical Metallurgy and Materials Science*, 40(4): 901–909, 2009. ISSN 10735623. doi: 10.1007/S11661-008-9761-5.

[37] Paul Kah, Markku Pirinen, Ramio Suoranta, and Jukka Martikainen. Welding of Ultra High Strength Steels. *Advanced Materials Research*, 849:357–365, 2014. ISSN 1662-8985. doi: 10.4028/WWW.SCIENTIFIC.NET/AMR.849.357.

[38] Behzad Barzin. *Simulation and material calibration of ultra high strength steel*

(UHSS) S960 welded joint under static tensile test utilizing finite element method (FEM). Master thesis, Lappeenranta University of Technology, 2015.

[39] Rui Yan, Haohui Xin, Fei Yang, Hagar El Bamby, Milan Veljkovic, and Kristo Mela. A method for determining the constitutive model of the heat-affected zone using digital image correlation. *Construction and Building Materials*, 342:127981, 8 2022. ISSN 0950-0618. doi: 10.1016/J.CONBUILDMAT.2022.127981.

[40] Edward A. Bender. *An introduction to mathematical modeling.* Wiley, 1978. ISBN 0471029513.

[41] Junuthula Narasimha Reddy. *Introduction to the finite element method.* McGraw-Hill Education, 2019.

[42] Matthew Huang. *Vehicle crash mechanics.* CRC press, 2002.

[43] Crash Simulation Vehicle Models | NHTSA. URL `https://www.nhtsa.gov/crash-simulation-vehicle-models`. Accessed: 2022-09-30.

[44] John O Hallquist. LS-DYNA ® THEORY MANUAL. Technical report, 2006. URL `www.lstc.com`.

[45] Isaac Newton. Philosophiae Naturalis Principia Mathematica. Technical report, 1967.

[46] Feliks Ruvimovich Gantmakher. *Lectures in Analytical Mechanics.* Mir Publishers, 1970.

[47] *Direct Dynamics: Newton–Euler Equations of Motion*, pages 183–207. Springer London, London, 2009. ISBN 978-1-84800-391-0. doi: 10.1007/978-1-84800-391-0_5. URL `https://doi.org/10.1007/978-1-84800-391-0_5`.

[48] Dipendra Subedi, Ilya Tyapin, and Geir Hovland. Review on Modeling and Control of Flexible Link Manipulators. *Identification and Control*, 41(3):141–163, 2020. doi: 10.4173/mic.2020.3.2.

[49] Fernando Malvezzi, Renato M.M. Orsino, and Tarcisio Antonio Hess Coelho. Lagrange's, Maggi's and Kane's equations applied to the dynamic modelling of serial manipulator. *Lecture Notes in Mechanical Engineering*, Part F6:291–304, 2018. ISSN 21954364. doi: 10.1007/978-3-319-91217-2{_}20/TABLES/3.

[50] Leonard Meirovitch. *Methods of Analytical Dynamics.* McGraw-Hill, New York, ed. edition, 1970.

[51] Oscar Cyrén and Sofia Johansson. *Modeling of Occupant Kinematic Response in Pre-crash Maneuvers A simplified human 3D-model for simulation of occupant kinematics in maneuvers.* Master thesis, Chalmers University of Technology, 2018.

[52] Test protocols and technical information. URL `https://www.iihs.org/ratings/about-our-tests/test-protocols-and-technical-information`. Accessed: 2022-09-30.

[53] J Davis, R. *Tensile Testing.* ASM International, 2004. ISBN 978-0-87170-806-9.

[54] Euro NCAP | The European New Car Assessment Programme. URL `https://www.euroncap.com/en`. Accessed: 2022-10-20.

[55] H Singh, C-D Kan, D Marzougui, and S Quong. Update to Future Midsize Lightweight Vehicle Findings in Response to Manufacturer Review and IIHS Small-Overlap Testing. Technical report, 2 2016.

[56] SIRIUS Technical Specifications | Dewesoft. URL `https://dewesoft.com/products/daq-systems/sirius/tech-specs`. Accessed: 2022-12-17.

[57] J211 Instrumentation for Impact Test, Part 1 - Electronic Instrumentation - SAE International. *Safety Test Instrumentation Standards Committee*, page 29, 2022. doi: https://doi.org/10.4271/J211/1_202208.

[58] Azmin Sham Rambely, Norhafiza AB Halim, and Rokiah Rozita Ahmad. A NUMERICAL COMPARISON OF LANGRANGE AND KANE'S METHODS OF AN ARM SEGMENT. *International Journal of Modern Physics: Conference Series*, 9:68–75, 2011. doi: 10.1142/S2010194512005119. URL `www.worldscientific.com`.

Paper A

Mathematical Models for Assessment of Vehicle Crashworthiness: A Review

Gulshan Noorsumar, Svitlana Rogovchenko, Kjell G. Robbersmyr, Dmitry Vysochinsky

This paper has been published as:

Gulshan Noorsumar, Kjell G. Robbersmyr, Svitlana Rogovchenko and Dmitry Vysochinskiy. Mathematical Models for Assessment of Vehicle Crashworthiness: A Review. *International Journal of Crashworthiness*, 1-15, 2021. doi: 10.1080/13588265.2021.1929760.

Mathematical Models for Assessment of Vehicle Crashworthiness: A Review

Gulshan Noorsumar, Svitlana Rogovchenko, Kjell G. Robbersmyr and Dmitry Vysochinskiy

Department of Engineering Sciences
University of Agder
4879 Grimstad, Norway

Abstract **This paper reviews approaches to mathematical modeling of a vehicle crash. The growing focus on vehicle and occupant safety in car crashes has triggered the need to study vehicle crashworthiness in the initial stages of vehicle development. The major motivation for this work is to support vehicle crashworthiness design during the product development process.The paper is divided into two parts; the first one overviews existing mathematical models used to solve engineering problems. The second part describes modeling strategies applied for replicating non-linear vehicle crash event and occupant kinematics in an occupant protection loadcase. We also highlight alternative modeling strategies using hybrid modeling techniques aimed at the improvement of the vehicle development process.**

A.1 Introduction

The notion of 'crashworthiness', first used in the aerospace industry in the early 1950's, introduced the measure of the ability of the structure to protect its occupants in survivable crashes [1]. In the automotive industry, the term refers to vehicle's structural abilities to plastically deform and absorb sudden impact loads maintaining enough survival space for the occupants. Crashworthy vehicle structures should be stiff in bending and torsion for proper ride and handling and should minimize fore-aft vibrations that give rise to harshness.
According to Du Bois et al. [1], the vehicle should be able to: (i) deform plastically in the front end and absorb crash energy in case of a frontal crash and prevent intrusions in the driver compartment; (ii) deform plastically in the rear end to protect occupants in case of a rear impact; and (iii) have well-designed side structures preventing intrusion into passenger compartment and opening of doors due to loading in a crash. [2]

Most safety regulations require crash testing at a specialized facility to determine the crashworthiness parameters. Car manufacturers conduct full vehicle or sled

tests to ensure that the car design meets the regulations. Usually, crash-testing is time consuming and costly. Mathematical models are employed to represent crash dynamics, for example, in the case of a car impacting a barrier or another car. These models involve differential equations of motion describing the deformation of the parts in the vehicle. The occupants in the car can also be included in a mathematical model to predict injury values during a crash.

Construction of an appropriate model involves the elimination and minimization of effects deemed to be negligible. The quantities that are modeled are expressed as functions depending on independent and controllable variables. Non-linear physical systems very often are modeled by ordinary and partial differential equations. To find specific solutions of such differential equations one needs initial and/or boundary conditions. Solutions can be validated with empirical data from the physical experiment, see, for instance, [3].

The classes of differential equations to which the analytical solutions exist are very limited; therefore, numerical methods are being employed. In this case computational inaccuracies add up to the inherent inaccuracies of the model and the result must be compared with the experimental data. As suggested by Marion and Lawson [4], one of possible approaches to mathematical modeling involves the following steps: (a) building; (b) studying; (c) testing; and (d) use of the model. Vehicle crashes are highly non-linear transient dynamic phenomena. In an impact, a non-linear relation holds between applied force and displacements; it appears due to geometrical non-linearity (non-linear behaviour of highly deformable bodies leading to non-linear strain-displacement relations), material nonlinearity (elasto-plastic material) and combinations of these two types of non-linearities. Material nonlinearity depends on a number of factors: rate of deformation, temperature, pressure, humidity, age of the material and the deformation history [5]. In case of vehicle impacts, it has a significant influence on the deformation and it is important to replicate material and geometrical non-linearity in vehicles while modeling the crash phenomenon. To deal with such non-linearities, Finite Element Method (FEM) is often employed. It has higher accuracy but includes manual efforts to mesh the parts along with increased computational efforts. In contrast, simplified mathematical models are less resource-consuming yet they have lower prediction levels. In several studies models which replicate the collision mechanics with considerable confidence were developed, however a compromise between computational time and accuracy is always present.

This paper reviews the existing approaches to mathematical modeling of car crashes. Although the use of models helps to reduce the dependence of automotive design on physical crash test data for determining crash parameters and injury values to occupants, they do not fully replace real time tests due to certain inevitable assumptions which restrict the analysis of the kinematics of the event in detail. The

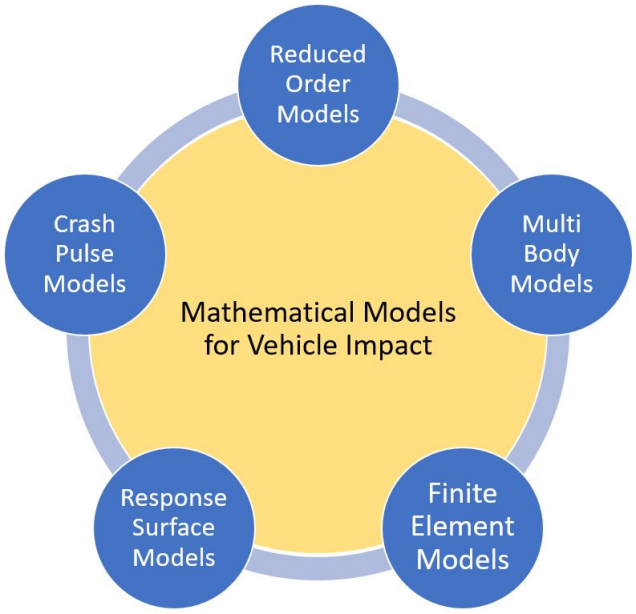

Figure A.1: Common used models for vehicle crash

research reported in the literature indicates the need to further improve the predictive power of existing models for efficient application in a vehicle design development. Figure A.1 presents the common models used for vehicle crash described in this study.

A.2 Methodology for Crash Modeling

A.2.1 Reduced Order Dynamic Models

These models have reduced complexity yet capture the kinematics of the crash with the load paths and components. The methodology includes the use of lumped parameter models, fine-grained lumped models and coarse mesh finite element models. One of the major challenges is that the accuracy of these models is affected by the simplifications and reduced number of degrees of freedom (DOF). Lumped parameter models are the most commonly used reduced order models; they include spring-damper systems replicating a deformable part and a concentrated mass representing the undeformed structures like engine and transmissions. Passenger compartment integrity is essential for vehicle structural loadcases; for simplicity, it is often assumed that the passenger compartment is integrated with the chassis as a lumped mass. However, occupant protection models need to accommodate for compartment deformations in order to understand the cabin intrusions and better predict possible crash scenarios. Lumped parameter models are also used to predict occupant movements and possible injuries

in a car crash. The use of lumped masses for head, torso and legs, all connected by springs replicating joints, helps to understand the head and neck deflections and torso movements in a crash.

The idea behind a reduced order model is to depict the rigid components as masses connected by springs and determine the forces acting on the masses from the external impact and the spring forces. These forces and energy conversion laws are used to determine the governing equations of motion which are set up using one of the following formulations.

Newtonian Mechanics: The Newtonian approach relies on three Newton's laws of motion [6]. The mechanics of particles can be described by the Newton's laws of motion which which describe the relationship between an object's motion and the forces acting on it.

Lagrangian Mechanics: The Lagrangian approach uses energies rather than forces to define the dynamics of a system. The Lagrangian is the central quantity in Lagrangian mechanics, it obeys the following equations:

$$\frac{d}{dt}\frac{\partial L}{\partial \dot{q}_i} - \frac{\partial L}{\partial q_i} = Q_i,$$

where, in general case, $L = T \breve{} V$, T is the total kinetic energy of the system equal to the sum of the kinetic energies of the particles, $q_i, i = 1, .., n$ are generalized coordinates and V is the potential energy of the system.

Hamiltonian Mechanics: In Hamiltonian mechanics, the time evolution is obtained by computing the Hamiltonian of the system in the generalized coordinates. The Hamiltonian principle describes the motion of those mechanical systems for which all forces are derivable from a generalized scalar potential that can be a function of the coordinates, velocities and time [6]. Lagrangian and Hamiltonian principles together form a compact invariant way of obtaining the mechanical equations of motion.

Reduced-order models allow prediction of large deformation structures, help in analyzing component level simulations during the early vehicle development process and assist in developing new vehicle architectures for automotive applications. They distinguish themselves from other methodologies by including design dimensions in the system; users are able to develop a predictive model which may not depend on vehicle crash data besides the validation phase of modeling.

A.2.2 Multi-body Models

A Multi Body System (MBS) is a system that consists of rigid bodies, or links, that are connected by joints which restrict relative motion of the parts. The study of MBS distinguishes forward dynamics which analyzes the motion of mechanical

systems under forces, whereas the inverse dynamics deals with the analysis of forces causing the motion of bodies [7]. Multi-body models are used for both dynamic and kinetic analysis [8]. Lagrange devised the formulation for the dynamics of multi body systems in 1788 in *Mecanique Analytique* [9] and since then is recognized as the father of multi-body dynamics. Important additions to this methodology include application of friction (by Coulomb [10]), beam elasticity (by Euler [11]), contact compliance (by Hertz [12]) and lubrication (by Reynolds [13]). Two hundred years after the formulation was proposed by Lagrange, the methodology gained further impetus with the introduction of improved matrix manipulation techniques by Denavit and Hartenberg [14]. During the past century, the improvements in solution methods and their computational efficiency supported applications of this methodology in different aspects of machine design including vehicle design analysis [8]. The analysis of linkage mechanisms developed by Wittenbauer in 1923 [15] was followed by the use of rigid body dynamics for the analysis of human gait by Fischer [16]. Segel [17] studied the motion of a vehicle on a flat road in response to steering control. Orlandea et al. [18] proposed a practical solution methodology for large rigid MBS based on the Lagrangian dynamics for constrained systems; this led to the development of ADAMS (automatic dynamic analysis of mechanical systems), the driving force behind many advancements in the automotive industry.

Constructing the governing equations for MBS is challenging; one of the classical approaches is based on the Lagrange method for setting up the equations which are solved numerically afterwards. However, this approach is time consuming, especially with systems having large number of components. Nikravesh in [19] has proposed a new methodology for constructing equations of motion for an MBS based on a body-coordinate formulation using Newton-Euler equations and a joint-coordinate formulation employing relative coordinates. The study also describes systematic transformation from the former to the latter formulation. The complexity of dynamic equations of motion makes such models challenging computationally; this stimulated the development of the software for computer simulation since 70's. The programming codes support different functionalities ranging from the generation of equations of motion to numerical simulations for solving the equations [7]. Examples of computer code guidelines can be found in the papers of Barley and Cripps [20] and Dopker [21].

Multi-body models are applied in vehicle development process for several decades to design vehicle handling and suspension systems [23]. One of the studies in this context is due to Hegazy et al. [24] where the vehicle structure is represented by rigid bodies connected by springs, dampers and joints. Recently MBSs have been also used to develop generic models for the study of crashworthiness in vehicles and for the prediction of the impact of crashes on vehicles during the development

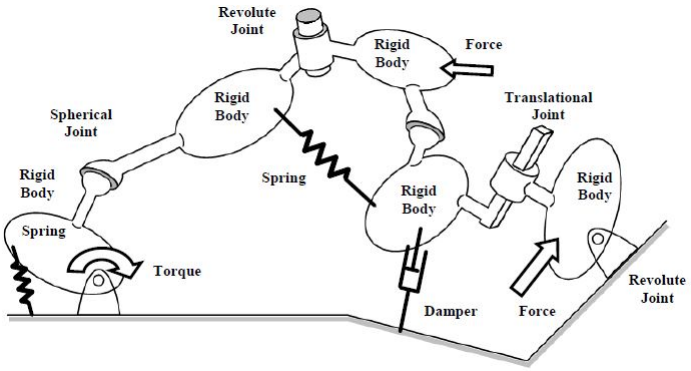

Figure A.2: Generic Multi Body Model [22]

process [25]. Lower accuracy and cumbersome process required for developing the model are the limitations of this methodology; although it is quite useful for early development phases of vehicle design. MBSs are used for the development of occupant and pedestrian models in crash analysis where one of the main challenges is related to the replication of the anthropometry of the human body. The representation of different joints of the body has been implemented in several commercial software programs like MADYMO. Similarly to reduced order models, this methodology has insufficient accuracy and less detailed modeling of the system. For instance, the occupant and pedestrian human body models lack details like skin and ligaments which might be critical for determining certain loadcase parameters in occupant and pedestrian protection.

A.2.3 Non-linear Finite Element Models

Finite element modeling uses finite element method (FEM) to solve boundary value problems (BVPs) for partial differential equations (PDEs) arising in many physical and engineering problems. The solution of such problems for PDEs can be considered in two forms: strong and weak. A strong form of the governing equations states that the solution must satisfy the problem at every point of the domain along with boundary conditions; it assumes that the classical solution to the problem exists. A weak form states that the solution must satisfy the problem in an integral sense and is used when the classical solution to a problem cannot be established. FEM is a special method which subdivides the original BVP into smaller problems called finite elements in order to approximate PDEs. The solution is derived using numerical methods for solving systems of algebraic equations and systems of ordinary differential equations. The basic steps of a FEM are [26]: establishing the strong formulation, obtaining the weak formulation, choosing approximations for the unknown functions, choosing the weight functions, and solving the system.

The finite element models are developed by discretizing the CAD surface into elements and nodes which cover the geometry of the vehicle (mesh) and the finite element BVPs are developed from the discretization. These problems are solved in order to determine the nodal displacements. The elemental stresses and strains can be derived from the explicit finite element method. In order to get a better approximation it is preferable to have a higher mesh size with more nodes covering the domain.

The FEM approach in engineering was developed in the early 1940s when Hrennikoff [27] and Courant [28] used mesh discretization for elasticity and structural analysis problems. Clough published the first paper on FEM in 1960 suggesting that two-dimensional elements connected to more than two nodes can be used to solve problems in continuum mechanics [29]. In 1965, NASA Structural Analysis software (Nastran) was developed to solve structural analysis problems; this paved the way to simulation of engineering stress strain problems with software codes. In the fololowing decade Alberto Peano developed the first professional FEM p-version code which was used by Szabo in an industrial implementation PROBE in 1982. The qualitative research of Spethmann et al. based on expert interviews analyzes the impact of the use of finite element methods in vehicle crash simulations on productivity and problem-solving [30]. The authors argue that since the 1960s, when the explicit FEM was developed and applied to crash events, it became not only an alternative to physical destructive testing but also a method for solving problems which formerly had been impossible to solve. Even though automotive industry gained trust in crash simulations, the lack of appropriate software and hardware brought them to a standstill in the late 1970s to early 1980s. The paper highlights the emergence of supercomputers in the late 1980s which aided research to improve the performance of passive safety systems in a crash. Since then the dependence of engineers on computer software programs and computer power has been constantly growing. The FEM approach is widely used by automakers to simulate crash although the process is time-consuming and requires skills to develop the full size finite element models. Another shortcoming of the FEM in crash simulations is the dependence of the results on CAD data for the structure and non-linear material properties of vehicle structure. The stiffness and dimensions of each component need to be defined before the solver is used to determine the acceleration and deformation in the crash event. The process of detailed intrinsic meshing is cumbersome and requires training to represent the entire CAD surface with a discretized mesh. This calls for research and predictive simulations at early design stages thus possibly reducing the number of re-design stages since the timescales tend to become shorter in automotive industry. Improvements can be achieved through the collaboration of car manufacturers with academic institutions in multidisciplinary research. An LS Dyna based FEM is

presented in Figure A.3 representing a full vehicle crash.

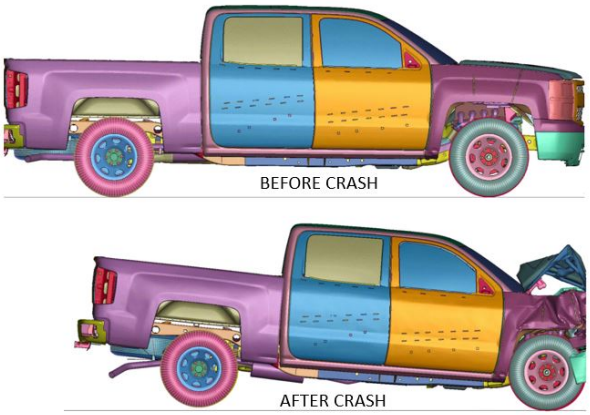

Figure A.3: LS Dyna FE model of a full vehicle crash

One of the major challenges in using software programs like LS-Dyna or PAM-CRASH for engineers transitioning into automotive industries is the extensive training required to understand the solver codes and assumptions made during the analysis. These complex programs are not a part of curriculum for engineering students or academic research and there is a need to bridge this gap between academia and specific requirements of the industry.

A.2.4 Response Surface Models

The Response Surface Models (RSM) are statistical approximation models which do not rely on the physical description of the objects but explore the relationship between the input (predictor, or design variable) and output response (dependent variable) using a number of experiments in which the predictor variables are changing. In automotive industry, RSM can be employed to measure the performance of the system and, in combination with numerical simulation methods, they are used to improve or optimize a product and its performance [31]. The methodology was developed by Box and Wilson who used the sequential method in chemical process design [32]. The motivation for their work was the problem of planning and analyzing experiments in search of desirable conditions on a set of controllable, or design, variables [33]. The response surface analysis can be viewed as analysis that deals with a fitted function and accommodates a large collection of techniques. RSM uses linear and quadratic models to fit a sequence of local regression models with experimental data.

The RSM algorithm consists of the four steps: (a) perform a statistically designed experiment, (b) estimate coefficients in the response surface equation, (c) check on

the adequacy of the equation (via lack-of-fit test) (d) study the response surface in the region of interest [33].

For engineering applications, the process of constructing models often includes the following three steps:

- design of experiments: this involves setting the factors at different levels for proper experiments and ensuring that the boundary values as well as the entire area of the interest of the model is tested for different combinations of variables;

- data collection: the process involves running the experiments to collect the data including FE simulations or real time crash tests.

- data fitting: this is the final step which involves using algorithms to fit the sample data matching specific requirements. The feasible design solution is obtained at this step and used for design recommendations or relevant changes aimed at meeting the crash loadcase requirements.

The RSM methodology was used in non-linear finite element models where accurate response surface models are constructed and evaluated for repeated replacement of the finite element model at each time step of the analysis [34]. In comparison with the modeling based on sensitivity analysis, the RSMs provide considerably more accurate predictions reducing dependence on FE models [35]. One of the shortcomings of the RSM technique is the dependence on real crash test/simulation data. Such models are unable to predict new scenarios in crash loadcase and have been found to be less accurate for non-linear impacts. It is crucial to know the algorithm behind the RSMs, otherwise it becomes a "black box" approach and finding the magnitude of approximation errors is difficult [36]. Another limitation of this technique is that the developed response surface is invalid for regions other than those set in the problem. The RS methodology fits the data to a second order polynomial, in which case the technique gives accurate prediction but may fail for problems with higher order polynomial approximations.

The RSM methodology is also useful in parameter identification models which help predict the stiffness and damping values for vehicle deformation; such models find extensive applications in accident reconstruction.

A.2.5 Crash Pulse Models

Crash pulses represent the dynamic response of a vehicle in a crash event and serve as a validation for most algorithms developed to predict crash responses. These models also help to explain the energy conversions in vehicle structure during the impact; structural optimizations are also based on crash pulses [35]. Furthermore, crash pulses are used in validation of crash simulations where most validation algorithms compare model simulations with real time crash data [37].

The crash pulses are modeled using the function representing the vehicle acceleration and the crash process. If $x(t)$ stands for the acceleration, the crash pulse model F_θ should ensure that

$$r_a(t_0) = x(t_0) - F_\theta(t_0) \approx 0,$$

$$r_v(t_0) = \int_0^{t_0} r_a(t)dt \approx 0,$$

$$r_d(t_0) = \int_0^{t_0} r_v(t)dt = \int_0^{t_0}\int_0^{t_0} r_a(t)dtdt \approx 0$$

at all times $t_0 \geq 0$ where $r_a(t), r_v(t), r_d(t)$ are the residual signals of acceleration, velocity and displacement respectively [37]. In the past, the crash pulse was represented using different pulse shapes including square, triangular, half-sine and even polynomial functions. In general, a crash pulse is defined only for a specified crash scenario and may not be applicable for different loadcases. There could be numerous factors influencing crash pulses such as velocity of impact, crash model and other collision conditions. However, researchers developed efficient schemes to overcome this problem in crash modeling. For instance, Wei has proposed a crash pulse model to determine crashworthiness of vehicles [37]. This methodology resembles reduced order modeling, however these models find applications in accident reconstruction and depend on crash pulses or crash data for model development and validation.

A.3 Applications of Modeling Strategies

A.3.1 Reduced Order Models

The standard approach for Lumped Mass Spring (LMS) models is that bodies are represented by concentrated point masses which are connected by linear/non-linear springs. The springs are defined by force-deformation and force-velocity curves and deform due to the application of a force. This approach was first introduced in automotive suspension design in the early 1900s and has been extensively used in automotive development since then.

The paper by Kamal [38] is one of the earliest studies in modeling of crash events using lumped parameter models. The model developed in this paper includes three mass components and eight resistances representing the deformable structures of the vehicle. The lumped masses represent the body chassis mass, the engine transmission and the vehicle bumper. The non-linear resistances along with the inertial components (lumped masses) are used to solve the basic equations of motion

numerically. The dynamic force acting on the resistances is approximated using static forces acting on the vehicle during the crash event, where the constant factor is assumed to be independent of the geometry of the structure. The model is presented in Figure A.4. It is assumed that the structure is two-dimensional with a closed rigid frame. This implies that the model may not predict the vehicle behaviour out of plane forces experienced by the structure in a crash. The study correlates well with physical test data for displacement while the acceleration peaks are not well correlated. However, the trend for the acceleration curves is similar which indicates that the model predicts the event's kinematics to a reasonable extent. The static and dynamics force-deformation curves show a lower peak for the static curve which is expected because the model does not account for the impact loading acting on the structure in a dynamic crash event. The study also includes elastic body analysis for the vehicle passenger compartment and calculates the forces exerted on the members in case when the occupant compartment is not considered a rigid lumped mass. A parameter study on the elastic passenger compartment indicates that the structure's capability to withstand crash increases with increasing metal thickness. This observation is in line with the basic understanding of bending forces, that is, the thickness of the structure contributes to the crashworthiness of the body.

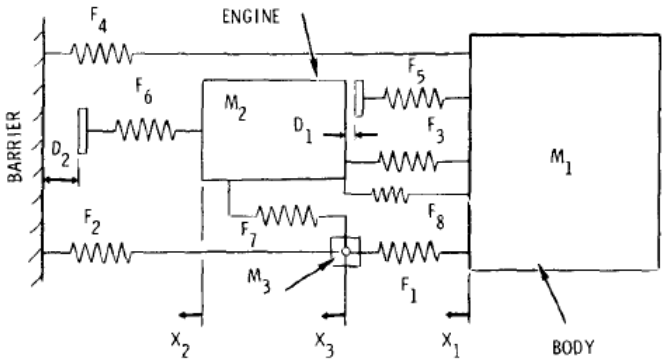

Figure A.4: Vehicle impact simulation model in Kamal [38]

Identification of parameters involves a range of approaches, for instance, a piece-wise linear approach where the force deformation characteristics are represented by the hat functions or Chebyshev polynomials. The studies conducted in [39] and [40] used optimization approaches to estimate crash parameters. The algorithm developed in [39] helps optimize the acceleration data for a full frontal crash using the force deformation curves for a few components in the vehicle. In [40], the solution space approach is used to develop an algorithm which is applied to three engineering vehicle crash scenarios. The algorithm determines the force deformation curves used for frontal crash components. This approach is illustrated with an example

where the algorithm is used to determine whether submarining occurs in the rear passenger seat and to design the car seat-belt and rear occupant structure which ensure the absence of submarining during a crash event. The optimization problem has a solution meeting the design constraints.

Sharp et al. used Lagrangian method to simulate vehicle motion [2]. The equations of motion take into consideration external forces acting on the vehicle and incorporate pitching, rolling and yawing effects on the car. The equations also include the sprung mass of the vehicle and unsprung masses per wheel along with the moment of inertia in the x, y and z axes. The numerical model predicts the body roll, pitch and yaw angles and the tire forces in the longitudinal and lateral directions. This mathematical model replicates the motion of an ideal vehicle with inertial forces and the coupling between pitch and bounce. The limitations of the model include the lack of non-linear springs and anti-roll bar to represent the suspension system in more detail.

A method for finding the parameter values for spring elongations was developed by Mentzer et al. [41] who used real time crash test data to determine the mass of the components from acceleration and wall contact forces. They obtained the force-deformation curves for the springs from the load paths under the condition that the system should have comparable motions of its masses so that the force and acceleration curves match the test data. This condition is difficult to achieve as the number of load paths could be higher than the mass elements. This is the reason why the least square method is used for the parameter identification in a full crash test data. Some of the drawbacks of this approach are: the energy absorption by the honeycomb structure during deformation was neglected; it is assumed that no rotational energy is lost in offset impacts. The rotational energy losses were accounted for in the SISAME 3D model adopted later by NHTSA where the masses were no longer considered as point masses which improved the model's reliability.

The early approaches to parameter determination in LMS models proved to be efficient and were further developed to improve agreement between model outputs and data sets; a number of parameter identification techniques used by researchers in vehicle modeling, will be discussed in our future research paper.

Cheva et al. [42] developed a lumped parameter model to replicate a zero degree frontal crash test and a 40% offset deformable barrier crash test. The barrier is defined as a large lumped mass as well as the firewall which represents the passenger compartment. The deformation of the firewall indicates the intrusion in the occupant compartment. The left and right sides of the vehicle were modeled separately so that the same model can be used with minor modifications for an offset crash event. The model includes mass components representing several parts in the deformable zone like the engine assembly, radiator, suspension components, and front rails. The crash

was simulated at 48 and 56 kmph and the results were validated against physical crash test data. The same model was used for 40% offset deformable barrier loadcase with the barrier imparting more load on one side. Then the upper rails have higher load from the deformable barrier causing higher deformation on the impacted side. The event kinematics are observed to be different in an offset crash scenario compared to a full frontal loading case.

A.3.1.1 Discrete Time Domain Simulations

The crash behaviour can also be described using discrete time domain simulation in lumped parameter models. The approach allows to predict and understand the crash response in terms of deformation, acceleration, velocity and rotation angles during the entire span of the crash event.

The research by Elkady et al. in [43] - [44] focuses on developing mathematical models for replicating a vehicle crash using non-linear springs for the vehicle bumper. The lumped parameter model developed in [43] and [45] uses a lumped mass representing the vehicle body and four spring damper units to replicate the suspension and wheels. It is assumed that the vehicle is moving on a flat asphalted road and the vertical motion of the tyres is neglected. The model is designed to explore the effects of Vehicle Dynamics Control Systems (VDCS) on the crash mitigation for an offset impact with a rigid barrier. The effect of ABS (anti-lock braking system) is also simulated by using a braking force component in the equation of motions. The front deformable members are presented by non-linear springs with force deformation characteristics and the forces on the springs during the crash are calculated using numerical methods. The model is validated by comparing the acceleration and deformation of the front end structures to the physical test data. The study concludes that the values of the post impact speed of the vehicle in the mathematical model and in the physical test agree well. The variation in the curves for the front end deformation suggests shortcomings of the model due to the inaccurate values of the system parameters. The paper also discusses the effects of VDCS on the collision response for a 50 percent offset impact.

The same 6 DOF mathematical model (shown in Figure A.5) is employed to solve the equations of motion using Euler's method for full frontal and offset impact [46].

It is demonstrated that in the case of the vehicle deformation and deceleration during the crash the effect of the active VDCS is negligible. However, the vehicle pitch angles show an improved vehicle behaviour with an active VDCS in the car. The model in this this study does not include the front bumper mass or a rigid mass like an engine or battery which may contribute to the deceleration and deformation of the vehicle. In Elkady et al. [47], the vehicle model is modified by adding a lumped mass for a front bumper which connects the front end members represented

by springs.

An offset impact with another identical vehicle is studied to understand the crash response of the vehicle and how it differs from the case of rigid barrier impact. The simulations are performed for the impact speed of 55 kmph with different car masses. The study could be extended to understand the deceleration in the vehicles for different impact speeds and vehicle masses.

Elmarakbi et al. [48] developed a mathematical model for smart structures which improves the crashworthiness response of a vehicle in a barrier impact. The smart structures are represented by spring mass damper systems for vehicle and occupant and are simulated numerically with the help of an optimization algorithm which minimizes the intrusion in the occupant compartment and the deceleration injury for the occupant. The injury curves obtained from the simulation are compared to the vehicle model without smart structures.

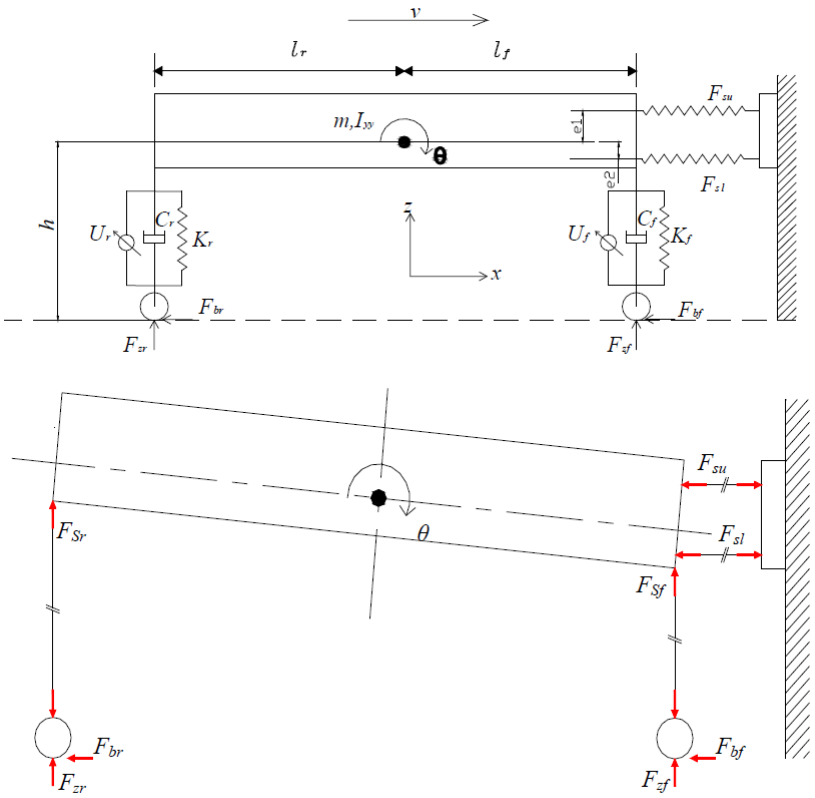

Figure A.5: Barrier impact simulation model in Elkady et al. [46]

Ionut et al. [49] developed a $2D$ mathematical model which includes 2 vehicles with 2 occupants to analyse the occupant kinematics in a frontal collision with another vehicle.

They use Lagrange's generalized formulation to obtain the system of five equations. The numerical solution provides the displacement and velocity of each of the vehicle

bodies and the velocities of the occupant's head and thorax. The model was validated against real test data demonstrating good correlation. The parameterization of the stiffness of the seat belt springs is used to understand the influence of the spring stiffness on the occupant deceleration and displacement.

A National Highway Transport Safety Administration (NHTSA) Lumped Parameter Model was developed by Deb et al. [50] for a side impact crash scenario. The authors identified lumped masses which were then added to the existing model based on finite element analysis of two passenger vehicles. The validation of this model was conducted with simulations of two vehicles Dodge Neon and Dodge Intrepid. The authors suggested the methodology of determining the spring characteristics from the FE model using contact introduced between two components. This gives the force displacement characteristics for the spring members.

The deformation characteristics of a vehicle under front-to-side impact were calculated by Prochowski et al. [51] using experimental and analytical equations. The combined deformation of both vehicle bodies due to the force was plotted for the impact duration. The stiffness of each vehicle was predicted based on equal force experienced by both vehicles, suggesting that for a medium size car the average side impact stiffness is a quarter of the front side stiffness. The authors challenge the existing method of calculating the side stiffness from force deformation curves asserting that it overestimates the side stiffness of the car body at a front-to-side collision. They argue that using only the central part of the deformation zone for calculating the stiffness is only a few percent lower than using the whole deformation zone for the measurements. The use of the central portion for the measurements does not only simplify them but also provides a higher accuracy of data for the measurements.

Jonsen et al. [52] propose a lumped parameter model to represent a bumper in a crash.

The system uses an optimization software INVSYS where an unconstrained subspace-searching subplex method is implemented. The algorithm identifies the local minima and can be applied for optimizing noisy objective functions. The objective function is defined to minimize the error between the calculated and measured displacements; constraints include masses, damping and stiffness constants along with total mass of the vehicle. The authors claim that if the DOF of the system is increased to two, the error is reduced. This result is validated using FE bumper system connected with a 2 DOF spring mass damper system allowing only longitudinal motion.

The research on LMS models for vehicle crash has progressed slowly from simple spring mass models to more complex multiple DOF models with spring-mass-damper systems and non-linear springs. We remark that the governing equations of mo-

tion usually use Newton-Euler formulation but in the models including occupants Lagrangian formulation has been employed.

A.3.2 Multi Body Models

Ambrosio et al. [53] developed a full vehicle crash model using an MBS with plastic hinge deformation. The entire vehicle is represented by kinematic joints, data for hinge deformation was derived from CAD data and finite element simulations. Sousa et al. [25] suggested a generic car model containing different parts including suspensions, tires, occupants and structural components contributing to loadpath. The representation of the structural components uses the plastic hinge approach. The model was validated against a completely known finite element vehicle model and can be fine-tuned to have the same crash responses as in the crash tests without the knowledge of the structure of the tested vehicle. The study emphasizes the need for simple mathematical models in early stages of vehicle development process. Carvalho et al. [54] use the plastic deformation methodology to develop an optimization algorithm for identifying multibody models for crash analysis. The solution to the problem is obtained through sequential application of genetic and gradient based optimization methods. This methodology has been also employed to define an MBS for a large family car for the case of front and side crashes.

King et al. [55] developed a mathematical model for an airbag which, in conjunction with a three DOF occupant model, can predict the effects of an airbag deployment on the occupant. The authors impose the following requirements to this model: the airbag is spherical and mounted on a steering wheel; the airbag is already inflated when the simulation starts but with a low pressure and is expected to expand radially due to gas filling in the bag; the pressure is distributed uniformly and the deformation of the wall of the airbag is linearly elastic. The three governing equations in this model are the elasticity equation, continuity equation and the equation for state of the gas. The equations describing what happens after the contact of the occupant with the airbag are proposed and the configuration of the deformed airbag is discussed. The mathematical model is implemented in a computer program written in FORTRAN IV where it is merged with the 3 DOF model of an occupant. The model describes the contact of the airbag with the occupant and the code reads contact information based on the occupant's position at any given time. The results of the simulation were validated at the sled facility at the Wayne State University using anthropometric dummies. The model's curves exibit good correlation with the experimental data.

Elkady et al. [44] developed a 3 DOF multi body mathematical model as shown in Figure A.6 to simulate a crash event of a car with an occupant.

Three masses representing the lower body replicate the legs and pelvic area of the occupant who can perform translation and rotation motion about the center of gravity (CG) of the body. The model replicates a seat belt with 2 spring damper systems and mitigates the impact for the occupant. The MBS is integrated with the vehicle model developed in the paper. Under the full frontal barrier crash the lower part of the body moves forward while the middle and upper body rotate slowly; the spring forces in the seat belt are introduced to reduce the rotation and movement of the body. Lagrange's method is employed to derive the equations of motion. The system of equations is solved numerically to compute the occupant body deceleration. The results from the vehicle crash model are used in the simulation of the crash impact on the occupant. The results highlight the importance of using seat belts, emphasizing that in crash events seat belts are the primary restraints in the vehicle safety system. The rotation angle of the middle body is similar to the pitch of the vehicle in the crash; the crash causes a neck rotation which could be fatal for an occupant. Remarkably, the change in the seat belts' spring stiffness positively affects the neck rotation and deceleration of the occupant. This study demonstrates that the use of a hybrid technique mixing LMS with MBS models improves the overall crash response prediction. Euler and Lagrangian equations are employed for vehicle and occupant models respectively; the advantages of using each of the approaches are discussed.

Hassan et al. [56] and Shi et al. [57] presented a multi body model of the cervical spine of a 50th percentile male occupant in a crash event performing FE simulations of two generic compact sedan cars in front and rear impact collisions. The single-DOF model included only rotational viscoelastic joints, and the two-DOF model allowed axial extension. It is shown that in a frontal collision, the highest risk of injury was for the lower cervical spine, and in a rear collision the most serious injury occurs in the upper to mid cervical spine. The MBS models were validated against FE data and are in agreement with the simulation data generated from FE tests.

Portal et al. [22] developed an accident reconstruction model using 3D rigid body mechanics. The rigid car body is modelled with nine rigid bodies and eight kinematic joints representing different vehicle components; the study includes also a motorcycle model and a human biomechanical model. The human biomechanical model features eight rigid bodies and thirteen kinematic joints which replicate different parts of the body. These models were used to study a frontal collision between a car and a motorcycle, an offset collision between two cars and a pedestrian impact.

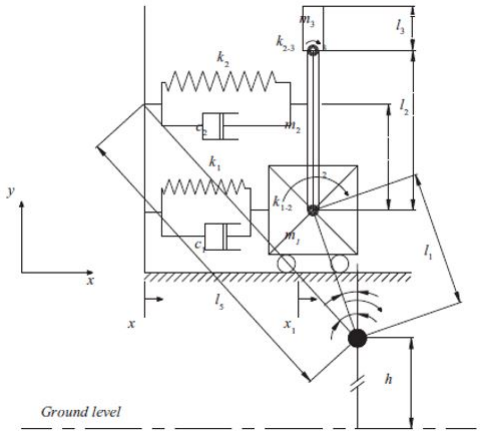

Figure A.6: 3-DOF occupant multi-body model in Elkady et al. [44]

A.3.3 Finite Element Models

Finite element models have applications in many engineering problems; a non-linear transient impact analysis of vehicle crash is one of the areas where these models produce reliable results. Thomke et al. [30] presented the evolution of crash simulations which originated in the military domains in the late 1960s. The automotive industry embraced this technique in the early 1970s, however the first full body vehicle crash simulation was conducted only in the mid 1980s. The authors highlight the importance of FEM simulations for predicting vehicle crashworthiness. Benson et al. [58] presented the calculations for crashworthiness design for automotive structures. This work layed the foundations for future FE models using different types of elements and mesh size for capturing the vehicle geometry and employing various techniques to measure the stress and strain from the simulations. Pifko and Winter [59] provide an overview of the theory behind FE, methods used to set up the governing equations based on Lagrangian equations and establish the failure criterion. They also draw parallels with the aircraft simulations to understand the application of FEM in the field of automotive safety pointing out the need for computational scientists to describe physical systems in detail prior to the solution of the associated differential equations.

Böttcher et al. [60] describe the progress with the use of FE models in automotive industry acknowledging that virtual simulations developed rapidly over the last 20 years. Virtual simulations have come a long way into supporting the vehicle development process from a smaller model size and lower accuracy to computationally intensive simulation models which capture almost every part of the vehicle geometry and achieve improved prediction levels. The authors point out that along with the standard loadcases, simulations nowadays feature even active sensing techniques like airbag deployment. Airbag sensing calibration technique using virtual simulations

has been demonstrated by Kiefer et al [61] who developed the algorithm for airbag deployment and discussed the advantages of using a virtual calibration technique for airbag sensing. The study shows that the model does not need to be too complex unlike the one for full vehicle loadcases, which reduces the computational costs. Recently, FEM has been used by the authors for determining the crash response in welded vehicles which contributed to the development of more stringent norms for improper repairs on UHSS structural members [62].

FEM have also been extensively used for developing simulation models to determine injuries to occupants in a crash. Kirkpatrick et al. [63] employed the software LS Dyna to develop and validate biofidelic models of varying degrees representing an occupant in a crash. In the automotive industry these virtual models replace real time tests with dummies or cadavers. The dummy modeling developed in this paper differs from the rigid body kinematics modeling of body parts like head, neck and abdomen because it accounts for the reflexes and joints in a human body during collisions. Putra [64] presented a head-neck FE model for an average female occupant utilizing an optimization strategy. The model employs an active neck muscle controller to represent human reflexes during whiplash induced rear-impact. The FEM was also used by several authors to develop pedestrian humanoid models which simulate the behaviour of pedestrian-vehicle crashes, see [65], [66] and [67]. Detailed FE models of a pedestrian replicate the anthropometry of a human head and legs and proved to be useful for predicting head and leg injuries in pedestrian collision scenarios.

Design of complex elastic and inelastic material models for simulation in crash loadcases has been a challenge for engineers since the accuracy of a finite element model is highly influenced by the replication of the behaviour of non-linear inelastic material in crash simulations. Ramaswamy et al. [68] highlight the need for the development and validation of material models for the simulations of loadcases identifying the parameters that influence the robustness of quasi-static bending simulation for the evaluation and performance of material model in out-of-plane loading scenarios.

Several researchers have used FEM to validate accident reconstruction models in the recent past, see, for instance, [69], [70] and [71]. Accident scenarios can be reproduced successfully in finite element models and reconstruction models can be validated in the absence of real time crash data.

It is worth mentioning that during the last decade there have been only small advancements in the finite element methodology; however applications of computer simulations for analysing crash scenarios have increased significantly. Researchers and industry experts rely on virtual crash simulation data for a big part of the product development process because this allows to reduce the product development timeline.

A.3.4 Response Surface Models

One of the approaches to the modeling of a vehicle crash which can address the drawbacks associated with LMS models employs Artificial Neural Networks (ANN). The new approach needs training on existing crash test data so that it can be used to predict crash scenarios. The data can be generated using finite element models as well, which makes it easier to collect necessary sets of curves for different crash scenarios. However, this approach is not very efficient for developing new car models or for the optimization and design of structures because it relies on existing data and predicts the impact characteristics only by using available crash test data. Omar et al. [72] use a recurrent neural network to predict the crashworthiness of a vehicle in a frontal crash demonstrating that ANN can be trained for non-linear impact models and produce satisfying results with good confidence levels.

Several researchers used identification of parameters for developing predictive models for crash loadcases. Joseph et al. [73] suggested a parameter identification method for a thoracic impact model predicting the chest injuries. The method minimizes the error between results from the mathematical model and experimental data using an optimization algorithm demonstrating a reasonable correlation between the curves which agrees with the known results. The use of the chest injury metrics for the validation of the mathematical model instead of real time acceleration data suggests that these models could also support occupant protection loadcases.

Ghannam et al. [74] present a mathematical model to determine the initial impact velocity of full frontal vehicle-to-vehicle test modes using the Barrier Equivalent Velocity (BEV) concept. The model is based on a basic mass-spring damper; it determines the velocity of a vehicle impacting another vehicle by calculating the crush energy of both vehicles and using the conservation of energy principles to define the initial velocity of the car. Two major assumptions require that the lateral and rotational energies are negligible compared to the initial kinetic energy of the bullet vehicle and the force-deformation curves in the vehicle front end for both vehicles are linear. The authors introduce a scaling factor to account for the non-linear force deformation characteristics, the lateral and rotational energies, thus ensuring that the model predicts correctly the real test velocity. The curves are validated with physical test data and scaling factors are added if necessary to adjust the graphs. It is concluded that the rotational and lateral energies have small influence on the initial velocity.

Several studies include optimization strategies to predict crash kinematics. The methodology uses a combination of LMS and FEM to define the system and then curve fitting techniques to determine parameters. B. Munyazikwiye et al. [75] use a double spring mass damper model with two masses representing the front rail and

the driver compartment respectively representing a car hitting a rigid barrier. The equations of motion are derived and solved with the help of a real time test crash pulse inputted into the MATLAB model. The spring stiffnesses and damper constants are derived by converting the state-space realization to transfer function. The mass distribution of the vehicle is verified by comparing the curve generated by the model with the physical test data to select the most feasible mass distribution based on the dynamic crush of the passenger compartment. The data from the four test cases is checked against the physical tests. The model does not account for material non-linearities and vehicle geometry for predicting the vehicle crashworthiness. However, the study gives an insight into the use of transfer functions for predicting crash injury values. B. Munyazikwiye et al. [76] use genetic algorithm for parameter optimization to estimate the front deformation characteristics in case of a vehicle-barrier impact and a vehicle-to-vehicle impact. Physical crash test data are used to fit the curves and determine piecewise linear spring deformation and damper characteristics. Usta et al [77] use a genetic algorithm and RSM to design crashworthy concentric circular tubes which crush on impact absorbing the impact energy.

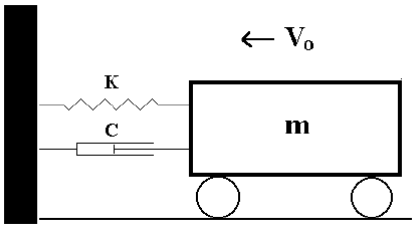

Figure A.7: Vehicle impact model in Kelvin [78]

A.3.5 Crash Pulse Model

Crash pulse models have been used to represent acceleration, velocity and displacement wave forms of a structure undergoing crash. The first step is to generate crash pulse data by running physical tests or FE simulations to gather an understanding on the type of impact. Signal pre-processing is an important step in the crash pulse methodology; it includes filtering, re-sampling, synchronizing and trimming the pulse [37]. This is followed by studying the crash stages and dividing the crash pulse into regions which better represent the deformation and intrusion behaviour. Woolley [79] proposed a crash pulse model which could be divided into two regimes: the dynamic compression and rebound phases. The compression phase is defined by the maximum dynamic crush in a vehicle impacting a barrier and its velocity becoming zero. The rebound phase in a vehicle-to-vehicle crash is the time when the two vehicles start moving away from each other which leads to their separation. The solutions to the

differential equations derived in this paper can have varying periodic characteristics (like sine or cosine) in the compression phase, and behave like polynomial functions in the rebound phase. The author introduced a transitional trigonometric function to model a crash pulse and validated the model against real time crash.

Cheng [80] analysed crash response using wavelets and wavelet packets decomposing stationary and transient crash signals into piece-wise stationary signals. The decomposed signals can undergo decomposition analysis if the signals from a non-stationary source become stationary after decomposition. The study uses a 1997 Honda Accord crash test data and the fifth order Daubechies wavelet (db5) to represent the motion of the structural components. The signal is compressed so that the time series contains a small number of coefficients for estimating body injuries during a crash. The authors also highlight another possible application of their methodology to predict best and worst performance in a sled test based on the impact pulse and for determining the range of performance using optimization techniques.

Crash pulse data with Haversine pulse were employed to study structural response of vehicle to impact [81]. The crash pulse was used for different speeds and it was observed that the energy absorption had a linear relationship with the displacement for a range of velocities. Similar behaviour is observed in the plots of absorbed energy vs deflection. When the data from sine model were plotted and compared with the real time crash data, acceleration curves showed good correlation. It was observed that the sine wave performed well for the full frontal barrier test while triangle pulse model showed good correlation for the offset model. The study does not explain why different models show good correlation to different loadcases; this indicates the need for more work on the loadcase comparison. Wei et al. [82] proposed a model using piecewise linear functions to describe the crash impulse based on CAE simulation data. They conclude that the model can be used to describe well the crash process exactly and can be used to predict crash under different conditions by varying the model parameters.

Prediction of crash pulses is an interesting area of research where different techniques including convolution methods [78] where a transfer function is employed for providing the output to the linear system. The vehicle crashing against a barrier can be represented as a spring damper system which is inputted with an excitation and an output response is expected; the process which transforms this input to an output in the time domain is described by the transfer function.

We recognize that this is a relatively new field of vehicle impact modeling and the opportunities to continue research in this domain should be further explored.

A.4 Discussion and Conclusions

Each of the modelling strategies discussed in this review have been applied across different engineering domains to solve complex non-linear dynamic problems. The research focused on the improvement of these methodologies to address problems which were difficult or impossible to solve. We observe the tremendous growth of application areas whereas the development of alternative modeling strategies was strongly influenced by the availability of increased computational power. The parallel growth in computational power from supercomputers to parallel CPUs helps solve complex equations with high level of accuracy and saves time.

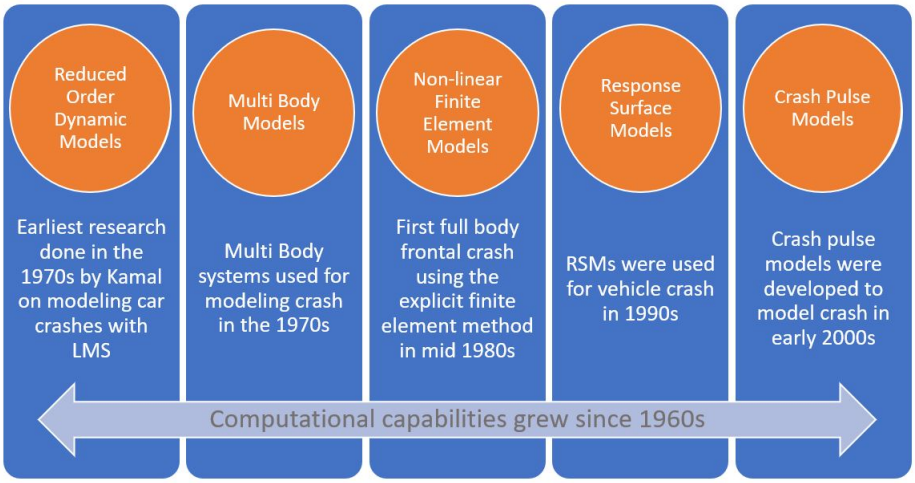

Figure A.8: Evolution of vehicle crash simulations

Although mathematical modeling of vehicle crash started to develop since the 1970's, the confidence in these models has significantly grown over the years. This is a positive trend reducing the dependence on physical crash tests. The evolution of vehicle crash simulations has been presented in Figure A.8. Mathematical models serve as a starting point for vehicle architecture development process providing recommendations to the studio and design teams; they are also employed during component design or for making changes in the existing components. Lumped parameter models show reasonable prediction power for frontal and side impacts. The major challenge faced in this field is the parameter identification which is partially resolved now using several identification strategies which however still have certain shortcomings. This hindered the use of LMS models in automotive industry during the development stages due to concerns related to new stringent safety regulations. The development of LMS models have slowly progressed from simple Kelvin models (Figure A.7) to complex spring-mass models with multiple springs and dampers representing the vehicle deformable features. The integration of occupant models in the car structure implies the addition of higher number of variables in the models

but yields far greater understanding of the loadpaths in a crash event.

Response surface methods have gained momentum in the recent past as well but their application is limited due to the fact that they cannot be used for new vehicle architectures or for changing structural and occupant protection regulations with new crash scenarios. However, reinforcement learning methods can be employed to overcome these limitations. RSMs have proved to be highly effective in modifying existing designs of vehicle structures and decision making has been easier without running virtual or physical tests based on data collection and using algorithms to interpret the feasible design space. This has helped determine feasible and non-feasible design regions for many component level loadcases and makes engineering judgements easier for design teams. The emergence of efficient machine learning tools and algorithms is a promising trend in the automotive industry which can increase confidence in the reliability of the analysis of non-linear transient impacts without physical tests.

Quantitative methods, although less significant for understanding the impact mechanics in detail, provide valuable observations on the crashworthiness of a vehicle, like the available crush space or coefficient of restitution. These methods are a backbone of most mathematical models which analyse the load paths of the vehicle impact.

It is imperative for engineers and academicians to be aware of important modeling strategies and carefully access the advantages and shortcomings of each of these methods in order to apply the most appropriate one based on the considerations of accuracy and efficiency required in the solution. The automotive industry is quite fast paced in terms of developing new products and improving existing architectures, the short product development cycle triggers the need for reliable virtual modeling methodologies which predict crashworthiness performance as close as within 5-10 % of the physical tests. In addition, the vehicle safety regulations have become more stringent over time as the focus on vehicle safety has gained momentum during the recent years. This in turn puts pressure on vehicle manufacturers who have to fulfill these regulations developing new products. This implies that industry experts resort to processes which are time consuming or computationally intensive to get the satisfactory confidence levels of their results; this sets a constraint on the adoption of new strategies or mathematical models for the development cycle which should be less complex yet explain the dynamics of the problem equally well. The experts look for methodologies which solve engineering problems with software automation or data science and help to come up with new products for the competitive automotive market. On the other hand, the academic community is equipped with the opportunity to explore different strategies but sometimes lacks the infrastructure and computational power to resolve complex modelling problems. There is a strong need to bridge this

knowledge gap between research groups and engineering applications to ensure the improvement of the product development process.

The non-linearity of dynamic impact in a vehicle crash along with the need for energy absorbing features to establish structural integrity in the vehicle is one part of a larger problem which also involves replication of anthropometric data of a human body model under the crash impact for the analysis of the injury values for different body parts. There is a need to explore hybrid modeling strategies which could combine methodologies reviewed in this paper to achieve the right balance of accuracy and efficiency in the solution; several relevant studies combining different modeling strategies aimed to overcome existing limitations.

This paper provides the concise overview of the existing research and challenges arising in the mathematical modeling of vehicle crashes. We identify possible areas of improvements in this domain and emphasize a strong need to build more confidence towards replacing physical tests with simplified but accurate mathematical models. The literature review conducted in this paper also highlights opportunities for improving mathematical models with vehicle structure and occupants to understand the impact dynamics under different crash scenarios. There is also a need to implement parameter identification strategies which incorporate the non-linear material properties of the front end members in the LMS models and validate them against physical test data. The growing need for infrastructural developments which allow to run finite element simulations on hundreds of parallel CPUs instead of running multiple physical tests to determine crashworthiness requirements calls for research in the area of reliable reduced order FEM models which are computationally less intensive. We also recognize the remarkable advancements in the field of machine learning and data science and the opportunities they bring for the development of robust models for predicting crash responses.

A.5 Acknowledgement

The authors would like to thank University of Agder (Norway) for support during the research and helping us with the resources.

References – Paper A

[1] Paul Du Bois, Clifford C Chou, Bahig B Fileta, Tawfik B Khalil, Albert I King, Hikmat F Mahmood, Harold J Mertz, Jac Wismans, Priya Prasad, and Jamel E Belwafa. Vehicle crashworthiness and occupant protection. 2004.

[2] RS Sharp and JR Goodall. A mathematical model for the simulation of vehicle motions. *Journal of Engineering Mathematics*, 3(3):219–237, 1969.

[3] Douglas R Shier and KT Wallenius. *Applied mathematical modeling: A multidisciplinary approach*. CRC Press, 1999.

[4] G. Marion and D. Lawson. An introduction to mathematical modelling. 2015.

[5] Muthukrishnan Sathyamoorthy. *Nonlinear analysis of structures*, volume 8. CRC Press, 1997.

[6] Herbert Goldstein, Charles Poole, and John Safko. *Classical mechanics, third ed.* Addison Wesley, San Franscisco, 2001.

[7] Tobias Larsson. *Multibody dynamic simulation in product development*. PhD thesis, Luleå University of Technology, 2001.

[8] Homer Rahnejat. Multi-body dynamics: historical evolution and application. *Proceedings of the Institution of Mechanical Engineers, Part C: Journal of Mechanical Engineering Science*, 214(1):149–173, 2000.

[9] Joseph Louis de Lagrange. *Mécanique analytique*, volume 1. Mallet-Bachelier, 1853.

[10] C.A. Coulomb. *Theorie des machines simple*. Bachelier, Paris, 1821.

[11] Leonhard Euler. Novi commentarii academiae scientiarum petropolitanae. *Nr*, 20:189–207, 1776.

[12] Heinrich Hertz, Daniel Evan Jones, and George Adolphus Schott. *Miscellaneous papers*. Macmillan and Company, 1896.

[13] Osborne Reynolds. Iv. on the theory of lubrication and its application to mr. beauchamp tower's experiments, including an experimental determination of the viscosity of olive oil. *Philosophical transactions of the Royal Society of London*, (177):157–234, 1886.

[14] Richard S Hartenberg and Jacques Denavit. A kinematic notation for lower pair mechanisms based on matrices. *Journal of applied mechanics*, 77(2):215–221, 1955.

[15] Ferdinant Wittenbauer. *Graphische Dynamik*. Springer Verlag, Berlin, 1923.

[16] O Fischer. Einführung in die mechanik lebender mechanismen. *Teubner, Leipzig*, 1906.

[17] Leonard Segel. Theoretical prediction and experimental substantiation of the response of the automobile to steering control. *Proceedings of the Institution of Mechanical Engineers: Automobile Division*, 10(1):310–330, 1956.

[18] Nicolae Orlandea, Milton A Chace, and Donald Albert Calahan. A sparsity-oriented approach to the dynamic analysis and design of mechanical systems—part 1. 1977.

[19] Parviz E Nikravesh. Multibody dynamics formulation. In *Grasping in Robotics*, pages 57–76. Springer, 2013.

[20] Stephen A Barley and Robert J Cripps. Executive-centred system design for cad applications. *Computer-aided design*, 24(5):235–242, 1992.

[21] Bernhard Dopker. Developments in interdisciplinary simulation and design software for mechanical systems. *Engineering with computers*, 4(4):229–238, 1988.

[22] RF Portal, JP Dias, and CA Mota Soares. Multibody models for vehicle accident reconstruction. In *ECCM 2006-III European Conference on Computational Mechanics-Solids, Structures and Coupled Problems in Engineering*, 2006.

[23] W Kortum and RS Sharp. Multibody computer codes in vehicle system dynamics: Supplement to vehicle system dynamics, vol 22. 1993. 1973.

[24] S Hegazy, Homer Rahnejat, and Khalid Hussain. Multi-body dynamics in full-vehicle handling analysis. *Proceedings of the Institution of Mechanical Engineers, Part K: Journal of Multi-body Dynamics*, 213(1):19–31, 1999.

[25] Luís Sousa, Paulo Veríssimo, and Jorge Ambrósio. Development of generic multibody road vehicle models for crashworthiness. *Multibody System Dynamics*, 19(1-2):133–158, 2008.

[26] Gagandeep Singh. Short introduction to finite element method. *Norwegian University of Science and Technology*, 2009.

[27] Alexander A-Hrennikov. "solution of problems in elasticity by the framework method. *Journal of Applied Mechanics*, 8:169–175, 1941.

[28] Richard Courant. Variational method for the solution of problems of equilibrium and vibrations. *Bulletin of American Mathematical Society*, 49:1–23, 1943.

[29] Ray W. Clough. The finite element method in plane stress analysis. *Proceedings 2nd ASCE Conference On Electronic Computation*, 1960.

[30] Philipp Spethmann, Stefan H Thomke, and Cornelius Herstatt. The impact of crash simulation on productivity and problem-solving in automotive r&d. Technical report, Working Paper, 2006.

[31] Arzu Eren Şenaras. Parameter optimization using the surface response technique in automated guided vehicles. In *Sustainable Engineering Products and Manufacturing Technologies*, pages 187–197. Elsevier, 2019.

[32] George EP Box and Kenneth B Wilson. On the experimental attainment of optimum conditions. *Journal of the royal statistical society: Series b (Methodological)*, 13(1):1–38, 1951.

[33] Raymond H Myers, Andre I Khuri, and Walter H Carter. Response surface methodology: 1966-1986. Technical report, Florida Univ Gainesville Dept of Statistics, 1986.

[34] Golnaz Shahidi and Shamim N Pakzad. Response surface model updating for nonlinear structures. In *Topics in Dynamics of Civil Structures, Volume 4*, pages 283–288. Springer, 2013.

[35] Lei Gu, Ren-Jye Yang, Guosong Li, and T Tyan. Structural optimization for crash pulse. *SAE transactions*, pages 786–792, 2005.

[36] David C. Cox and Paul Baybutt. Methods for uncertainty analysis: A comparative survey. *Risk analysis*, 1(4):251–258, 2006.

[37] Zoulong Wei. *Analysis, Modeling and CAE Validation of Vehicle Crashes using Advanced Signal Processing Tools*. PhD thesis, University of Agder, 2017.

[38] Mounir M Kamal. Analysis and simulation of vehicle to barrier impact. *SAE Transactions*, pages 1498–1503, 1970.

[39] Lavinia Graff, Helmut Harbrecht, and Markus Zimmermann. On the computation of solution spaces in high dimensions. *Structural and Multidisciplinary Optimization*, 54(4):811–829, 2016.

[40] Lavinia Graff. *A stochastic algorithm for the identification of solution spaces in high-dimensional design spaces*. PhD thesis, University of Basel, 2013.

[41] Stuart G Mentzer, Randa A Radwan, and William T Hollowell. The sisame methodology for extraction of optimal lumped parameter structural crash models. Technical report, SAE Technical Paper, 1992.

[42] Wichai Cheva, Tsuyoshi Yasuki, Vikas Gupta, and Kolita Mendis. Vehicle development for frontal/offset crash using lumped parameter modeling. Technical report, SAE Technical Paper, 1996.

[43] Mustafa Elkady, Ahmed Elmarakbi, and Dave Crolla. A numerical study for optimizing vehicle dynamics control systems in offset impacts. Technical report, SAE Technical Paper, 2011.

[44] Mustafa Elkady, Ahmed Elmarakbi, and John MacIntyre. The influence of a vehicle dynamics control system on the occupant's dynamic response during a vehicle collision. *Proceedings of the Institution of Mechanical Engineers, Part D: Journal of automobile engineering*, 226(11):1454–1471, 2012.

[45] Mustafa Elkady, Ahmed Elmarakbi, and John MacIntyre. Enhancement of vehicle safety and improving vehicle yaw behaviour due to offset collisions using vehicle dynamics. *International journal of vehicle safety*, 6(2):110–133, 2012.

[46] Mustafa Elkady and Ahmed Elmarakbi. Modelling and analysis of vehicle crash system integrated with different vdcs under high speed impacts. *Central European Journal of Engineering*, 2(4):585–602, 2012.

[47] Ahmed Elmarakbi, Mustafa Elkady, and John MacIntyre. Numerical analysis of vehicle-to-vehicle impact using vehicle dynamics control systems for collision mitigation. *International Journal of Dynamics and Control*, 1(2):172–191, 2013.

[48] AM Elmarakbi and JW Zu. Crashworthiness improvement of vehicle-to-rigid fixed barrier in full frontal impact using novel vehicle's front-end structures. *International journal of automotive technology*, 6(5):491–499, 2005.

[49] Radu Alexandru Ionut, Cofaru Corneliu, and Tolea Bogdan. Mathematical model validated by a crash test for studying the occupant's kinematics and dynamics in a cars' frontal collision. *International Journal of Automotive Technology*, 18 (6):1017–1025, 2017.

[50] A Deb and KC Srinivas. Development of a new lumped-parameter model for vehicle side-impact safety simulation. *Proceedings of the Institution of Mechanical Engineers, Part D: Journal of Automobile Engineering*, 222(10): 1793–1811, 2008.

[51] L Prochowski, M Ziubiński, and T Pusty. Experimental and analytic determining of the characteristics of deformation and side stiffness of a motor car body based on results of side-impact crash tests. In *IOP Conference Series: Materials Science and Engineering*, volume 421, page 032025. IOP Publishing, 2018.

[52] Pär Jonsén, Erik Isaksson, Karl-Gustaf Sundin, and Mats Oldenburg. Identification of lumped parameter automotive crash models for bumper system development. *International Journal of Crashworthiness*, 14(6):533–541, 2009.

[53] Jorge Ambrosio and J Dias. A road vehicle multibody model for crash simulation based on the plastic hinges approach to structural deformations. *International Journal of Crashworthiness*, 12(1):77–92, 2007.

[54] Marta Carvalho and Jorge Ambrósio. Identification of multibody vehicle models for crash analysis using an optimization methodology. *Multibody System Dynamics*, 24(3):325–345, 2010.

[55] Albert I King, Clifford C Chou, and James A Mackinder. Mathematical model of an airbag for a three-dimensional occupant simulation. Technical report, SAE Technical Paper, 1972.

[56] Mohamed TZ Hassan, Mo Gabriel Shi, and SA Meguid. Nonlinear multibody dynamics and finite element modeling of occupant response: part i—rear vehicle collision. *International Journal of Mechanics and Materials in Design*, 15(1): 3–21, 2019.

[57] Mo Gabriel Shi, Mohamed TZ Hassan, and SA Meguid. Nonlinear multibody dynamics and finite element modeling of occupant response: part ii—frontal and lateral vehicle collisions. *International Journal of Mechanics and Materials in Design*, 15:23–41, 2019.

[58] DJ Benson and JO Hallquist. The application of dyna3d in large scale crashworthiness calculations, lawrence livermore national laboratory. *Report No. UCRL*, 94028, 1986.

[59] AB Pifko and R Winter. Theory and application of finite element analysis to structural crash simulation. In *Computational Methods in Nonlinear Structural and Solid Mechanics*, pages 277–285. Elsevier, 1981.

[60] Curd-Sigmund Böttcher, Steffen Frik, and Bernd Gosolits. 20 years of crash simulation at opel-experiences for future challenges, 2005.

[61] Thomas Kiefer, Peter Erb, Bernd Gosolits, and Radu Visinescu. Simulation of airbag sensing signals using finite element method. In *LS-DYNA User Forum*, 2004.

[62] Gulshan Noorsumar, Kjell Robbersmyr, Svitlana Rogovchenko, and Dmitry Vysochinskiy. Crash response of a repaired vehicle-influence of welding uhss members. Technical report, SAE Technical Paper, 2020.

[63] Steven W Kirkpatrick, Robert MacNeill, and Robert T Bocchieri. Development of an ls-dyna occupant model for use in crash analyses of roadside safety features. In *Transportation Research Board 82nd Annual Meeting, Washington, DC, Jan*, pages 12–16. Citeseer, 2003.

[64] I Putu Alit Putra. An average female head-neck finite element model with reflexive neck muscles. Technical report, Chalmers University of Technology, 2020.

[65] Mark Howard, Alan Thomas, Werner Koch, James Watson, and Roger Hardy. Validation and application of a finite element pedestrian humanoid model for use in pedestrian accident simulations. In *Proceedings of IRCOBI Conference*, pages 101–119, 2000.

[66] Wansoo Pak, Yunzhu Meng, Jeremy Schap, Bharath Koya, Scott F Gayzik, and Costin D Untaroiu. Finite element model of a high-stature male pedestrian for simulating car-to-pedestrian collisions. *International journal of automotive technology*, 20(3):445–453, 2019.

[67] Yunzhu Meng, Wansoo Pak, Berkan Guleyupoglu, Bharath Koya, F Scott Gayzik, and Costin D Untaroiu. A finite element model of a six-year-old child for simulating pedestrian accidents. *Accident Analysis & Prevention*, 98:206–213, 2017.

[68] Karthik Ramaswamy, Jayaraj Radhakrishnan, Bhaskar Patham, and Vesna Savic. Fast and stable quasi-static bending simulations in ls-dyna: Identification of optimal finite element model parameters. Technical report, SAE Technical Paper, 2016.

[69] Shusuke Numata, Koji Mizuno, Daisuke Ito, Dai Okumura, and Hisashi Kinoshita. Validation of crush energy calculation methods for use in accident reconstructions by finite element analysis. *SAE International journal of transportation safety*, 6(2):133–146, 2018.

[70] Chao Yu, Fang Wang, Bingyu Wang, Guibing Li, and Fan Li. A computational biomechanics human body model coupling finite element and multibody segments for assessment of head/brain injuries in car-to-pedestrian collisions. *International journal of environmental research and public health*, 17(2):492, 2020.

[71] Yang Xueyan, Qian Yubin, and Wang Ying. Establishment and verification of finite element model of pedestrian head based on accident reconstruction. In *2019 2nd World Conference on Mechanical Engineering and Intelligent Manufacturing (WCMEIM)*, pages 716–721. IEEE, 2019.

[72] T Omar, A Eskandarian, and N Bedewi. Vehicle crash modelling using recurrent neural networks. *Mathematical and computer Modelling*, 28(9):31–42, 1998.

[73] Joseph C Free, James W Hall, and Cesar A Montano. Identification of mathematical models from impact data: application to thoracic impact. Technical report, SAE Technical Paper, 1976.

[74] Mahmoud Yousef Ghannam, Todd Clark, Yeruva Reddy, and Jinkoo Lee. A study of crash energy and severity in frontal vehicle-to-vehicle crash tests. Technical report, SAE Technical Paper, 2011.

[75] Bernard B Mnyazikwiye, Hamid R Karimi, and Kjell Gunnar Robbersmyr. Mathematical modeling of vehicle frontal crash by a double spring-mass-damper model. In *2013 XXIV International Conference on Information, Communication and Automation Technologies (ICAT)*, pages 1–6. IEEE, 2013.

[76] Bernard B Munyazikwiye, Hamid R Karimi, and Kjell G Robbersmyr. Application of genetic algorithm on parameter optimization of three vehicle crash scenarios. *IFAC-PapersOnLine*, 50(1):3697–3701, 2017.

[77] Fatih Usta, Zana Eren, Hasan Kurtaran, Halit S Türkmen, Zafer Kazancı, and Zahit Mecitoglu. Crashworthiness optimization of nested and concentric circular tubes using response surface methodology and genetic algorithm. *Latin American Journal of Solids and Structures*, 15(5), 2018.

[78] Matthew Huang. *Vehicle crash mechanics*. CRC press, 2002.

[79] Ronald Lee Woolley. Crash pulse modeling of force limiting structures. Technical report, SAE Technical Paper, 2008.

[80] Zhiqing Cheng. Analysis of automobile crash responses using wavelets. *SAE Transactions*, pages 285–291, 2002.

[81] MS Varat and Stein E Husher. Crash pulse modelling for vehicle safety research. In *Proceedings: International technical conference on the enhanced safety of vehicles*, volume 2003, pages 9–p. National Highway Traffic Safety Administration, 2003.

[82] Z Wei, HR Karimi, and KG Robbersmyr. A model of vehicle-fixed barrier frontal crash and its application in the estimation of crash kinematics. In *ESV Conference, Seoul, South Korea*, 2015.

Paper B

A novel technique for modeling vehicle crash using lumped parameter models

Gulshan Noorsumar, Svitlana Rogovchenko, Kjell G. Robbersmyr, Dmitry Vysochinskiy and Andreas Klausen

This paper has been published as:

Gulshan Noorsumar, Svitlana Rogovchenko, Kjell G. Robbersmyr, Dmitry Vysochinskiy and Andreas Klausen. A novel technique for modeling vehicle crash using lumped parameter models. *Proceedings of the 11th International Conference on Simulation and Modeling Methodologies, Technologies and Applications - SIMULTECH,*, ISBN 978-989-758-528-9; ISSN 2184-2841, pages 62-70, 2021. doi: 10.5220/0010529200620070.

A novel technique for modeling vehicle crash using lumped parameter models

Gulshan Noorsumar, Svitlana Rogovchenko, Kjell G. Robbersmyr, Dmitry Vysochinskiy and Andreas Klausen

Department of Engineering Sciences
University of Agder
4879 Grimstad, Norway

Abstract **This paper presents a novel technique for modeling a full frontal vehicle crash. The crash event is divided into two phases; the first until maximum crush and the second part when the vehicle starts pitching forward. This novel technique will help develop a three degrees of freedom (DOF) lumped parameter model (LPM) for crash and support in the vehicle development process. The paper also highlights the design process for reducing vehicle pitching in occupant protection load cases. The model has been validated against a finite element (FE) simulation of a full frontal crash of a Chevrolet Silverado developed by the National Highway Traffic Safety Administration (NHTSA), and the LPM shows good correlation with the FE test data.**

B.1 Introduction

Vehicle crashes have been among the major causes of mortality in recent times [1]. In October 2015, the European Commission had launched a study to identify the most common crash scenarios leading to serious injuries in a vehicle crash. The results of this study point to the fact that a frontal crash is the most common crash scenario, followed by a side impact, where occupants are severely injured [2]. Euro NCAP is a voluntary car safety assessment program introduced to ensure safer cars for occupants and vulnerable road users. This program has been instrumental in driving regulations across the globe and improving vehicle safety standards. During the past decades, several crash mitigation and avoidance techniques have been employed by vehicle design engineers to meet these stringent regulations. The vehicle front-end and side structures have been modified to improve energy absorption capability [3]. Vehicle design engineers have resorted to various methodologies to improve the vehicle structure to absorb energy in case of a crash and prevent intrusions in the occupant compartment. These methodologies have been partially successful in

replacing full-time physical tests in the vehicle development process. The vehicle industry still conducts a lot of physical crash tests to validate the crash response generated from mathematical models.

One of the recent approaches is using finite element methods (FEM) to model the full vehicle impact scenario and conduct simulations to predict the vehicle and occupant injury values. Benson et al. [4] presented the calculations of crashworthiness design thereby, laying the foundations for application of FEM in the automotive industry. This technique has high accuracy in predicting injury values, however the process involves manual efforts and is computationally intensive. Lumped parameter models (LPM) were first used in modeling vehicle crash by [5]. In this paper the vehicle was represented by three lumped mass components and eight resistances representing the deformable parts in the vehicle. Mentzer et al. [6] employed real time crash data to determine parameters for LPM used to represent the crash scenario. The force deformation curves derived from these models helped determine predictive models aiding in vehicle development.

Recently, LPMs were used by Elkady et al. to develop a multi-DOF mathematical model to simulate a crash event with active vehicle dynamics control systems (VDCS) [3, 7]. The model replicated a full frontal and offset impact between two vehicles and compared the performance of a baseline vehicle with a vehicle equipped with VDCS features. It also includes a 3-DOF occupant impact model using Lagrangian formulation. Munyazikwiye et al. use a mass-spring-damper model with two lumped mass components representing a vehicle impacting a rigid barrier. After identifying the parameters, the model in this study shows good correlation with test data which demonstrates that a simple LPM can be used to represent the impact dynamics successfully [8]. Multi body modeling has also been used in the past for simulating vehicle dynamics model for realistic applications [9].

Occupant injury prediction is an area of research where the vehicle-occupant interaction in a vehicle impact scenario is studied and the injury patterns of occupants in the car are determined with mathematical models. Large vehicle deceleration has been identified as one of the main causes of head and chest injuries, and vehicle rotational motions in different axis also lead to occupant injuries [10]. In a full frontal impact, vehicle pitch and drop are significantly greater compared to rolling and yawing motions. In the recent past, increasing focus on unbelted occupants to meet FMVSS 208 (Federal Motor Vehicle Safety Standards) requirements has led researchers to observe that vehicle pitch and drop contributed to higher head and neck injury values. The objective of a vehicle structure is not just to absorb energy and optimize crash pulses, but also to minimize vehicle pitch and drop [10, 11]. Chang et al. have developed an FE model to study vehicle pitch and drop in body-on-frame vehicles. The model is correlated to barrier tests and also tries to predict factors

affecting vehicle pitch and drop in a crash event [12]. The research from Chang et al. points to the fact that design of vehicle rails plays an important role in the load distribution during an impact scenario for body-on-frame vehicles. The out-of-plane bending of the vehicle rails increases the role of a vertical component of the barrier force, causing an imbalance in the vehicle, leading to forward pitching on the vehicle. Wei et al. have estimated the relationship between energy absorbing components and the crash pulse, establishing the fact that the bumper and the front rails both significantly contributing to the energy absorption in a full frontal crash event [13].

In this paper, we simplify the system by splitting the vehicle motion into two phases corresponding to

- the horizontal linear motion, and
- the rotation of the vehicle body.

We have decided to replicate a full frontal vehicle crash event at 56 kilometers per hour (kmph) employing an LPM with multiple DOFs to predict

- the maximum deformation in the vehicle to absorb energy, and
- the pitch angle of the vehicle due to the crash response.

B.2 Methodology

Literature documents that a crash event leads to pitching, rolling and yawing of the vehicle along with the deceleration of the vehicle and movement in horizontal and vertical directions. It is difficult to model the impact scenario in different axes and generating the governing equations. It was also observed that the time for the vehicle to attain minimum velocity after impact also coincides with the maximum deformation on the vehicle.

In this study, we separate the horizontal translational motion from the vertical motion during the impact event. In a full frontal crash event the vehicle is observed to be experiencing forward pitching; whereas the effect of rolling and yawing can be neglected. Taking into account these assumptions we split the crash event into two phases:

- time till maximum deformation and minimum vehicle velocity after start of crash event t_1, and
- time after maximum deformation to the end of the crash event t_2.

B.2.0.1 FEM Simulations

In this study, finite element simulation for a 2014 Chevrolet Silverado [14] running at 56 kmph and hitting a frontal barrier at 0% offset was conducted. The FE model was developed by National Crash Analysis Center (NCAC) in collaboration with NHTSA (National Highway Traffic Safety Administration) through the reverse engineering process [14]. The FE model consisting of 1476 parts, 2,741,848 nodes and 2,870,507 elements has been correlated to NHTSA Oblique Test and Insurance Institute for Highway Safety (IIHS) Small Overlap Front Test. The FE model weighs 2582 kg which is close to the physical test vehicle weighing 2624 kg. It replicates the material and geometrical properties of the physical vehicle [15].

The FE model was run on LS-DYNA with 32 CPUs in an HPC environment and the corresponding curves generated were used for the parameter estimation and validation of the LPM in MATLAB Simulink. In the FE simulation, the acceleration of some nodes on the vehicle body are recorded by the solver LS-DYNA. These nodes are selected by the user at the preprocessing stage. This process was employed to determine the acceleration of the vehicle CG as well as the barrier forces, to be used for validation in this study. Figure B.1 shows the FE model used in the simulations.

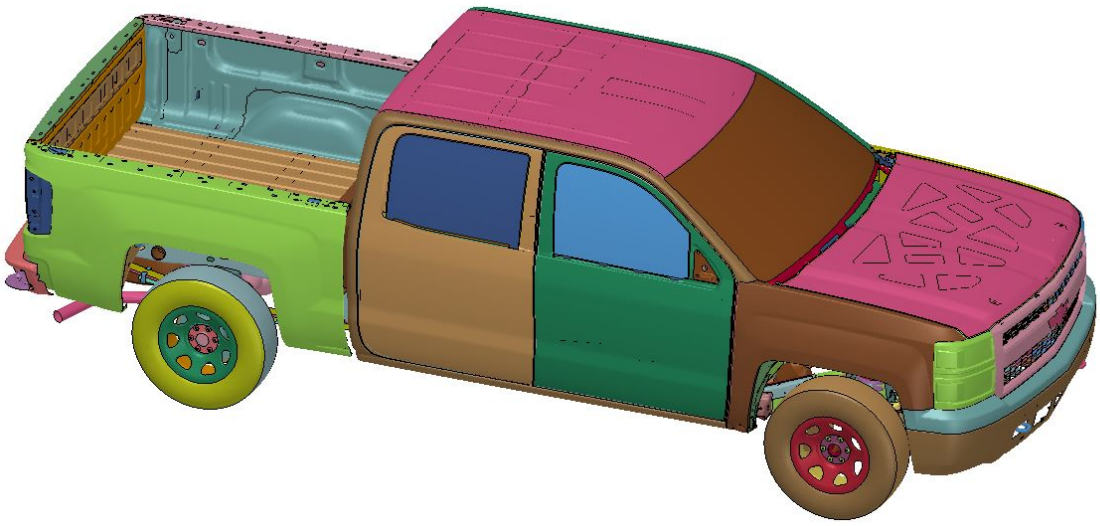

Figure B.1: FE Model of a 2014 Chevrolet Silverado developed by NCAC

This FE model generated the piecewise linear curve data for spring and damper coefficients. The algorithm uses Newton-Euler numerical integration to achieve the computed values and predict the time for maximum dynamic crush of the vehicle. The algorithm developed is explained in the next section.

B.2.1 Lumped parameter model

The LPM developed is a single-mass system with a spring and damper unit in the front, known as Kelvin model, representing the bumper system and the deformable system. The front springs allow translational motion only in the direction of x-axis [16]. The suspension of the vehicle is represented by a pair of springs and dampers which allow translation in the vertical z-axis and rotation around the y-axis. The center of mass of the vehicle has 3 DOFs making this system fairly complex to solve in a single system. The lumped mass body can move in the direction of horizontal (x) and vertical (z) axes along with rotation around one (y) axis. The center of gravity (CG) of the vehicle is located at a distance l_f from the front end and l_r from the rear end suspension points. The distance l_0 represents the distance of the CG from the front occupant compartment zone.

B.2.2 Vehicle Crash Model - Phase I

First we model only the translational movement of the vehicle along the horizontal axis and hitting the barrier at 0% offset. The mathematical model is developed in Simulink which replicates the maximum vehicle deformation till the time of maximum crush t_m. This value also corresponds to the time when the vehicle attains zero or minimum velocity. It should be noted that the vehicle may not achieve zero velocity by the time of maximum deformation if the vehicle front end is not able to absorb energy to undergo plastic deformation. The mathematical model uses a single DOF equation with a front spring-damper unit. The stiffness of the spring is tuned to represent the maximum deformation of the vehicle at a particular speed. For this problem we have assumed a speed of 56 kmph (NHTSA regulations for frontal crash). The motion of suspension system in the model has been neglected during this phase of the event scenario. Figure B.2 represents the vehicle in a deformed state. The Simulink model predicts the time till maximum deformation of the vehicle and the maximum displacement of the vehicle CG.

The prediction of the values of spring deformation coefficient k and damper coefficient c used in the general equation of motion have been a challenge for researchers in the past [17], [18]. There have been several parameter estimation studies conducted in the past to determine the stiffness of the vehicle front in a crash event. The behaviour of the front end system is highly nonlinear but it has been approximated by a piecewise linear relationship [19, 20].

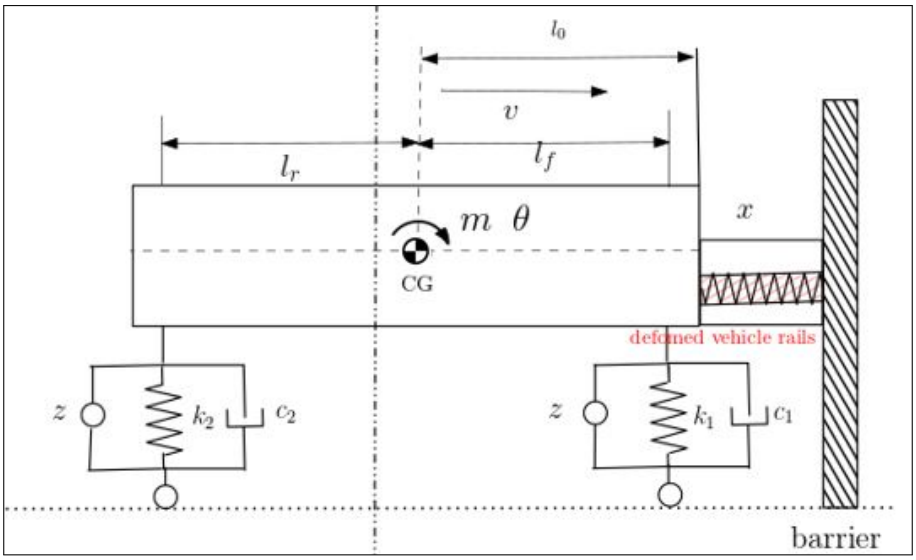

Figure B.2: Vehicle representation in Phase 1 of the event: Deformed front end

Equation of Motion:

$$m\ddot{x} + c\dot{x} + kx = Q_i \tag{B.1}$$

where, $Q_i = 0$ (i.e. no force component is added here); k is the spring coefficient; c is the damper coefficient for the bumper model.

In the model developed for the first phase, the spring and damper coefficients are parameterized using a gradient-descent optimization algorithm developed in [21] for a single mass-spring-damper system. The code searches for a global minima by performing 100 re-runs of gradient descent optimization, each with randomly generated initial parameter values. The algorithm was modified to improve the correlation between the test and computed values. The non-linear force-deformation curve for spring-damper system has been assumed to be piecewise-linear with six breakpoints in the curve. The forces on the spring are calculated using the general relationship between the force and deformation for a spring-damper system [3], see Figure B.3. The stiffness of the spring k and the spring force component F_k vary according to the deflection values in the spring and are defined as follows.

The spring stiffness and damping coefficients in the model, are defined as the

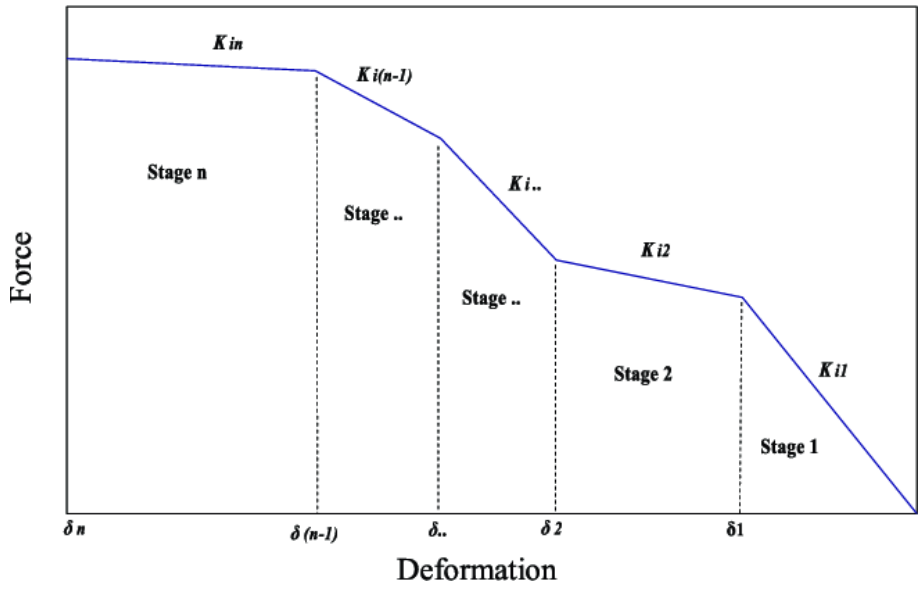

Figure B.3: General piecewise force-deformation characteristics [3].

piecewise-linear functions of x and $\dot{x}$, respectively. These functions are:

$$k(x) = \begin{cases} \frac{(k_2-k_1)\cdot|\hat{x}|}{x_1} + k_1 & \text{for, } |\hat{x}| \leq x_1, \\ \frac{(k_3-k_2)\cdot(|\hat{x}|-x_1)}{(x_2-x_1)} + k_2 & \text{for, } x_1 \leq |\hat{x}| \leq x_2 \\ \frac{(k_4-k_3)\cdot(|\hat{x}|-x_2)}{(x_3-x_2)} + k_3 & \text{for, } x_2 \leq |\hat{x}| \leq x_3 \\ \frac{(k_5-k_4)\cdot(|\hat{x}|-x_3)}{(x_4-x_3)} + k_4 & \text{for, } x_3 \leq |\hat{x}| \leq x_4 \\ \frac{(k_6-k_5)\cdot(|\hat{x}|-x_4)}{(x_5-x_4)} + k_5 & \text{for, } x_4 \leq |\hat{x}| \leq x_5 \\ \frac{(k_7-k_6)\cdot(|\hat{x}|-x_5)}{(C-x_5)} + k_6 & \text{for, } x_5 \leq |\hat{x}| \leq C \end{cases}$$

The damper characteristics are defined similar to the spring characteristics in the model

$$c(\dot{x}) = \begin{cases} \frac{(c_2-c_1)\cdot|\hat{\dot{x}}|}{\dot{x}_1} + c_1 & \text{for, } |\hat{\dot{x}}| \leq \dot{x}_1, \\ \frac{(c_3-c_2)\cdot(|\hat{\dot{x}}|-\dot{x}_1)}{(\dot{x}_2-\dot{x}_1)} + c_2 & \text{for, } \dot{x}_1 \leq |\hat{\dot{x}}| \leq \dot{x}_2 \\ \frac{(c_4-c_3)\cdot(|\hat{\dot{x}}|-\dot{x}_2)}{(\dot{x}_3-\dot{x}_2)} + c_3 & \text{for, } \dot{x}_2 \leq |\hat{\dot{x}}| \leq \dot{x}_3 \\ \frac{(c_5-c_4)\cdot(|\hat{\dot{x}}|-\dot{x}_3)}{(\dot{x}_4-\dot{x}_3)} + c_4 & \text{for, } \dot{x}_3 \leq |\hat{\dot{x}}| \leq \dot{x}_4 \\ \frac{(c_6-c_5)\cdot(|\hat{\dot{x}}|-\dot{x}_4)}{(\dot{x}_5-\dot{x}_4)} + c_5 & \text{for, } \dot{x}_4 \leq |\hat{\dot{x}}| \leq \dot{x}_5 \\ \frac{(c_7-c_6)\cdot(|\hat{\dot{x}}|-\dot{x}_5)}{(v_0-\dot{x}_5)} + c_6 & \text{for, } \dot{x}_5 \leq |\hat{\dot{x}}| \leq v_0 \end{cases}$$

where, k is the spring coefficient; c is the damper coefficient; $\hat{x}$ is the computed vehicle deformation; $\dot{x}$ is the vehicle velocity; $\hat{\dot{x}}$ is the computed vehicle velocity; v_0 is the velocity at the time of maximum dynamic crush; C is the maximum dynamic crush;

F_k and F_c are the built-up spring and damping forces defined by the following equations

$$F_k = k(x) \cdot x, \tag{B.2}$$

$$F_c = c(\dot{x}) \cdot \dot{x} \tag{B.3}$$

The proposed algorithm uses an optimization approach to minimize an objective function. The objective function to be minimized is the error function $E(\Theta, t)$ where Θ denotes the unknown variables in the mode. The error function is defined as follows:

$$E(\Theta, t) = E_1(\Theta, t) + E_2(\Theta, t) + E_3(\Theta, t), \text{where} \tag{B.4a}$$

$$E_1(\Theta, t) = |(a_{FE} - a_{LPM})| \tag{B.4b}$$

$$E_2(\Theta, t) = |(v_{FE} - v_{LPM})| \tag{B.4c}$$

$$E_3(\Theta, t) = |(x_{FE} - x_{LPM})| \tag{B.4d}$$

where, a is the acceleration; v is the vehicle velocity; and x is the displacement.

The error function $E(\Theta, t)$ determines the difference between the FE and computed values at every point, and the optimization algorithm tries to minimize these error values by altering $\Theta = [k_i, c_i] \, \forall i \in [1, 7]$. The corresponding spring and damper coefficient values developed from this minimization algorithm have been discussed in

the results section of the paper.

B.2.3 Vehicle Crash Model - Phase II

The second phase for the model describes what happens after the instant the vehicle achieves maximum dynamic crush and minimum velocity. The vehicle starts to pitch forward at this instant. Several studies were conducted to understand the reason behind the vehicle pitching forward [10, 12], suggesting that for body-on-frame vehicles one of the reasons is the out of plane bending in vehicle rails leading to a vertical force component in the moment balance equation. The vertical force component is added to gravity force acting downwards and creates an imbalance of loading which leads to the vehicle pitching. The prediction of this pitching angle is important for determining the injury to occupants and a low pitching angle influences occupant protection design in a vehicle. In this phase of the event as shown in Figure B.4 and Figure B.5, we consider only vertical motion of the suspension springs and a rotation about the y-axis with angle θ.

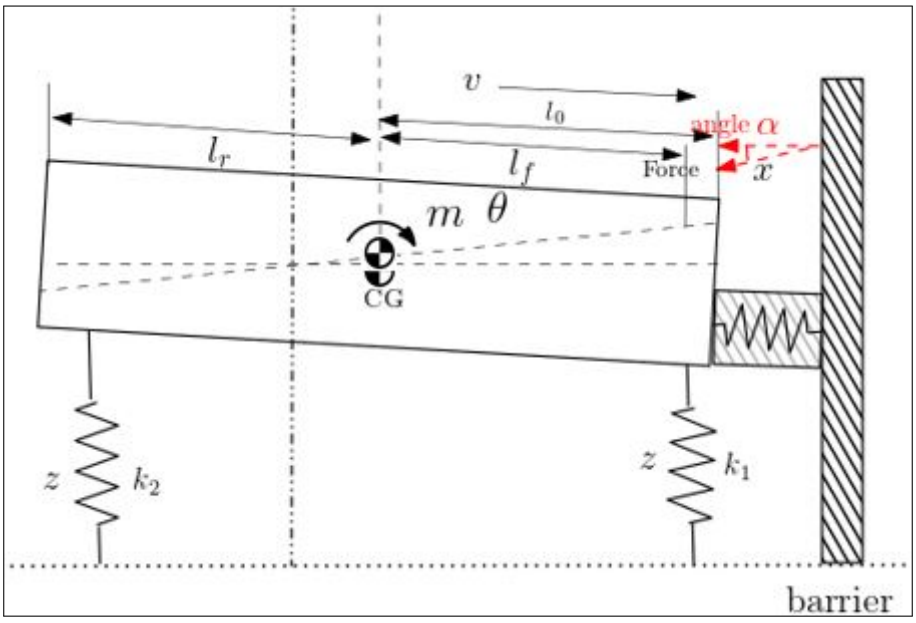

Figure B.4: Vehicle representation in Phase II of the event: Vehicle Pitching forward

$$\frac{d}{dt}\frac{\partial L}{\partial \dot{q}_i} - \frac{\partial L}{\partial q_i} + \frac{\partial D}{\partial q_i} = Q_i \tag{B.5}$$

where, in the general case, $L = T - V$, T is the total kinetic energy of the system equal to the sum of the kinetic energies of the particles, $q_i\, i = 1..n$ are generalized coordinates and V is the potential energy of the system. For dissipation forces a special function D must be introduced alongside L, Q_i is the external force acting on the system, which in this case is the vertical force component experienced by the vehicle at the time of maximum dynamic crush.

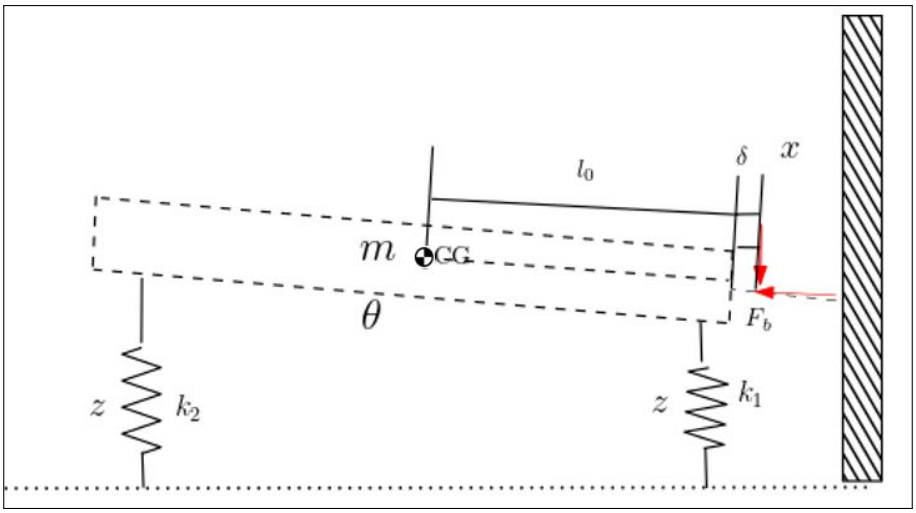

Figure B.5: Vehicle representation in Phase II with forces acting on the vehicle and suspension springs in play

Kinetic Energy:

$$T = \frac{1}{2}J\dot{\theta}^2 + \frac{1}{2}m\dot{x}^2 \tag{B.6}$$

Potential Energy :

$$V = \frac{1}{2}k_1(x - l_f\theta)^2 + \frac{1}{2}k_2(x + l_r\theta)^2 \tag{B.7}$$

Dissipation Energy :

$$D = \frac{1}{2}c_1(\dot{x} - l_f\dot{\theta})^2 + \frac{1}{2}c_2(\dot{x} + l_r\dot{\theta})^2 \tag{B.8}$$

The values of k_1, k_2, c_1, c_2, l_f and l_r are taken from standard automotive parameters from literature data [22]. Table B.1 shows the parameter values adopted from this study.

The value of the vehicle mass m and the moment of inertia J for the lumped mass system has been calculated from the FE model of the vehicle. The governing equations of motion are

$$\begin{aligned} Q_i =& J\ddot{\theta} + (k_1l_f^2 + k_2l_r^2)\theta + (c_1l_f^2 + c_2l_r^2)\dot{\theta} \\ &+ (k_2l_r - k_1l_f)x + (c_2l_r - c_1l_f)\dot{x} \end{aligned} \tag{B.9}$$

$$\begin{aligned} Q_i =& m\ddot{x} + (k_1 + k_2)x + (c_1l_f + c_2l_r)\dot{\theta} \\ &+ (k_2l_r - k_1l_f)\theta + (c_1 + c_2)\dot{x} \end{aligned} \tag{B.10}$$

Table B.1: Automotive Parameters set [22]

Symbol	Value	Unit	Meaning
M	400	kg	Sprung mass
m_{ij}	50	kg	Unsprung masses (i = front, rear and j = left, right)
I_x	250	kg.m^2	Roll inertia
I_y	1400	kg.m^2	Pitch inertia
t	1.4	m	Front and rear axle
l_f	1.4	m	COG-front distance
l_r	1	m	COG-rear distance
r	0.3	m	Nominal wheel radius
h	0.7	m	Chassis COG height
k_f	30,000	N/m	Front suspension linearized stiffness (left, right)
k_r	20,000	N/m	Rear suspension linearized stiffness (left, right)
c_f	1500	N/m/s	Front suspension linearized damping (left, right)
c_r	3000	N/m/s	Rear suspension linearized damping (left, right)
k_t	200,000	N/m	Tire stiffness (front, rear and left, right)
β	50	rad/s	Suspension actuator bandwidth

B.3 Results and Discussion

In this section we compare the results of the LPM model with FE data generated from LS-DYNA simulations for a Chevrolet Silverado vehicle at 56kmph with a full frontal impact loadcase.

B.3.1 Phase I

As mentioned in the previous section, Part I of the event simulates the time till maximum deformation of the vehicle; the spring and damper coefficients are determined using the Gradient Descent Optimization with an error function explained in the previous section. The computed and test (FE) values are plotted in Figure B.6 and shows good correlation of results. The algorithm predicts the stiffness and damping coefficient values as shown in Figures B.7 and B.8.

The output from the Gradient Descent Optimization algorithm is used to predict the deformation and vehicle velocity in a MATLAB Simulink model;

Figure B.9 shows a plot of maximum vehicle deformation vs test deformation and the plot shows good correlation. A similar plot (Figure B.10) was generated to

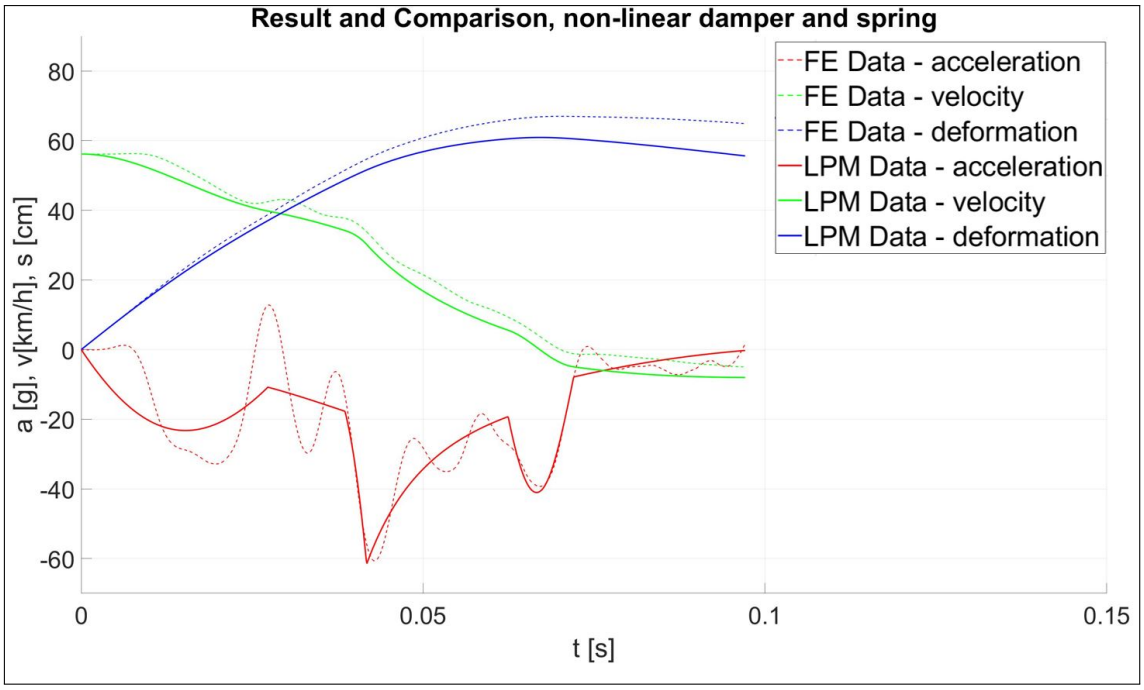

Figure B.6: Plot of computed and test values for parameter model

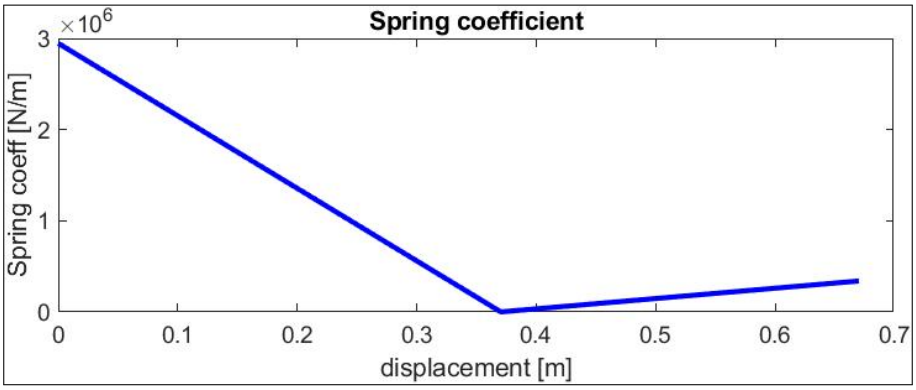

Figure B.7: Spring coefficient obtained from the algorithm

compare the velocity of the vehicle at the CG (in the case of LPM at the CG of the lumped mass). The time the vehicle attains zero velocity is similar in the plots but there is a small difference after 0.04s. The reason for this deviation can be attributed to the spring and damper characteristics which are approximated for this study using a piece-wise linear function. The model can be improved using a non-linear function for the spring stiffness and damping characteristics. If the model is simulated beyond the time the vehicle attains zero velocity, a rebound is observed in the velocity. This velocity rebound could be due to the internal strain energy store in the springs, and it would be interesting to investigate this further in future research.

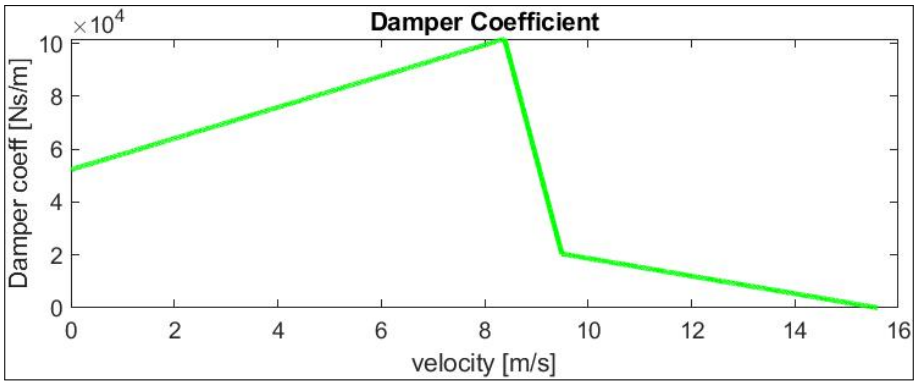

Figure B.8: Damper Coefficient obtained from the algorithm

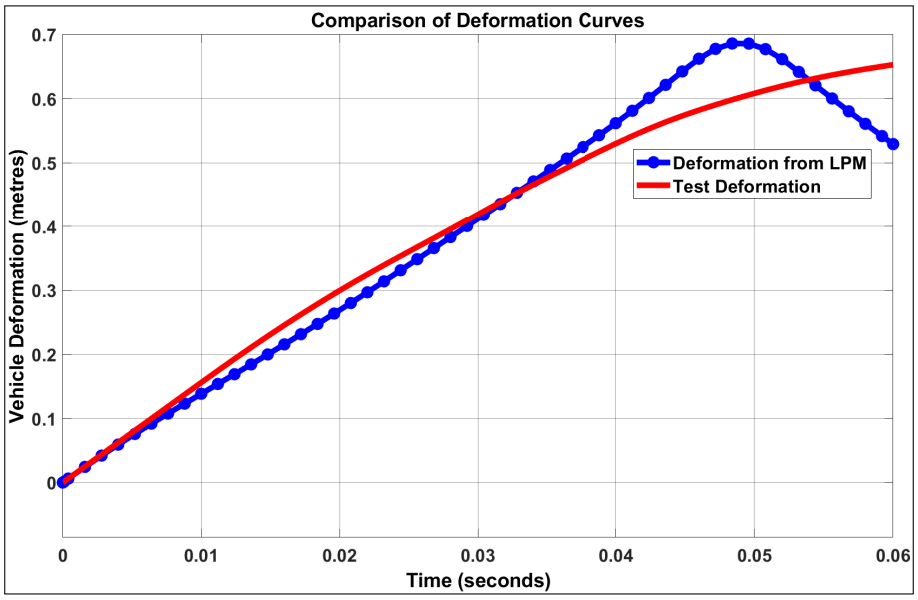

Figure B.9: Displacement of the vehicle CG curves comparison for LPM vs FE model

B.3.2 Phase II

The prediction for the second part of the model using Simulink was conducted and plotted against the data from FE model. The force Q_i in the governing equations is the vertical component of the barrier force experienced by the vehicle in the crash. The force curve is derived from the FE model and inputted into the Simulink model to improve prediction. However, it will be of interest to mathematically explain this force component in terms of residual impact energy after absorption. The Simulink model is run with numerical integration (variable timestep- ode 45) and the velocity of the lumped mass in z-direction along with the pitching angle is compared to data from FE model.The comparison with other numerical integration methods was kept out of scope of this study.

Figure B.11 compares the forward pitching angle for the FE model and the LPM developed in this study. The pitch angle comparison shows a similar trend observed in both the curves; the vehicle starts to pitch around the same time during the crash

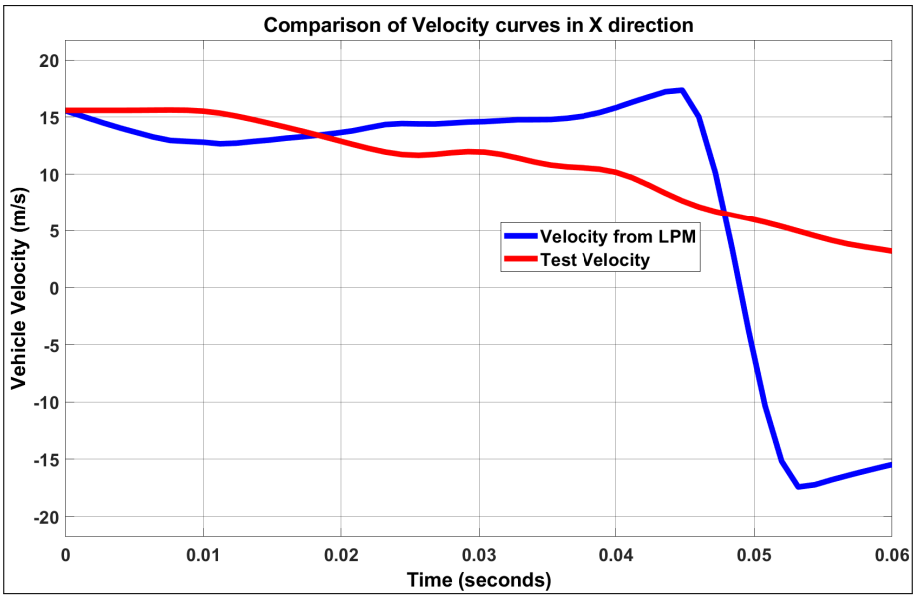

Figure B.10: X-Velocity curve comparison for LPM vs FE model

event which is crucial to designers planning airbag deployment in vehicles and other active features on cars. The pitch angle curve for the simulation LPM peaks higher than the FE data at the start of the vehicle rotation but slowly follows the FE data curve showing comparable maximum pitch angle values which is also an important observation for a vehicle safety design team. The linear approximation for the spring and damper coefficients can be a contributing factor to the difference in the values between the curves along with the barrier force definition in the model. There might be energy losses in the model which have not been accounted for in this study.

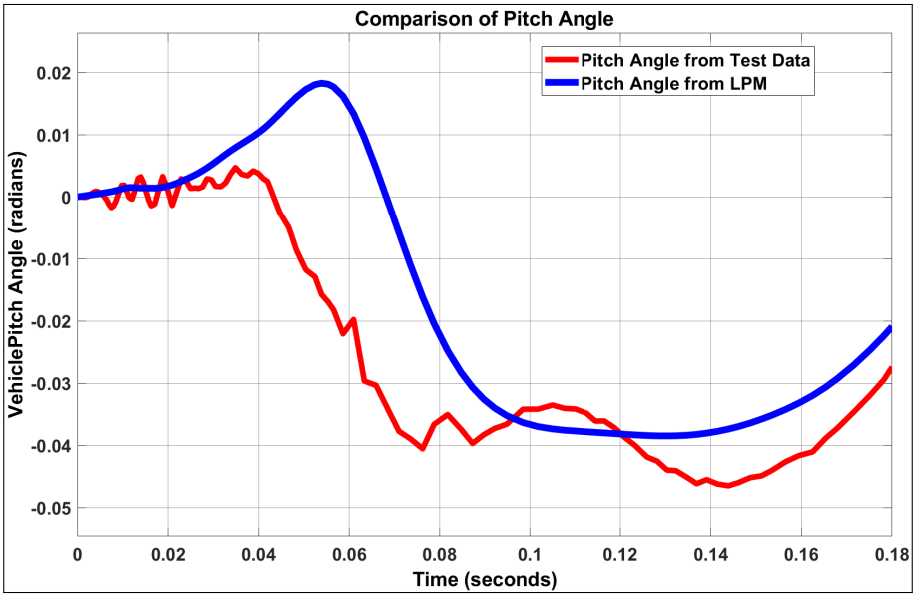

Figure B.11: Forward Pitch Angle curve overlay for LPM vs FE model

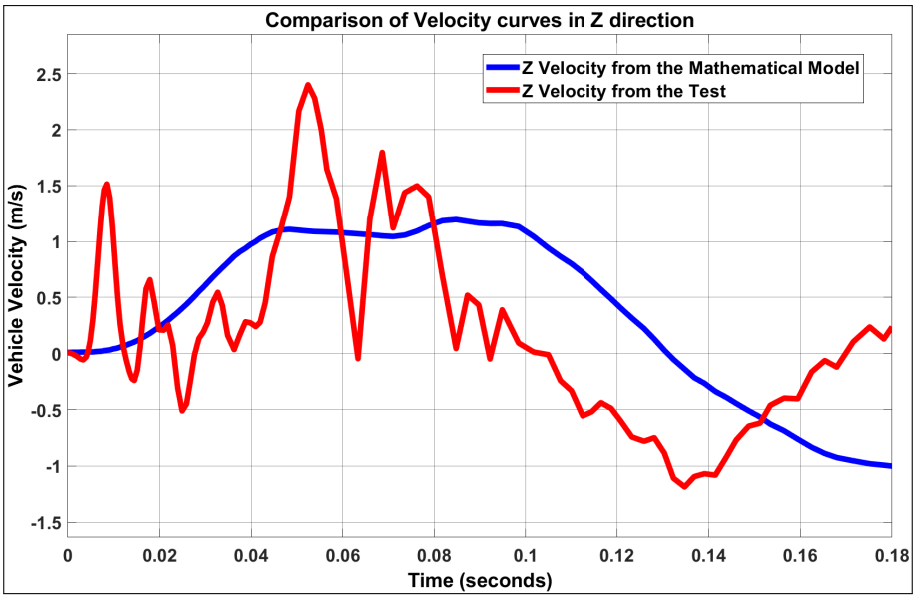

Figure B.12: Z-Velocity curve comparison for LPM vs FE model

Figure B.12 compares the z-velocity (vertical velocity) in the body with the curves generated from FE data. The trend in the curve is similar but the peak values are not matching in this simulation model. One of the contributing factors to this deviation is the use of standard linear spring and damper coefficient values for the model (used from literature data). The linear value for the spring and damper coefficients can lead to the difference in the values for this parameter as well. The values of l_f and l_r can also be tuned further to represent the Chevrolet Silverado (2014) model used in this study. However, the authors have intentionally avoided fine tuning these values assuming that this data may not be available to vehicle development team at the start of the design process. This makes it inevitable to use standard values for automotive parameters.

B.4 Conclusion and Next steps

The novel technique developed in this paper for modeling a full frontal vehicle crash event successfully predicts the event kinematics. The study demonstrates that the two phase simulation model can describe a highly complex dynamical multiple DOF system with few equations and parameters, making the process of using LPMs very simple and reliable for safety design engineers. The study also highlights that parameter identification is an important part of accident reconstruction process and its correlation has an influence on the deformation and velocity during vehicle crash. One of the major implications from the model developed in this study is the design of vehicle rails, as a contributing factor to vehicle pitching forward.

This assumption used to arrive at a simpler LPM model providing reliable results

include the following:

- The spring and damper characteristics are assumed to be piecewise-linear with six breakpoints although they are non-linear in physical systems.
- The vehicle acceleration is assumed to be zero at the time pitching starts in the crash event.
- Energy losses like friction and heat losses in the vehicle during the crash event are neglected to simplify the problem.
- Only vehicle rotations about the y-axis (pitching) are considered for modeling in the full frontal impact scenario; rotations about other axes are considered negligible and not impacting the occupant injuries.

B.5 Acknowledgments

The authors would like to thank University of Agder for the support to conduct this research.

References – Paper B

[1] Paul Du Bois, Clifford C Chou, Bahig B Fileta, Tawfik B Khalil, Albert I King, Hikmat F Mahmood, Harold J Mertz, Jac Wismans, Priya Prasad, and Jamel E Belwafa. Vehicle crashworthiness and occupant protection. 2004.

[2] Gulshan Noorsumar, Kjell Robbersmyr, Svitlana Rogovchenko, and Dmitry Vysochinskiy. Crash response of a repaired vehicle-influence of welding uhss members. Technical report, SAE Technical Paper, 2020.

[3] Mustafa Elkady and Ahmed Elmarakbi. Modelling and analysis of vehicle crash system integrated with different vdcs under high speed impacts. *Open Engineering*, 2(4):585–602, 2012.

[4] DJ Benson, JO Hallquist, M Igarashi, K Shimomaki, and M Mizuno. Application of dyna3d in large scale crashworthiness calculations. Technical report, Lawrence Livermore National Lab., 1986.

[5] Mounir M Kamal. Analysis and simulation of vehicle to barrier impact. *SAE Transactions*, pages 1498–1503, 1970.

[6] Stuart G Mentzer, Randa A Radwan, and William T Hollowell. The sisame methodology for extraction of optimal lumped parameter structural crash models. Technical report, SAE Technical Paper, 1992.

[7] Mustafa Elkady, Ahmed Elmarakbi, and John MacIntyre. Enhancement of vehicle safety and improving vehicle yaw behaviour due to offset collisions using vehicle dynamics. *International journal of vehicle safety*, 6(2):110–133, 2012.

[8] Bernard B Munyazikwiye, Hamid R Karimi, and Kjell Gunnar Robbersmyr. Mathematical modeling of vehicle frontal crash by a double spring-mass-damper model. In *2013 XXIV International Conference on Information, Communication and Automation Technologies (ICAT)*, pages 1–6. IEEE, 2013.

[9] Peter Riegl and Andreas Gaull. Modeling and validation of a complex vehicle dynamics model for real-time applications. In *Proceedings of 8th International*

Conference on Simulation and Modeling Methodologies, Technologies and Applications - SIMULTECH,, pages 403–413. INSTICC, SciTePress, 2018. ISBN 978-989-758-323-0. doi: 10.5220/0006856304030413.

[10] J Michael Chang, Mohammad Ali, Ryan Craig, Tau Tyan, Marwan El-Bkaily, and James Cheng. Important modeling practices in cae simulation for vehicle pitch and drop. *SAE Transactions*, pages 62–72, 2006.

[11] Gernot Woitsch and Wolfgang Sinz. Influence of pitching and yawing during frontal passenger vehicle crash tests on driver occupant's kinematics and injury. *International journal of crashworthiness*, 18(4):356–370, 2013.

[12] J Michael Chang, Mohammed Rahman, Mohammad Ali, Tau Tyan, Marwan El-Bkaily, and James Cheng. Modeling and design for vehicle pitch and drop of body-on-frame vehicles. *SAE transactions*, pages 329–338, 2005.

[13] Zuolong Wei, Hamid Reza Karimi, and Kjell Gunnar Robbersmyr. Analysis of the relationship between energy absorbing components and vehicle crash response. Technical report, SAE Technical Paper, 2016.

[14] National Highway Traffic Safety Administration et al. Crash simulation vehicle models. *URL: https://www. nhtsa. gov/research-data/databasesand-software*, 2016.

[15] Harry Singh, Velayudham Ganesan, James Davies, Mahendran Paramasuwom, Lorenz Gradischnig, Patrick Wood, and Vikrant Mogal. Structural countermeasure/research program mass and cost increase due to oblique offset moving deformable barrier impact test. Technical report, 2018.

[16] Matthew Huang. *Vehicle crash mechanics*. CRC press, 2002.

[17] Javad Marzbanrad and Mostafa Pahlavani. A system identification algorithm for vehicle lumped parameter model in crash analysis. *International Journal of Modeling and Optimization*, 1(2):163, 2011.

[18] Witold Pawlus, Hamid Reza Karimi, and Kjell Gunnar Robbersmyr. Development of lumped-parameter mathematical models for a vehicle localized impact. *Journal of mechanical science and technology*, 25(7):1737–1747, 2011.

[19] Bernard B Munyazikwiye, Hamid R Karimi, and Kjell G Robbersmyr. Application of genetic algorithm on parameter optimization of three vehicle crash scenarios. *IFAC-PapersOnLine*, 50(1):3697–3701, 2017.

[20] Bernard B Munyazikwiye, Dmitry Vysochinskiy, Mikhail Khadyko, and Kjell G Robbersmyr. Prediction of vehicle crashworthiness parameters using piecewise lumped parameters and finite element models. *Designs*, 2(4):43, 2018.

[21] Andreas Klausen, Sondre Sanden Tørdal, Hamid Reza Karimi, Kjell G Robbersmyr, Mladen Ječmenica, and Ole Melteig. Mathematical modeling and optimization of a vehicle crash test based on a single-mass. In *Proceeding of the 11th World Congress on Intelligent Control and Automation*, pages 3588–3593. IEEE, 2014.

[22] Sergio M Savaresi, Charles Poussot-Vassal, Cristiano Spelta, Olivier Sename, and Luc Dugard. *Semi-active suspension control design for vehicles*. Elsevier, 2010.

Paper C

Development and extended validation of a lumped parameter prediction model for analysing injury parameters in a vehicle crash

Gulshan Noorsumar, Svitlana Rogovchenko, Kjell G. Robbersmyr, Dmitry Vysochinskiy and Andreas Klausen

This paper has been published as:

Gulshan Noorsumar, Svitlana Rogovchenko, Kjell G. Robbersmyr, Dmitry Vysochinskiy and Andreas Klausen. Development and extended validation of a lumped parameter prediction model for analysing injury parameters in a vehicle crash. Submitted to *Lecture Notes in Networks and Systems - Springer*.

Development and extended validation of a lumped parameter prediction model for analysing injury parameters in a vehicle crash

Gulshan Noorsumar[1], Svitlana Rogovchenko[1], Kjell G. Robbersmyr[1], Dmitry Vysochinskiy[1] and Andreas Klausen[2]

[1]Department of Engineering Sciences
University of Agder

[2]MotionTech, Norway

Abstract **We present a lumped parameter model (LPM) for improving vehicle crashworthiness analysis. The novel methodology divides the event into two phases: until maximum crush and when the vehicle starts pitching forward. We built a three degrees of freedom (DOF) model for the analysis of a crash event supporting the vehicle development process. The model has been validated against the National Highway Traffic Safety Administration (NHTSA) finite element (FE) simulation of a truck and a sedan. The LPM shows good correlation with the FE test data. A parameter variation study, changing the thickness of the metal parts by 10% and 20%, is presented to improve the vehicle crash performance resulting in the reduction in pitching of the vehicle. The Simulink based simulation captures the change in the performance confirming the reliability of the model to predict event kinematics.**

C.1 Introduction

Each year 1.23 million people are reported to die in road accidents and vehicle crashes have been among the major causes of mortality [1]. Even a larger number of people suffers from non-fatal injuries with many incurring a disability due to the injury. Production of vehicles that ensure safety for all road users including occupants is crucial to reduce the road related injuries.

Most vehicle safety regulations require crash testing at a specialized facility to determine the crashworthiness parameters. Car manufacturers conduct full vehicle or Vulnerable Road User (VRU) tests to ensure that the car design meets the regulations. Usually, crash-testing is time consuming and costly. Mathematical models are employed to represent crash dynamics, for example, in the case of a car impacting a barrier or another car. These models involve differential equations of

motion describing the deformation of the parts in the vehicle. The occupants inside the car can also be included in a mathematical model to predict injury values during a crash, models of a human present a valuable complement to other models, such as animal models and crash dummies. The vehicle front-end and side structures have been modified to improve energy absorption capability [2]. Finite Element Methods (FEM) have received impetus in vehicle crash modeling in the past decades. With improved computational speeds the models became more accurate and reliable for vehicle development. Benson et al. [3] presented the calculations of crashworthiness design laying the foundations for application of FEM in the automotive industry. However, development of FE models is time-consuming and needs CAD data which is not available during the early stages of vehicle design. Lumped parameter models (LPM) were first applied for modeling vehicle crash events in [4] where the vehicle was represented by three lumped mass components and eight resistances representing the deformable parts in the vehicle. The citeCd paper paved the way for many more studies using LPMs to represent the behaviour of a vehicle and occupants under impact. Recently, LPMs were used by Elkady et al. [2, 5] to develop a multi-DOF mathematical model to simulate a crash event with active vehicle dynamics control systems (VDCS). The model replicated a full frontal and offset impact between two vehicles comparing the performance of a baseline vehicle with a vehicle equipped with VDCS features. It also includes a 3-DOF occupant impact model derived using Lagrangian formulation. Munyazikwiye et al. [6] use a mass-spring-damper model with two lumped mass components to represent a full frontal impact with a rigid barrier. The study shows good correlation with test data suggesting that a simple LPM can replicate the impact kinematics successfully.

Occupant injury prediction is an important area of research where the vehicle-occupant interaction in a vehicle impact scenario is studied and the injury patterns of occupants in the car are determined with a help of mathematical models. Large vehicle deceleration has been identified as one of the main causes of head and chest injuries, and vehicle rotational motions in different axes also lead to occupant injuries [7].

In a full frontal impact, vehicle pitch and drop are significantly larger compared to rolling and yawing motions. Neck injury is one of the most common types of injury in vehicle accidents [8]. In a vehicle crash, unbelted occupants could interact with the vehicle interiors leading to severe injuries. In the recent past, the research focusing on unbelted occupants to meet Federal Motor Vehicle Safety Standards (FMVSS 208) requirements demonstrated that vehicle pitch and drop contributed to higher head and neck injury values.

The objective of a vehicle structure is not just to absorb energy and optimize crash pulses, but also to minimize vehicle pitch and drop [7, 9]. Chang et al. [10] have

developed an FE model to study vehicle pitch and drop in body-on-frame vehicles. The model is correlated to barrier tests and predicts factors affecting vehicle pitch and drop in a crash event. This research points to the fact that design of vehicle rails plays an important role in the load distribution during an impact scenario for body-on-frame vehicles. The out-of-plane bending of the vehicle rails increases the role of a vertical component of the barrier force, causing an imbalance in the vehicle, leading to forward pitching on the vehicle. Wei et al. [11] have estimated the relationship between energy absorbing components and the crash pulse, establishing that the bumper and the front rails both significantly contribute to the energy absorption in a full frontal crash event.

Researchers use different methodologies to improve vehicle crashworthiness modifying the vehicle structure or materials used to manufacture different vehicle parts. Genetic algorithm to estimate and optimize the vehicle parameters for a vehicle-vehicle impact was used in [12]. Li et al. [13] used lightweight optimization and material modification to meet crashworthiness requirements balancing contradictory vehicle dynamics and fuel economy requirements. The design optimization using a DOE to develop surrogate models reducing the pitch and drop in an FE model that improves interactions between the occupant's head and vehicle interior parts was presented in [14]. Our paper is an extension of the work presented by the authors at the conference SIMULTECH 2021 [15]. The model developed has been extended to validate a sedan FE model. We establish the robustness of the model to predict the impact of changes in stiffness of the vehicle on the reduction of vehicle pitching. To this end, we simplify the system splitting the vehicle motion into two phases as in [15]:

- the horizontal linear motion, and
- the rotation of the vehicle body.

We replicate a full frontal vehicle crash event at 56 kilometers per hour (kmph) employing an LPM with multiple DOFs to predict

- the maximum deformation in the vehicle to absorb energy, and
- the pitch angle of the vehicle due to the crash response.

The model has been validated with a 2014 pickup truck (Chevrolet Silverado) and a 2010 sedan (Toyota Yaris). FE model simulations of the two cars were used to compare the LPM results. The Toyota Yaris FE model has also been modified to study stiffness variations in the crashworthiness of the vehicle. The LPM is robust to predict the changes in stiffness of the vehicle making this model suitable for prediction of injury parameters in a vehicle crash.

C.2 Methodology

Literature documents that a crash event leads to pitching, rolling and yawing of the vehicle along with the deceleration of the vehicle and movement in horizontal and vertical directions. It is difficult to model the impact scenario in different axes and to generate the governing equations. It was observed that the time for the vehicle to attain minimum velocity after impact coincides with the maximum deformation on the vehicle.

In this study, we separate the horizontal translational motion from the vertical motion during the impact event. In a full frontal crash event the vehicle experiences forward pitching; whereas the effect of rolling and yawing can be neglected. Taking into account these assumptions we split the crash event into two phases:

- time interval until maximum deformation and minimum vehicle velocity after start of crash event t_1, and
- time interval after maximum deformation to the end of the crash event t_2.

C.2.1 FEM Simulations for Validation

We conducted a FE simulation for a 2014 Chevrolet Silverado and a 2010 Toyota Yaris running at 56 kmph and hitting a frontal barrier at 0% offset. These FE models were developed by National Crash Analysis Center (NCAC) in collaboration with NHTSA (National Highway Traffic Safety Administration) through the reverse engineering process [16].

Chevrolet Silverado model The FE model in Figure C.1 consisting of 1,476 parts, 2,741,848 nodes and 2,870,507 elements has been correlated to NHTSA Oblique Test and Insurance Institute for Highway Safety (IIHS) Small Overlap Front Test. The FE model weighs 2,582 kg which is close to the physical test vehicle weighing 2,624 kg. It replicates the material and geometrical properties of the physical vehicle [17].

Toyota Yaris model The FE model replicates a 2010 four-door passenger sedan consisting of 917 parts, 1,480,422 nodes and 1,514,068 elements. The FE model weighs 1,100 kg which is close to the physical test vehicle weighing 1,078 kg. The validation is conducted against an NCAP frontal wall impact with actual data from NHTSA Tests 5677 and 6221. It replicates the material and geometrical properties of the physical vehicle [18]. The model was also validated against test data from other scenarios. The curves correlate well with the test data and the FE model has been used by several authors [19].

The FE models were run on LS-DYNA with 32 CPUs in an HPC environment and the corresponding curves generated were used for the parameter estimation and

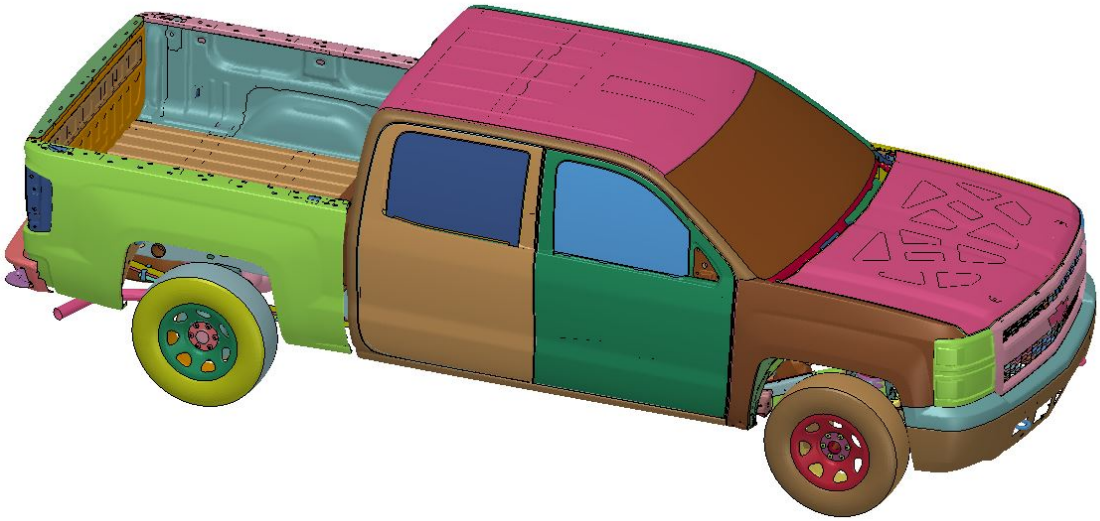

Figure C.1: An FE Model of a 2014 Chevrolet Silverado developed by NCAC [15]

validation of the LPM in MATLAB Simulink. In the FE simulation, the acceleration of some nodes on the vehicle body are recorded by the solver LS-DYNA. These nodes are selected by the user at the pre-processing stage. This process was employed to determine the acceleration of the vehicle center of gravity (CG) as well as the barrier forces, employed for the validation. Figure C.1 and C.2 shows the FE model used in the simulations. These FE model generated the piecewise linear curve data for

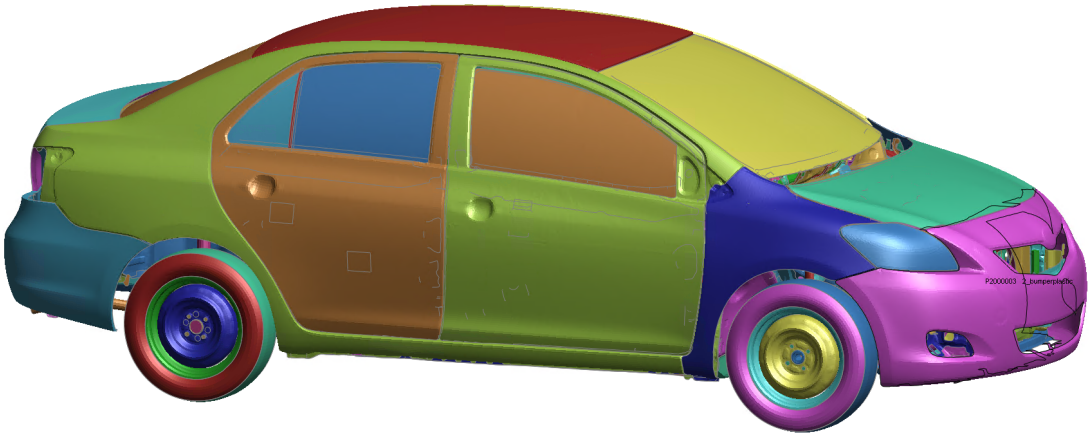

Figure C.2: An FE model of a 2010 Toyota Yaris developed by NCAC

the spring and damper coefficients. Newton-Euler numerical integration is used to calculate the values and predict the time for maximum dynamic crush of the vehicle. The algorithm is discussed in the following section.

The Toyota Yaris FE model was further updated to increase the stiffness by changing the thickness of all the metal parts by 10% and 20%. This was achieved by changing the shell element thickness on the FE regardless of the parts being load bearing or deformable members. The parts undergoing thickness change are

represented in Figure C.3. The increase in vehicle mass, mass moment of inertia and, change in vehicle CG were noted and updated in the LPM. The FE simulations were run and validated against the LPM to compare the performance.

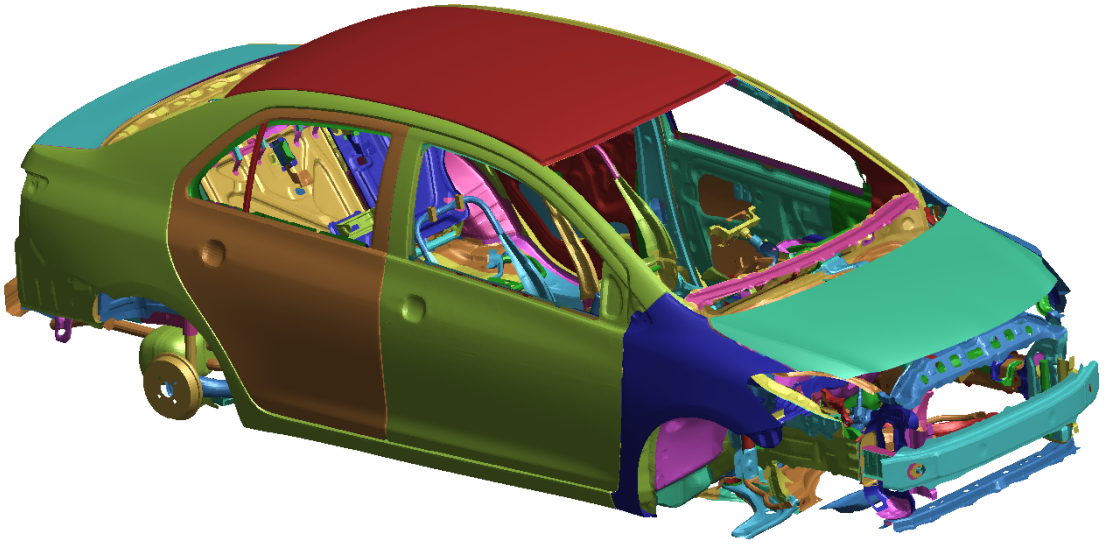

Figure C.3: Toyota Yaris metal parts undergoing thickness change for robustness study

C.2.2 Description of the Lumped parameter model

As a single-mass system, the LPM developed utilizes a spring and damper system in the front side as the bumper and deformable system; this is commonly known as the Kelvin model. The front springs allow translational motion only in the direction of x-axis [20]. There are two pairs of springs and dampers in the suspension of the vehicle, allowing translation in the z axis and rotation around the y-axis. There are three degrees of freedom in this system, making it quite challenging to solve. The lumped mass body can move in the direction of horizontal (x) and vertical (z) axes along with the rotation around one (y) axis. The CG of the vehicle is located at a distance l_f from the front end and l_r from the rear end suspension points; l_0 represents the distance between the CG and the front occupant compartment zone. The two phases are described below.

C.2.3 Vehicle Crash Model - Phase I

First we model only the translational movement along the horizontal axis of the vehicle hitting the barrier at 0% offset. The LPM developed in Simulink replicates the maximum vehicle deformation until the time of maximum crush t_m. Additionally, this value corresponds to the instant the vehicle reaches its zero velocity or minimum speed. If the vehicle front end does not absorb energy by deforming plastically, then

it is possible that it will not reach zero velocity by the time of maximum deformation. A single DOF equation with a spring-damper unit is used in the mathematical model. The stiffness of the spring is tuned to represent the maximum deformation of the vehicle at a particular speed. For this problem we have assumed the speed of 56 kmph (NHTSA regulations for frontal crash). The motion of suspension system in the model has been neglected during this phase of the event. Figure C.4 represents the vehicle in a deformed state. The Simulink model predicts the time until the maximum deformation of the vehicle and the maximum displacement of the vehicle CG.

The prediction of the values of spring deformation coefficient k and damper coefficient c used in the general equation of motion has been a challenge for researchers in the past [21], [22]. The stiffness of the vehicle front in a crash was estimated using various parameter estimation studies. Despite the highly nonlinear behavior of the front end, it was approximated by a piecewise linear relationship [23, 24].

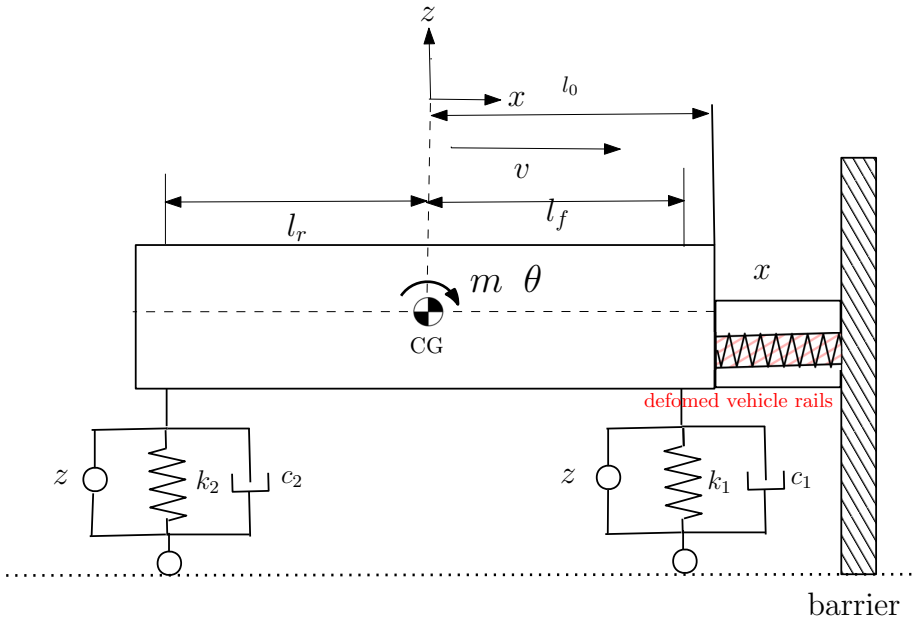

Figure C.4: Vehicle representation in Phase 1 of the event: Deformed front end [15]

In our case the equation of motion assumes the form:

$$m\ddot{x} + c\dot{x} + kx = Q_i \tag{C.1}$$

where $Q_i = 0$ (i.e. no force component is added here); k is the spring coefficient; c is the damper coefficient for the bumper model.

Optimization algorithm

At this stage, the spring and damper coefficients are parameterized using a gradient-descent optimization algorithm developed in [25] for a single mass-spring-damper system. The code searches for a global minima by performing 100 re-runs of gradient

descent optimization, each with randomly generated initial parameter values. The algorithm was modified to improve the correlation between the test and computed values. The non-linear force-deformation curve for the spring-damper system is assumed to be piecewise-linear with six breakpoints in the curve. The forces on the spring are calculated using the general relationship between the force and deformation for a spring-damper system [2], see Figure C.5. The stiffness of the spring k and the spring force component F_k vary according to the deflection values in the spring.

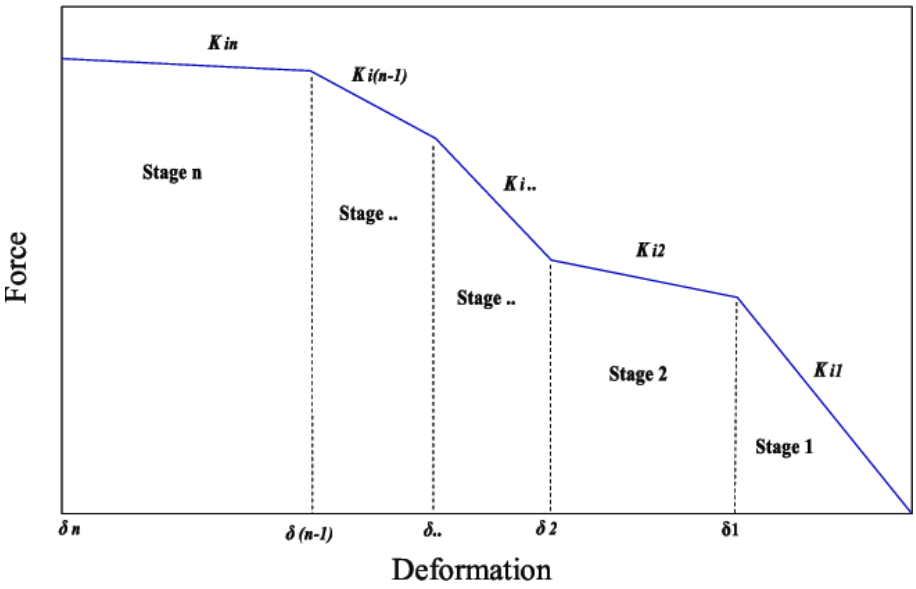

Figure C.5: General piecewise force-deformation characteristics [2], [15]

The spring stiffness and damping coefficients in the model are defined as the piecewise-linear functions of x and $\dot{x}$, respectively:

$$k(x) = \begin{cases} \frac{(k_2-k_1)\cdot|\hat{x}|}{x_1} + k_1, & \text{for } |\hat{x}| \le x_1, \\ \frac{(k_3-k_2)\cdot(|\hat{x}|-x_1)}{(x_2-x_1)} + k_2, & \text{for } x_1 \le |\hat{x}| \le x_2, \\ \frac{(k_4-k_3)\cdot(|\hat{x}|-x_2)}{(x_3-x_2)} + k_3, & \text{for } x_2 \le |\hat{x}| \le x_3, \\ \frac{(k_5-k_4)\cdot(|\hat{x}|-x_3)}{(x_4-x_3)} + k_4, & \text{for } x_3 \le |\hat{x}| \le x_4, \\ \frac{(k_6-k_5)\cdot(|\hat{x}|-x_4)}{(x_5-x_4)} + k_5, & \text{for } x_4 \le |\hat{x}| \le x_5, \\ \frac{(k_7-k_6)\cdot(|\hat{x}|-x_5)}{(C-x_5)} + k_6, & \text{for } x_5 \le |\hat{x}| \le C. \end{cases}$$

The damper characteristics are defined similarly to the spring characteristics:

$$c(\dot{x}) = \begin{cases} \frac{(c_2-c_1)\cdot|\hat{\dot{x}}|}{\dot{x}_1} + c_1, & \text{for } |\hat{\dot{x}}| \leq \dot{x}_1, \\ \frac{(c_3-c_2)\cdot(|\hat{\dot{x}}|-\dot{x}_1)}{(\dot{x}_2-\dot{x}_1)} + c_2, & \text{for } \dot{x}_1 \leq |\hat{\dot{x}}| \leq \dot{x}_2, \\ \frac{(c_4-c_3)\cdot(|\hat{\dot{x}}|-\dot{x}_2)}{(\dot{x}_3-\dot{x}_2)} + c_3, & \text{for } \dot{x}_2 \leq |\hat{\dot{x}}| \leq \dot{x}_3, \\ \frac{(c_5-c_4)\cdot(|\hat{\dot{x}}|-\dot{x}_3)}{(\dot{x}_4-\dot{x}_3)} + c_4, & \text{for } \dot{x}_3 \leq |\hat{\dot{x}}| \leq \dot{x}_4, \\ \frac{(c_6-c_5)\cdot(|\hat{\dot{x}}|-\dot{x}_4)}{(\dot{x}_5-\dot{x}_4)} + c_5, & \text{for } \dot{x}_4 \leq |\hat{\dot{x}}| \leq \dot{x}_5, \\ \frac{(c_7-c_6)\cdot(|\hat{\dot{x}}|-\dot{x}_5)}{(v_0-\dot{x}_5)} + c_6, & \text{for } \dot{x}_5 \leq |\hat{\dot{x}}| \leq v_0, \end{cases}$$

where k is the spring coefficient, c is the damper coefficient, $\hat{x}$ is the computed vehicle deformation, $\dot{x}$ is the vehicle velocity, $\hat{\dot{x}}$ is the computed vehicle velocity, v_0 is the velocity at the time of maximum dynamic crush, C is the maximum dynamic crush, F_k and F_c are the built-up spring and damping forces defined by the following equations

$$F_k = k(x) \cdot x, \tag{C.2}$$

$$F_c = c(\dot{x}) \cdot \dot{x}. \tag{C.3}$$

The proposed algorithm uses an optimization approach to minimize an objective function. The objective function to be minimized is the error function $E(\Theta, t)$ where Θ denotes the unknown variables in the mode. The error function is defined as follows: $E(\Theta, t) = E_1(\Theta, t) + E_2(\Theta, t) + E_3(\Theta, t)$ where

$$E_1(\Theta, t) = |(a_{FE} - a_{LPM})|, \tag{C.4a}$$

$$E_2(\Theta, t) = |(v_{FE} - v_{LPM})|, \tag{C.4b}$$

$$E_3(\Theta, t) = |(x_{FE} - x_{LPM})|, \tag{C.4c}$$

where a is the acceleration, v is the vehicle velocity, and x is the displacement. The error function $E(\Theta, t)$ determines the difference between the FE values and LPM values at every point, and the optimization algorithm minimizes the error values by altering $\Theta = [k_i, c_i], \quad \forall i \in [1, 7]$. The corresponding spring and damper coefficient values obtained from this minimization algorithm are discussed in the results section.

C.2.4 Vehicle Crash Model - Phase II

The second phase for the model describes what happens after the instant the vehicle achieves maximum dynamic crush and minimum velocity. At this instant the vehicle starts to pitch forward. Several studies were conducted to understand the vehicle pitching forward [7, 26] suggesting that for the body-on-frame vehicles one of the reasons is the out-of-plane bending in vehicle rails which leads to the appearance of a vertical force component in the moment balance equation. This vertical force component is added to gravity force acting downwards and creates an imbalance of loading resulting in the vehicle pitching. The prediction of the pitching angle is important for determining the injury to occupants. Low pitching angles influences occupant protection design in a vehicle. This phase of the event is shown in Figure C.6 and Figure C.7. We consider here only vertical motion of the suspension springs and the rotation about the y-axis with angle θ.

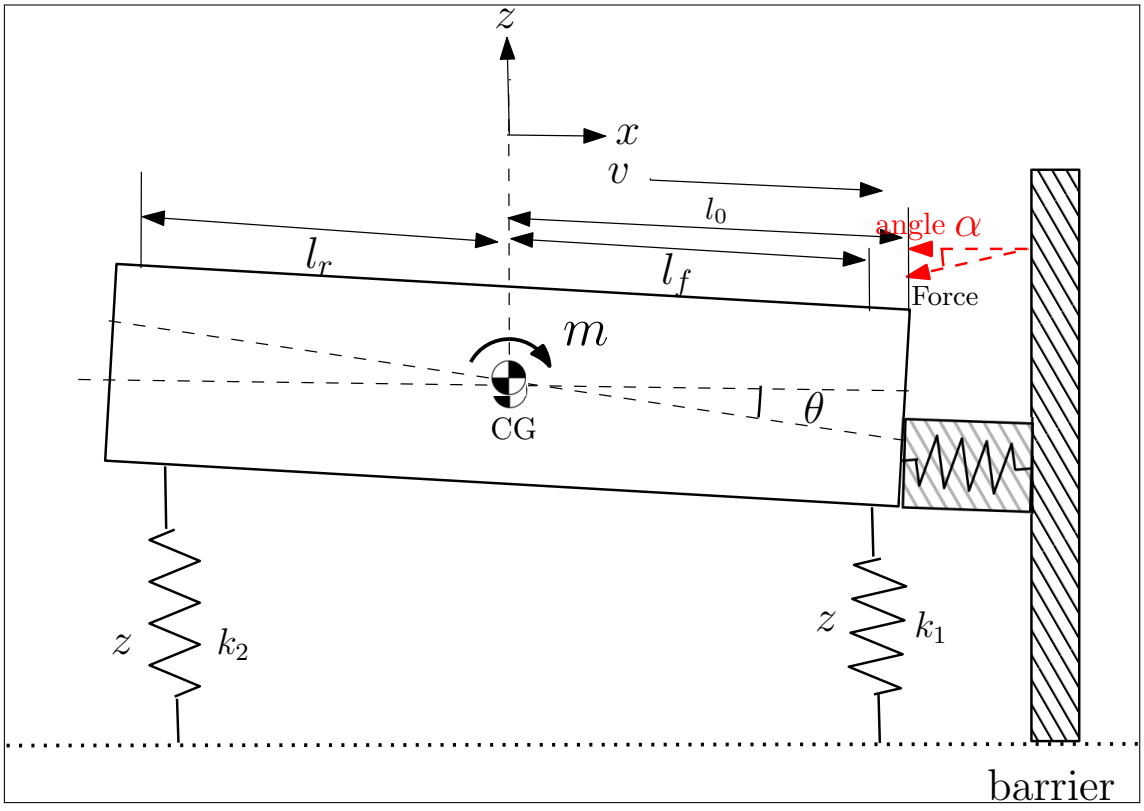

Figure C.6: Vehicle representation in Phase II of the event: Vehicle Pitching forward [15]

The dynamics in the Lagrangian formulation is described by the equation [27]:

$$\frac{d}{dt}\frac{\partial L}{\partial \dot{q}_i} - \frac{\partial L}{\partial q_i} + \frac{\partial D}{\partial q_i} = Q_i \tag{C.5}$$

where, in the general case, $L = T - V$, T is the total kinetic energy of the system

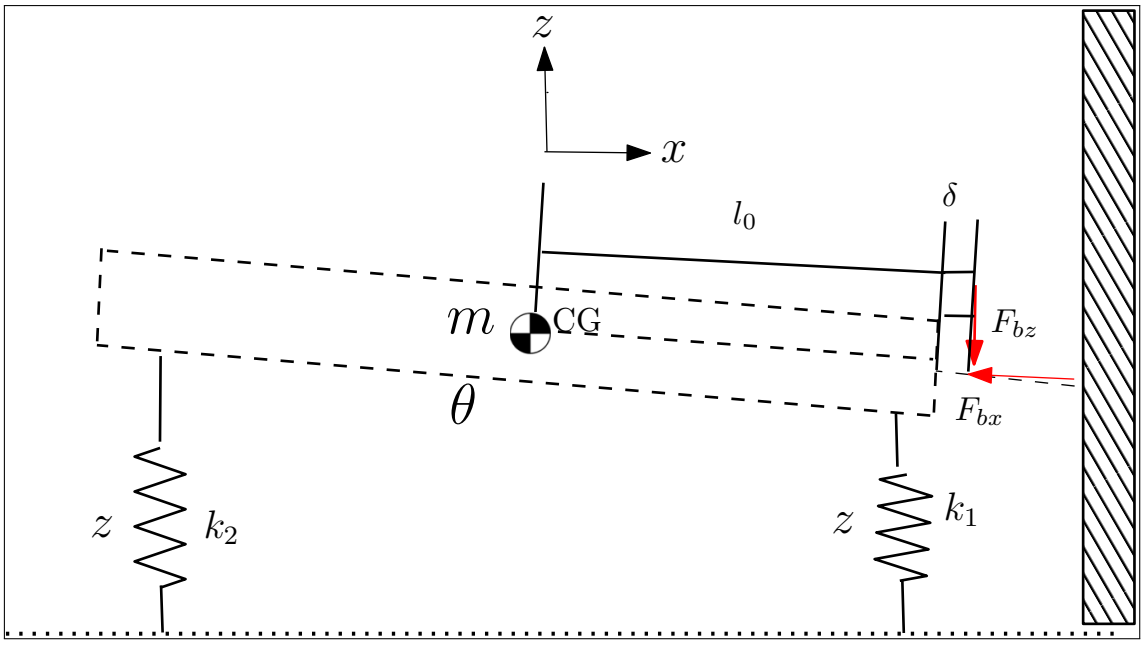

Figure C.7: Vehicle representation in Phase II with forces acting on the vehicle and suspension springs in play [15]

equal to the sum of the kinetic energies of the particles, $q_i\, i = 1, \ldots, n$ are generalized coordinates, Q_i is the external force acting on the system, which in this case is the vertical force component experienced by the vehicle at the time of maximum dynamic crush, and V is the potential energy of the system. For dissipation forces, a special function D must be introduced alongside L.

The equations for the kinetic, potential and dissipation energy are:

$$T = \frac{1}{2}J\dot{\theta}^2 + \frac{1}{2}m\dot{x}^2, \tag{C.6}$$

$$V = \frac{1}{2}k_1(x - l_f\theta)^2 + \frac{1}{2}k_2(x + l_r\theta)^2, \tag{C.7}$$

and

$$D = \frac{1}{2}c_1(\dot{x} - l_f\dot{\theta})^2 + \frac{1}{2}c_2(\dot{x} + l_r\dot{\theta})^2. \tag{C.8}$$

The values of standard automotive parameters k_1, k_2, c_1, c_2, l_f and l_r are taken from the literature, [28], see Table C.1.

Table C.1: Automotive Parameters set [28]

Symbol	Value	Unit	Meaning
M	400	kg	Sprung mass
m_{ij}	50	kg	Unsprung masses (i = front, rear and j = left, right)
I_x	250	kg.m^2	Roll inertia
I_y	1400	kg.m^2	Pitch inertia
t	1.4	m	Front and rear axle
l_f	1.4	m	COG-front distance
l_r	1	m	COG-rear distance
r	0.3	m	Nominal wheel radius
h	0.7	m	Chassis COG height
k_f	30,000	N/m	Front suspension linearized stiffness (left, right)
k_r	20,000	N/m	Rear suspension linearized stiffness (left, right)
c_f	1500	N/m/s	Front suspension linearized damping (left, right)
c_r	3000	N/m/s	Rear suspension linearized damping (left, right)
k_t	200,000	N/m	Tire stiffness (front, rear and left, right)
β	50	rad/s	Suspension actuator bandwidth

The values of the vehicle mass m and the moment of inertia J for the lumped mass system are calculated from the FE model of the vehicle. The governing equations of motion are [15]:

$$\begin{aligned} Q_i =& J\ddot{\theta} + (k_1 l_f^2 + k_2 l_r^2)\theta + (c_1 l_f^2 + c_2 l_r^2)\dot{\theta} \\ &+ (k_2 l_r - k_1 l_f)x + (c_2 l_r - c_1 l_f)\dot{x}, \end{aligned} \tag{C.9}$$

$$\begin{aligned} Q_i =& m\ddot{x} + (k_1 + k_2)x + (c_1 l_f + c_2 l_r)\dot{\theta} \\ &+ (k_2 l_r - k_1 l_f)\theta + (c_1 + c_2)\dot{x}. \end{aligned} \tag{C.10}$$

C.2.5 Robustness Check

The LPM predicts important vehicle parameters, thus, contributing to analysis of vehicle crashworthiness. The model was validated to estimate the injury parameters for a truck and a sedan. The sensitivity of the model to stiffness is assessed by changing the thickness of the material; analyzing the spring and damper coefficient curves generated with the help of the optimization algorithm described in Section C.2.3. The methodology for determining the vehicle parameters (maximum displacement, time for zero velocity and maximum pitch angle) is similar to the baseline model. It is interesting to observe the changes in vehicle pitching angle and acceleration by adding mass to the system in terms of elemental thickness to the metal parts.

The changes in mass and moment of inertia for the model are presented in Table C.2 below. These changes have been incorporated in the LPM to determine injury values.

Table C.2: FE Model specifications

Parameter	Yaris Baseline	10% stiffness	20% stiffness
Mass, (kg)	1253.5	1303.9	1353.6
Mass Moment of Inertia, (kgm^2) (I_{xx})	425128	445472	465782
Vehicle CG x, (mm)	1025	1033.6	1039
Vehicle CG y, (mm)	-3.0	-2.1	-1.5
Vehicle CG z, (mm)	557	560	563 [1ex]

C.3 Results and Discussion

In this section we compare the results of the LPM with FE data generated from LS-DYNA simulations for a Chevrolet Silverado and Toyota Yaris vehicle at 56 kmph with a full frontal impact loadcase.

C.3.1 Phase I

Baseline Chevrolet Silverado Model First we simulate the time until maximum deformation of the vehicle; the spring and damper coefficients are determined using the Gradient Descent Optimization with an error function defined in Section C.2.3. The computed and test (FE) values are plotted in Figure C.8; They show good correlation of results. The predicted values of the stiffness and damping coefficients are shown in Figures C.9 and C.10.

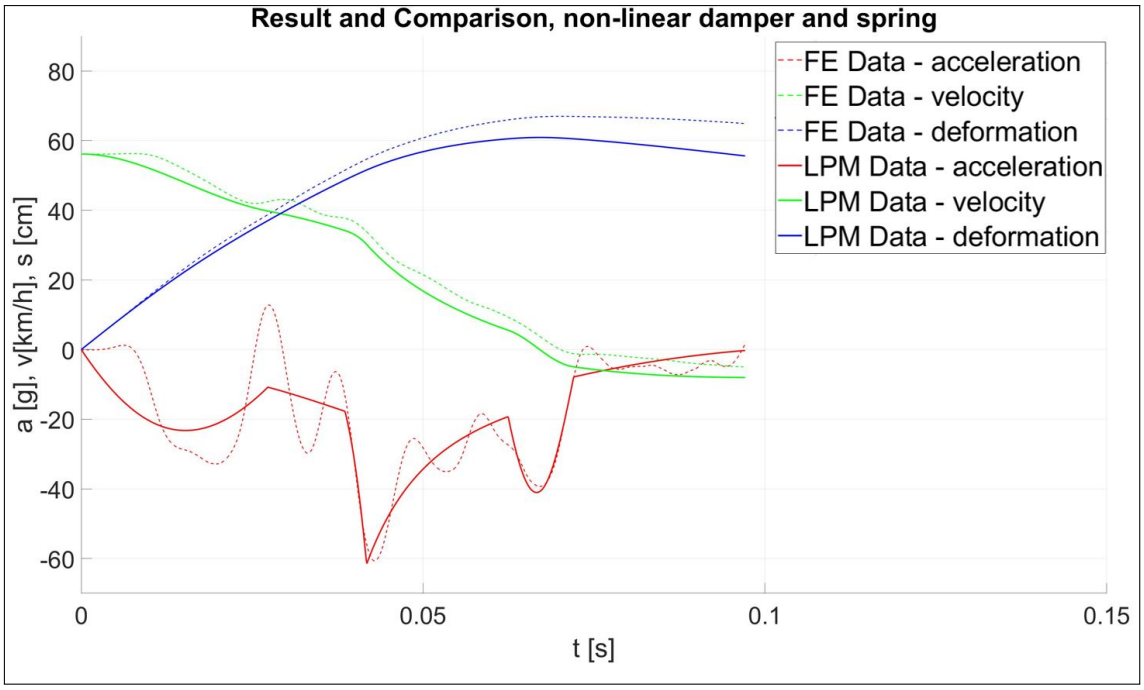

Figure C.8: Plot of computed and test values for parameter model for a Chevrolet Silverado Model

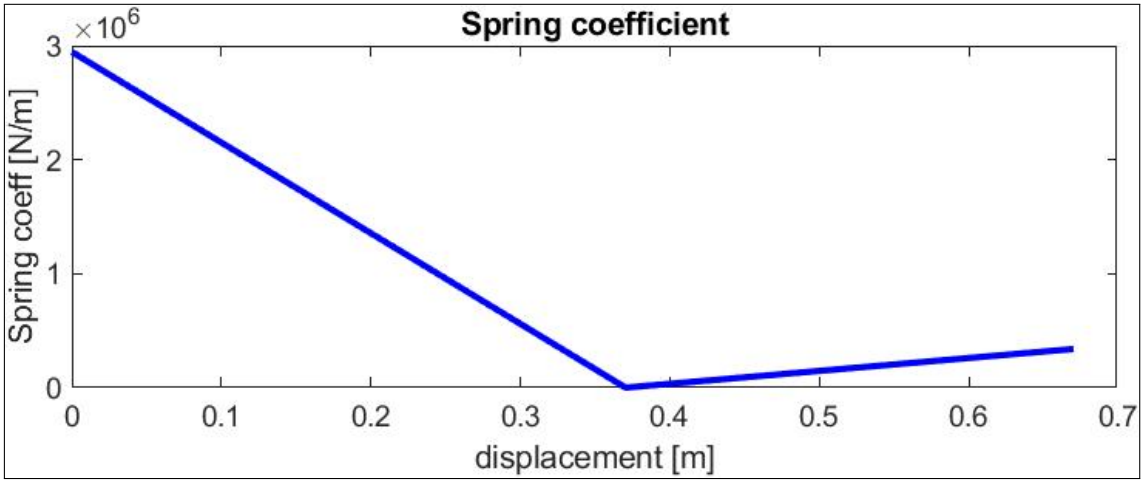

Figure C.9: Spring coefficient obtained from the algorithm for Chevrolet Silverado Baseline model

The output from the Gradient Descent Optimization algorithm is used to predict the deformation and vehicle velocity in a MATLAB Simulink model.

The plots of maximum FE vehicle deformation and LPM deformation in Figure C.11(**a**) show good correlation. A similar plot (Figure C.11(**b**)) was generated to compare the velocity of the vehicle at the CG; in the case of LPM at the lumped mass center. The LPM is represented by the mathematical model in the plots. The time the vehicle attains zero velocity is closely correlated in the plots but there is a small deviation after 40 ms. The reason for this deviation can be attributed to

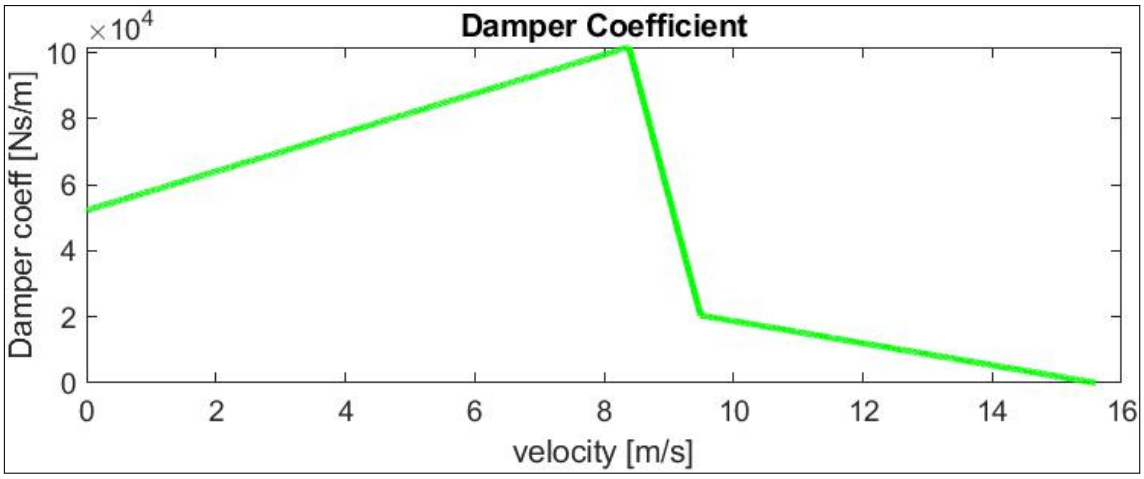

Figure C.10: Damper Coefficient obtained from the algorithm for Chevrolet Silverado Baseline model

the spring and damper characteristics which are approximated in this study using a piece-wise linear function. The model can be improved using a non-linear function for the spring stiffness and damping characteristics. If the model is simulated beyond the time the vehicle attains zero velocity, a rebound is observed in the velocity. This velocity rebound could be due to the internal strain energy stored in the springs, and it would be interesting to investigate this further in the future.

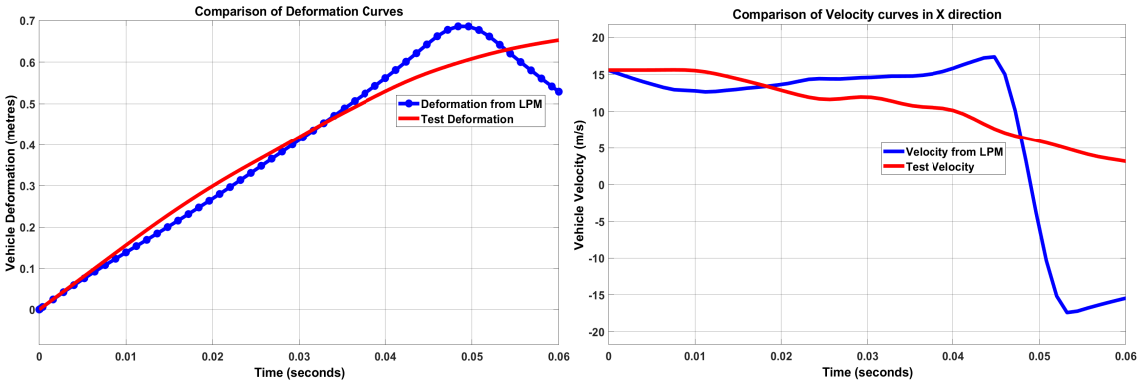

(**a**) (**b**)

Figure C.11: (a) Displacement of the vehicle CG curves comparison for LPM vs FE model, (b) velocity of the vehicle CG curves comparison for LPM vs FE model Chevrolet Silverado Baseline model - Phase I

Baseline Toyota Yaris Model The baseline 2010 Yaris model FE simulations were used for estimating the front-end spring-damper characteristics shown in Figure C.13; acceleration, velocity and deformation plots are compared in C.12. These characteristics are used in Phase I of the Simulink model to determine the displacement and time for the vehicle to attain zero velocity. The curves are overlayed in Figure C.14.

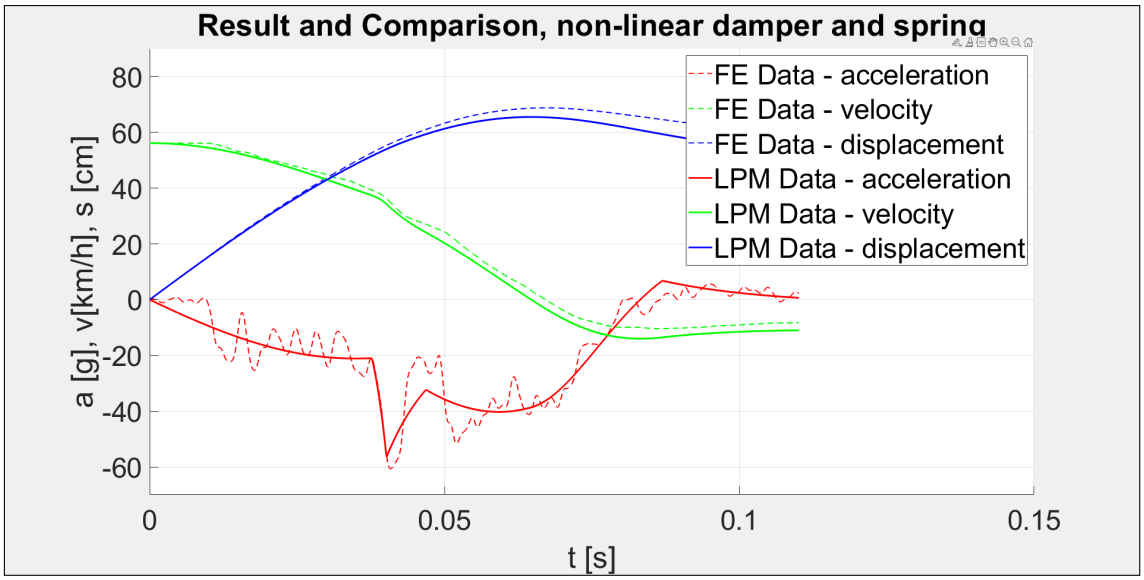

Figure C.12: Plot of computed and FE test values for lumped parameter model for a Toyota Yaris Model

C.3.2 Phase II

The prediction for the second part of the lumped model using Simulink was conducted and plotted against the data from FE model. The quantity Q_i in the governing equations is the vertical component of the barrier force experienced by the vehicle in the crash. The force curve is derived from the FE model and inputted into the Simulink model to improve the prediction; it will be of interest to mathematically explain this force component in terms of residual impact energy after absorption. The Simulink model is run with numerical integration (variable timestep- ode 45) and the velocity of the lumped mass in z-direction along with the pitching angle is compared to the data from FE model.

C.3.2.1 Baseline Chevrolet Silverado Model

Figure C.15(**a**) compares the z-velocity (vertical velocity) in the body with the curves generated from the FE data. The trend in the curve is similar but the peak values are not matching. One of the contributing factors to this deviation is the use of standard linear spring and damper coefficient values for the model. The use of the linear approximation for the spring and damper coefficients can lead to the difference in the values for this parameter as well. The values of l_f and l_r can also be further tuned to represent the Chevrolet Silverado (2014) model. However, we intentionally avoided fine tuning these values assuming that this data may not be available to vehicle development team at the start of the design process and it makes sense to use

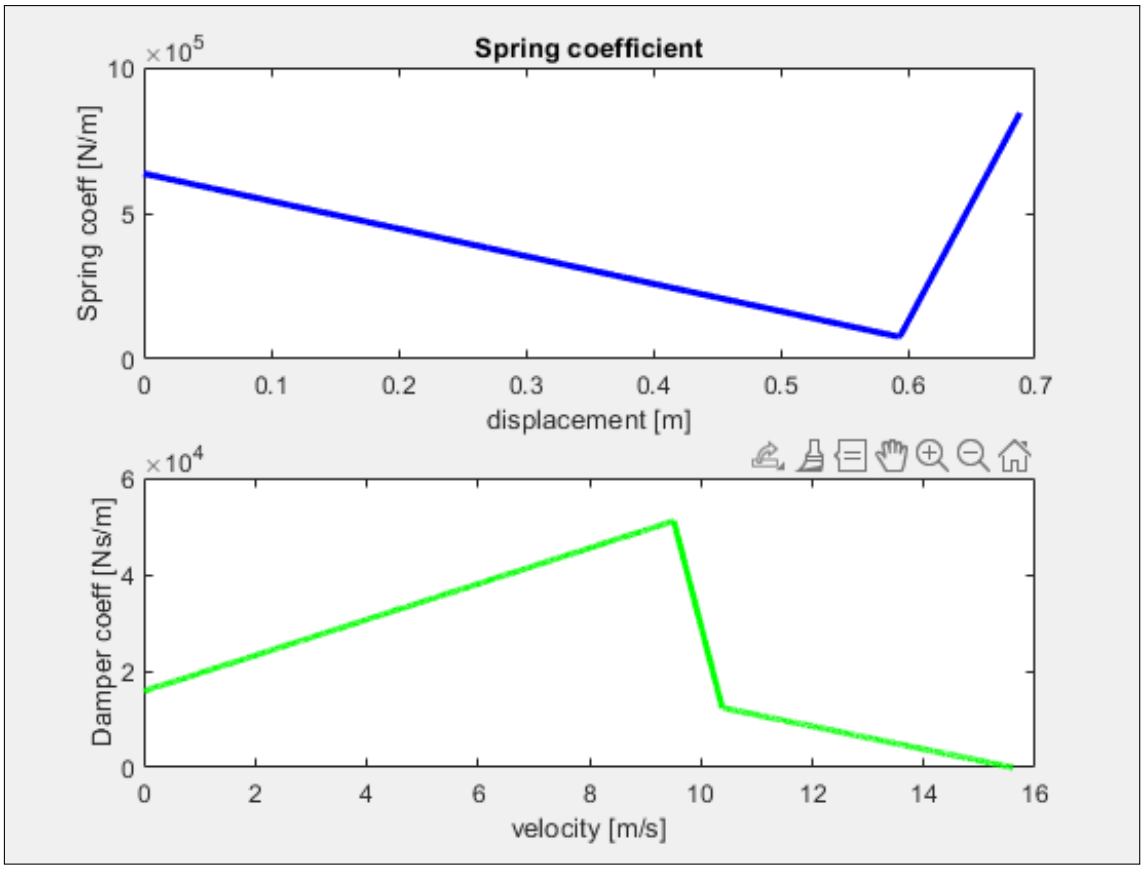

Figure C.13: Damper Coefficient obtained from the algorithm for Toyota Yaris Baseline model

standard values for automotive parameters. Figure C.15(**b**) compares the forward pitching angle for the FE model and the LPM developed in this study. The pitch angle comparison shows a similar trend observed in both curves. The vehicle starts to pitch around the same time during the crash event; this is crucial for designers planning airbag deployment in vehicles and other active protection features. The pitch angle curve for the simulation LPM peaks higher than the FE data at the start of the vehicle rotation but slowly follows the FE data curve showing comparable maximum pitch angle values. In addition, this is also a very important observation for vehicle safety designers. The difference between the curves can be explained by the linear approximation for the spring and damper coefficients and the barrier force definition. The study did not account for energy losses that may exist in the model.

C.3.2.2 Baseline Toyota Yaris Model

Similar to Phase I, the z velocity and pitch of the vehicle is overlaid for the Yaris model in Phase II of the impact presented in Fig C.16. The observations for the prediction of the injury parameters are consistent with the truck model prompting the reliability of the model for different vehicle platforms.

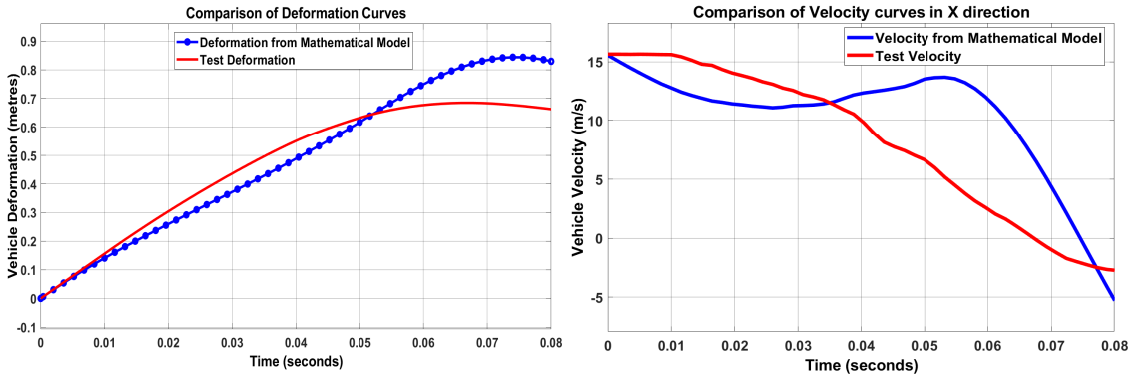

(a) (b)

Figure C.14: (a)Displacement curves overlaid, (b) Velocity curves overlaid
Toyota Yaris Baseline model Phase I : Overlay of curves for LPM and FEM

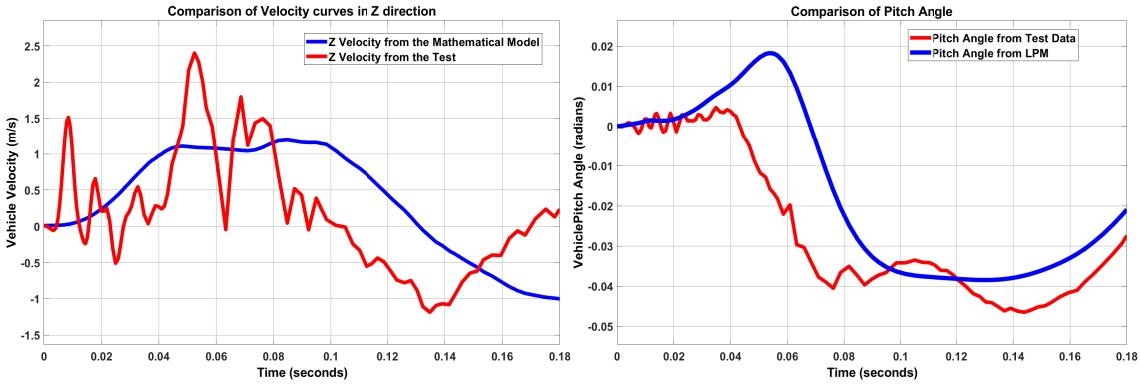

(a) (b)

Figure C.15: (a) Z-Velocity curve overlay for LPM vs FE model, (b) Forward Pitch Angle curve overlay for LPM vs FE model
Chevrolet Silverado Baseline Model Phase II : Overlay of curves for LPM and FEM

C.3.3 Robustness Check

According to Section C.2.5 the LPM was used to predict stiffness changes in the model by changing the thickness of the model by

- increasing thickness of all metal parts by 10%
- increasing thickness of all metal parts by 20%

Figure C.17 shows the acceleration and pitch curves for the baseline Toyota Yaris model and the modified models. It is observed that increasing the thickness of the parts reduces the peak acceleration values along with the vehicle pitching forward. However, the trend is non-linear indicating that only increasing the thickness is not a possible countermeasure to improve vehicle crashworthiness. There are other contributing variables which could help reduce the injury values in a crash.

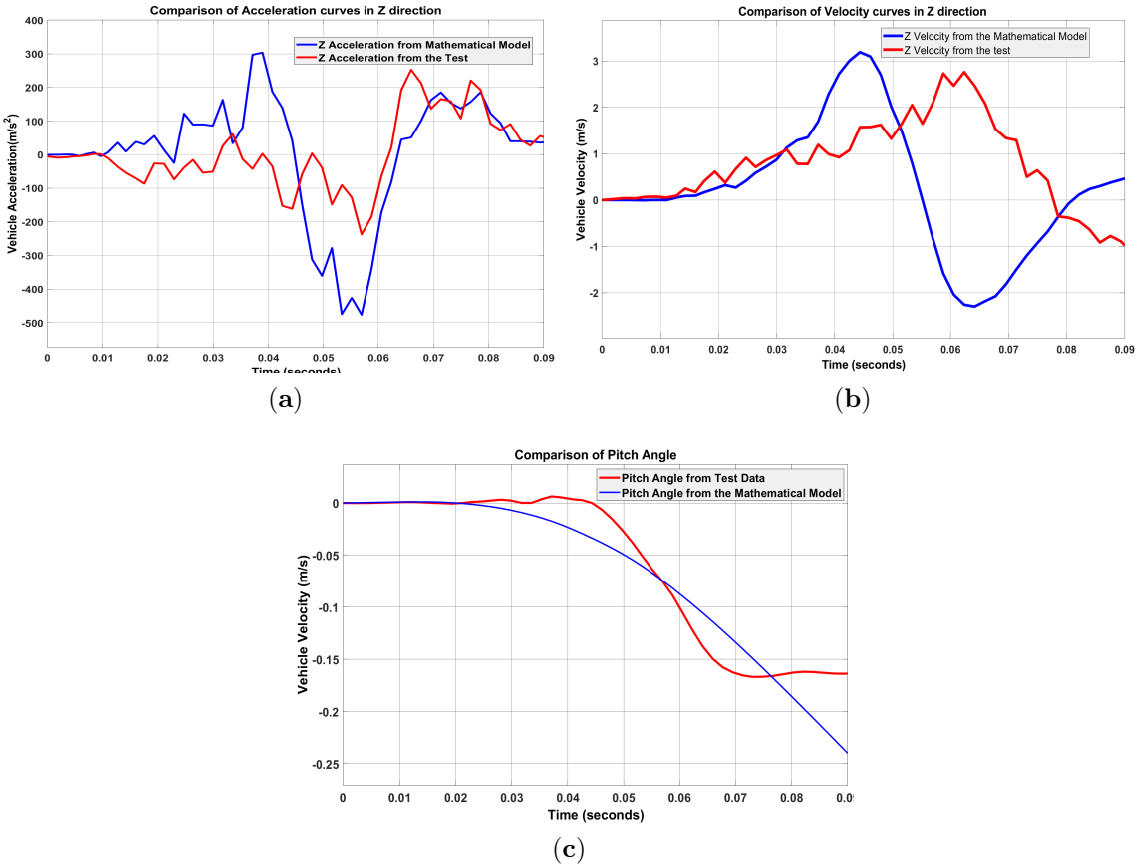

Figure C.16: (a)Z Acceleration curve, (b) Z Velocity curve, (c)Pitch curve Toyota Yaris Baseline Phase II : Overlay of curves for LPM and FEM

C.3.3.1 Phase I - 10% thickness

The spring and damper coefficient curves; mass/moment of inertia changes are updated in the Simulink model to determine the performance of the LPM in both phases of impact. The maximum displacement is closely correlated to the test data in Figure C.18(**a**) and the time the vehicle attains zero velocity is predicted with a variation of approximately 10 ms.

C.3.3.2 Phase II - 10% thickness

The simulation was repeated for the 10% stiffness model using Simulink to simulate the impact kinematics and predict the front-end deformation to absorb the energy of the impact; along with the forward pitching of the vehicle. The model predicts the maximum pitching angle and the z acceleration curve is closely replicated in the LPM simulations, see Figure C.20.

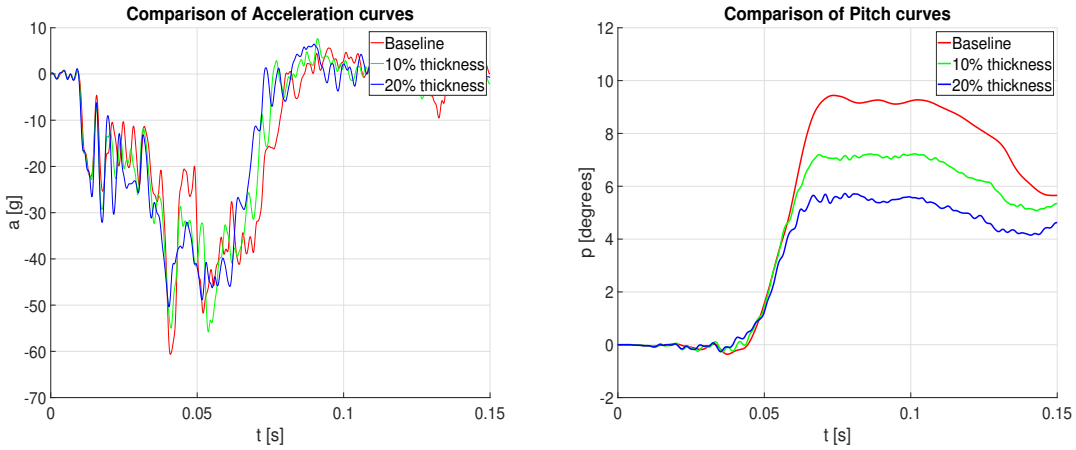

(a) (b)

Figure C.17: (a) X-acceleration comparison for baseline and modified models, (b) Forward Pitch Angle comparison for baseline and modified models
Toyota Yaris Model: Stiffness Variation

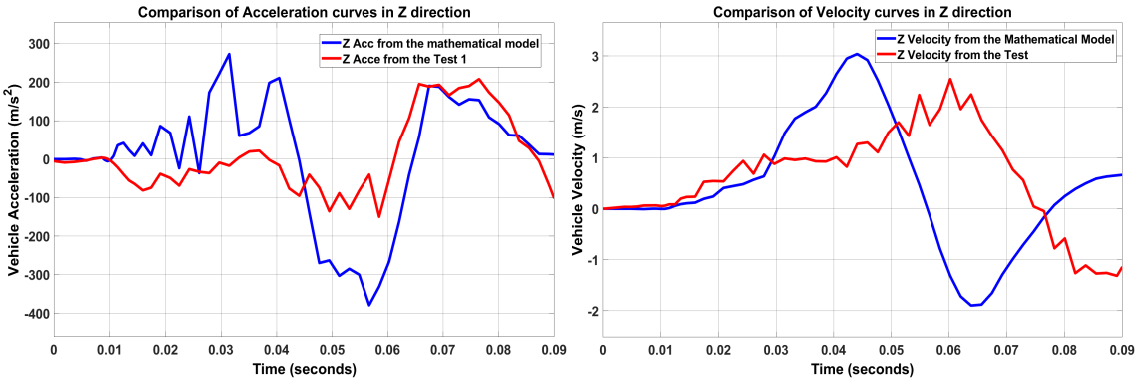

(a) (b)

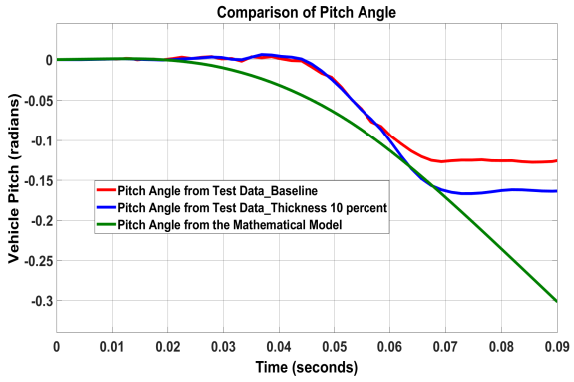

(c)

Figure C.19: (a) Z Acceleration curves overlaid, (b) Z Velocity curves overlaid, (c) Forward Pitching curves overlaid
Toyota Yaris Model - 10% Thickness Variation - Phase II : Overlay of curves for LPM and FEM

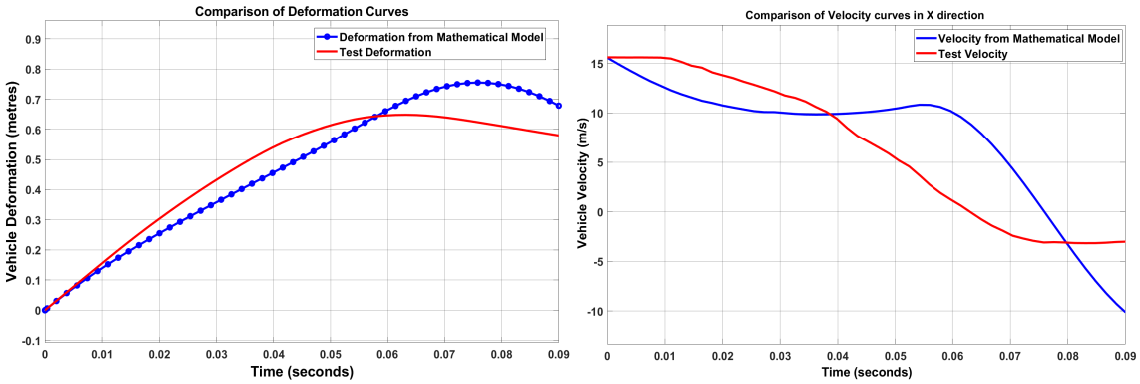

(**a**) (**b**)

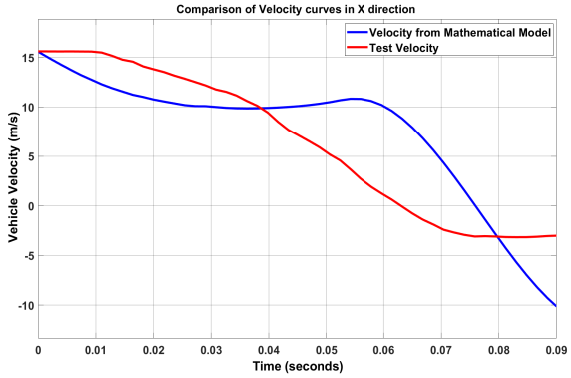

(**c**)

Figure C.18: (a)Deformation curves overlaid, (b) Velocity curves overlaid, (c) Pitch curve
Toyota Yaris Model - 10% Thickness Variation - Phase I : Overlay of curves for LPM and FEM

.

C.3.3.3 Phase I - 20% thickness

The results of Phase I with thickness modification are presented in Figure C.20 and show good correlation with the results. The gap in correlation is consistent with the observations outlined with the Silverado model.

C.3.3.4 Phase II - 20% thickness

The pitching curve in Figure C.21(**c**) follows the trend of the FE test data, however, the LPM simulation deviates from the test curve after the time of maximum pitching. This can be attributed to the constant stiffness of the suspension springs and damper coefficients. The LPM can be further improved by providing non-linear stiffness and damper characteristics representing the vehicle suspension system.

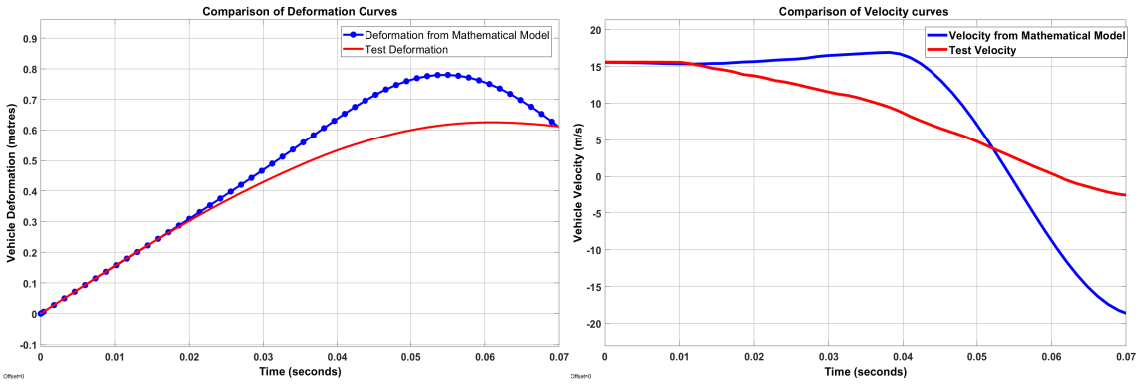

(**a**) (**b**)

Figure C.20: (a)Deformation curves overlaid, (b) X velocity curves overlaid
Toyota Yaris Model - 20% Thickness Variation Phase I : Overlay of curves for LPM and FEM

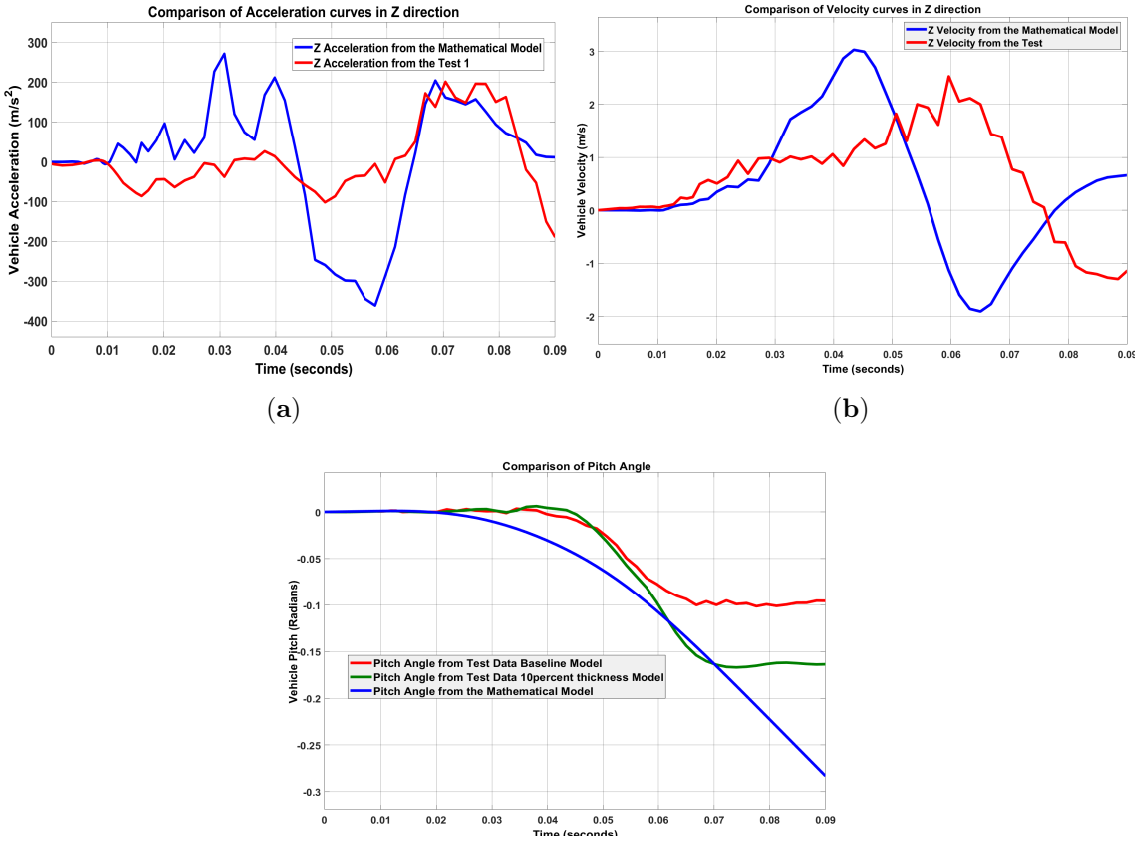

(**a**) (**b**)

(**c**)

Figure C.21: (a)z Acceleration curves overlaid, (b) z Velocity curves overlaid, (c) Forward Pitch curves overlaid
Toyota Yaris Model - 20% Thickness Variation - Phase II : Overlay of curves for LPM and FEM

The change in stiffness is closely predicted in both models for the z acceleration and maximum pitching angle indicating a high reliability of the model. The maximum

deformation and time to attain zero velocity is also correlated well in the LPM simulations; the differences in the result can be attributed to the assumption of linear characteristics for non-linear front-end spring data.

C.4 Conclusions

The novel technique developed in this paper for modeling a full frontal vehicle crash event successfully predicts the event kinematics. The study demonstrates that the two phase simulation model can describe a highly complex dynamical multiple DOF system with few equations and parameters, making the process of using LPMs very simple and reliable for safety design engineers. The robustness check and stiffness variation analysis indicates that the model is reliable and predicts variations in the parameters to determine injury values. The increase in thickness of the model by 10% and 20% improved the crashworthiness of the vehicle. Reducing the pitching angle would reduce the likelihood of injury to the occupants. The study highlights that parameter identification is an important part of the accident reconstruction process and influences the crashworthiness performance of the vehicle.

The assumptions used to arrive at a simpler LPM model providing reliable results include the following:

- The spring and damper characteristics are assumed to be piecewise-linear with six breakpoints although they are non-linear in physical systems.
- The suspension spring and damper coefficients were assumed same for the truck and sedan model used in the validation study.
- The vehicle acceleration is assumed to be zero at the time pitching starts in the crash event.
- Energy losses like friction and heat losses in the vehicle during the crash event are neglected to simplify the problem.
- Only vehicle rotations about the y-axis (pitching) are considered for modeling in the full frontal impact scenario; rotations about other axes are considered negligible and not impacting the occupant injuries.

References – Paper C

[1] Paul Du Bois, Clifford C Chou, Bahig B Fileta, Tawfik B Khalil, Albert I King, Hikmat F Mahmood, Harold J Mertz, Jac Wismans, Priya Prasad, and Jamel E Belwafa. Vehicle crashworthiness and occupant protection. 2004.

[2] Mustafa Elkady and Ahmed Elmarakbi. Modelling and analysis of vehicle crash system integrated with different vdcs under high speed impacts. *Open Engineering*, 2(4):585–602, 2012.

[3] DJ Benson, JO Hallquist, M Igarashi, K Shimomaki, and M Mizuno. Application of dyna3d in large scale crashworthiness calculations. Technical report, Lawrence Livermore National Lab., 1986.

[4] Mounir M Kamal. Analysis and simulation of vehicle to barrier impact. *SAE Transactions*, pages 1498–1503, 1970.

[5] Mustafa Elkady, Ahmed Elmarakbi, and John MacIntyre. Enhancement of vehicle safety and improving vehicle yaw behaviour due to offset collisions using vehicle dynamics. *International journal of vehicle safety*, 6(2):110–133, 2012.

[6] Bernard B Munyazikwiye, Hamid R Karimi, and Kjell Gunnar Robbersmyr. Mathematical modeling of vehicle frontal crash by a double spring-mass-damper model. In *2013 XXIV International Conference on Information, Communication and Automation Technologies (ICAT)*, pages 1–6. IEEE, 2013.

[7] J Michael Chang, Mohammad Ali, Ryan Craig, Tau Tyan, Marwan El-Bkaily, and James Cheng. Important modeling practices in cae simulation for vehicle pitch and drop. *SAE Transactions*, pages 62–72, 2006.

[8] Fan Li, Nian Song Liu, Hong Geng Li, Biao Zhang, Shi Wei Tian, Ming Gang Tan, and Baptiste Sandoz. A review of neck injury and protection in vehicle accidents. *Transportation Safety and Environment*, 1(2):89–105, 11 2019. ISSN 26314428. doi: 10.1093/TSE/TDZ012. URL `https://academic.oup.com/tse/article/1/2/89/5618803`.

[9] Gernot Woitsch and Wolfgang Sinz. Influence of pitching and yawing during frontal passenger vehicle crash tests on driver occupant's kinematics and injury. *International journal of crashworthiness*, 18(4):356–370, 2013.

[10] J Michael Chang, Mohammed Rahman, Mohammad Ali, Tau Tyan, Marwan El-Bkaily, and James Cheng. Modeling and design for vehicle pitch and drop of body-on-frame vehicles. *SAE transactions*, pages 329–338, 2005.

[11] Zuolong Wei, Hamid Reza Karimi, and Kjell Gunnar Robbersmyr. Analysis of the relationship between energy absorbing components and vehicle crash response. Technical report, SAE Technical Paper, 2016.

[12] Bernard B. Munyazikwiye, Hamid Reza Karimi, and Kjell G. Robbersmyr. Optimization of vehicle-to-vehicle frontal crash model based on measured data using genetic algorithm. *IEEE Access*, 5:3131–3138, 2017. ISSN 21693536. doi: 10.1109/ACCESS.2017.2671357.

[13] Zhaokai Li, Qiang Yu, Xuan Zhao, Man Yu, Peilong Shi, and Cilei Yan. Crashworthiness and lightweight optimization to applied multiple materials and foam-filled front end structure of auto-body:. *http://dx.doi.org/10.1177/1687814017702806*, 9(8):1–21, 8 2017. ISSN 16878140. doi: 10.1177/1687814017702806. URL `https://journals.sagepub.com/doi/full/10.1177/1687814017702806`.

[14] J. Michael Chang, Miinshiou Huang, Tau Tyan, G. Li, and L. Gu. Structural optimization for vehicle pitch and drop. In *SAE Technical Papers*. SAE International, 4 2006. doi: 10.4271/2006-01-0316. URL `https://www.sae.org/publications/technical-papers/content/2006-01-0316/`.

[15] Gulshan Noorsumar, Svitlana Rogovchenko, Kjell G. Robbersmyr, Dmitry Vysochinskiy, and Andreas Klausen. A novel technique for modeling vehicle crash using lumped parameter models. *Proceedings of the 11th International Conference on Simulation and Modeling Methodologies, Technologies and Applications, SIMULTECH 2021*, pages 62–70, 2021. doi: 10.5220/0010529200620070.

[16] National Highway Traffic Safety Administration et al. Crash simulation vehicle models. *URL: https://www. nhtsa. gov/research-data/databasesand-software*, 2016.

[17] Harry Singh, Velayudham Ganesan, James Davies, Mahendran Paramasuwom, Lorenz Gradischnig, Patrick Wood, and Vikrant Mogal. Structural countermeasure/research program mass and cost increase due to oblique offset moving deformable barrier impact test. Technical report, 2018.

[18] D Marzougui, D Brown, H K Park, C D Kan, and K S Opiela. Development & Validation of a Finite Element Model for a Mid-Sized Passenger Sedan. In *3 th International LS-DYNA Users Conference Session: Automotive*, 2014.

[19] Center for Collision Safety and Analysis – 2010 Toyota Yaris. URL `https://www.ccsa.gmu.edu/models/2010-toyota-yaris/`.

[20] Matthew Huang. *Vehicle crash mechanics*. CRC press, 2002.

[21] Javad Marzbanrad and Mostafa Pahlavani. A system identification algorithm for vehicle lumped parameter model in crash analysis. *International Journal of Modeling and Optimization*, 1(2):163, 2011.

[22] Witold Pawlus, Hamid Reza Karimi, and Kjell Gunnar Robbersmyr. Development of lumped-parameter mathematical models for a vehicle localized impact. *Journal of mechanical science and technology*, 25(7):1737–1747, 2011.

[23] Bernard B Munyazikwiye, Dmitry Vysochinskiy, Mikhail Khadyko, and Kjell G Robbersmyr. Prediction of vehicle crashworthiness parameters using piecewise lumped parameters and finite element models. *Designs*, 2(4):43, 2018.

[24] Bernard B Munyazikwiye, Hamid R Karimi, and Kjell G Robbersmyr. Application of genetic algorithm on parameter optimization of three vehicle crash scenarios. *IFAC-PapersOnLine*, 50(1):3697–3701, 2017.

[25] Andreas Klausen, Sondre Sanden Tørdal, Hamid Reza Karimi, Kjell G Robbersmyr, Mladen Ječmenica, and Ole Melteig. Mathematical modeling and optimization of a vehicle crash test based on a single-mass. In *Proceeding of the 11th World Congress on Intelligent Control and Automation*, pages 3588–3593. IEEE, 2014.

[26] Gulshan Noorsumar, Kjell Robbersmyr, Svitlana Rogovchenko, and Dmitry Vysochinskiy. Crash Response of a Repaired Vehicle - Influence of Welding UHSS Members. In *WCX SAE World Congress Experience*. SAE International, 4 2020. doi: https://doi.org/10.4271/2020-01-0197. URL `https://doi.org/10.4271/2020-01-0197`.

[27] Herbert Goldstein, Charles Poole, John Safko, and Stephen R. Addison. Classical Mechanics, 3rd ed. *American Journal of Physics*, 70(7):782–783, 7 2002. ISSN 0002-9505. doi: 10.1119/1.1484149. URL `http://aapt.scitation.org/doi/10.1119/1.1484149`.

[28] Sergio M Savaresi, Charles Poussot-Vassal, Cristiano Spelta, Olivier Sename, and Luc Dugard. *Semi-active suspension control design for vehicles*. Elsevier, 2010.

Paper D

Vehicle crashworthiness performance in frontal impact: mathematical model using elastic pendulum

Gulshan Noorsumar, Svitlana Rogovchenko, Kjell G. Robbersmyr and Dmitry Vysochinskiy

This paper has been published as:

Gulshan Noorsumar, Svitlana Rogovchenko, Kjell G. Robbersmyr and Dmitry Vysochinskiy. Vehicle crashworthiness performance in frontal impact: mathematical model using elastic pendulum. *Mechanics Research Communications*; ISSN 0093-6413, pages 103954, volume 124, 2022. doi: 10.1016/j.mechrescom.2022.103954..

Vehicle crashworthiness performance in frontal impact: mathematical model using elastic pendulum

Gulshan Noorsumar, Svitlana Rogovchenko, Kjell G. Robbersmyr and Dmitry Vysochinskiy
Department of Engineering Sciences
University of Agder
4879 Grimstad, Norway

Abstract **Vehicle occupant injuries due to collisions cause many fatalities every year. Safe vehicle design plays a critical role in averting serious injuries to occupants and vulnerable road users in the event of a crash. In this paper we study a full frontal vehicle crash against a rigid barrier introducing a Lumped Parameter Model (LPM) inspired by the elastic pendulum motion. The model uses polar coordinates to simplify the problem and the governing equations have been defined using Lagrangian formulation. The Simulink model has been validated against Finite Element (FE) data demonstrating good correlation with pitching angle and maximum crush of the vehicle. These parameters are crucial for designing vehicles which efficiently protect occupants.**

D.1 Introduction

Vehicle collisions are the one of the major causes of occupant injuries in a vehicle crash event. The 2015 European Commission report identifies a frontal impact as the most common crash scenario leading to serious injuries, followed by a side impact. These injuries are caused by different forces acting on the cage protecting the occupants in a collision in various impact scenarios. [1], [2]. The report also suggests further studies of mechanisms and measures aimed at reducing injury severity in a crash. Factors leading to occupant head and neck injuries are the vehicle pitch and drop in case of a full frontal impact [3]. Occupant interaction with vehicle cage leads to severe injuries in a crash, especially in case of unbelted occupants. In order to prevent head to roof/header contacts it is imperative to include vehicle pitch and drop in design considerations for full frontal impact injury mitigation [3].

The geometry and deformation of the front end members are important for predicting the forward pitching of a vehicle. In fact, downward bending of the rails generated by the imbalance of forces acting on the part in the vertical direction

is a key reason for pitching in full frontal impacts [4], [5]. The rotation of the vehicle that leads to yawing and rolling is not included in most simulation models predicting the injury response because they are negligible in case of a full frontal impact. Designing an ideal straight frame vehicle safety engineers face challenges due to package constraints (engine compartment); this leads to vertical downward bending of frame rail structures in body-on-frame vehicles during deformation. Such out of plane bending not only causes less efficient energy absorption but also adds a downward moment causing an imbalance of forces acting on the vehicle. The vehicle pitch was simulated using CAE modeling by Chang et al. who concluded that the modeling and design of vehicle rails play a crucial role in vehicle pitch and drop [6], [7]. Vehicle rotations were also predicted by Lumped Parameter Models (LPM) in [4], [8] using a 6 DOF (Degrees of Freedom) vehicle model with an active vehicle dynamics control system.

Mathematical modeling is used in vehicle development process to respond to changing safety norms and to ensure that new vehicles are designed to protect pedestrians and occupants in a crash. Mathematical models replace physical testing to predict the injury values in a collision scenario; Finite Element (FE) models have good accuracy in correlating the kinematics of an impact and have been used in several applications in the automotive industry [9], [10]. LPMs are usually designed as simplified spring-damper systems representing a deformable part and a rigid lumped mass component replicating the non-deformable occupant compartment. The study by Kamal was one of the first applications of LPM in automotive crashworthiness modeling [11]. In the last decade several researchers employed parameter estimation techniques to study impact dynamics using LPM models [12], [13]. Pavlov [14] represented a vehicle as a pendulum in motion and predicted vehicle pitching using an inverted pendulum. Occupant modeling using inverted spherical pendulum model was conducted by Cyrén and Johansson [15], who derived the equations of motion of the pendulum using Lagrangian formulation. Inverted pendulum has also been used in explaining the dynamics of a two-wheeled vehicle with self-tilt motion by Miao [16].

This paper introduces an elastic pendulum model to explain the impact kinematics for a full frontal impact model (0% offset) of a vehicle which is undergoing impact at 56 kmph against a rigid barrier; the vehicle occupant cage is represented by a compound pendulum. The equations of motion of the system are derived using the Lagrangian formulation. The model is validated against an FE model simulation, details are explained in the next section.

D.2 Methodology

Our model represents a non-linear vehicle impact as a pendulum in motion. The vehicle hitting a rigid impactor goes through three stages:

- front end deformation (modeled as in an elastic pendulum),
- rotation about the impact point acting like a pivot in case of a pendulum,
- restoring force due to gravity bringing the vehicle back to the rest position.

Some of the assumptions in the model include [5]:

- Only vehicle rotations about the y-axis (pitching) were considered in the model; rotations in other axes have been neglected.
- Energy losses like friction and heat losses were neglected.
- Although the system behaves non-linearly in a crash, the front-end spring and damper characteristics were assumed to be piece-wise linear with four breakpoints.

The periodic pendulum motion shown in Figure D.1 is adopted for this model; the pendulum is allowed to swing back and forth from its rest position. In the case of the vehicle under impact, the occupant compartment acts like a pendulum bob rotating about the pivot point leading to vehicle pitching. The vehicle is not allowed to swing back and forth due to the ground acting as a constraint. The vehicle suspension system also acts as a constraint to restrict the motion of the pendulum. Figure D.2 shows the model with the constraints, the barrier defined for the LPM is a non deformable 0% offset impactor. The LPM used is a 5 DOF system, similar to the one developed in [5]. The non deformable occupant compartment is represented in the model by the concentrated mass. The deformable front end comprising of vehicle rails, crush cans and the plastic parts is represented by a spring and damper system in Figure D.3.

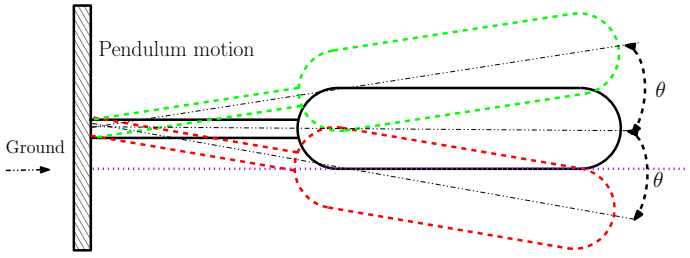

Figure D.1: Vehicle body rotating like a pendulum about the impact point.

The vehicle front end undergoes deformation to absorb energy which leads to the deceleration of the vehicle; the time of maximum crush generally coincides with the

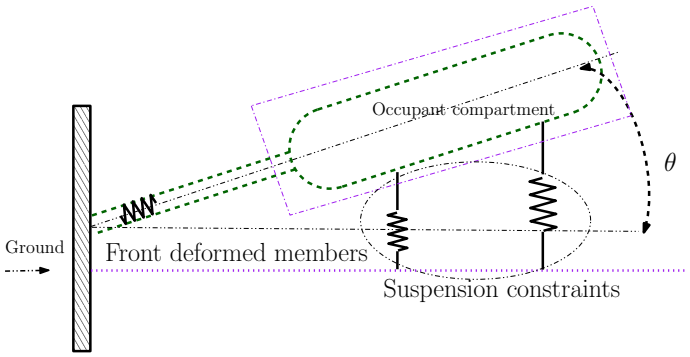

Figure D.2: Elastic pendulum with constraints representing a vehicle under impact.

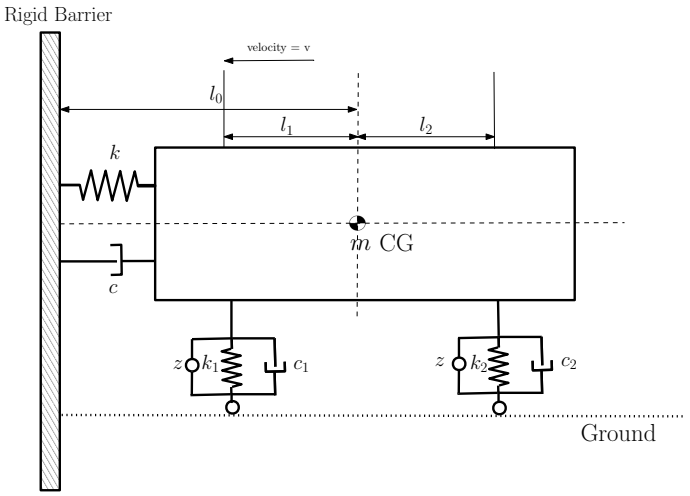

Figure D.3: LPM Model of a vehicle impacting a rigid barrier.

instant when the vehicle attains zero velocity. The pendulum LPM uses a spring damper system to absorb the impact energy as shown in Figure D.4. In a full frontal impact against a rigid barrier the vehicle starts pitching forward due to the imbalance of forces as explained by Chang et al. [3], [6]; this behaviour has been replicated in the LPM (Figure D.5) and modeled as an elastic pendulum.

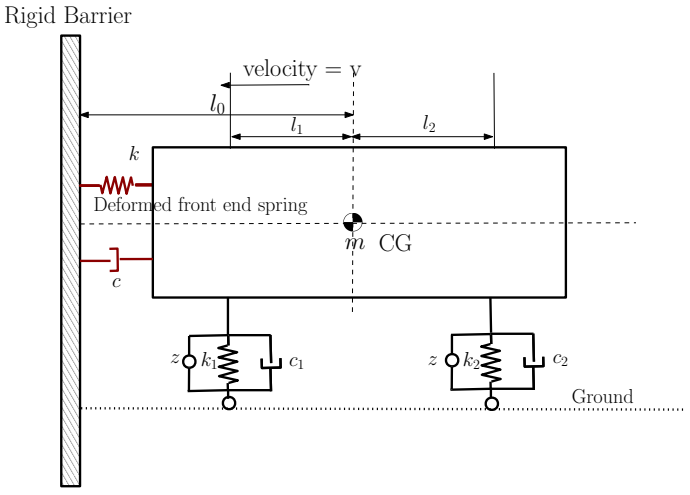

Figure D.4: Vehicle front end members undergoing deformation.

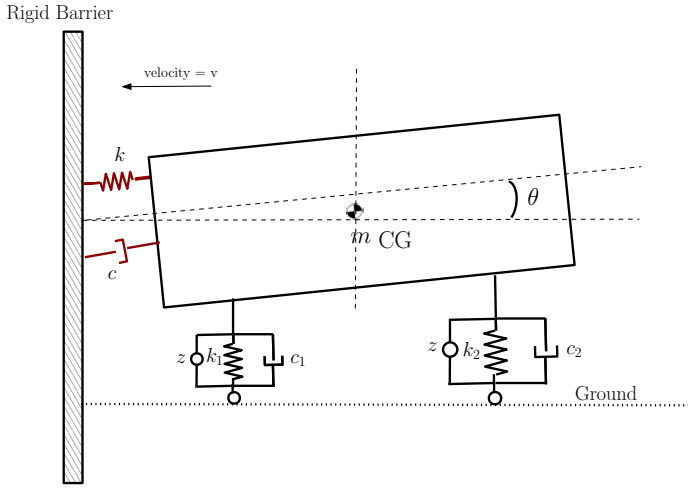

Figure D.5: LPM representation of vehicle pitching forward in the event.

D.2.1 Finite Element (FE) Model

The LPM is validated by an FE model similar to that considered in [5]. The FE simulations conducted for a vehicle impact at 56 kmph were used to validate this model. The FE model developed by National Highway Traffic Safety Administration (NHTSA) through the reverse engineering process [17] was used to compare the simulation curves. Parameter identification was conducted to determine the spring and damper characteristics for the non-linear deformation in the vehicle front.

D.2.2 Parameter identification for front end spring and damper characteristics

The spring and damper characteristics are derived using the algorithm developed by the authors in [5], [18]. The gradient descent optimization algorithm developed in [5] is modified to include deformation and pitching of the vehicle during the entire event of collision. The non-linear force-deformation curve is assumed to be piece-wise linear with four breakpoints in the curve. The stiffness k and spring force F_k are related by the equation (D.1). Similarly, the damper coefficient c is related to the damping force F_c by the equation (D.2) [19].

$$F_k = k(x) \cdot x, \tag{D.1}$$

$$F_c = c(\dot{x}) \cdot \dot{x}, \tag{D.2}$$

where

$$k(x) = \begin{cases} \frac{(k_2-k_1)\cdot|\hat{x}|}{x_1} + k_1, & \text{for } |\hat{x}| \le x_1, \\ \frac{(k_3-k_2)\cdot(|\hat{x}|-x_1)}{(x_2-x_1)} + k_2, & \text{for } x_1 \le |\hat{x}| \le x_2, \\ \frac{(k_4-k_3)\cdot(|\hat{x}|-x_2)}{(x_3-x_2)} + k_3, & \text{for } x_2 \le |\hat{x}| \le x_3, \\ \frac{(k_5-k_4)\cdot(|\hat{x}|-x_3)}{(x_4-x_3)} + k_4, & \text{for } x_3 \le |\hat{x}| \le x_4, \\ \frac{(k_6-k_5)\cdot(|\hat{x}|-x_4)}{(x_5-x_4)} + k_5, & \text{for } x_4 \le |\hat{x}| \le x_5, \\ \frac{(k_7-k_6)\cdot(|\hat{x}|-x_5)}{(C-x_5)} + k_6, & \text{for } x_5 \le |\hat{x}| \le C. \end{cases}$$

The damper characteristics are defined similar to the spring characteristics in the model:

$$c(\dot{x}) = \begin{cases} \frac{(c_2-c_1)\cdot|\hat{\dot{x}}|}{\dot{x}_1} + c_1, & \text{for } |\hat{\dot{x}}| \le \dot{x}_1, \\ \frac{(c_3-c_2)\cdot(|\hat{\dot{x}}|-\dot{x}_1)}{(\dot{x}_2-\dot{x}_1)} + c_2, & \text{for } \dot{x}_1 \le |\hat{\dot{x}}| \le \dot{x}_2, \\ \frac{(c_4-c_3)\cdot(|\hat{\dot{x}}|-\dot{x}_2)}{(\dot{x}_3-\dot{x}_2)} + c_3, & \text{for } \dot{x}_2 \le |\hat{\dot{x}}| \le \dot{x}_3, \\ \frac{(c_5-c_4)\cdot(|\hat{\dot{x}}|-\dot{x}_3)}{(\dot{x}_4-\dot{x}_3)} + c_4, & \text{for } \dot{x}_3 \le |\hat{\dot{x}}| \le \dot{x}_4, \\ \frac{(c_6-c_5)\cdot(|\hat{\dot{x}}|-\dot{x}_4)}{(\dot{x}_5-\dot{x}_4)} + c_5, & \text{for } \dot{x}_4 \le |\hat{\dot{x}}| \le \dot{x}_5, \\ \frac{(c_7-c_6)\cdot(|\hat{\dot{x}}|-\dot{x}_5)}{(v_0-\dot{x}_5)} + c_6, & \text{for } \dot{x}_5 \le |\hat{\dot{x}}| \le v_0, \end{cases}$$

where k is the spring coefficient, c is the damper coefficient, $\hat{x}$ is the computed vehicle deformation, $\dot{x}$ is the vehicle velocity, $\hat{\dot{x}}$ is the computed vehicle velocity, C is the maximum dynamic crush, v_0 is the velocity at the time of maximum dynamic crush. The optimization algorithm which minimizes the error between the test and computed values has been used to determine the acceleration, velocity and deformation of the vehicle. The validation data from FE model and optimization algorithm are plotted in Figure D.6.

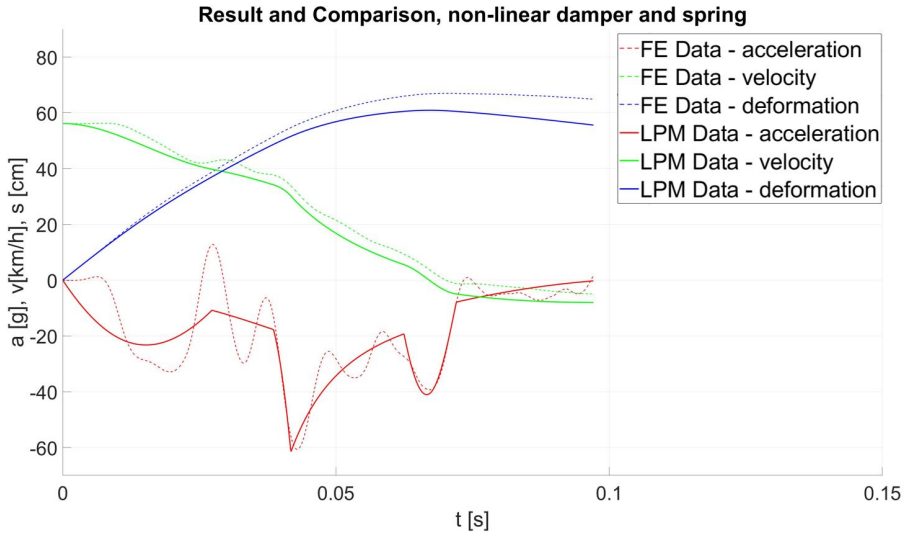

Figure D.6: Plot of computed and test values from parameterization algorithm.

D.2.3 Governing equations of motion

The governing equations of motion for the vehicle impacting the barrier have been modeled using the relativistic Lagrangian formulation [20]:

$$\frac{d}{dt}\frac{\partial L}{\partial \dot{q}_i} - \frac{\partial L}{\partial q_i} + \frac{\partial D}{\partial q_i} = Q_i,$$

where, in general case, $L = T - V$, T is the total kinetic energy of the system equal to the sum of the kinetic energies of the particles, $q_i, i = 1, ..., n$ are generalized coordinates and V is the potential energy of the system. Here D is the dissipation function and Q_i is the external force acting on the system; in this case it is the vertical component of the force experienced by the vehicle at the time of maximum dynamic crush [21].

For the purpose of simplifying the system, we converted the cartesian coordinates to polar coordinates: the horizontal (x) and vertical (z) coordinates and the angle of rotation θ about the y axis, were represented in polar coordinates by the following expressions:

$$x = [l_0 + r(t)] \cos\theta(t), \tag{D.3}$$

$$y = [l_0 + r(t)] \sin\theta(t), \tag{D.4}$$

where l_0 is the distance from the center of gravity (CG) to the point of impact of the vehicle, t is the time, and r and θ are the radius and angle in polar coordinates respectively. Taking the derivatives of x and z with respect to time t we obtain:

$$\dot{x} = \dot{r}\cos\theta - (l_0 + r)\sin\theta \cdot \dot{\theta}, \tag{D.5}$$

$$\dot{z} = \dot{r}\sin\theta + (l_0 + r)cos\theta \cdot \dot{\theta}, \tag{D.6}$$

where $\dot{x}$ and $\dot{z}$ represent the velocity of the vehicle in horizontal and vertical directions. Squaring both sides of the equations gives us:

$$\begin{aligned}\dot{x}^2 =& \dot{r}^2\cos^2\theta + (l_0 + r)^2\sin^2\theta \cdot \dot{\theta}^2 \\ & - 2\dot{r}\cos\theta \cdot (l_0 + r)\sin\theta \cdot \dot{\theta},\end{aligned} \tag{D.7}$$

$$\begin{aligned}\dot{z}^2 =& \dot{r}^2\sin^2\theta + (l_0 + r)^2\cos^2\theta \cdot \dot{\theta}^2 \\ & + 2\dot{r}\cos\theta \cdot (l_0 + r)\sin\theta \cdot \dot{\theta}.\end{aligned} \tag{D.8}$$

Adding the terms we have:

$$\begin{aligned}\dot{x}^2 + \dot{z}^2 =& \dot{r}^2(\cos^2\theta + \sin^2\theta) \\ & + (l_0 + r)^2 \cdot \dot{\theta}^2(\cos^2\theta + \sin^2\theta).\end{aligned} \tag{D.9}$$

The kinetic energy of the system is given by

$$T = \frac{1}{2}m(\dot{x}^2 + \dot{z}^2), \tag{D.10}$$

or, in polar coordinates,

$$T = \frac{1}{2}m[\dot{r}^2 + (l_0 + r)^2\dot{\theta}^2]. \tag{D.11}$$

The potential energy of the system can be found as

$$V = mg(l_0 + r)\sin\theta + \frac{1}{2}kr^2 + \frac{1}{2}k_1r_1^2 + \frac{1}{2}k_2r_2^2, \tag{D.12}$$

where r_1 and r_2 are expressed in terms of r and θ as follows:

$$r_1 = (l_0 + r - l_1)\theta, \tag{D.13}$$

$$r_2 = (l_0 + r - l_2)\theta. \tag{D.14}$$

Here m is the mass of the lumped body, l_1 is the distance from the CG to the front suspension, l_2 is the distance from the CG to the rear suspension. Simplifying the expression for potential energy in equation (D.12), we obtain:

$$\begin{aligned}V =& mg(l_0 + r)\sin\theta + \frac{1}{2}kr^2 + \frac{1}{2}k_1(l_0 + r - l_1)^2\theta^2 \\ & + \frac{1}{2}k_2(l_0 + r - l_2)^2\theta^2.\end{aligned} \tag{D.15}$$

Here k_1 and k_2 are the suspension spring coefficients for the front and rear suspension

respectively. Using equations (D.11) and (D.15) and Lagrangian formulation, $L = T - V$, we conclude that

$$\begin{aligned} L =& \frac{1}{2}m[\dot{r}^2 + (l_0 + r)^2\dot{\theta}^2 - mg(l_0 + r)\sin\theta - \frac{1}{2}kr^2 \\ & - \frac{1}{2}k_1(l_0 + r - l_1)^2\theta^2 - \frac{1}{2}k_2(l_0 + r - l_2)^2\theta^2. \end{aligned} \tag{D.16}$$

The governing equations of motion are:

$$\begin{aligned} Q_r^{ext} =& m\ddot{r} - mr\dot{\theta}^2 - ml_0\dot{\theta}^2 + mg\sin\theta \\ & + kr + \frac{1}{2}k_1(2r - l_0r - l_1)\theta^2 \\ & + \frac{1}{2}k_2\theta^2(2r + l_0r + 2l_2), \end{aligned} \tag{D.17}$$

$$\begin{aligned} Q_\theta^{ext} =& m(l_0 + r)^2\ddot{\theta} + mg(l_0 + r)cos\theta \\ & + k_1(l_0 + r - l_1)^2\theta + k_2(l_0 + r + l_2)^2\theta, \end{aligned} \tag{D.18}$$

where Q_r^{ext} and Q_θ^{ext} are the external forces experienced by the vehicle. The non-conservative forces experienced by the system are included in the Lagrange's equation of motion in the form of generalized forces expressed with the formulation of virtual work δU [15]:

$$\delta U = \sum_{j=1}^{m} F_j \cdot \delta r_j, \tag{D.19}$$

where F_j are the force components, δr_j are the virtual displacements given by

$$\delta r_j = \sum_{i=1}^{N} \frac{\partial r_j}{\partial q_i}\delta q_i \tag{D.20}$$

for $j = 1, 2, 3, \ldots, m$. This yields the following equation for virtual work as:

$$\begin{aligned} \delta U = F_1 \cdot \sum_{i=1}^{N} \frac{\partial r_j}{\partial q_i}\delta q_i + F_2 \cdot \sum_{i=1}^{N} \frac{\partial r_j}{\partial q_i}\delta q_i + \cdots \\ + F_m \cdot \sum_{i=1}^{N} \frac{\partial r_j}{\partial q_i}\delta q_i. \end{aligned} \tag{D.21}$$

Using equation (D.21), we compute the generalized forces experienced by the system.

$$\begin{aligned} \delta U = F_x \cdot \left(\frac{\partial z}{\partial r} \cdot \delta r + \frac{\partial z}{\partial \theta} \cdot \delta\theta\right) \\ + F_z \cdot \left(\frac{\partial z}{\partial r} \cdot \delta r + \frac{\partial z}{\partial \theta} \cdot \delta\theta\right). \end{aligned} \tag{D.22}$$

Substituting equations (D.3) and (D.4) in equation (D.22), we get

$$\begin{aligned} dU = F_x \cdot [(\cos(\theta)\delta r - (l_0 + r)\sin(\theta)\delta\theta] \\ + F_z \cdot [(\sin(\theta)\delta r + (l_0 + r)\cos(\theta)\delta\theta]. \end{aligned} \tag{D.23}$$

The external forces included in this LPM are barrier forces, damper forces including front end spring damper system and suspension damper system forces. The corresponding equations are:

$$Q_r^{ext} = Q_r^{bar} + Q_r^{damp}, \tag{D.24}$$

$$Q_\theta^{ext} = Q_\theta^{bar} + Q_\theta^{damp}. \tag{D.25}$$

Here F_x and F_z are the horizontal and vertical force components acting on the vehicle; Q_r^{bar} and Q_θ^{damp} are the non-conservative barrier and damper forces acting on the system.
Then δU becomes:

$$\begin{aligned} \delta U = Q_r^{damp} \cdot \delta r + Q_\theta^{damp} \cdot \delta\theta \\ + Q_r^{bar} \cdot \delta r + Q_\theta^{damp} \cdot \delta\theta, \end{aligned} \tag{D.26}$$

where

$$Q_r^{bar} = F_{bx}\cos(\theta) + F_{bz}\sin(\theta), \tag{D.27}$$

$$Q_\theta^{bar} = -F_{bx}(l_0 + r)\sin(\theta) + F_{bz}(l_0 + r)\cos(\theta), \tag{D.28}$$

where F_{bx} and F_{bz} are the barrier forces experienced by the vehicle in the horizontal and vertical directions. These values are included from the FE simulation data. Damper forces are presented below:

$$\begin{aligned} D = \frac{1}{2}c\dot{r}^2 + \frac{1}{2}c_1[(l_0 - l_1 + r)^2 + \dot{r}\theta]^2 \\ + \frac{1}{2}c_2[(l_0 + l_2 + r)^2 + \dot{r}\theta]^2, \end{aligned} \tag{D.29}$$

$$\begin{aligned} Q_r^{damp} = c\dot{r}\cos(\theta) + c_1[(l_0 + r - l_1) + + \dot{r}\theta] \\ + c_2[(l_0 + r + l_2) + \dot{r}\theta]\sin(\theta), \end{aligned} \tag{D.30}$$

$$\begin{aligned} Q_\theta^{damp} = -c\dot{r}(l_0 + r)\sin(\theta) + [c_1(l_0 + r - l_1)\dot{\theta} + \\ + c_2[(l_0 + r + l_2)\dot{\theta}](l_0 + r)\cos(\theta), \end{aligned} \tag{D.31}$$

where c_1 and c_2 are the damper coefficients for the front and rear suspensions.

D.3 Results and Discussion

The LPM was simulated in Simulink and the results were compared with the data generated from the FE model for a 2014 Chevrolet Silverado impacting a rigid barrier at 56 kmph. The curve outputs from LS Dyna were converted to polar coordinates before overlaying them with LPM results. The Simulink model was run with an ode 45 (fixed solver) and the change of the solver type did not improve or deteriorate the performance of the model. Prediction of the velocity of the vehicle after impact for the entire impact event is crucial for vehicle design in the development stages; in most cases the time of maximum crush coincides with the instant when the vehicle stops. The maximum crush (displacement) contributes to the energy absorbed by the front end members and is an important parameter for vehicle injury prediction. As described in the previous section, in a full vehicle impact scenario, the vehicle pitches forward which may lead to serious head and neck injuries to occupants. Vehicle pitch angle plays an important role in designing active safety measures like airbags by helping to mitigate occupant injuries. The pendulum inspired model developed in this study predicts these parameters; the maximum displacement of the vehicle in the LPM is overlayed with FE data in Figure D.7.

The values of k_1, k_2, c_1, c_2, l_1, l_2 and l_0 in Table D.1 were taken from [22]. The

Table D.1: Automotive Parameters set [22]

Symbol	Value	Unit	Meaning
M	400	kg	Sprung mass
m_{ij}	50	kg	Unsprung masses (i = front, rear and j = left, right)
I_x	250	kg.m^2	Roll inertia
I_y	1400	kg.m^2	Pitch inertia
t	1.4	m	Front and rear axle
l_f	1.4	m	COG-front distance
l_r	1	m	COG-rear distance
r	0.3	m	Nominal wheel radius
h	0.7	m	Chassis COG height
k_f	30,000	N/m	Front suspension linearized stiffness (left, right)
k_r	20,000	N/m	Rear suspension linearized stiffness (left, right)
c_f	1500	N/m/s	Front suspension linearized damping (left, right)
c_r	3000	N/m/s	Rear suspension linearized damping (left, right)
k_t	200,000	N/m	Tire stiffness (front, rear and left, right)
β	50	rad/s	Suspension actuator bandwidth

vehicle deformation recorded from the LPM was plotted against the test data in Figure D.7. The maximum displacement in the vehicle front end is very closely

correlated with the test data; this indicates that the prediction of vehicle deformation with model is accurate. The LPM curves, however, drop after 100 ms which can be attributed to the spring rebound in the model. The time the vehicle velocity

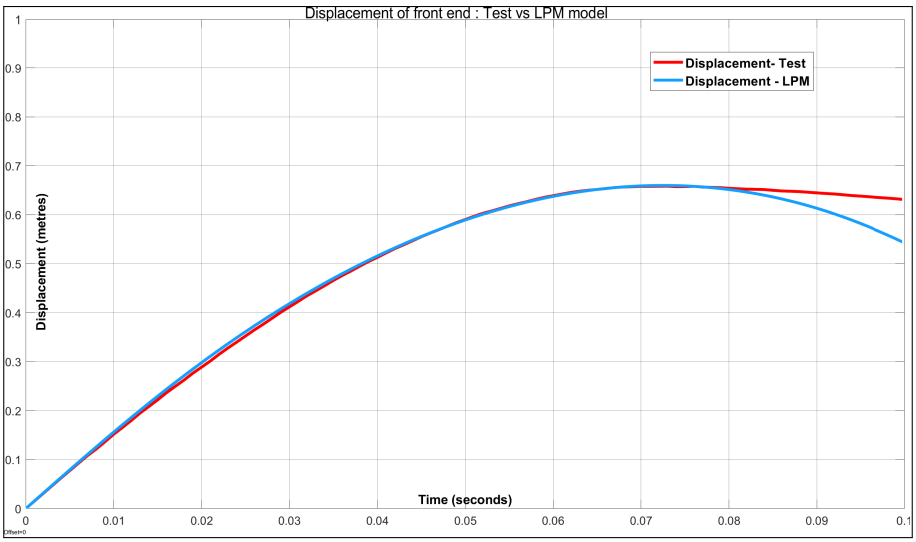

Figure D.7: LPM simulation vehicle deformation curves compared with FE simulation data

becomes zero generally coincides with the instant for maximum crush making the prediction of velocity change on the vehicle an important parameter for improving crash performance. The curves comparing the test and LPM velocity curves show good correlation with close prediction of the time when the vehicle attains zero velocity as shown in Figure D.8. The vehicle pitching angle is an important parameter to determine the injury to occupants; the LPM and test curves were overlayed to observe acceptable prediction values of the pitching angle in Figure D.9. The vehicle rotations in the other axes were neglected in this study. The model over-predicts in case of pitching which can be addressed by taking into account spring rebound, however, the close correlation between the LPM and the FE data increases confidence in using LPMs for predicting occupant injuries in the future.

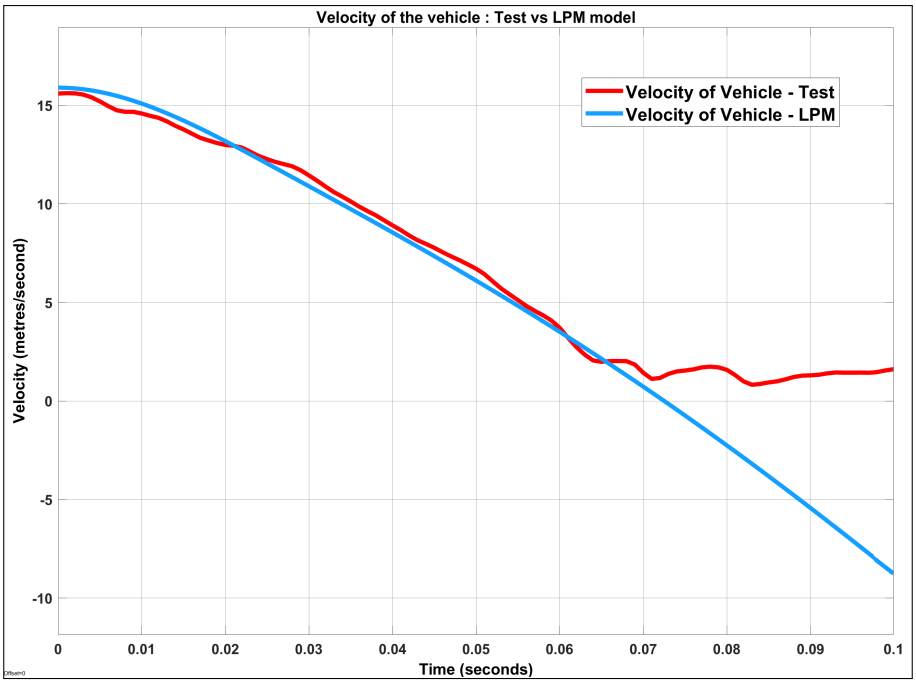

Figure D.8: LPM simulation vehicle velocity curves compared with FE simulation data.

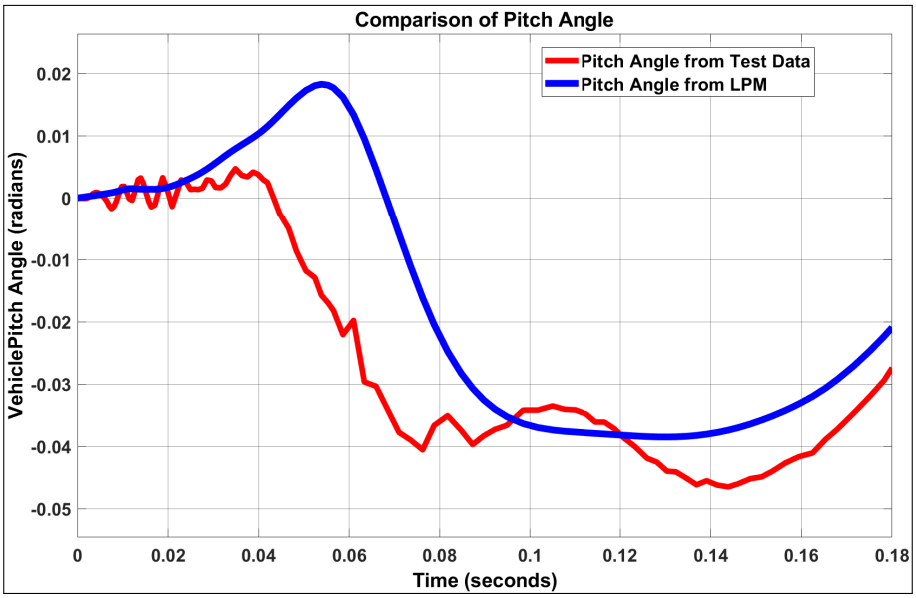

Figure D.9: LPM simulation vehicle deformation curves compared with FE simulation data.

D.4 Conclusions

Vehicle safety is one of the major concerns both for the customers and for the automotive industry. Safety standards become more and more stringent, comprehensive safety tests are being meticulously conducted on new vehicles, and serious injuries in road crashes are being constantly monitored, documented and analyzed for improving vehicle safety. Identifying a frontal impact as the most common scenario resulting

in serious injuries, a recent report of the European Commission [1] calls for further research into vehicle safety. During the last decade there has been a noticeable progress in the development of reliable mathematical models that can be used for the analysis of various aspects of a vehicle crash [21]. Mathematical modeling and computer simulation successfully complement and even replace physical crash tests because they combine a high predictive power with substantially lower modeling costs.

In this paper, we suggest a novel mathematical model for a full frontal vehicle crash. The following key aspects distinguish our model from those reported in the literature. First, instead of focusing on the pitching about the center of gravity as most existing models do, we simulate the vehicle pitching during a full frontal crash about the point of impact. Second, contrary to traditional approaches based on the use of Newtonian formulation [4], [8] for the derivation of the governing equations of motion, we use relativistic Lagrangian formulation; the model equations are further simplified by conversion to polar coordinates. Third, we model the motion of the occupant compartment during the frontal impact as a rotation of a compound elastic pendulum about a pivot point; the pendulum uses a spring damper system for absorbing the impact energy. An LPM model with five DOF designed in the paper has been simulated in Simulink. The results of the simulation correlate quite well with the data obtained in an FE simulation model developed by NHTSA. Since our model successfully replicates vehicle dynamics during the crash against a rigid barrier, predicted parameter values for the front end deformation and pitching can be used by the automotive industry at initial stages of vehicle design.

References – Paper D

[1] Wendy Weijermars, Niels Bos, Annelies Schoeters, Jean-Christophe Meunier, Nina Nuyttens, Emmanuelle Dupont, Klaus Machata, Robert Bauer, Katherine Perez, Jean-Louis Martin, Heiko Johansson, Ashleigh Filtness, Laurie Brown, and Pete Thomas. Serious Road Traffic Injuries in Europe, Lessons from the EU Research Project SafetyCube. *Transportation Research Record: Journal of the Transportation Research Board*, 2672(32):1–9, 12 2018. ISSN 0361-1981. doi: 10.1177/0361198118758055. URL `http://journals.sagepub.com/doi/10.1177/0361198118758055`.

[2] Gulshan Noorsumar, Kjell Robbersmyr, Svitlana Rogovchenko, and Dmitry Vysochinskiy. Crash Response of a Repaired Vehicle - Influence of Welding UHSS Members. In *WCX SAE World Congress Experience*. SAE International, 4 2020. doi: https://doi.org/10.4271/2020-01-0197. URL `https://doi.org/10.4271/2020-01-0197`.

[3] J. Michael Chang, Mohammed Rahman, Mohammad Ali, Tau Tyan, Marwan El-Bkaily, and James Cheng. Modeling and design for vehicle pitch and drop of body-on-frame vehicles. *SAE Technical Papers*, 114(2005):329–338, 2005. ISSN 26883627. doi: 10.4271/2005-01-0356.

[4] Ahmed Elmarakbi, Mustafa Elkady, and John MacIntyre. Numerical analysis of vehicle-to-vehicle impact using vehicle dynamics control systems for collision mitigation. *International Journal of Dynamics and Control*, 1(2):172–191, 6 2013. ISSN 21952698. doi: 10.1007/s40435-013-0017-x.

[5] Gulshan Noorsumar, Svitlana Rogovchenko, Kjell Robbersmyr, Dmitry Vysochinskiy, and Andreas Klausen. A Novel Technique for Modeling Vehicle Crash using Lumped Parameter Models. pages 62–70, 7 2021. doi: 10.5220/0010529200620070.

[6] J. Michael Chang, Miinshiou Huang, Tau Tyan, G. Li, and L. Gu. Structural optimization for vehicle pitch and drop. In *SAE Technical Papers*. SAE International, 4 2006. doi: 10.4271/2006-01-0316. URL `https://www.sae.org/publications/technical-papers/content/2006-01-0316/`.

[7] J. Michael Chang, Mohammad Ali, Ryan Craig, Tau Tyan, Marwan El-Bkaily, and James Cheng. Important modeling practices in CAE simulation for vehicle pitch and drop. In *SAE Technical Papers*. SAE International, 4 2006. doi: 10.4271/2006-01-0124. URL `https://www.sae.org/publications/technical-papers/content/2006-01-0124/https://www.sae.org/publications/technical-papers/content/2006-01-0124/?PC=DL2BUY`.

[8] Mustafa Elkady, Ahmed Elmarakbi, and John Macintyre. Enhancement of vehicle safety and improving vehicle yaw behaviour due to offset collision using vehicle dynamics. *International Journal of Vehicle Safety*, 6(2):110–133, 2012. ISSN 14793113. doi: 10.1504/IJVS.2012.049011.

[9] D.J. Benson, J.O. Hallquist, M. Igarashi, K. Shimomaki, and M. Mizuno. Application of DYNA3D in large scale crashworthiness calculations, 1986. URL `http://inis.iaea.org/Search/search.aspx?orig_q=RN:17073039`.

[10] C.-S Böttcher, S Frik, and B Gosolits. 20 Years of Crash Simulation at Opel-Experiences for Future Challenge. Technical report, 2005.

[11] M. M. Kamal. Analysis and simulation of vehicle to barrier impact. In *SAE Technical Papers*. SAE International, 1970. doi: 10.4271/700414.

[12] Bernard B. Munyazikwiye, Dmitry Vysochinskiy, Mikhail Khadyko, and Kjell G. Robbersmyr. Prediction of Vehicle Crashworthiness Parameters Using Piecewise Lumped Parameters and Finite Element Models. *Designs*, 2(4):43, 10 2018. ISSN 24119660. doi: 10.3390/designs2040043.

[13] A. Deb and K. C. Srinivas. Development of a new lumped-parameter model for vehicle side-impact safety simulation. *Proceedings of the Institution of Mechanical Engineers, Part D: Journal of Automobile Engineering*, 222(10): 1793–1811, 2008. ISSN 09544070. doi: 10.1243/09544070JAUTO801.

[14] Nikolay Pavlov. Study the vehicle pitch motion by spring inverted pendulum model. (February), 2019.

[15] Oscar Cyrén and Sofia Johansson. Modeling of Occupant Kinematic Response in Pre-crash Maneuvers A simplified human 3D-model for simulation of occupant kinematics in maneuvers. Technical report.

[16] Shouhong Miao and Qixin Cao. Modeling of self-tilt-up motion for a two-wheeled inverted pendulum. *Industrial Robot*, 38(1):76–85, 2011. ISSN 0143991X. doi: 10.1108/01439911111097878.

[17] Crash Simulation Vehicle Models | NHTSA. URL https://www.nhtsa.gov/crash-simulation-vehicle-models.

[18] Andreas Klausen, Sondre Sanden Tordal, Hamid Reza Karimi, Kjell G. Robbersmyr, Mladen Jecmenica, and Ole Melteig. Mathematical modeling and optimization of a vehicle crash test based on a single-mass. *Proceedings of the World Congress on Intelligent Control and Automation (WCICA)*, 2015-March (March):3588–3593, 3 2015. doi: 10.1109/WCICA.2014.7053313.

[19] Mustafa Elkady and Ahmed Elmarakbi. Modelling and analysis of vehicle crash system integrated with different VDCS under high speed impacts. *Central European Journal of Engineering*, 2(4):585–602, 2012. doi: 10.2478/S13531-012-0035-Z.

[20] Herbert Goldstein, Charles Poole, John Safko, and Stephen R. Addison. Classical Mechanics, 3rd ed. . *American Journal of Physics*, 70(7):782–783, 7 2002. ISSN 0002-9505. doi: 10.1119/1.1484149. URL http://aapt.scitation.org/doi/10.1119/1.1484149.

[21] Gulshan Noorsumar, Svitlana Rogovchenko, Kjell G. Robbersmyr, and Dmitry Vysochinskiy. Mathematical models for assessment of vehicle crashworthiness: a review. *https://doi.org/10.1080/13588265.2021.1929760*, 2021. doi: 10.1080/13588265.2021.1929760. URL https://www.tandfonline.com/doi/abs/10.1080/13588265.2021.1929760.

[22] Sergio Savaresi, Charles Poussot-Vassal, Cristiano Spelta, Olivier Sename, and Luc Dugard. Semi-Active Suspension Control Design for Vehicles. *Semi-Active Suspension Control Design for Vehicles*, 2010. doi: 10.1016/C2009-0-63839-3.

Paper E

Crash Response of a Repaired Vehicle - Influence of Welding UHSS Members

Gulshan Noorsumar, Kjell G. Robbersmyr, Svitlana Rogovchenko and Dmitry Vysochinskiy

This paper has been published as:

Gulshan Noorsumar, Kjell G. Robbersmyr, Svitlana Rogovchenko and Dmitry Vysochinskiy. Crash Response of a Repaired Vehicle - Influence of Welding UHSS Members. *SAE Technical Paper* 2020-01-0197, 2020, doi: 10.4271/2020-01-0197, ISSN: 0148-7191, e-ISSN: 2688-3627.

Crash Response of a Repaired Vehicle - Influence of Welding UHSS Members

Gulshan Noorsumar, Kjell G. Robbersmyr, Svitlana Rogovchenko and Dmitry Vysochinskiy.
Department of Engineering Sciences
University of Agder
4879 Grimstad, Norway

Abstract **Automakers generally recommend not to weld structural parts after a vehicle crash, and these should be replaced as a whole part in case of a crash event. Sectioning of these members is also not recommended, and use of the repair manual is mandatory in case of fracture of such parts. However, repair shops may not adhere to these instructions and use incorrect repair procedures on these members which would modify their strength properties. This study analyses the impact of welding structural members in a vehicle like the A-pillar which use Ultra-High Strength Steels (UHSS) for reducing the weight of the vehicle and improving the crashworthiness of the structure. The research conducted in this paper highlights the differences in the crash performance of a repaired vehicle as opposed to baseline injury values for the vehicle. The performance of the modified vehicle when tested for different loadcases shows reduced crash performance as compared to the baseline performance and it can be concluded that welding or sectioning the UHSS parts would influence the crashworthiness of a vehicle. This paper only focuses on structural integrity of the repaired vehicle in a crash event. The performance of the vehicle in occupant injury is kept out of scope for this study.**

E.1 Introduction

The word 'crashworthiness', first used in the aerospace industry around the early 1950's provided a measure of the ability of the structure to protect its occupants in survivable crashes [1]. In the automotive industry the term refers to the measure of vehicle's structural abilities to plastically deform and absorb sudden impact loads while maintaining enough survival space for the occupants. The goal of crashworthiness: Vehicle structures should be stiff in bending and torsion for proper ride and handling. The vehicle structures should minimize fore-aft vibrations that give rise to harshness. The vehicle structure should [1]:

- Deform plastically in the vehicle front end and absorb crash energy in case of a frontal crash and prevent intrusions in the driver compartment
- Deformable rear structure to protect rear occupants in case of a rear impact and well-designed side structures to prevent intrusion into passenger compartment and preventing opening of doors due to loading in a crash

In October 2015, the European Commission launched a study to analyse crashes in order to identify a number of most common crash scenarios with serious injuries as an outcome. In all datasets frontal impacts are most common followed by side-impacts in crashes where car occupants get severely injured. This might be related to the differences in impact and the force at which the cage of the car protects the occupant when hit from different sides as well as a reflection of the probability that a car is hit on a particular side [2]. Some of the recommendations provided by the report suggest further study of mechanisms and effective measures directed at severe injuries in road accidents. EuroNCAP is one of the global New Car Assessment Programme (NCAP) that has been influential in bringing about improvements in vehicle safety. However, it's commonly referred to as 'consumer metric' because it is not based on government regulations/legislations. Car makers across the globe treat this as a common metric to determine the crashworthiness of their products and achieve a target star rating [3]. These regulations and consumer ratings have led automakers to use innovative technologies in the form of active and passive safety to meet the performance requirements [4]. One of the conventional design solutions used by automakers to meet front end crash requirements is to increase the gauge of the structural load bearing members. This leads to increased durability of the members and improved occupant protection. However, upsizing the thickness led to mass increase and reduced fuel economy. According to the research in [3] the automobile weight loss is 10%, the consumption of fuel reduced by 8% and the emissions reduced by 4%. This propelled the need for automakers to optimize the vehicle mass while meeting the crash requirements leading to use of Advanced High Strength Steel (AHSS) in structural members of the vehicle. Steels with yield strength levels in excess of 550MPa are generally referred to as AHSS. These are also sometimes called Ultra-High Strength Steels (UHSS) for tensile strengths exceeding 780 MPa [5]. The research conducted in [4] emphasized the influence of AHSS parts in crash behavior and concluded that using these steel grades improves the crashworthiness of the vehicle. The study in [6] introduced AHSS to auto-roof strength application and studied by FEA simulation to demonstrate that AHSS design can meet the proposed more stringent roof crush requirement. The excellent properties of steel are achieved by employing common alloying elements (carbon, manganese, boron, silicon, nickel, chromium and molybdenum) and other metallurgical strengthening mechanisms

which help in its excellent tensile strength [7]. However, these strength properties come with difficulties associated with the welding and joining processes for these materials which can affect its properties. The research paper [7] lists down the difficulties encountered during welding and Heat Affected Zone (HAZ) softening of UHSS and the possible impact of these processes on the material behavior [7].

Collision repair of vehicle is a process which is outlined by an automaker for every product in its portfolio and it includes the procedure to repair/replace a part in the vehicle. The repair manual is a detailed document which explains the process for every part in the vehicle based on its structural properties, influence of heat treatment and crashworthiness abilities. The manual also lists down the circuits diagrams for electrical components to help the technicians who have the specific tools/facilities to repair cars. Most automakers suggest replacement of structural components after plastic deformation and prohibit heat repair for body and frame parts. The parts using UHSS are recommended not to undergo reinforcement repair to ensure the crashworthiness of the vehicle and occupant protection features are not modified. This is crucial to the safety of occupants because in the event of a crash of the repaired car the structural integrity of the vehicle should prevent occupant compartment intrusions.

However, it has been observed in certain cases that the repair shops/technicians may not follow the procedures outlined by the automakers which could lead to safety issues for the occupants of the vehicle in a crash. Unprofessional repairs could result due to the following reasons: [8]

- Repair of parts when replacement is necessary or recommended
- Insufficient knowledge of repairing the parts leading to wrong assembly or processes
- Incorrect process to repair the parts
- Absence of special tools
- Use of poor/low quality spares and components
- Incorrect connections and wiring of electrical harnesses or subsystems

The recommended procedures for UHSS parts are replacement of the complete part and following the repair manual from the Original Equipment Manufacturer (OEM) strictly. This would prevent compromising the structural integrity of the vehicle and occupants in a crash. Recent trends involve car manufacturers resort to Computer Aided Engineering (CAE) using an FE (finite element) model of the vehicle which represents the geometry of the vehicle and includes material non-linearities. These models help to test the vehicle for different crash scenarios instead

of conducting a physical test. These FE models aid in the vehicle development cycle and are updated during different stages of vehicle development. Automakers also put huge focus on CAE modeling strategies to accurately represent different parts of the vehicle and their interactions. There are commercially available solvers like LS Dyna and PamCrash which help predict the crash scenario in vehicle FE models. These solvers can support complex geometries and fine mesh sizes to accurately predict injury values. This has led to the automotive CAE engineers use complex models with mesh refinement to capture the geometry and material characteristics. The result is accurate representation of crash mechanics at the expense of huge computational times and high solver capacities required to run these simulations.

Several attempts have been made to reduce computational time of full vehicle models by using simplified structural modeling. The simplified model developed by Michael et. al. [9] is validated against a full-frontal barrier model and shows encouraging results. The use of beam grid model is a growing trend in CAE to represent a vehicle crash model. Reducing run time of an FE model using beam grid approach was attempted and shows considerable reduction in computational time [10].

Crash performance of vehicle structures in different impact scenarios was studied in detail in [11]. The paper focusses on developing a simplified crash model for analysis and then validating the simulation results with physical test data. Several similar studies have been conducted to compare the FE models with physical test data to gain confidence on using LS Dyna simulations to predict crash injury values. In this study we attempt to examine the impact of unprofessional repairs on a vehicle which uses UHSS and conduct crash test simulations on the vehicle after a repair which does not follow standard repair procedures. This paper addresses different scenarios of improper repairs and the possible consequences after an impact. The crash tests simulations are performed on a Finite Element (FE) model using LS Dyna non-linear analysis solver. The study also compares the iteration results with Finite Element simulations performed using the baseline FE model.

This study was conducted on the 2011 Honda Accord (Sedan) vehicle. These models were selected because they use UHSS for the load bearing members. The finite element models were developed by National Highway Traffic Safety Administration (NHTSA) along with National Crash Analysis Center (NCAC) [12]. It is to be noted that this study uses the FE models from the NHTSA database but it does not try to replicate the light weight study or change the content of the report published by the team at NHTSA.

E.2 FE Model Description

The Honda Accord Model (2011), a 4 door mid-size sedan was developed by a research team led by NHTSA to represent this vehicle with a detailed finite element model and used to replicate multiple impact scenarios. The research project modified the vehicle to a light-weight version using UHSS having high yield strength (1250-1500 MPa) and improve performance for crash regulations [13]. The study conducted for this paper uses the modified vehicle as a baseline model and modifications are made on the vehicle to replicate unprofessional repair procedures. The study also employs different Computer Aided Engineering (CAE) methodologies to represent repair strategies and observe the changes in the results. The FE model was run for baseline impact with the following front and side impact regulations.

- IIHS Small-Overlap Frontal Barrier Test
- NCAP Front Impact Test
- IIHS Moderate Frontal Offset Test
- IIHS Lateral Moving Deformable Barrier Test
- NCAP Side Impact Test
- Lateral NCAP Pole Side

The modifications made to the baseline vehicle were updated to all the models and run for evaluating all the loadcases and observe the differences in the performance in comparison to the base vehicle.

E.3 Loadcase Requirements

The instrumentation needed for these tests measures the severity of impact on the structural integrity and occupant dummies used for the test. Occupant protection has been kept out of scope for this study.

E.3.1 IIHS Small-Overlap Frontal Barrier Test (IIHS SOL)

This test is conducted at 40 mph vehicle speed when the vehicle hits a 5-foot tall rigid barrier. This test tries to replicate a scenario of a vehicle hitting another vehicle, an object or a utility pole. The test conducted on the driver side strikes the barrier at 25% width of the vehicle from the vehicle centerline.

The regulation rates the vehicle on the basis of structural integrity of the vehicle at 7 points of the vehicle interior plus, movement of three points along the door

frame. This is a total of 18 points on the vehicle [14]. The 18 points are distributed as follows: Steering Column (1), Left Instrument Panel (1), Brake Pedal (1), Parking Brake Pedal(1), Footrest (1), Seat Bolts(2), Left Toepan (1), Upper Dash (1), Lower (three points) and upper (three points) hinge pillar, Rocker panel (three points),

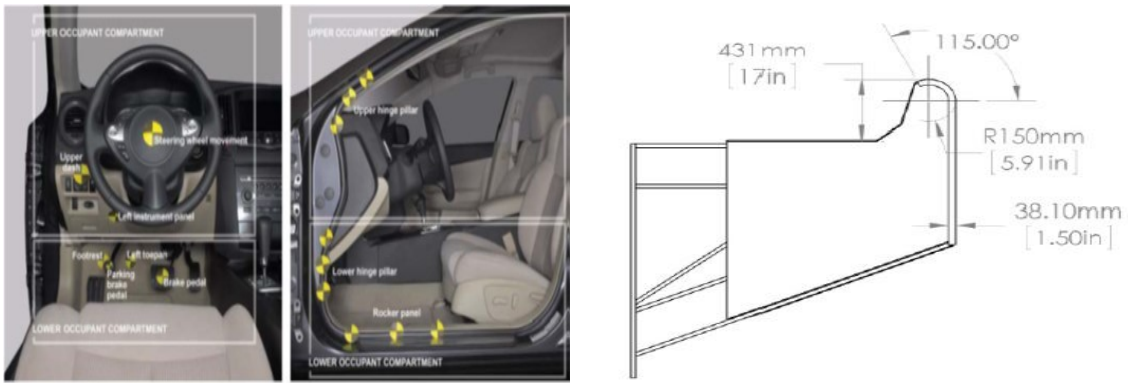

(**a**) (**b**)

Figure E.1: (a) Locations used for measuring vehicle intrusion, (b) SOL Barrier, Top and Isometric Views

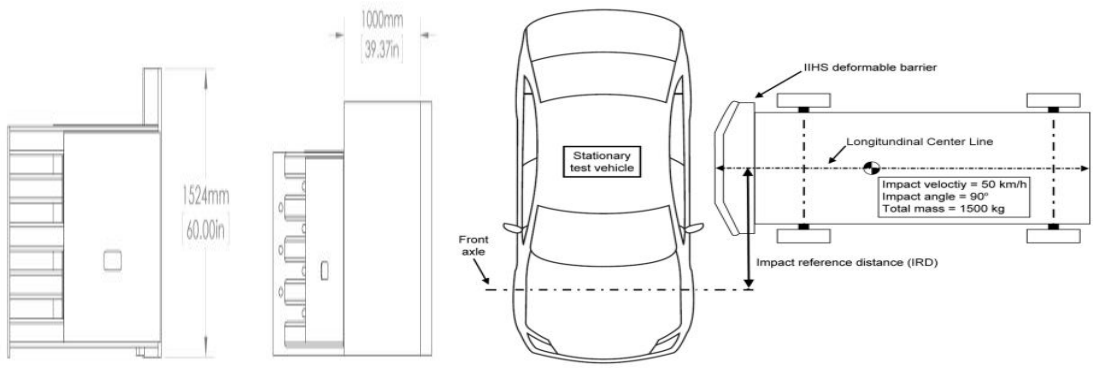

(**a**) (**b**)

Figure E.2: (a) SOL Barrier, Side and Front Views, (b) IIHS Lateral Moving Deformable Barrier aligned with the test vehicle [

The points of measurement on the vehicle lower occupant compartment and upper occupant compartment are shown in Figure E.1(**a**) below [14]. Figure E.1(**b**) and E.2(**a**) indicate the SOL barrier top, isometric, side and front views.

E.3.2 NCAP Front Impact Test

This is a full-width impact on the vehicle front. This test is run with a rigid barrier and the vehicle meeting a head-on collision at 56 kmph. The NCAP test for full frontal impact has shorter pulse time width and lower occupant compartment intrusion [13].

E.3.3 IIHS Moderate Frontal Offset Test

This test, as the name suggests, is a frontal offset crash test with the vehicle hitting a 40% overlap barrier. The vehicle speed is 64 kmph and the intrusions on the driver side are measured at 14 locations on the interior and exterior of the vehicle. The coordinates of these 14 locations before and after the crash are recorded and compared to understand the intrusion in the driver compartment. The barrier has a rigid base unit, an extension and a deformable face. The barrier specification has been outlined in the IIHS protocol.

E.3.4 IIHS Lateral Moving Deformable Barrier Test

This test includes a 1500 kg moving deformable barrier hitting a stationary vehicle at a speed of 50 kmph. The barrier strikes the vehicle at 90 degrees angle to the driver side and the longitudinal impact point of the barrier on the side of the test vehicle is dependent on the wheelbase. The impact reference distance is defined as the distance rearward from the test vehicle's front axle to the closest edge of the deformable barrier when it first contacts the vehicle. The standard barrier is a trolley vehicle with a deformable front end. The intrusion measured on the vehicle at different ground heights at the vehicle B-pillar helps document the IIHS safety rating. Figure E.2(**b**) shows the IIHS Lateral Moving Deformable Barrier loadcase setup.

E.3.5 NCAP Side Impact Test

The Lateral NCAP moving deformable barrier test is a side impact test with a moving deformable barrier, weighing 1368 kgs and it strikes a stationary vehicle (positioned at an angle of 63 degrees to the line of forward motion).The barrier moves with a speed of 62kmph. Figure E.3 shows the orientation of the trolley for NCAP side test.

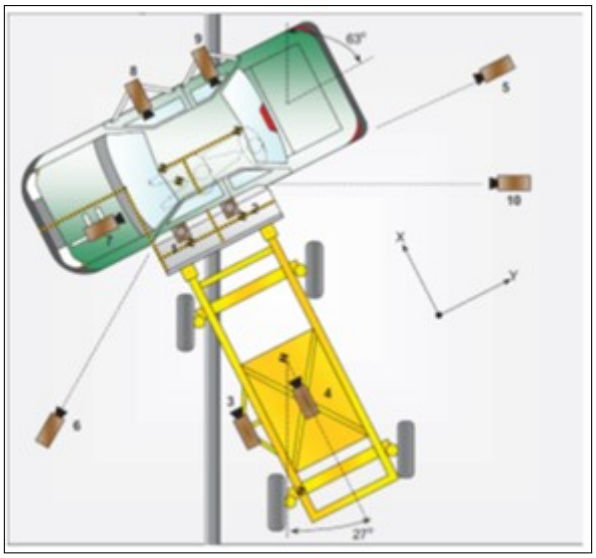

Figure E.3: Orientation of trolley to struck vehicle in NCAP side impact test with moving deformable barrier

E.3.6 IIHS Moderate Frontal Offset Test

This test, as the name suggests, is a frontal offset crash test with the vehicle hitting a 40% overlap barrier. The vehicle speed is 64 kmph and the intrusions on the driver side are measured at 14 locations on the interior and exterior of the vehicle. The coordinates of these 14 locations before and after the crash are recorded and compared to understand the intrusion in the driver compartment. The barrier has a rigid base unit, an extension and a deformable face. The barrier specification has been outlined in the IIHS protocol.

E.4 CAE Methodology

The study includes setting up finite element crash tests for the loadcases and using LS Dyna solver to simulate the impacts. The FE model chosen for this study uses UHSS on the A-pillar reinforcements and some rocker reinforcements. The baseline model was run with the crash loadcases and the results compared to data furnished in the report from NHTSA in [13]. The baseline model meets all safety loadcase requirements with a good margin and was a good candidate to investigate if the performance deteriorated with inclusion of incorrect repairing strategies. A preliminary study was conducted on the FE model with removing few rows of elements from the A-Pillar part to investigate its influence on the crash regulations. (Figure E.4) This modified vehicle representing cracks on a vehicle A-Pillar was simulated with the crash loadcases and the results were compared with baseline performance of the vehicle. The IIHS SOL loadcase showed considerable performance deterioration

over the base model. This modification emphasized the need to investigate more on the A-Pillar contribution on the load distribution in a crash event. Figure E.5 shows A-Pillar failure in the modified model. The baseline model in yellow and the modified (iteration) in blue show comparisons between the two animations.

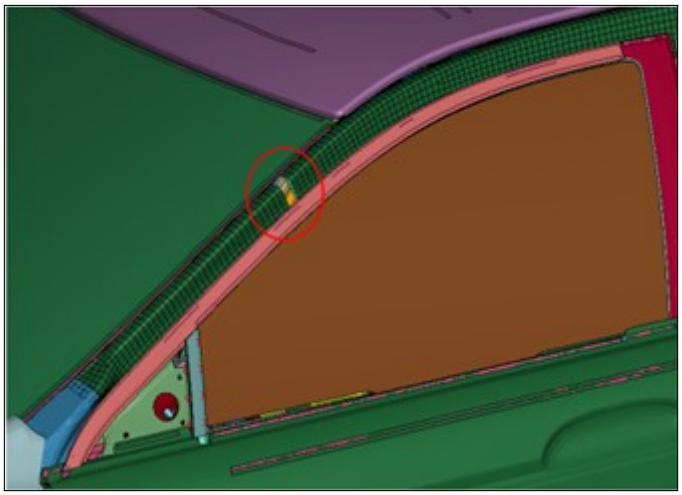

Figure E.4: Encircled zones show A-Pillar failure in the modified model (in blue) and absence of buckling in the baseline model (in yellow).

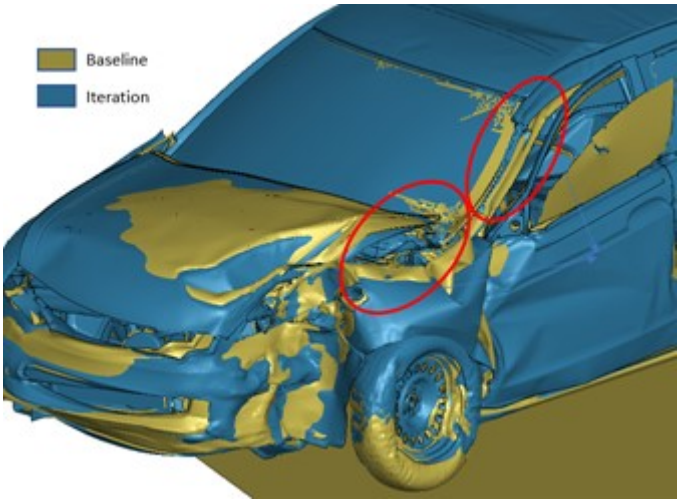

Figure E.5: Encircled zone shows A-Pillar elements removed for the preliminary study.

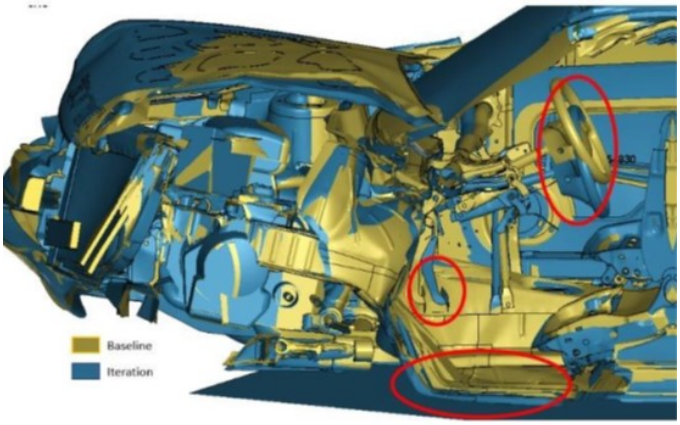

Figure E.6: Vehicle cut section showing higher intrusion in the vehicle compartment.

The modified model is observed to have more deformation in the A-Pillar and door structural members (Figure E.5). This indicated that the load distribution of a crash model is changed by a small fracture in the UHSS part. The buckling in the A-pillar shows reduced structural performance in the iteration model. Figure E.6 shows higher intrusion in the driver compartment, steering wheel axial and lateral movement and brake pedal movement in the occupant zone.

E.4.1 Representation of Welding of UHSS:

One of the incorrect repair procedures is welding the UHSS steel members which considerably reduces its yield strength and causes it to yield much before the expected time. The baseline FE model was modified to include butt welds in the A-Pillar to represent the Heat Affected Zone (HAZ). Different CAE strategies were employed to represent the weak zone in the structural steel part. It is to be noted that only UHSS parts on the A-Pillar were modified for the study, the parts with mild steel were not modified on the A-Pillar.

- Representing a small zone on the UHSS member with a part having low yield strength material
- Using beam elements to represent the weld material in the part
- Incorporating beams in the weld zone and surrounding elements being assigned with low yield strength dyna material model to represent the HAZ.

These strategies were simulated to understand the crash event kinematics.

The strategy (a) showed buckling in the A-Pillar and could be used for the study but the challenge was to determine the yield strength of the heat affected zone after welding the part. This could be investigated with tensile tests conducted on the welded specimen, but it was omitted in this study.

The strategy (c) above provided unrealistic results and was discarded for this study.

The strategy to use welding beams (b) was used for this study and compared against all crash loadcases of the baseline model. The weld material assigned to the parts was dyna material card used for other welds in the finite element model. The beam elements are connected to the A-Pillar with nodes shared to the shell elements in the A-Pillar. This represents a butt weld which connects two pieces of metal. The figure E.7 below shows the material data for beams representing the weld.

MAT SPOTWELD CARD FROM LS DYNA (SI Units)

Mass Density	Young's Modulus	Poisson's Ratio	Yield Stress	Plastic Hardening Modulus
1.8 E-9	20000	0.3	120	2000

Effective Plastic Strain in weld material at failure	Axial Force Resultant at Failure	Force Resultant at Failure
1.5	60000	30000

Figure E.7: LS Dyna Weld Material Data for Beam Elements used in the model.

E.5 Results of crash loadcase comparison with welded beams.

E.5.1 IIHS Small-Overlap Frontal Barrier Test (IIHS SOL)

The IIHS SOL test was run with baseline model and butt welds added to the vehicle A-Pillar. The CAE model represents a butt weld and the acceleration at the vehicle CG and at points on the A-Pillar show differences in baseline performance. The A-Pillar in the baseline does not show buckling, however the welded model buckles and shows higher intrusion in the driver compartment (Figure E.8 and E.9)This is an alarming observation because the A-Pillar is a structural member which distributes the load during the impact and failure of this part also leads to cracking of the windshield. Another important observation in this iterative model is that the A-Pillar buckles at a point away from the weld and closer to the hood edge. This failure was not observed on the baseline model. The windshield impact could lead to change in airbag timing [7]. This is, however not investigated as part of this study. The intrusion numbers for IIHS swings to the acceptable zone from the 'Good' zone for the

vehicle. It is to be noted that the IIHS SOL baseline performance for this model was comfortably within the targets, however, welding a model with marginal performance could possibly lead to shifting the performance to the 'Poor' zone. (Figure E.9). The dashed lines in the figure represent the performance metrics for IIHS SOL test as laid down by the crash regulatory agency (IIHS) for this loadcase.

Another important observation for this model is the structure of the driver side door looks compromised and may not open properly post-crash for occupant ejection. Figure E.11 shows the door deformation compared to the baseline model and it shows higher deformation. It is important the door stays closed during a crash to avoid occupants being thrown out of the vehicle and assists in airbag deployment. The acceleration measured in the A-Pillar region is shown in Figure E.12 below. The acceleration curves show changes in load distribution in the vehicle structural members. The unexpected peaks in the acceleration curve for the modified vehicle explains the energy being distributed to the driver compartment which is not the intended path for a crash event. The acceleration pulses at the vehicle CG shows similar magnitude and duration for the two models (Figure E.13)

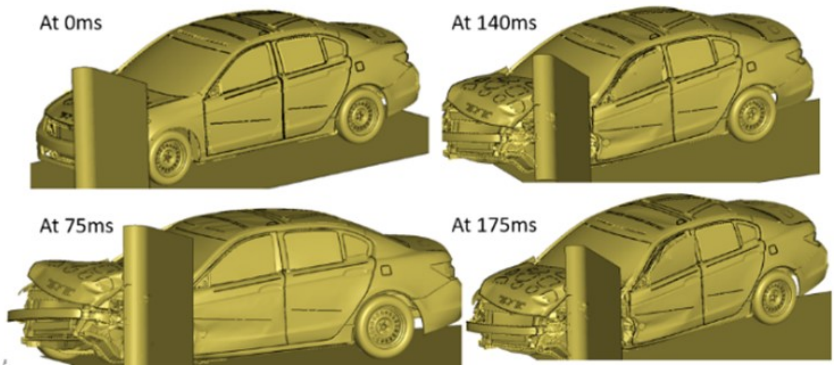

Figure E.8: Baseline performance of Honda Accord for IIHS Small Overlap Test.

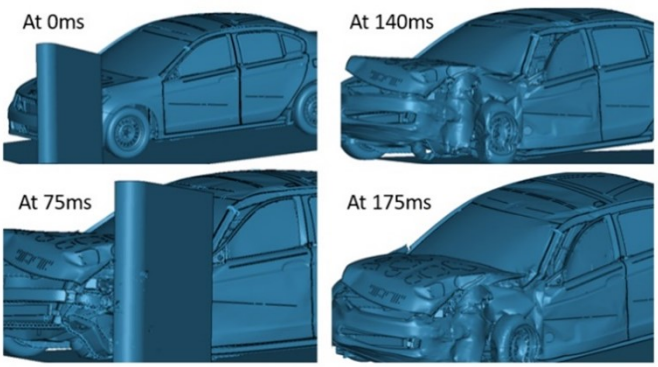

Figure E.9: Modified model Honda Accord with IIHS Small Overlap.

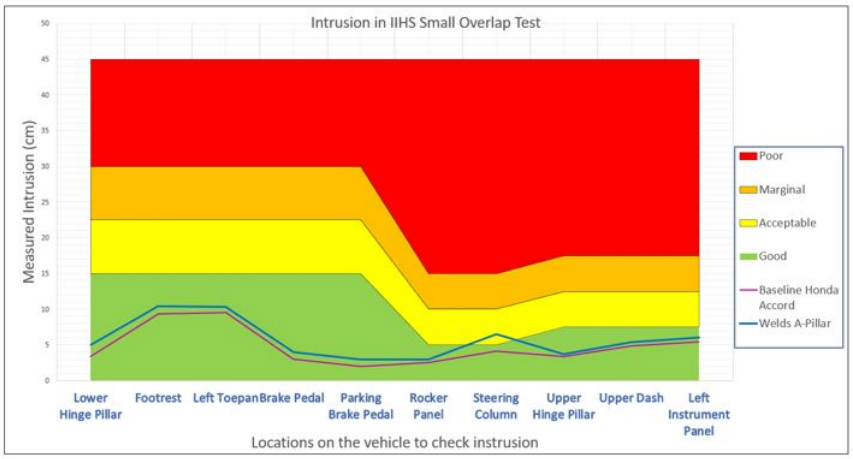

Figure E.10: Measured Intrusion against different positions in the driver compartment for baseline and modified vehicle.

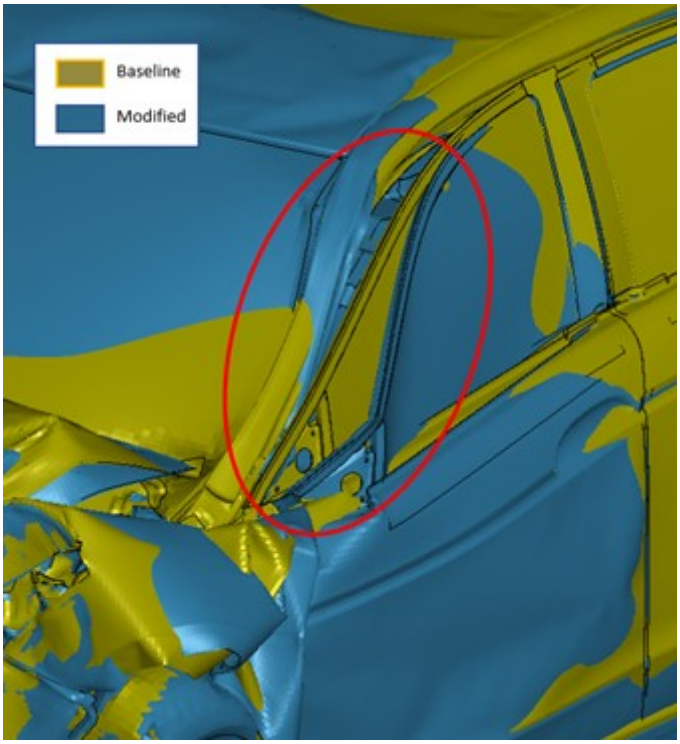

Figure E.11: Vehicle structural changes in the driver compartment for baseline and modified vehicle.

E.5.2 NCAP Front Impact

The front impact test conducted on the baseline and iteration model yields similar performance indicating nominal impact on the performance of the model with welds. One of the reasons for this reduced impact is enough crush space on the baseline vehicle which does not allow the forces to reach the A-Pillar. The acceleration pulses as shown in Figure E.14 and E.15 on the passenger and driver side of the vehicle

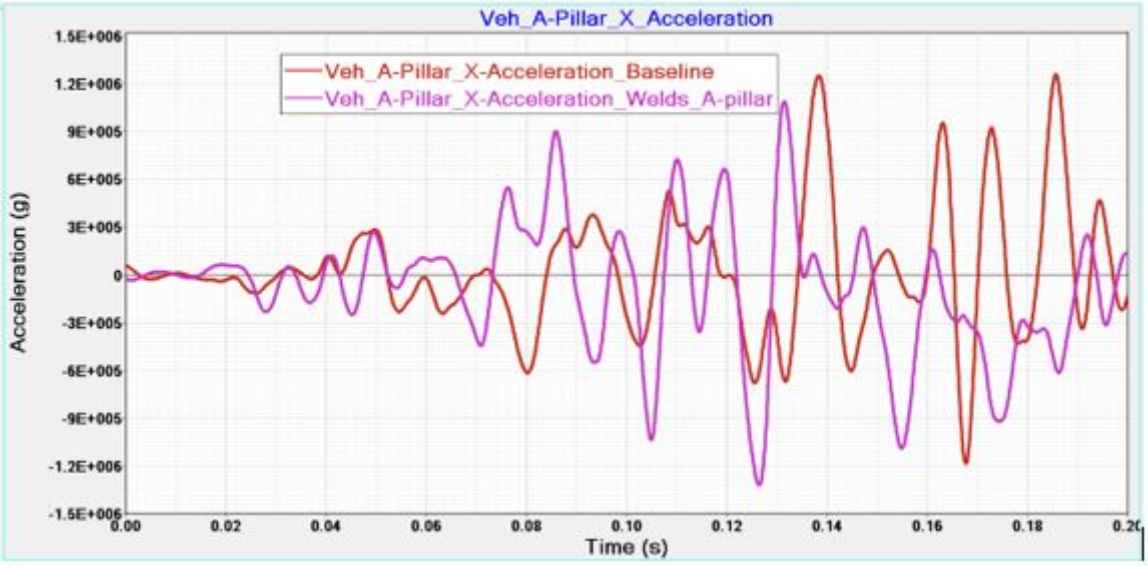

Figure E.12: Vehicle A-Pillar X-Acceleration for baseline and welded A-Pillar model

show similar magnitude and duration. The acceleration on the vehicle CG is also comparable to the baseline (Figure E.16) and simulation animation reveals similar crash kinematics This indicates that the intrusion in the occupant compartment is minimal and the vehicle performs as intended after a repair on the A-Pillar. The position of this weld might affect the performance and can be investigated for research purposes.

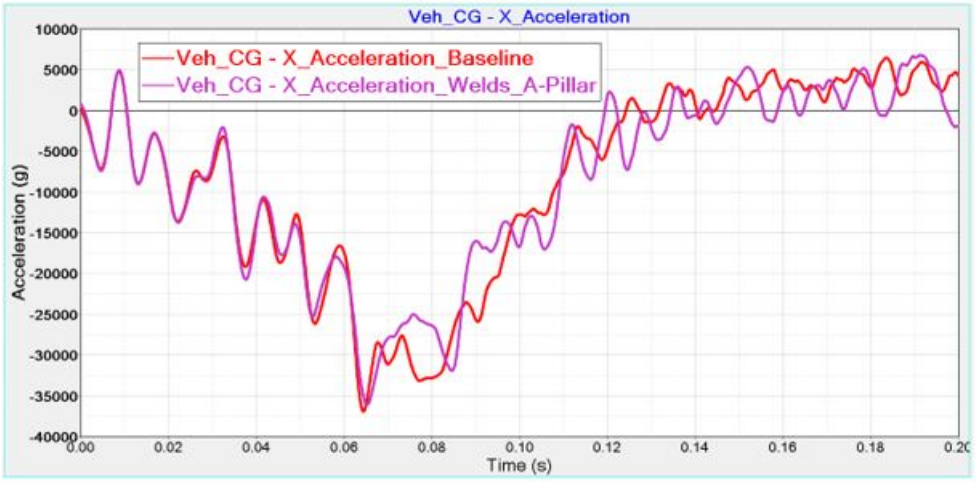

Figure E.13: X-Acceleration at vehicle CG.

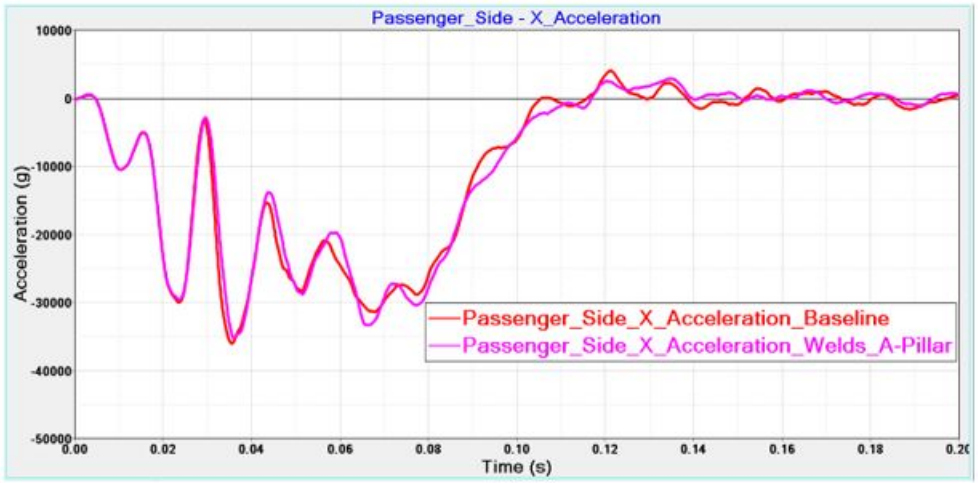

Figure E.14: Passenger side x-Acceleration for NCAP Front Impact

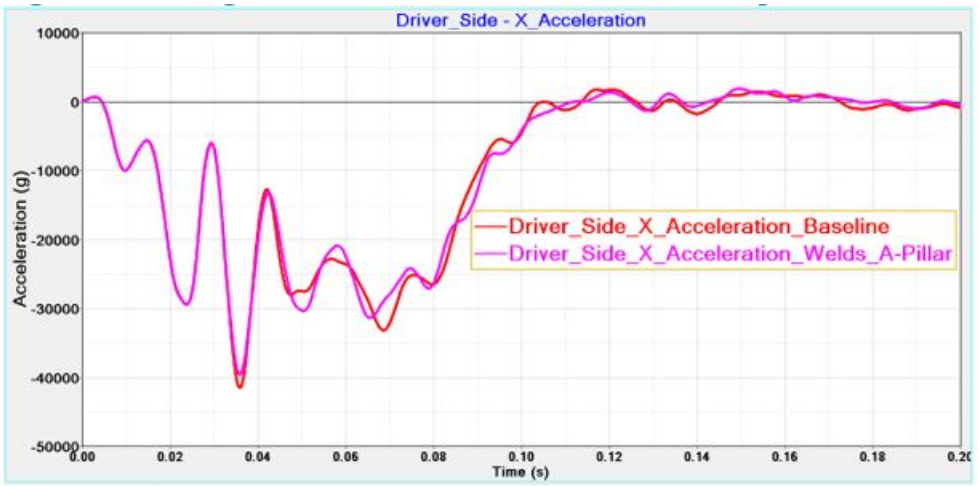

Figure E.15: Driver side X-Acceleration for NCAP Front Impact

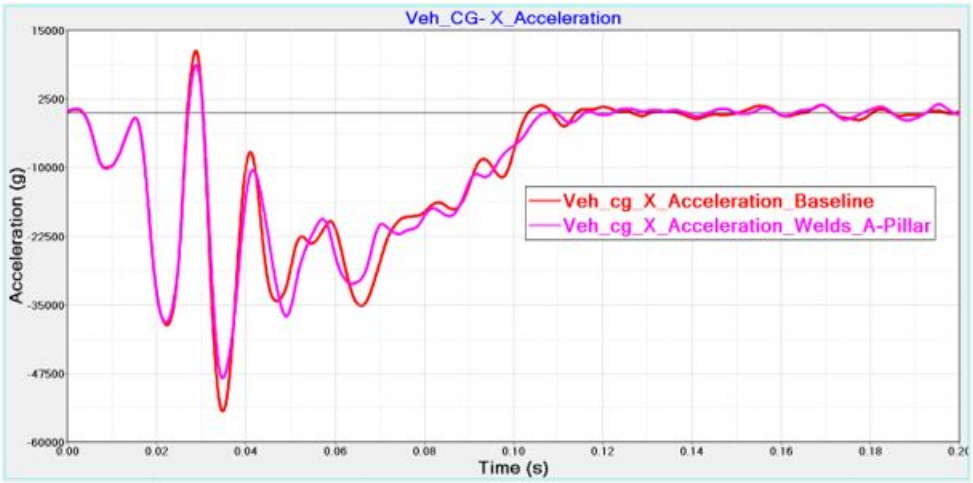

Figure E.16: Vehicle CG X-Acceleration

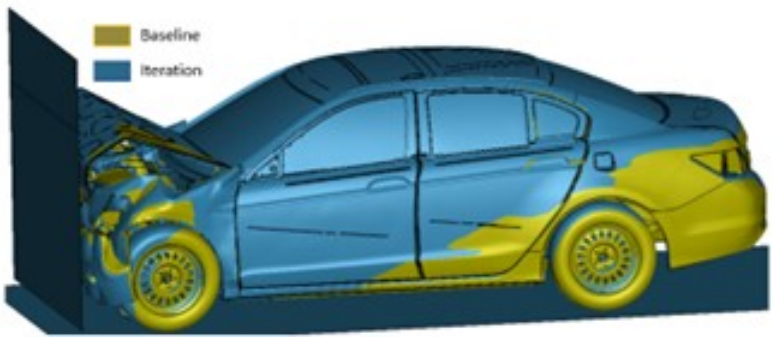

Figure E.17: Isometric view of front impact test with baseline and modified vehicle

E.5.3 IIHS Moderate Frontal Offset Test

The modified car was also run with the Moderate Frontal Offset test and it shows small variation with the addition of welds. The baseline intrusion profile for this vehicle was comfortably meeting the IIHS performance and falls under 'Good' rating. The iteration results show higher intrusion numbers for the model, but the rating does not change and hence this loadcase was not investigated in detail for the changes on the vehicle. Figure E.19 and E.20 show the acceleration response measured on the CG and A-Pillar.

Figure E.21 above indicates the x-displacement in the baseline and iteration model for a front impact model. The intrusions in the occupant compartment are more than the baseline model, it can be concluded that the loads from the crash have been transferred to the occupant compartment which is not safe for the occupants. The areas around the dash and steering column show higher intrusions when compared to the factory model.

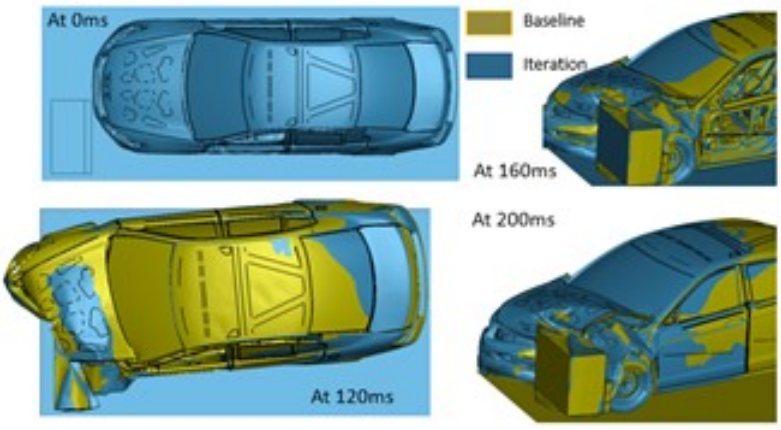

Figure E.18: Moderate Frontal Offset Test for baseline and modified vehicle showing intrusion in the driver compartment

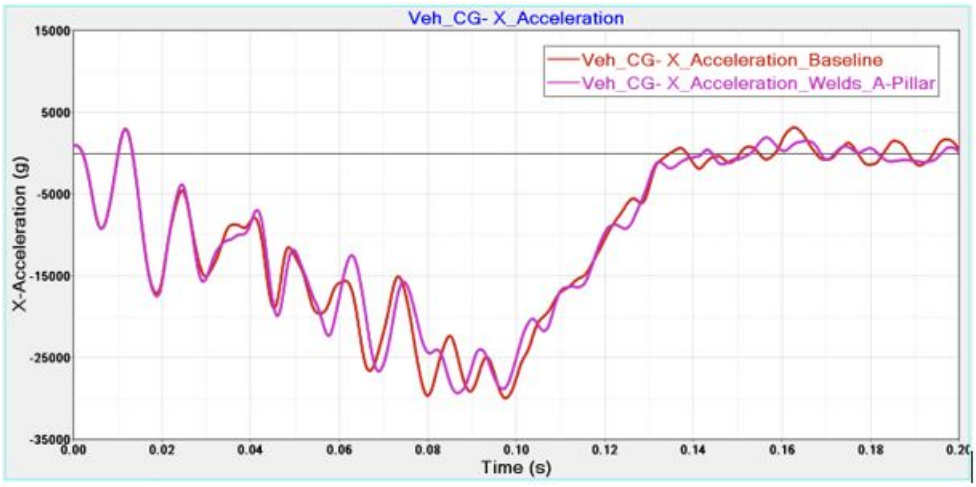

Figure E.19: Vehicle CG X-Acceleration

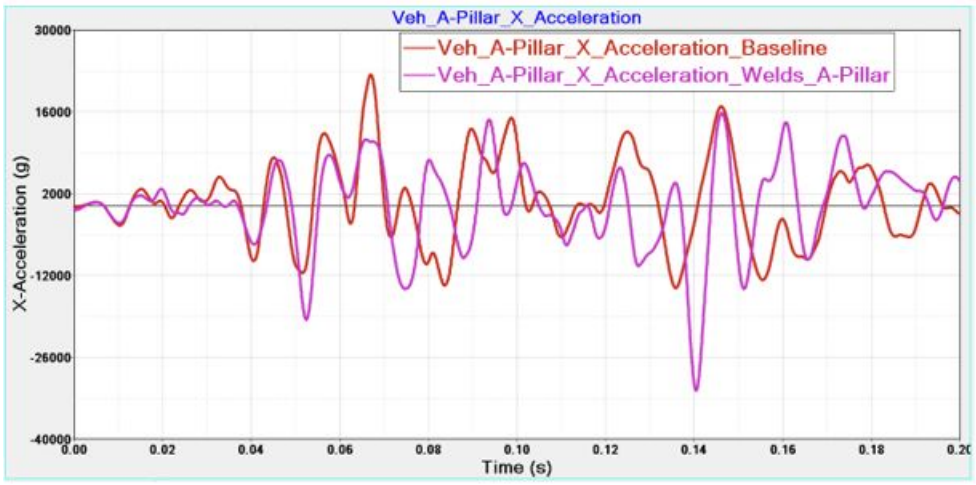

Figure E.20: X-Acceleration plot at A-Pillar

E.5.4 IIHS Lateral Moving Deformable Barrier Test (IIHS Side Impact)

The baseline and iteration model were tested for the IIHS Lateral Moving Deformable Barrier test and the side intrusions observed for the B-Pillar. The baseline performance of this model was 'Good', and addition of welds leads to a shift of the performance to 'Acceptable' and closer to the 'Marginal' zone for this loadcase (Figure E.22). Figure E.24 shows the iteration model in cut section showing higher intrusion in the occupant compartment. The load distribution in the vehicle is also affected by this small change thus emphasizing the OEM recommendation of not welding the UHSS members to ensure same performance. The X-Acceleration at the vehicle CG does not show too many changes however it would be interesting to

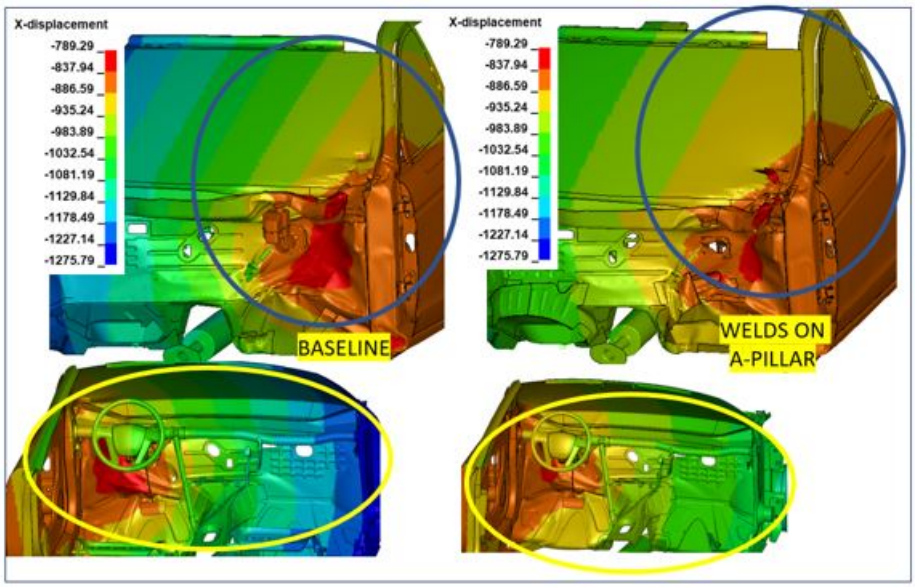

Figure E.21: X-displacement intrusion in the vehicle compartment for baseline and iteration case.

observe if there are multiple welds on the vehicle and how the performance would be affected by this change. It would be interesting to understand how the position of these welds would affect the results.

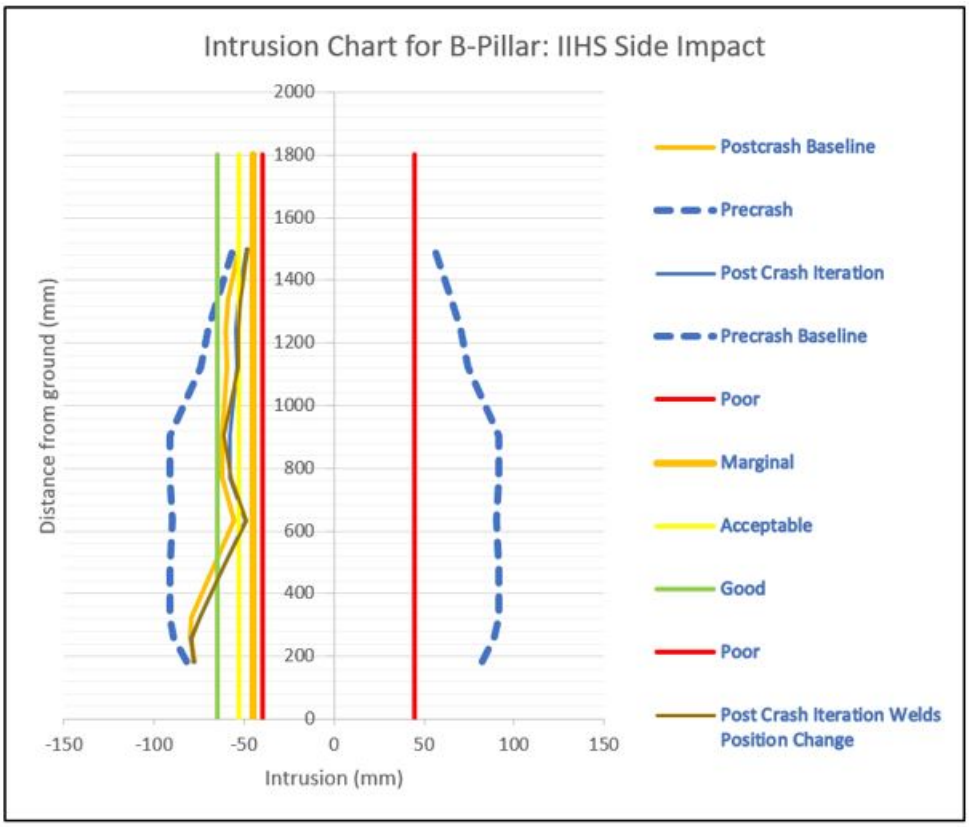

Figure E.22: IIHS Intrusion Chart for B-Pillar Side Impact Intrusions; Baseline and Modified Model compared

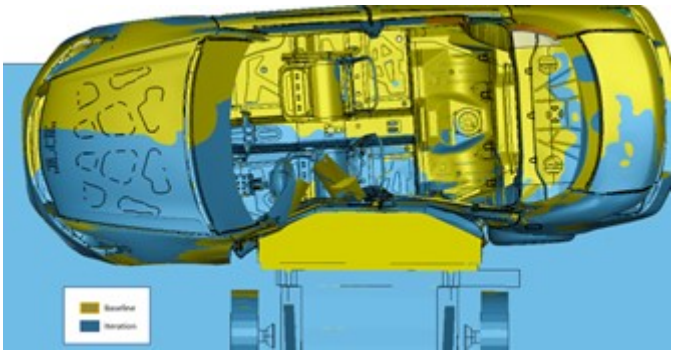

Figure E.23: Side Intrusion comparison for Baseline and Modified Model: Iteration model showing higher intrusion

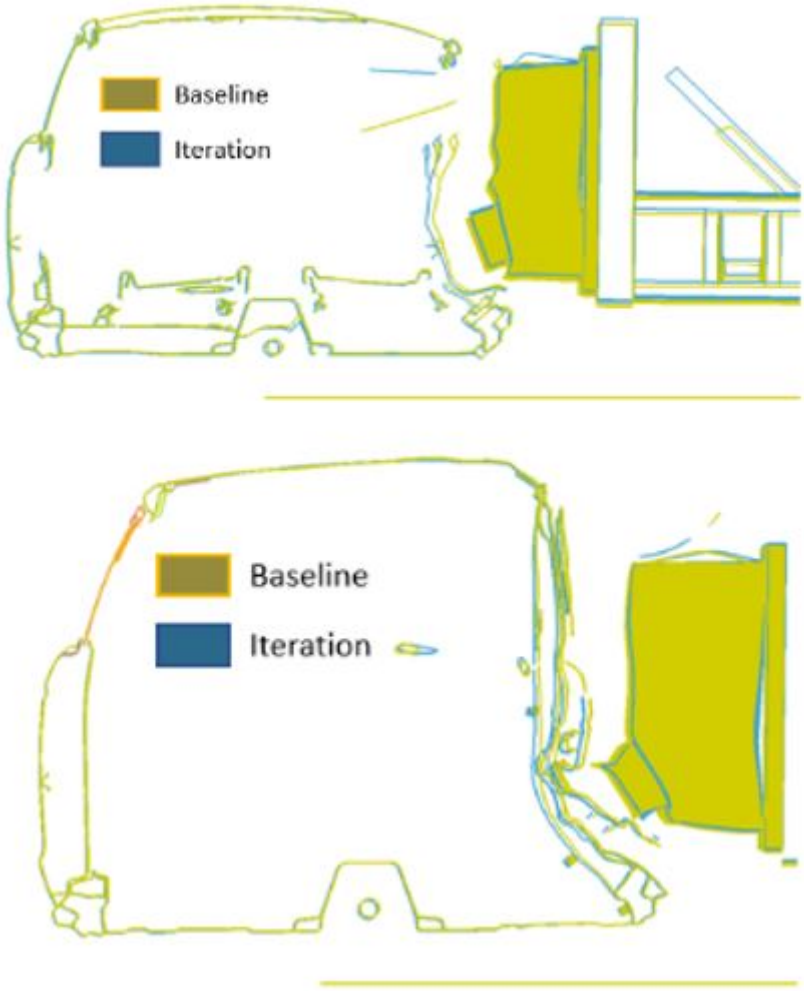

Figure E.24: Cut section views of IIHS Impact Barrier Test at the B-Pillar

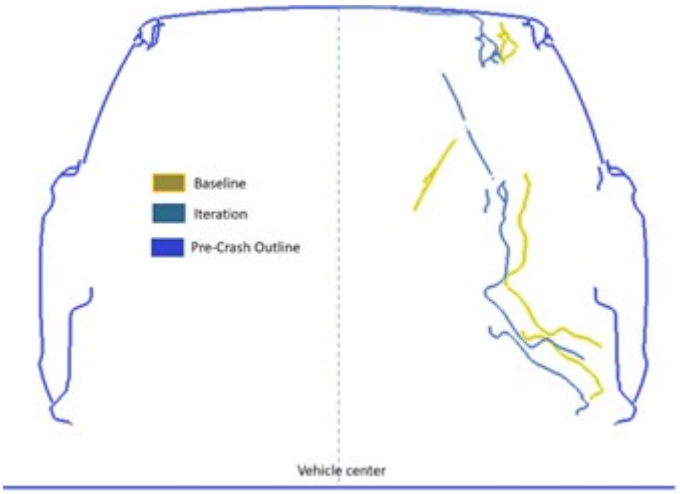

Figure E.25: Comparison of maximum intrusion on the B-Pillar for baseline and modified FE model

E.5.5 NCAP Side Impact Test (Lateral Moving Deformable Barrier Test)

This test was performed on the modified vehicle and shows improved intrusion values as compared to the baseline results. This observation can be attributed to the low height of this barrier compared to the IIHS side impact barrier. The weld in the A-Pillar allows the barrier load to be distributed to the vehicle body and reduced intrusion in the driver compartment. This explanation could be investigated in more details; however, it has been kept out of scope for this study.

E.5.6 Lateral NCAP Pole Impact

The NCAP Pole test was performed on the modified models and compared with the baseline performance. The B-Pillar velocity for the modified model shows small changes compared to the baseline but it does not change the performance of the vehicle for this loadcase. (Figure E.27) The X-acceleration measured at the CG and A-Pillar show the load path variations in the model due to the weld but the performance variation is small due to the area of impact of the pole being closer to the B-Pillar, a change in the rocker or B-Pillar region would show greater influence for this loadcase. Figure E.28 shows the simulation comparison for both cases at 180ms.

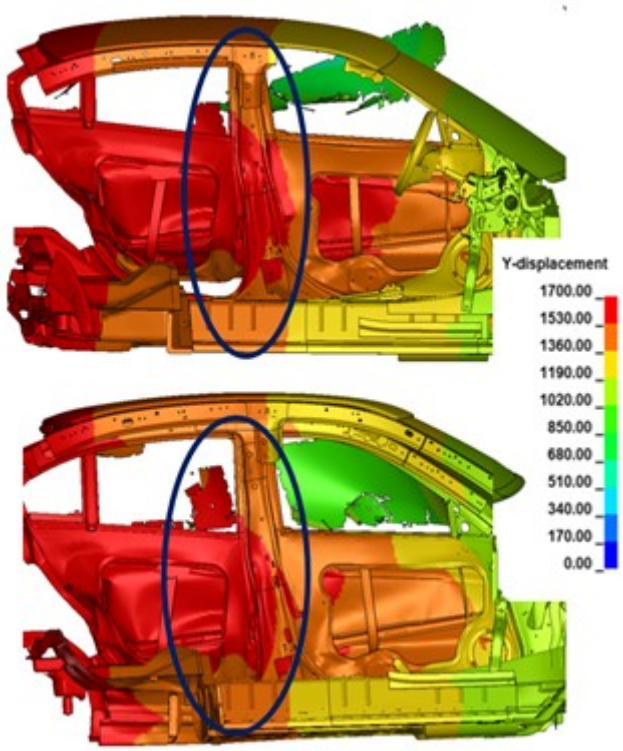

Figure E.26: Y-Displacement on the driver side during NCAP Side Impact test

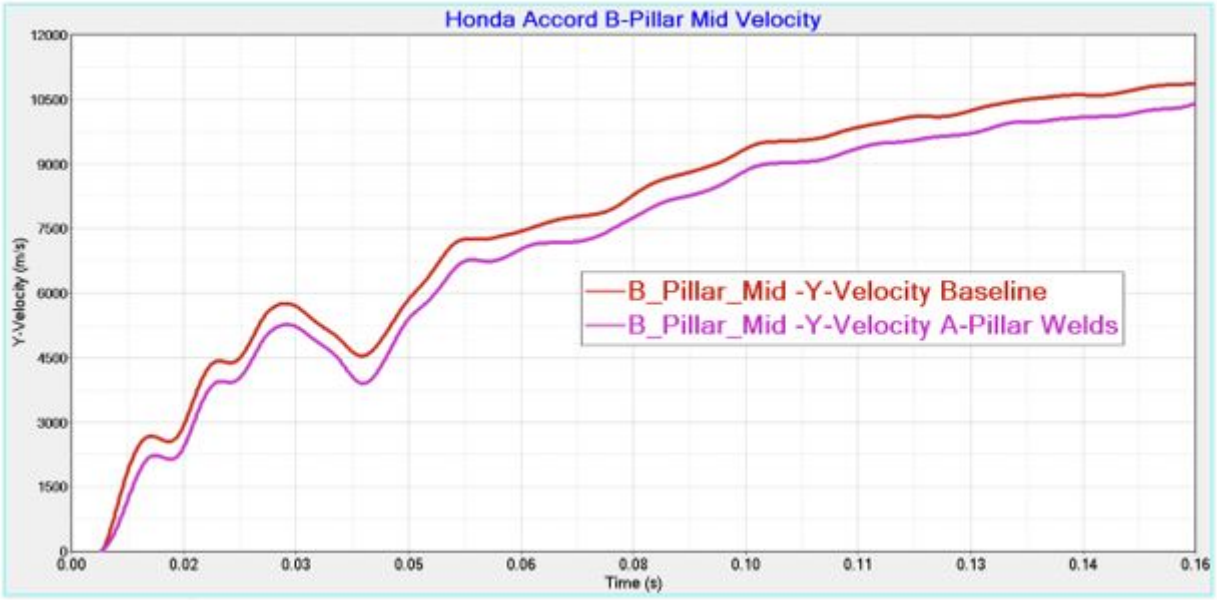

Figure E.27: B-Pillar (Mid) Velocity plot

E.5.7 Weld Position Analysis

It was observed that the A-Pillar buckled at a few points during IIHS SOL impact, these points were far from the position of the welds. This observation brought out the need to understand the influence of the position of these welds on the A-Pillar or

any structural member. The same Honda Accord model was chosen for this analysis and welds were assigned to 3 different points on the A-Pillar to understand the influence of these welds on the performance of the vehicle for IIHS SOL test. This test was chosen to perform the weld position analysis because it is most sensitive to changes on the A-Pillar (as observed during this study). Figure E.29 shows the 3 positions of welds on the A-Pillar (marked as Iteration 1,2 and 3).

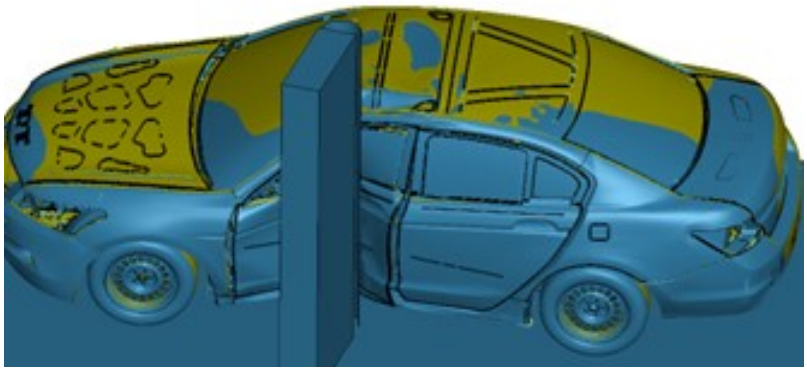

Figure E.28: Lateral NCAP Pole Test at time 180ms

E.5.8 Weld Position Analysis

The corresponding X-Acceleration for a point on the A-Pillar shown in Figure E.30 below shows that Iteration 3 has the maximum influence on the performance when compared to the baseline. It is also interesting that different positions of welding render a relatively different response in terms of acceleration pulse for the vehicle. This study does not investigate the worst position of welding on the member because every case yields an acceleration higher than the baseline values indicating the fact that welding on the member would create a new unintended load path for the impact. Figure E.31 shows higher X-intrusion in the iteration models as compared to the baseline plots. One of the possible reasons Iteration 3 has the maximum influence on the crash performance is its position in the middle of the A-Pillar and the buckling of the A-Pillar leads to maximum deformation and intrusion in the driver compartments

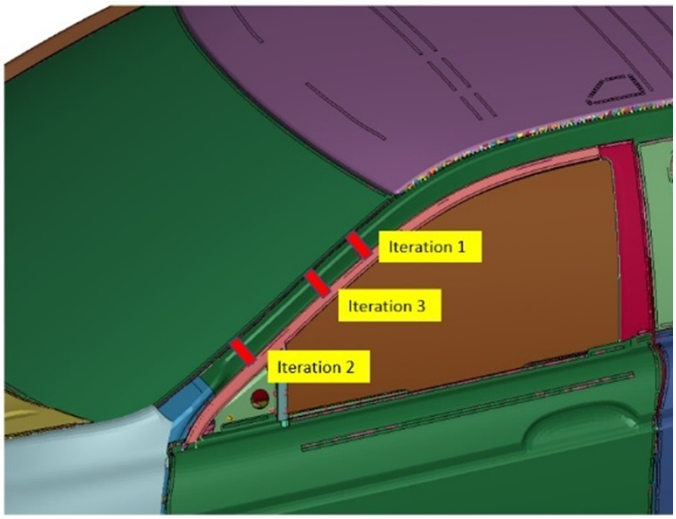

Figure E.29: Position of welds on the A-Pillar for analyzing influence of position on the performance

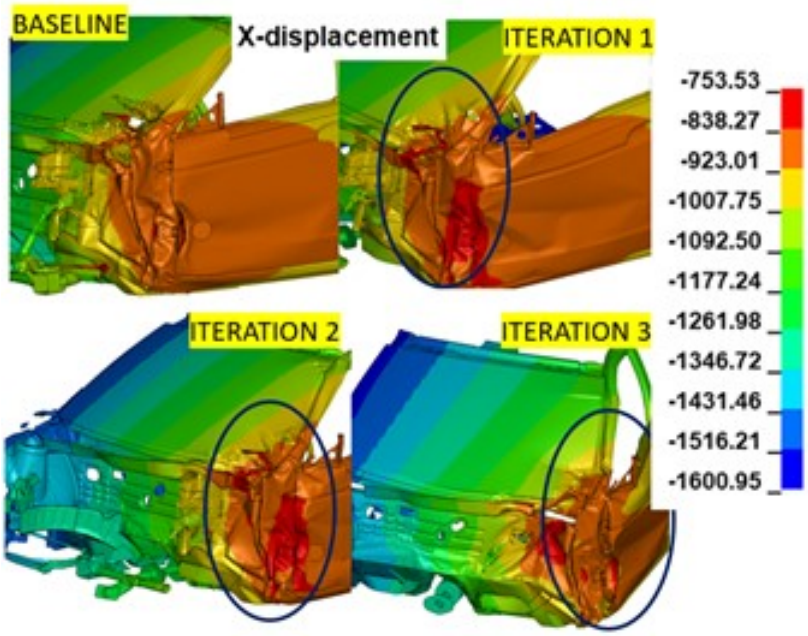

Figure E.31: X-displacement (intrusion) in the driver compartment for different weld positions on the A-Pillar

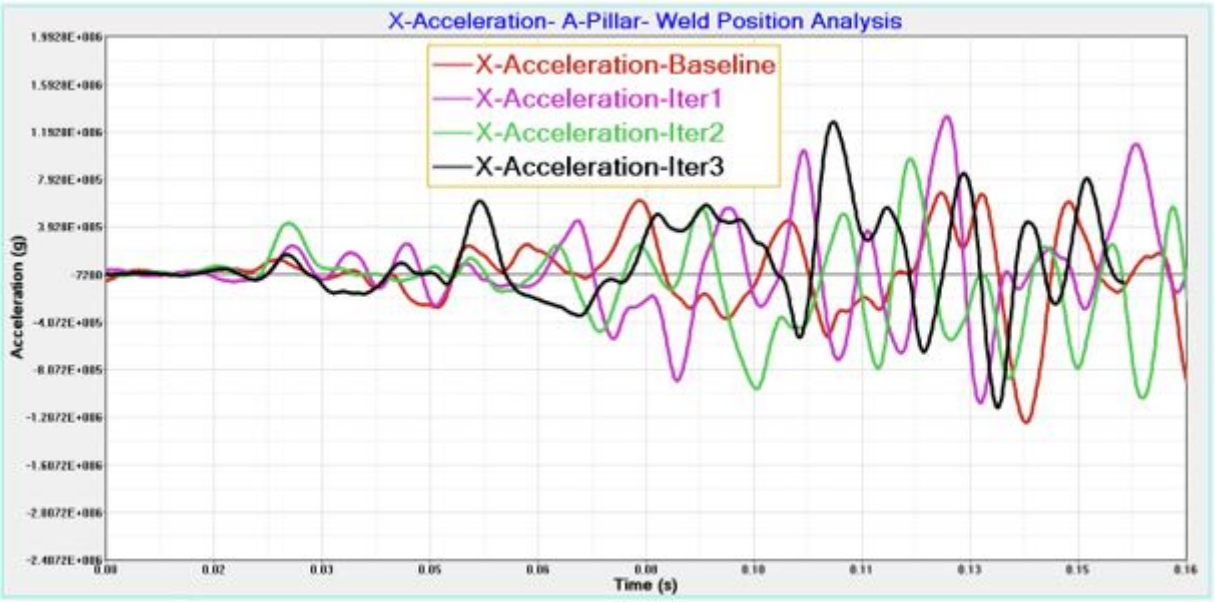

Figure E.30: X-Acceleration on A-Pillar for Weld Position Analysis

E.6 Conclusions

The addition of UHSS steel members to a vehicle helps to improve structural integrity of the vehicle while also contributing to weight reduction of the vehicle. The strong material has its constraints while repairing the members and a knowledge about the influence of welding on these materials is crucial to ensure that safety performance is retained on the vehicle after a repair. This study brings to light the fact that the safety performance of a vehicle is modified after improper repairs are conducted on the vehicle as shown in Table E.32 The load path in the event of a crash is changed after structural UHSS members are welded. It is also observed that the impact of improper repairs on a vehicle is more sensitive in a few crash scenarios as opposed to some other loadcases. This study involves only welding at a single point on the A-Pillar, further research will be done in order to understand the influence of multiple welds on different UHSS members. It will include the study of impact of repairs on different structural members with respect to the crash loadcases. We plan to conduct a similar study on different vehicle types to understand if the impact of welding and improper repairs is higher on small vehicles or if it's same for all vehicle types.

Loadcase	Crash Performance Evaluation	
	Baseline	Weld Added to A-Pillar
IIHS Small-Overlap Frontal Barrier Test	✓	✓
NCAP Front Impact Test	✓	✓
IIHS Moderate Frontal Offset Test	✓	✓
IIHS Lateral Moving Deformable Barrier Test	✓	✓
Lateral NCAP Pole Test	✓	✓
NCAP Side Impact Test	✓	✓

Figure E.32: Comparison of baseline vs modified vehicle crash performance across different loadcases

E.7 Contact Information

Gulshan Noorsumar: gulshan.noorsumar@uia.com University of Agder, Norway

E.8 Acknowledgments

The authors of this paper would like to acknowledge National Highway Traffic Safety Administration (NHTSA) and National Crash Analysis Center (U.S.) along with George Mason University for sharing access to the finite element models used during the study.

References – Paper E

[1] Paul Du Bois, Clifford C Chou, Bahig B Fileta, Tawfik B Khalil, Albert I King, Hikmat F Mahmood, Harold J Mertz, Jac Wismans, Priya Prasad, and Jamel E Belwafa. 2004.

[2] Laetitia Theodora Aarts, JJ Commandeur, Ruth Welsh, S Niesen, Markus Lerner, Pete Thomas, Niels Bos, and Ragnhild Johanna Davidse. Study on serious road traffic injuries in the eu. *Luxembourg: Publications Office of the European Union*, 2016.

[3] Zhaokai Li, Qiang Yu, Xuan Zhao, Man Yu, Peilong Shi, and Cilei Yan. Crashworthiness and lightweight optimization to applied multiple materials and foam-filled front end structure of auto-body:. *Advances in Mechanical Engineering*, 9:1–21, 8 2017. ISSN 16878140. doi: 10.1177/1687814017702806. URL `https://journals.sagepub.com/doi/10.1177/1687814017702806`.

[4] Guofei Chen and Aleksy A. Konieczny. Influence of ahss part geometric features on crash behavior. *SAE Technical Papers*, 4 2006. ISSN 0148-7191. doi: 10.4271/2006-01-1588. URL `https://www.sae.org/publications/technical-papers/content/2006-01-1588/`.

[5] Advanced high-strength steel (ahss) definitions - worldautosteel, . URL `https://www.worldautosteel.org/steel-basics/automotive-steel-definitions/`.

[6] Liang Huang, Min Kuo, and Benda Yan. Ahss application in roof strength. *SAE Technical Papers*, 2007. ISSN 26883627. doi: 10.4271/2007-01-0339.

[7] Paul Kah, Markku Pirinen, Ramio Suoranta, and Jukka Martikainen. Welding of ultra high strength steels. *Advanced Materials Research*, 849:357–365, 2014. ISSN 1662-8985. doi: 10.4028/WWW.SCIENTIFIC.NET/AMR.849.357. URL `https://www.scientific.net/AMR.849.357`.

[8] Uwe Schmortte. Crash-test results to analyse the impact of non-professional repair on the performance of side structure of a car. 2011.

[9] Michael Schäffer, Ralf Sturm, and Horst E. Friedrich. Methodological approach for reducing computational costs of vehicle frontal crashworthiness analysis by using simplified structural modelling. *International Journal of Crashworthiness*, 24:39–53, 1 2019. ISSN 17542111. doi: 10.1080/13588265.2017.1389631.

[10] Biswajit Tripathy and Sampath Vanimisetti. The beam-grid: Development of a full vehicle reduced order model for frontal, offset and side impact f2018/f2018-stn-024 - fisita. 10 2018.

[11] Yucheng Liu. Development of simplified truck chassis model for crash analysis in different impact scenarios. *International Journal of Crashworthiness*, 15(5): 457–467, 2010.

[12] Crash Simulation Vehicle Models | NHTSA, . URL `https://www.nhtsa.gov/crash-simulation-vehicle-models`.

[13] H Singh, CD Kan, D Marzougui, and S Quong. Update to future midsize lightweight vehicle findings in response to manufacturer review and iihs small-overlap testing. *Report No. DOT HS*, 812:237.

[14] IIHS. Small overlap frontal crashworthiness evaluation — crash test protocol, 2021.

Paper F

Effect of welding and heat treatment on the properties of UHSS used in automotive industry

Gulshan Noorsumar, Dmitry Vysochinskiy, Even Englund, Kjell G. Robbersmyr and Svitlana Rogovchenko

This paper has been published as:

Gulshan Noorsumar, Dmitry Vysochinskiy, Even Englund, Kjell G. Robbersmyr and Svitlana Rogovchenko. Effect of welding and heat treatment on the properties of UHSS used in automotive industry. *EPJ Web of Conferences*, 250, 05015 (2021),ISSN: 2101-6275 doi: 10.1051/epjconf/202125005015.

Effect of welding and heat treatment on the properties of UHSS used in automotive industry

Gulshan Noorsumar, Dmitry Vysochinskiy, Even Englund, Kjell G. Robbersmyr and Svitlana Rogovchenko
Department of Engineering Sciences
University of Agder
4879 Grimstad, Norway

Abstract **This paper deals with the undesired effects of the heat treatments on the mechanical properties of Ultra High Strength Steel (UHSS) used nowadays in automotive industry to improve crashworthiness performance of vehicles. The UHSS specimens were extracted from certain parts of the car body and subjected to different heat treatments. Four types of specimens were tested: untreated, welded with metal inert gas welding, heat treated at 800 °C, and heat treated at 1250 °C. All heat-treated specimens showed dramatically reduced values of strength. The results suggest that it is important to follow the official repair manuals avoiding unnecessary welding and improper heat treatments of UHSS. The experiments provide the data necessary for constructing a constitutive model and performing a finite-element analysis of improperly repaired UHSS parts.**

F.1 Introduction

Main challenges in vehicle design are related to the concerns with passenger safety, lighter weight and higher stiffness is required for the vehicle safety. Passenger and, more recently, pedestrian safety requirements entail the use of high energy absorbing materials and a smart geometry to mitigate the injuries in a crash event. Vehicles also need a stiff and durable passenger compartment to reduce intrusions in a crash scenario. A light-weight vehicle structure is ideal for improved fuel economy, ride, and handling of the vehicle [1]. Several metal grades have been proposed to replace mild steel in automotive crash applications to achieve a higher strength while retaining the properties of steel, thus, reducing the thickness and weight of components in a vehicle [2]. AHSS (Advanced High Strength Steels) were developed to support these requirements and applied in the automotive industry replacing mild steel in structural members. A study by the World Steel Dynamics anticipated that by

2025 the usage of AHSS would reach 23.7 million tons replacing mild steel [3], [4]. In vehicles, AHSSs have been used in structural body-in-white parts like A, B, and C Pillars, roof rails, door beams, front and side members; these parts protect from intrusions in the occupant compartment in the event of a vehicle collision [3]. AHSSs are multiphase steels that contain various concentrations of ferrite, bainite, martensite and retained austenite phases; the proportions of which are modified to obtain functional requirements of steel [3], [5].

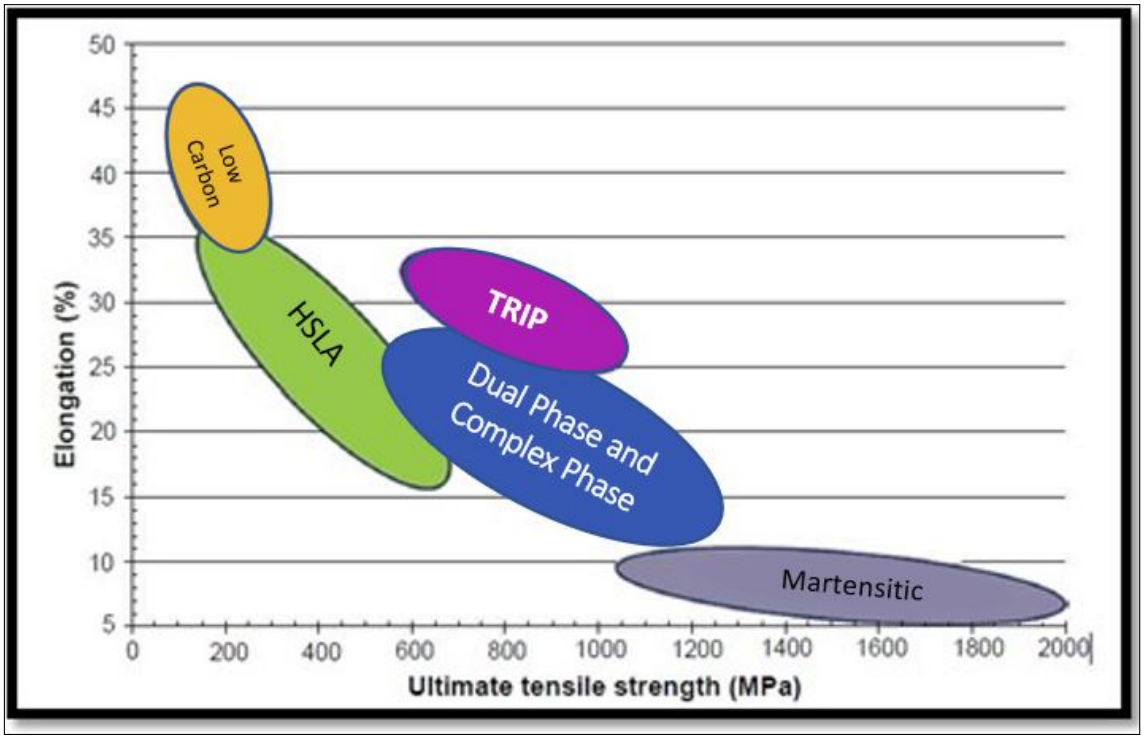

Figure F.1: Strength vs elongation relationship for the first generation of advanced high-strength steels

- Dual Phase (DP) steels have an ultimate strength roughly between 500 to 1180 MPa; TRIP and CP are available up to 980 MPa. These steel types are used in a car area requiring high strength, high ductility, and good weldability

- Martensitic steel is currently available with strength in the range of 900-1900 MPa. The yield stress ranges from 900 to 1600 MPa. These steels are alloyed with carbon, manganese and chromium to achieve the required strength. They have high carbon content leading to high stiffness; anti-intrusion properties are used in parts which are not welded in general, for example, bumper and door intrusion beams. They have low elongation (close to 6%) and therefore are not considered for energy absorption applications. The use of this steel type poses welding and forming challenges because the heat produced in these processes alters the microstructure of the material thereby changing its mechanical

properties. As per a study conducted on the heat treatment of these material the HAZ (Heat Affected Zone) produced by welding causes significant austenite growth followed by phase transformation in the material [3].

- Boron Steels are produced by adding higher carbon percentage in the range of 0.2 to 0.25% with approximately 1.2% manganese and 0.0005-0.001% boron increasing the hardenability of steel [6]. This type of steel has high deformation resistance, thus making it suitable for the use in passenger safety cage applications

Collision repair for AHSS has been a challenge for automakers leading to new repair procedures outlined in repair manuals to prevent undesired heat treatment of structural parts. These parts are recommended to be either replaced or repaired strictly according to the procedure in the manual. The report published by the American Iron and Steel Institute [7] presents the results of the collaborative project with General Motors which investigates the repairability of AHSS used in automobiles in order to determine the crashworthiness response of a vehicle after proper repairs were conducted on the vehicle parts. The micro-structure changes are observed in the material due to application of heat; the material reverts to soft equilibrium phases which reduces its crashworthiness response in a crash event [7]. Several studies have been conducted to support the hypothesis that the vehicle crash response is negatively affected due to improper repairs conducted on the vehicles [8], [9]. Material behaviour changes are reported after improper collision repair related to welding or heat treatment on the vehicle.

The literature review shows that there has been insufficient data for developing a material card to conduct FE simulations for an improperly heat-treated vehicle member. In this study, material characterization of coupon samples cut out from vehicle structural members was conducted to investigate the baseline material properties of the steel-type used in the parts. Welding and heat treatment of these samples was conducted to determine the impact of these processes on the strength and stiffness of the material. This coupon testing approach forms the basis for the development of a material model to replicate improper collision repair on a vehicle.

The coupon samples used in this study underwent tensile testing in a UTM (Universal Testing Machine) in the laboratory at the University of Agder and stress-strain curves were derived using the data from the extensometer and DIC (Digital Image Correlation) measurements. The next section on this paper explains the methodology of the experiment and the results/observations from this experimental data.

F.2 Methodology

The UHSS coupon test samples used for tensile testing were cut out from the parts of the car, structural parts are shown in Fig. 2 and were further cut into dog bone samples using water jet cutting to obtain the correct sample size. The standard specimen size selected for the tensile test specimen is an ASTM (American Society for Testing and Materials) E8 dog-bone specimen as shown in Fig. 3. The steel samples were taken from a car which uses UHSS for structural durability of its members, however we are not aware of the steel type and properties used in the vehicle and assume that it is boron steel referring to the metal in the sequel as UHSS.

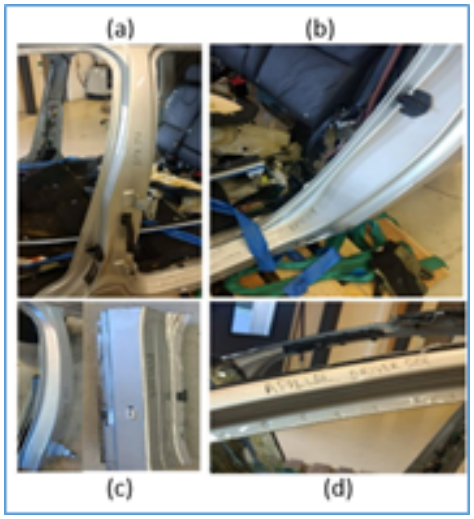

Figure F.2: Vehicle structural members using UHSS (a) B-Pillar, (b) C-pillar, (c) Rocker, (d) A-Pillar test (ASTM E8)

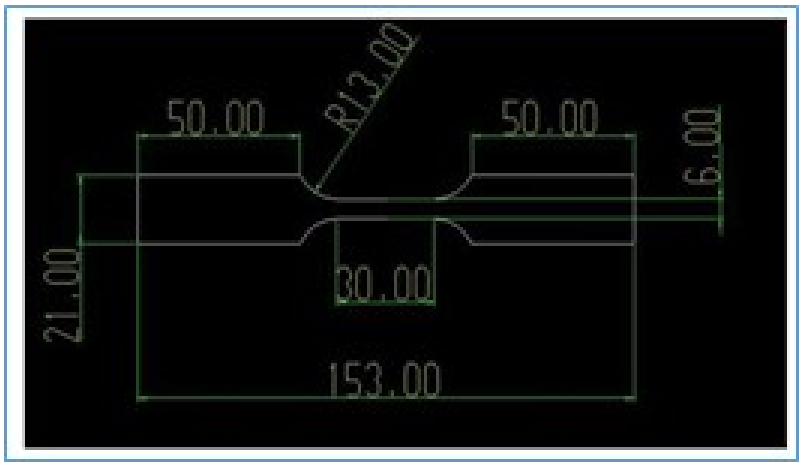

Figure F.3: Dimensions of the specimen used in the tensile test

Fig. F.4 above shows the water jet cutting process. The samples were further divided into 4 types as the table below (Table F.1).

Figure F.4: Water jet cutting of the samples, dog-bone samples

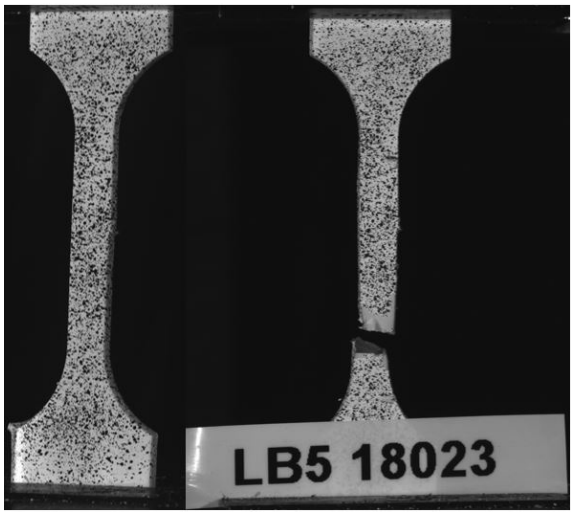

Figure F.5: Speckled sample for DIC

F.2.0.1 Sample Preparation

- Baseline Sample: After the water jet cutting the dog bone samples were used as a baseline UHSS sample. The samples were measured to ensure same thickness and test area to get consistent results for all tests.

- Welded Sample: The coupon was cut at the centre of the reduced section and welded using the metal inert gas Argon-CO2 (19l/min at 18V,106-114 Amp, filler rate; 3.5 mm/min). The two parts of the coupon were joined by a single V butt joint and grinding operation was conducted to make the sample edges smooth

SI No.	Sample Type	Total No. of Samples
1	Baseline	4
2	Welded	4
3	Heat Treated - 800°C	4
4	Heat Treated - 1250°C	4

Table F.1: Specimen types used for the material test

- Heat Treated at 800 °C: The baseline sample type was heat treated in a furnace at 800 °C for a period of 3 mins and then the sample was cooled with air before tensile testing. The intent was to introduce a change in the microstructure of the base material and test its behaviour.

- Heat Treated at 1250 °C: The process followed is similar to the heat treatment at 800 °C: leaving the sample in the furnace till the temperature reaches 1250 °C and keeping the furnace temperature fixed prior to removing the samples for air cooling process.

The samples produced with the processes described above were of a similar dimension. However, since the samples were cut out of vehicle parts, internal stresses could be present in the samples due to the manufacturing process of these parts. Therefore, the results might deviate from the manufacturer's baseline material data. The goal of the study is to detect any change in material properties in the vehicle parts during the repair process.

One of the best practices involved in conducting DIC is speckling the samples with a random pattern so that the samples can be identified by the camera [10]. The coupons were speckled with a spray gun before the tensile testing process as shown in Fig. 4 (c). The tensile test was conducted at a constant loading rate of 0.3 mm/s and the loading was terminated when the specimens underwent a fracture. The machine is equipped with load cell, build-in position sensor and clip-on LVDT-based extensometer with a measurement range of 25mm to 30 mm.

F.2.1 Experimental Results

The data from the extensometer and DIC were postprocessed to obtain the stress-strain curves for the samples as shown in Figure F.6. The load-elongation curves were constructed using a combination of machine build-in sensors and extensometer displacement data; compliance correction was applied where necessary.

Table F.2 shows the yield stress , ultimate stress, and ultimate strain in the four sets of samples; the mean values for individual tests are presented.

SI No.	Sample Type	Yield Strength (MPa)	Ultimate Tensile Strength (MPa)	Ultimate Strain
1	Baseline	1188	1325	0.043
2	Welded	730	758	0.016
3	Heat Treated - 800°C	386	582	0.191
4	Heat Treated - 1250°C	311	383	0.100

Table F.2: Yield Strength calculated from the tensile test results

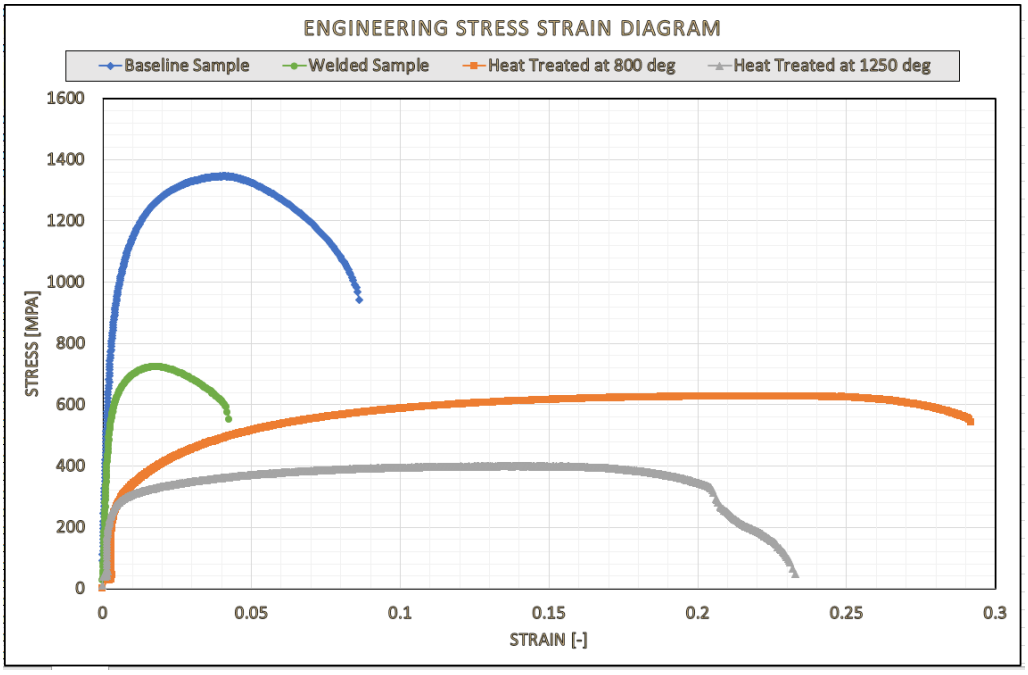

Figure F.6: Engineering Stress Strain Diagrams for (i) Baseline Sample (ii) Welded Sample (iii) Heat Treatment at 800 °C Sample (iv) Heat Treatment at 1250 °C Sample

F.3 Discussion

A high yield strength of a material indicates its capacity to withstand extreme structural loads before it deforms or fails. The results of the tensile tests indicate that the baseline sample has a high yield strength higher than 1100 MPa. The high yield strength value helps the vehicle structure to withstand the impact of a frontal or side crash event. However, the coupons which underwent welding or heat treatment before the tensile test show lower yield strength and ultimate strength values indicating reduced structural integrity in the vehicle occupant cage. This can be fatal to vehicle occupants in a crash; it may also lead to a change in the load distribution in the vehicle structure and cause more intrusions in the passenger compartment. It is also observed that the strains in the welded sample were lower compared to the baseline and heat-treated samples indicating lower ductility; this can be attributed to the filler material used for the welding.

The material parameters defined can serve as a starting point for developing a material card to be used in an explicit solver software like LS Dyna. The experimental values for improper heat treatment of structural members presented in this paper can be used to simulate an unprofessional repair in vehicles. FE simulations with the material card (e.g., MAT 24: Piecewise Linear Plasticity used in LS Dyna) developed using these reference values are out of scope for this paper.

There are several important observations and assumptions made during this study, for instance:

- The coupons may have internal stresses resulting from the manufacturing process of the parts, so the baseline results may not match the manufacturer data.

- The type of welding of the samples can significantly differ during repair, hence the material properties might vary due to the variations in the welding process affected by the welding conditions, experience of the welder, and the type of a joint made.

- The authors also recognize the minor variations between sample sizes because the samples were cut out from the vehicle parts and subsequently underwent water jet cutting to extract coupons; these variations can also introduce errors in the stress calculations. The tensile testing process on the UTM can also include minor variations which remain unaccounted for. To account for some of these variations, we conducted the minimum of 3 valid tests for each sample type and took the mean values.

F.4 Conclusions and Next Steps

In this study we observed the changes in the microstructure of UHSS samples subjected to tensile testing in a UTM. It was concluded that the lower yield strength of the material coupons results from the welding or heat treatment of the samples; it causes the change in the properties of steel and may lead to a poor crashworthiness response of a vehicle under impact. It would be interesting to conduct a spectral analysis on the samples to understand the microstructure changes in more detail, and a hardness test to further explore the material characteristics of the samples. It is also of interest to investigate microstructure around the weld to determine the reason for low ductility in the sample. The material data generated from this research can be also used to generate a material card to simulate the material behaviour in a non-linear full vehicle crash using an FE solver.

F.5 Acknowledgement

The authors would like to acknowledge the support of the employees, technicians, and engineers in the Mechatronics Lab. The authors would also like to express deep gratitude to collision investigator Bjarne Hæstad for acquiring the vehicle parts used for this study.

References – Paper F

[1] David L Greene and John DeCicco. Engineering-economic analyses of automotive fuel economy potential in the united states. *Annual Review of Energy and the Environment*, 25:477–535, 2000.

[2] Nader Abedrabbo, Robert Mayer, Alan Thompson, Christopher Salisbury, Michael Worswick, and Isadora Van Riemsdijk. Crash response of advanced high-strength steel tubes: Experiment and model. *International Journal of Impact Engineering*, 36:1044–1057, 2009.

[3] Mahadev Shome and Muralidhar Tumuluru. *Welding and joining of advanced high strength steels (AHSS)*. Elsevier, 2015.

[4] World steel dynamics, report of october 2014.

[5] Debanshu Bhattacharya. Metallurgical perspectives on advanced sheet steels for automotive applications, 2011.

[6] C D Horvath. Advanced steels for lightweight automotive structures, 2010.

[7] D Anderson. Application and repairability of advanced high-strength steels. *American Iron and Steel Institute: Charlotte, NC, USA*, 2008.

[8] Uwe Schmortte. Crash-test results to analyse the impact of non-professional repair on the performance of side structure of a car. 2011.

[9] Gulshan Noorsumar, Kjell Robbersmyr, Svitlana Rogovchenko, and Dmitry Vysochinskiy. Crash response of a repaired vehicle - influence of welding uhss members. SAE International, 4 2020. doi: https://doi.org/10.4271/2020-01-0197. URL `https://doi.org/10.4271/2020-01-0197`.

[10] Gustavo Quino, Yanhong Chen, Karthik Ram Ramakrishnan, Francisca Martínez-Hergueta, Giuseppe Zumpano, Antonio Pellegrino, and Nik Petrinic. Speckle patterns for dic in challenging scenarios: rapid application and impact endurance. *Measurement Science and Technology*, 32(1):015203, 2020.

Paper G

An experimental and numerical investigation into the dynamic crash testing of welded and heat treated TRIP steel members on a modern vehicle

Gulshan Noorsumar, Kjell G Robbersmyr, Kristian Muri Knausgård, Roy Werner Folgerø, Karl Berge Rød, Jan Christian Bjerke Strandene, Harald Sauvik, Bjarne Hæstad, Tore Helleland Næss, Dmitry Vysochinskiy, Svitlana Rogovchenko

This paper has been published as:

Gulshan Noorsumar, Kjell G. Robbersmyr, Kristian Muri Knausgård, Roy Werner Folgerø, Karl Berge Rød, Jan Christian Bjerke Strandene, Harald Sauvik, Bjarne Hæstad, Tore Helleland Næss, Dmitry Vysochinskiy and Svitlana Rogovchenko. An experimental and numerical investigation into the dynamic crash testing of welded and heat treated TRIP steel members on a modern vehicle. Submitted to *International Journal of Impact Engineering-Elsevier*.

An experimental and numerical investigation into the dynamic crash testing of welded and heat treated TRIP steel members on a modern vehicle

Gulshan Noorsumar, Kjell G. Robbersmyr, Kristian Muri Knausgård, Roy Werner Folgerø, Karl Berge Rød, Jan Christian Bjerke Strandene, Harald Sauvik, Bjarne Hæstad, Tore Helleland Næss, Dmitry Vysochinskiy, Svitlana Rogovchenko
Department of Engineering Sciences
University of Agder
4879 Grimstad, Norway

Abstract **The weldability and heat treatment of Transformation Induced Plasticity (TRIP) steel has been an active area of research with micro-structural changes observed in the material due to welding. This poses a constraint to its application in providing structural integrity and lightweight automotive members. This paper investigates the crashworthiness response of a vehicle undergoing unprofessional repairs on its TRIP steel structural members. The study describes the preparation of the dynamic full vehicle test against a rigid barrier at 0% offset along with welding and heat treating the TRIP steel members. The vehicle crash performance has been presented indicating reduced performance when compared to a baseline vehicle test. A Finite Element (FE) model has also been developed to replicate the non-linear impact scenario; correlation study shows FE model replicates the test closely.**

G.1 Introduction

The microstructure of Transformation Induced Plasticity (TRIP) steels contains a mixture of ferrite, with retained austenite, martensite and bainite in varying amounts. This effect can be defined as the transformation of retained austenite to martensite during straining leading to increased work hardening rate at higher strain, this forms the basis of TRIP steel [1], [2]. These steels are ideally suited for structural members to enhance safety in automotive applications. This microstructure change leads to superior high strain rate performance, resulting in large dynamic energy absorption [3], [4]. The addition of Si, Al, P alone or in combination suppresses the carbide

formation during the isothermal bainite transformation, this leaves the remaining austenite to be enriched in C resulting in room temperature stabilization. This results in the austenite-martensite transformation during straining and has proven to be useful in improving the strength-ductility balance in TRIP steels. The first observation of an unexpected increase in formability due to this transformation was observed in 1937 by Wasswemann [5]. It was later described in 1967 by Zackay et al. that highly-alloyed homogeneous metastable austenitic steels was the reason behind the enhancement in ductility [6]. The mechanical properties of TRIP steels are superior in terms of strength and elongation compared to other types of steels [7]

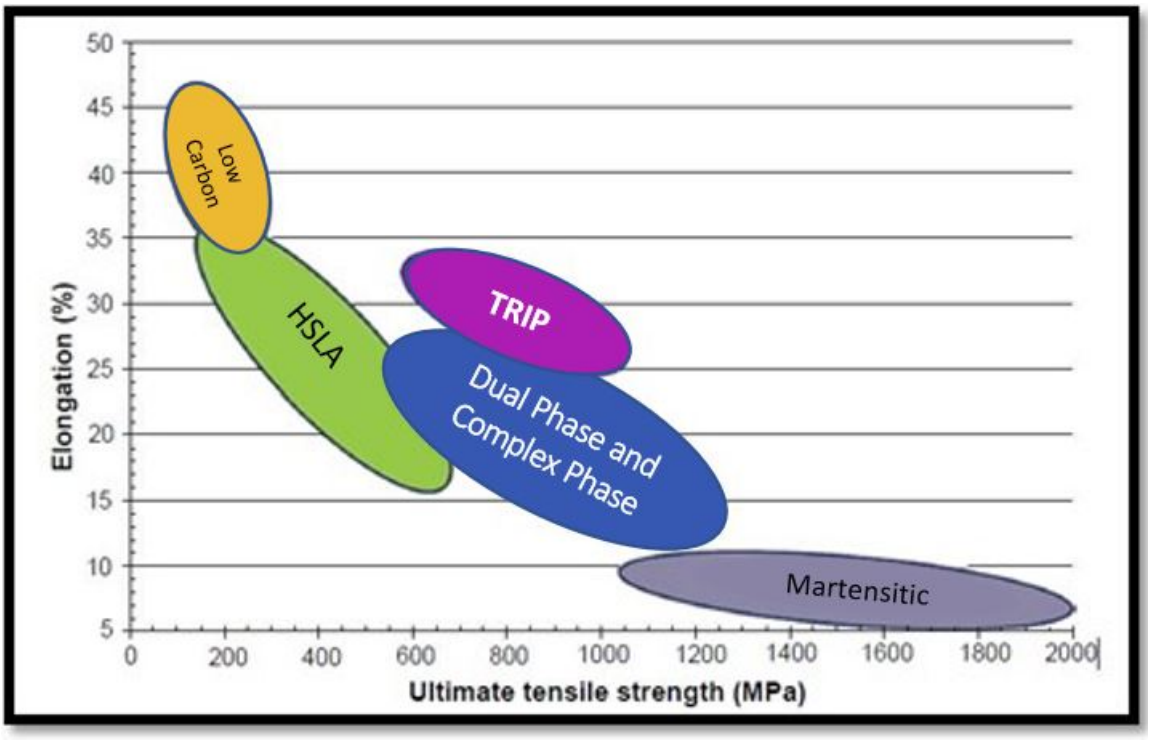

Figure G.1: Strength vs elongation relationship for the first-generation of advanced high-strength steels [7]

With the rapid increase in road accidents leading to death and severe injuries to road users, automakers have laid continued focus on developing safer cars. Along with this, increasing fuel economy demands and improved vehicle dynamics are contradicting requirements to improve the structural strength of vehicles. Light weighting of vehicles comes with an increased risk of vehicle safety for occupant cage intrusions in a vehicle crash, this has led automakers to use TRIP steels in structural members on vehicles [8]. In their application TRIP steels might be a part of several manufacturing and joining processes; such as welding, forming, coating and heat treatments. Welding is the one of the most popular joining processes for metallic materials and is widely used in the industry, however the heat conducted to the

workpiece during the process induces internal stresses and leads to deformation. In the case of TRIP steel the metallurgical zones created due to welding and heat affected zones causes microstructural changes in the material. As can be expected, the thermal cycle of the fusion joining process destroys the carefully designed microstructure of TRIP steel, especially affecting the retained austenite in the microstructure; which results in a deterioration of the mechanical properties in the weld region compared with the base metal. There were several papers investigating the weldability and heat treatment of TRIP steels and the material changes resulting due to the exposure of the workpiece to thermal changes [7], [9]. Amirthalingam [10] concluded in his thesis that Erichsen cupping test performed on welded samples showed that the formability of the welded TRIP steel is inferior to that of TRIP steel base metals. The properties of welded samples also changes with times at room temperature after welding; indicating changes in expected behaviour of this material by fusion welding. A study conducted by the authors of this paper [7] further highlights the findings from Amirthalingam; the study concluded the significant change in yield and ultimate strength of the dog bone samples undergoing tensile testing after welding and heat treatment compared to the baseline samples. These studies emphasize the need to avoid welding or heat treating TRIP steels in the absence of professional welding instructions outlined by the manufacturer.

Auto Collision Repair is a process when trained technicians repair a vehicle that has been damaged by an accident, weather, or any such conditions. Most automakers highly recommend following the collision repair manual to fix structural or part damages after an accident, this is to ensure that the parts which cannot be repaired or joined by a fusion process need to be replaced and the vehicle crashworthiness performance is restored. Unprofessional collision repairs could result due to a lot of reasons leading to a change in the safety performance of the vehicle after a repair [8], [11]. The study in [8] also outlines the crash performance of a vehicle after welding TRIP steel structural members. The FE (Finite Element) model used in the study replicates a Honda Accord undergoing impact under different scenarios and the performance evaluation showed the changes from the baseline performance of the vehicle. These changes can be attributed to the micro structural changes of the TRIP steel undergoing welding during the process of unprofessional collision repair. FE models have been used to replicate vehicle crashes in the industry as well as academia; this methodology has been accepted to replace physical testing in the industry for vehicle development because of the accuracy of the models generated by this method [12], [13]. However, FE models require computational time and modeling hours to prepare detailed models.

Based on the existing literature review conducted during this study, we recognized the need to conduct full scale tests to investigate the crashworthiness behaviour of

TRIP steel structural members undergoing welding and heat treatment. Conducting a full scale test is a challenge in regards to using the sensors, instrumentation and cameras for capturing the test data. The authors have used the report from Robbersmyr [14] and EuroNCAP full frontal test protocol for planning this test [15]. The experimental setup for the full frontal rigid barrier test at 0% offset and the corresponding results have been defined in the next section. A numerical simulation model was developed by the authors to correlate with the test data.

G.2 Methodology

G.2.1 Test Setup - Preparing the test vehicle

In order to perform the different tests, a test vehicle, onto which the sensors is mounted. The test vehicle used in the experiment was a model year 2015, 5 door hatchback as shown in Figure G.2. The basic specifications of the vehicle are outlined in the table below.

Vehicle Parameters	
Total Weight	1450 kg
Width	1700 mm
Length	3950 mm
Height	1510 mm
Wheelbase	2510 mm
Track width	1485 mm

Table G.1: Test Vehicle Parameters

Figure G.2: Model Year - 2015 Hatchback - Test Vehicle.

To include unprofessional repairs, the vehicle was cut at four points; A-pillar (driver and passenger side) and the Rocker (driver and passenger side). It was ensured

that all the panels were cut through; including the TRIP steel material on the parts. The repair process outlined by the collision manual was not followed and the parts were welded together with MIG (Metal Inert Gas) welding. After welding; grinding was conducted on the weld zone to remove excess filler material. Figure G.3 outlines the process followed for cutting and welding the parts.

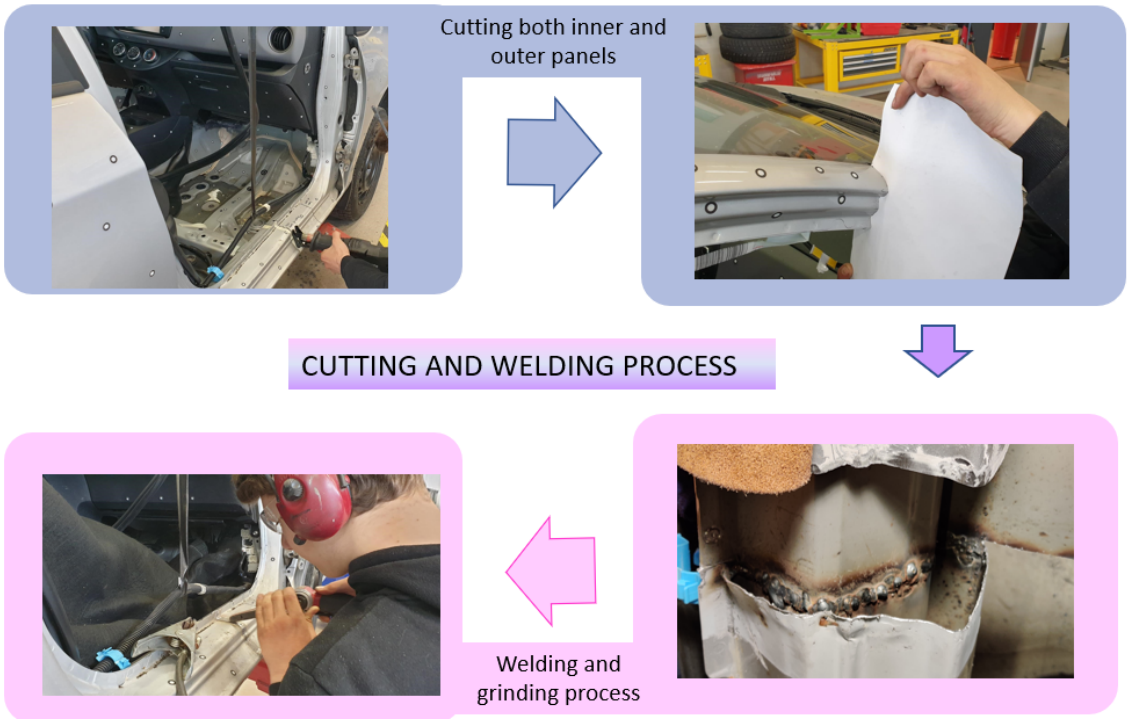

Figure G.3: Cutting and welding process followed for preparing the test vehicle

G.2.2 Instrumentation

The test was conducted with several on-board sensors and instrumentation to capture the forces acting on the vehicle during the impact. This subsection describes the instrumentation and datalogging systems used during this test.

G.2.2.1 Datalogger

The Data Acquisition System (DAS) is an important part of the data collection process: In this study we used was a Dewesoft SIRIUS Waterproof Rugged IP67. The shock rating of the logger is 100 g; it has 8x2 channels; each one is capable of 3x digital inputs, 1x event counter, encoder, period, pulse-width and duty-cycle. The DAS was placed in a box with power input from a 12V battery in the rear passenger seat to avoid impact during the test [16].

G.2.2.2 Accelerometers

There were 7 accelerometers mounted on the test vehicle to capture data from the impact. We used piezoresistive accelerometers (triaxial and uniaxial) designed for crash applications; low mass is preferred while using instrumentation on the vehicle and these sensors weighed less than 10 grams. They utilize three advanced micro machined, full-bridge sensors with gas damping and integral mechanical stops to ensure ruggedness, high output, high accuracy and high resonant frequency. Table G.2 highlights some of the specifications relevant to accelerometers used in this study [17], [18].

Parameter	Uniaxial	Triaxial
Sensitivity(100Hz and 10g)	0.30mV/g	0.3mV/g
Range	1000g	2000g
Excitation voltage	2-10V	2-10V
Frequency Response	20 to 1500 Hz, Referenced 100 Hz	20 to 1500 Hz, Referenced 100 Hz
Number of units	4	3

Table G.2: Uniaxial and triaxial accelerometer specifications.

G.2.2.3 Mounting of accelerometers

Table G.3 and Figure G.4 shows the accelerometer mounting locations on the test vehicle. The 3-Dimensional (3D) accelerometers were mounted on brackets designed to absorb initial shocks from the impact.

Table G.3: Accelerometer mounting locations.

Accelerometer Type	Mounting	Measurement
Triaxial - 1	Vehicle Center of Gravity (CG)	Vehicle CG on a steel bracket designed for the purpose
Triaxial - 2	In front of the vehicle CG	Mounted 25 cm in front of the vehicle CG and before the welded zone to capture the accelerations
Triaxial - 3	Rear of the vehicle CG	Mounted rear of the vehicle - 210 cm from the vehicle CG
Uniaxial - 1	Rocker	Acceleration in structural members in x axis
Uniaxial - 2	A-Pillar	mounted on a bracket designed to fit on the A-pillar measuring acceleration in x axis
Uniaxial - 3	Driver seat	Driver seat acceleration in x axis
Uniaxial - 4	Engine	Engine top in z axis

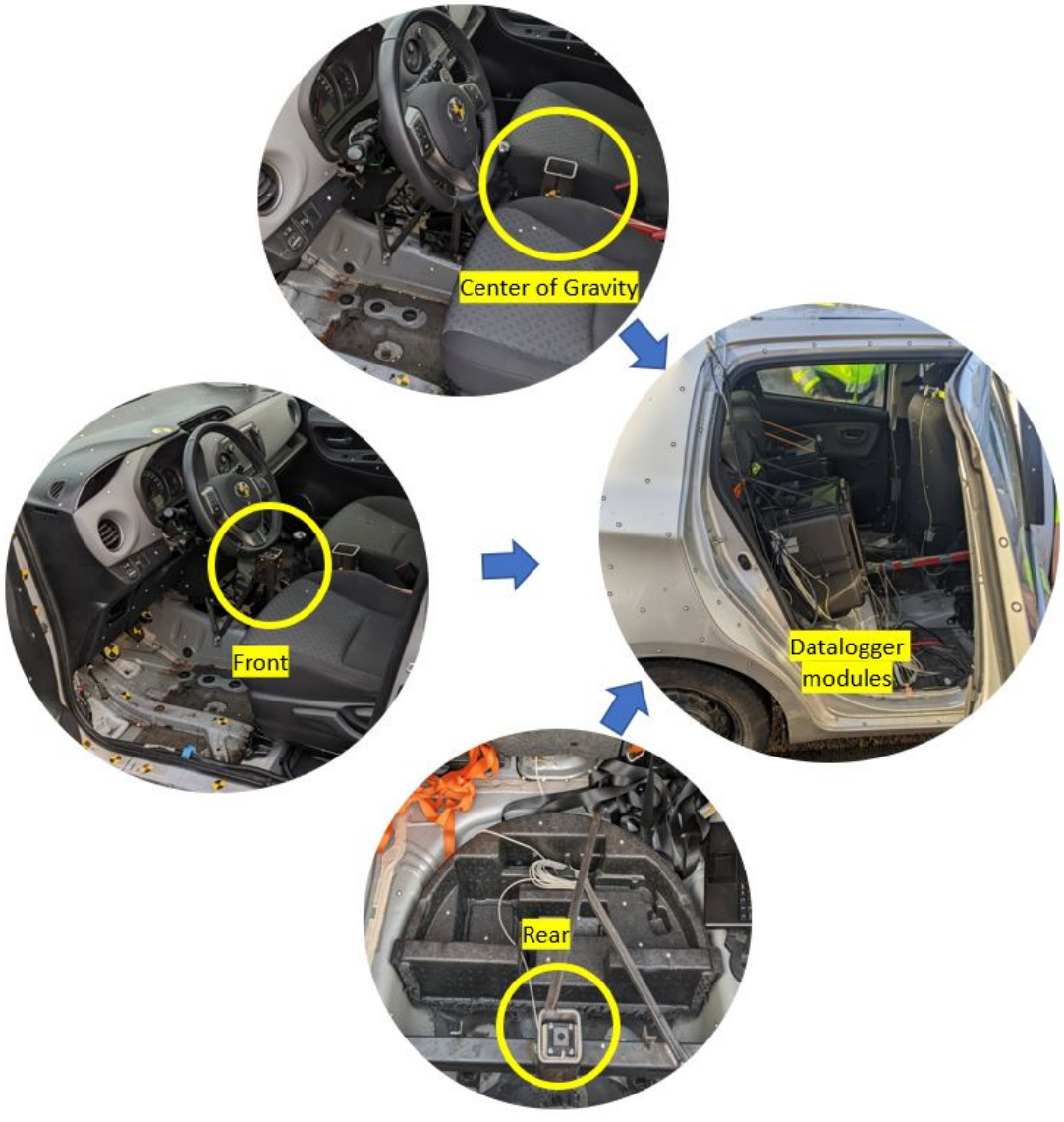

Figure G.4: 3D Accelerometer mounting locations on the test vehicle.

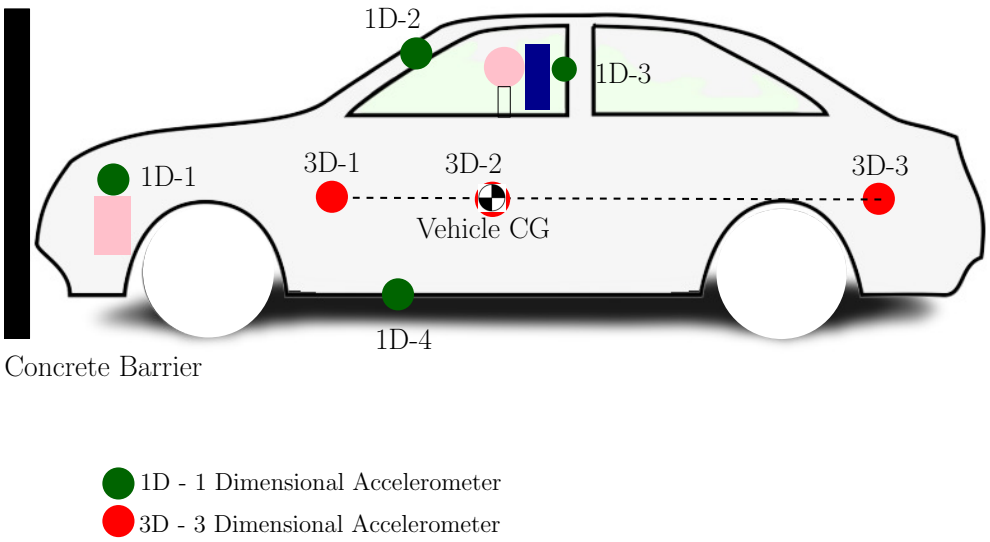

Figure G.5: Vehicle axes with accelerometer positions.

Eigen Frequency of each mounting bracket for the accelerometer

The eigen frequency of each bracket mounting for the accelerometer was measured with the DAS; the frequency of each axis in the 3D accelerometer was plotted with FFT (Fast Fourier Transform) and the maximum frequency was identified using a Matlab code. The eigen frequency of all brackets was desired to be above 2000 Hz so that it can be easily filtered from the test data. The measured frequencies are presented in Table G.4. The accelerometer on the driver seat was mounted on the

Accelerometer Type	Direction of Measurement	Eigen Frequency (Hz)
3D Accelerometer at CG	x axis	7272
3D Accelerometer at CG	y axis	3076
3D Accelerometer at CG	z axis	7272
3D Accelerometer at Front	x axis	2222
3D Accelerometer at Front	y axis	2577
3D Accelerometer at Front	z axis	9050
3D Accelerometer at Rear	x axis	2297
3D Accelerometer at Rear	y axis	1058
3D Accelerometer at Rear	z axis	7913
1D Accelerometer at Rocker	x axis	3756
1D Accelerometer at A-Pillar	x axis	699
1D Accelereomter at Engine	x axis	2357

Table G.4: Eigen Frequency Measurement.

cushion without a mounting bracket; hence it was excluded while measuring the eigen frequencies. The frequencies for all accelerometer brackets was above 1000 Hz except the 3D printed mount for the A-Pillar which was close to 700 Hz.

G.2.3 Center of Gravity Measurement

One 3D accelerometer needed to be mounted on the vehicle center of gravity (CG) to measure accelerations around the vehicle center of mass. The CG was calculated by installing 4 tensile loadcells on either wheel to measure the load on each wheel; the x and y and z coordinates of the CG are calculated based on the following measurements.

The vehicle was first lifted with zero inclination, and the static normal forces of the front and rear wheels, F_1, F_2, F_3 and F_4, were measured by the loadcells (Figure G.7 - 1). Then, after the front wheels were jacked up with an inclination angle θ; the normal forces were measured again.

Position of CG on wheel base R_f and R_r are the total loads at the front and rear wheels respectively.

$$R_f = F_2 + F_3 \tag{G.1}$$

$$R_r = F_1 + F_4 \tag{G.2}$$

where F_2 and F_3 are the reaction forces at the front left and right wheel; F_1 and F_4 are the reaction forces at the rear left and right wheel. Now taking moment at rear wheel $\sum M_x = 0$

$$R_f * b - W * x = 0 \tag{G.3}$$

$$CG_x = (R_f * b)/W; \tag{G.4}$$

where x is the distance of the CG point from the center of the rear wheel; W is the weight of the vehicle; b is the wheelbase of the vehicle. Similarly, Position of C.G. on Track width

$$R_L = F_1 + F_2 \tag{G.5}$$

$$R_R = F_3 + F_4 \tag{G.6}$$

Now taking moment at left wheel $\sum M_y = 0$

$$CG_y = (R_r * a)/W; \tag{G.7}$$

CG_y is the distance of the CG point from the center of the left wheel; a is the track width of the vehicle.

Determination of the height of the CG Let d is the diameter of the wheel; h is the height of the CG

$$CG_z = \frac{R_f - F_z}{W \tan\theta} \cdot b \tag{G.8}$$

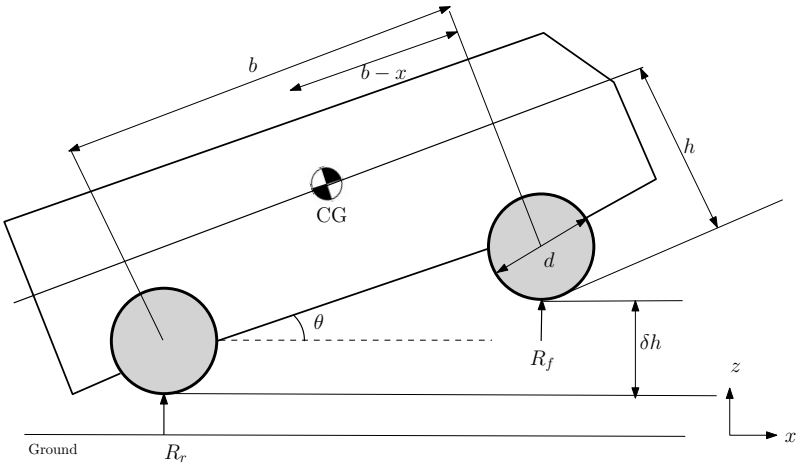

Figure G.6: Vehicle CG Measurement in tilted position.

where, F_z is the front weight in tilted position with angle θ Substituting the values in Equations G.4, G.7 and G.8 gives us the coordinates of the CG in x, y and z coordinates as $CG_{x,y,z} = [100.69, 1.4, 60.04]$ (units in cm)

Figure G.7: CG measurement; 1) Measurement of forces without tilting the vehicle; 2) Tilting vehicle front by 30 degrees

G.2.4 Rigid Concrete Barrier

The barrier; a concrete block with a steel-plate mounted on it is shown in Figure G.8. The concrete barrier was manufactured with 20 concrete blocks stacked in 3 rows with 8-8-4 blocks to generate a large reactive force. The dimension of each block is $(1.8x0.8x0.8)$ metres, and weights ≈ 2 tonnes. The entire concrete structure weighs ≈ 50 tonnes with dimensions of 3.2 x 3.2 metres in length and width; and 2.4 metres height. There was a steel plate fixed in-front of the concrete block to distribute the impact load across the structure; the plate weighs 200 kgs.

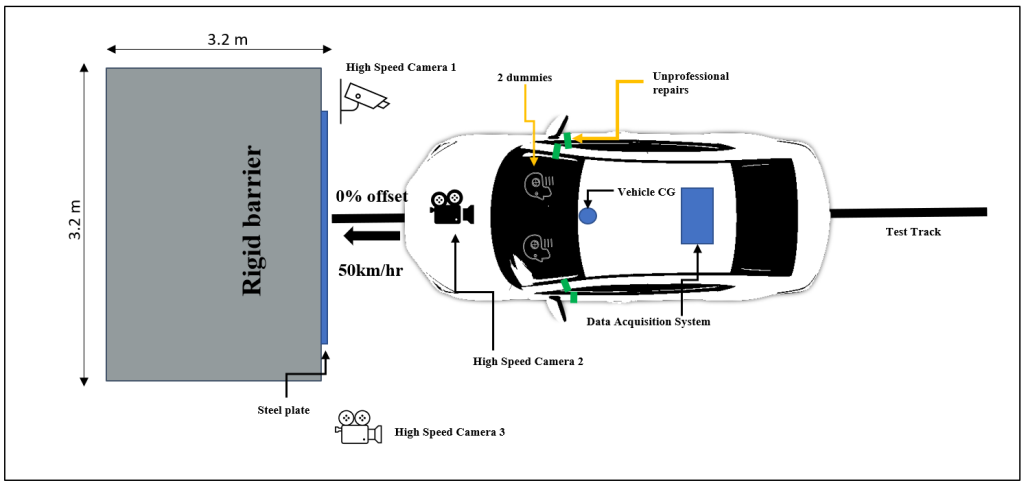

Figure G.9: Schematic of the test setup .

Figure G.8: Concrete barrier used in the test.

G.2.5 Test Conditions

The test schematic is presented below in Figure G.9. The planned test speed was 56 km/hr with a deviation of $+/-3$ km/hr; the speed of the vehicle was measured with an encoder based speed sensor developed for the test and a GPS speed sensor installed in the DAS. The sensors, as shown in Figure G.10 were affixed to the vehicle to measure the speed. Triggers are generally used in crash tests to determine the impact time and synchronizing all data signals from the acquisition system; triggers can be mechanical (contact based), flash bulb type for camera systems or electrical signals to synchronize impact times. We used a contact type trigger which generates a signal on impact with the vehicle; (Figure G.11) the trigger was mounted on the vehicle front (outermost part of the vehicle) to initiate a signal to the acquisition system.

The occupant head rotations and airbag deployment timings for a crash event

(**a**) (**b**)

Figure G.10: (a) Encoder based speed sensor developed to measure test speed, (b) GPS sensor for measuring test speed
Speed sensors on the vehicle

are important to study the injuries to driver and passengers in the vehicle. This test was conducted with a driver and a passenger belted dummy in the vehicle seats. The dummies were not instrumented crash test dummies; however they represent a 50^{th} percentile male with a weight of 75 kgs. The face and knee of the dummies were painted with fresh paint to determine the contact areas with the interior of the vehicle and also with the driver and passenger airbag (Figure G.12).

Figure G.11: Contact based trigger mounted on the vehicle.

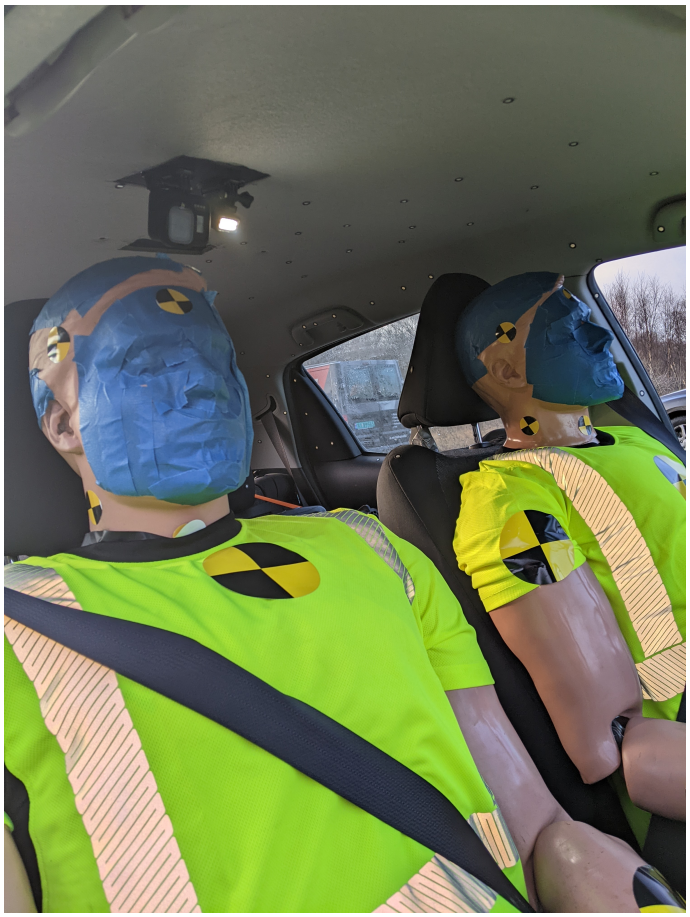

Figure G.12: Crash test dummies used in the test .

G.2.5.1 Videos to capture the Impact

As presented in Figure G.9 the crash test was captured with high speed cameras mounted at specific locations on the test site. The specifications of the videos captured is presented in Table G.5. The test videos are used to analyse the airbag deployment timings; deformation of the vehicle along with supporting in correlation with the FE simulations

Camera Type	Mounting	Resolution/fps
PROMON U1000 High speed camera	Side View	800*600/604
PROMON U1000 High speed camera	Front Side View	800*600/604
PROMON U1000 High speed camera	Top View	800*600/604
Go Pro Hero 8	Mounted on the barrier, captures front view	50 fps
Go Pro Hero 8	Mounted on vehicle roof, captures airbag deployment	50 fps
Professional Camera	Side View Wide Angle	50 fps

Table G.5: Camera Specifications.

G.2.5.2 Safety Considerations

It was imperative to include safety consideration while planing the test because it was not conducted in a crash laboratory designed for running vehicle safety tests; the crash was conducted on an outdoor test site in Farsund Airport, Lista in South Norway. A few safety considerations are outlined below:

- Marking safe walking areas in the test site; both near the track and the concrete barrier
- Using reflective vests for all engineers on-site; along with using safety glasses and shoes for everyone
- Removing the fuel from the test vehicle

G.2.6 Finite Element Modeling

The impact against the rigid barrier on an improperly repaired vehicle was replicated on an LS Dyna simulation using the modified 2010 Toyota Yaris model (developed by NHTSA (National Highway Transport Safety Administration[19]).The FE model developed by NHTSA was updated with material and thickness for the structural

members to replicate a 2015 Toyota Yaris model. It is modified with welds on the structural members replicating the crash test vehicle as defined in Subsection G.2.1. The FE model was cut at the A-Pillar and Rocker regions; the methodology defined by Noorsumar et al. in [8] was adopted to model the welds on the TRIP steel along with weld material properties used in the study conducted in [8]. The LS Dyna material properties used for the butt welds is presented in Figure G.13. The HAZ generated due to welding the members was also defined in the cross section of the structural members around the weld. The material properties of the HAZ have been used from the results of the study conducted by the authors in [7]; the paper determines the change in yield strength and ultimate strength of welded and heat treated UHSS (Ultra High Strength Steel) coupon samples.

MAT SPOTWELD CARD FROM LS DYNA (SI Units)

Mass Density	Young's Modulus	Poisson's Ratio	Yield Stress	Plastic Hardening Modulus
1.8 E-9	20000	0.3	120	2000

Effective Plastic Strain in weld material at failure	Axial Force Resultant at Failure	Force Resultant at Failure
1.5	60000	30000

Figure G.13: Weld properties in LS Dyna [8]

G.3 Results and Discussion

G.3.1 Test Results

The test acceleration curves for different sensors have been presented in Figure G.14. This data is generated from the raw unfiltered data by making use of CFC-180 method according to the ISO-6487:1987 standard. The channel class uses cut off frequency that is 300 Hz for CFC-180. The cut off frequency is a boundary condition for allowing low frequencies to pass through and attenuates the high ones. This is due to high disturbances and noise from a full scale vehicle crash which might cause bad signal processing. The 3D accelerometers at the vehicle CG, front and the rear have been represented with resultant curves and the 1-D accelerometers at other locations measures the acceleration in the direction of impact (x axis in this case).

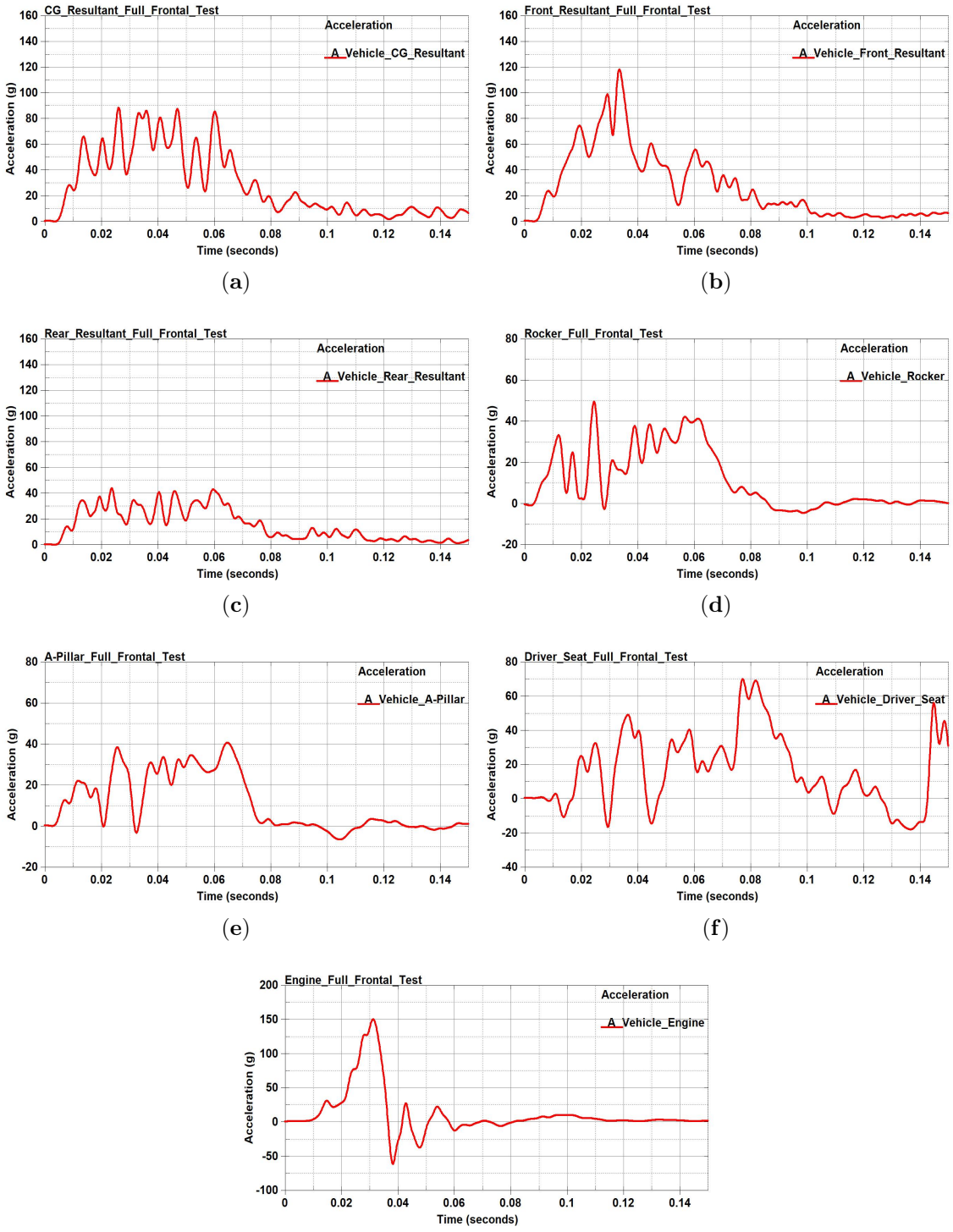

Figure G.14: (a) Acceleration at the vehicle CG - Resultant of the curves, (b) Acceleration at the front of the vehicle - Resultant of the curves,
(c) Acceleration at the rear of the vehicle - Resultant of the curves, (d) Engine Acceleration curves
(e) Acceleration at the A-Pillar, (f) Acceleration at the Rocker
(g) Acceleration at the Driver Seat,
Acceleration plots for different parts of the vehicle

The table below presents the maximum acceleration in the direction of impact for all the accelerometers G.6

Accelerometer Type	Mounting	Peak Acceleration (g) - Filtered data
Triaxial - 1	Vehicle Center of Gravity (CG) - Resultant	88.4
Triaxial - 2	Front of the vehicle CG - Resultant	118.27
Triaxial - 3	Rear of the vehicle CG - Resultant	43.80
Uniaxial - 1	Rocker	49.49
Uniaxial - 2	A-Pillar	70.10
Uniaxial - 3	Driver seat	114.37
Uniaxial - 4	Engine	150.29

Table G.6: Uniaxial and triaxial accelerometer maximum acceleration.

The pre and post-test images have been presented in Figure G.15 - G.17 showing deformation after impact and the position of the dummies post impact. The front-end was observed to be deformed symmetrically indicating 0% offset during the crash.

Figure G.15: Test vehicle in Side View pre and post impact.

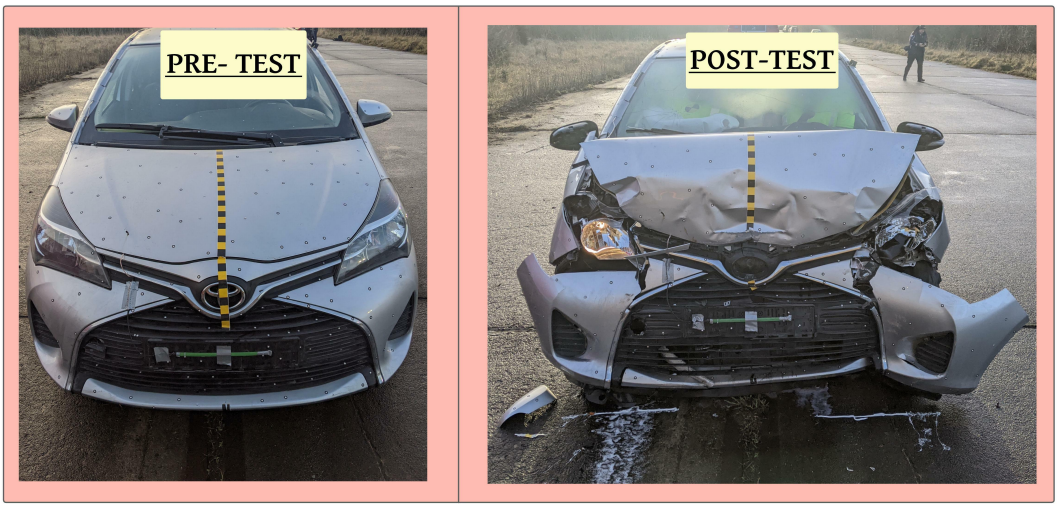

Figure G.16: Test vehicle in Front View pre and post impact.

Figure G.17: Test vehicle in Side View with Dummies and Airbag Deployment - pre and post impact.

The speed of the test vehicle measured with GPS and an in-house developed encoder based speed sensor has been presented in Figure G.18. The velocity measured by the GPS mounted on the vehicle (Figure G.18(**a**)) shows an unrealistic dip at 40-60 ms indicating the time of maximum deformation; we recognize the data is unreliable and a limitation to using GPS for a highly dynamic event as the vehicle crash. The correlation with FE data uses the curves obtained from the encoder sensor instead because it indicates more reliable values.

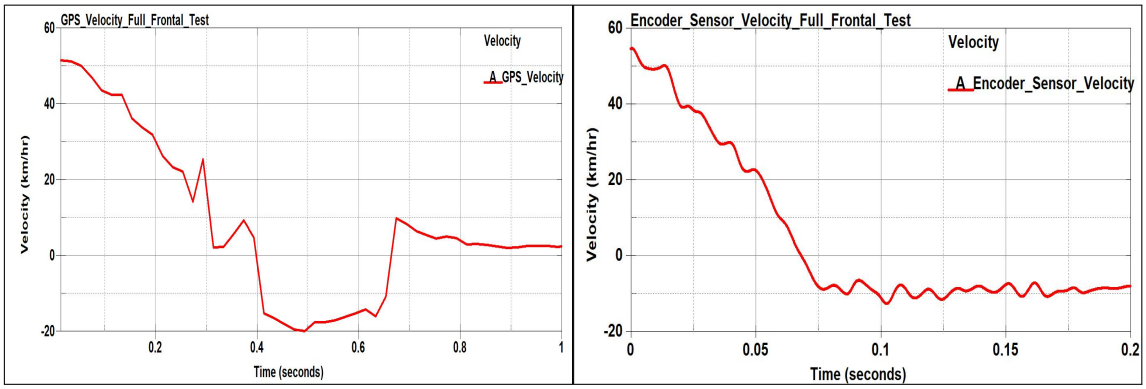

(**a**) (**b**)

Figure G.18: (a) Velocity curves from GPS, (b) Velocity curve from Encoder Speed sensor
Impact speed

The videos captured on the test indicate the airbag deployment time which is a crucial element in occupant injury protection; the deployment time was compared to a test conducted on the same vehicle by NHTSA (Crash Test Database). It was observed that the airbag deployed later than expected deployment time indicating higher occupant injuries in the modified vehicle. Figure G.19 - G.20 show the images captured at different time intervals and compare the airbag in the two vehicles. It was observed that the airbag deployment is delayed by $\approx$ 11 ms in the modified vehicle. The loadcase specifications on the two tests is similar (0% offset rigid barrier) along with the make, model and velocities for the tests.

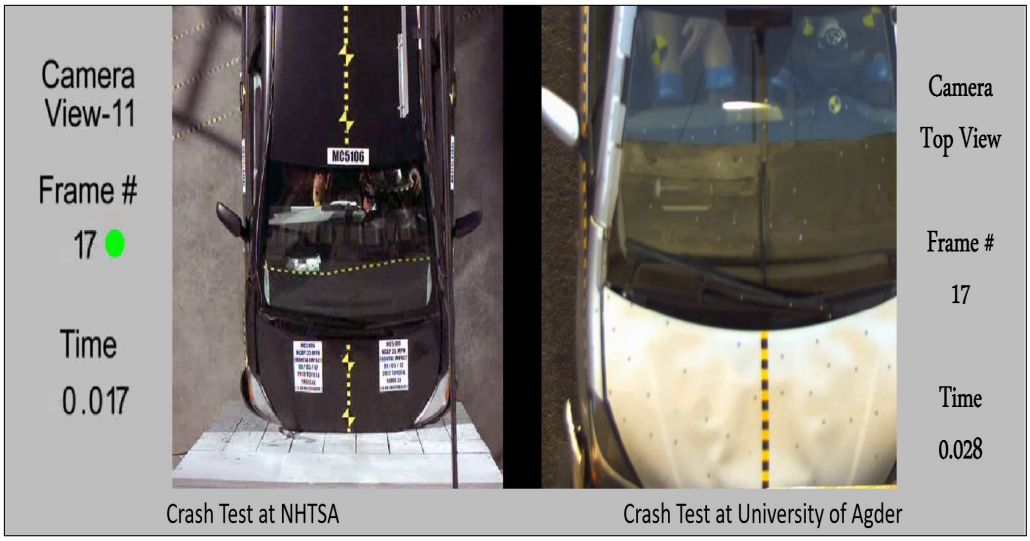

Figure G.19: Airbag deployment timings compared NHTSA vs Crash test at UiA - start of deployment

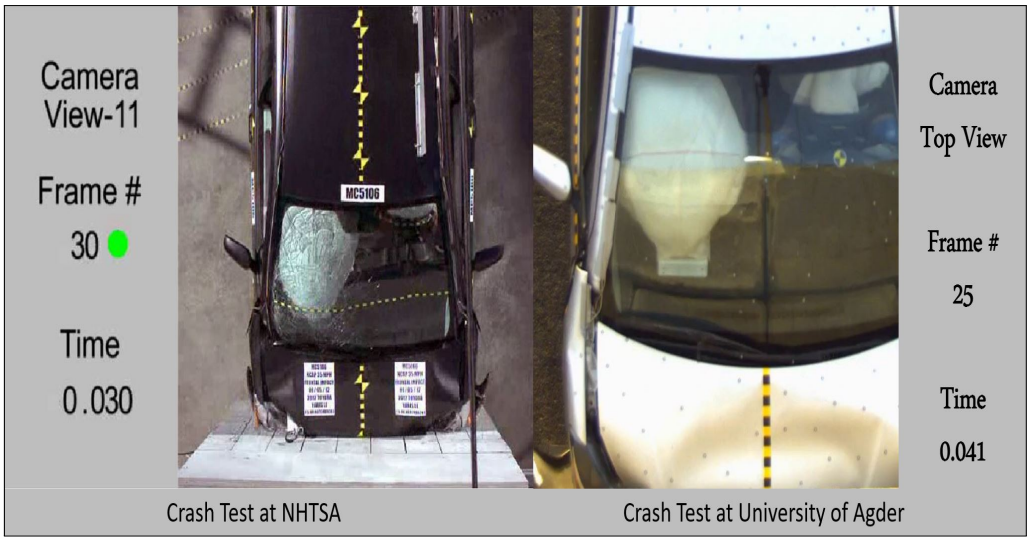

Figure G.20: Airbag deployment timings compared NHTSA vs Crash test at UiA - close to end of deployment

G.3.2 Validation with FE Models

The LS Dyna model developed in Section G.2 was simulated to compare the impact kinematics to the test data generated from the sensors and the video. The FE model does not include a dummy or airbags because occupant protection was kept out of scope.. The correlation with FE dummy models and airbag deployment will be discussed in a separate study. Figure G.21-G.22 represents the side view and top view of the comparison with test data. The simulations were observed to be closely following the videos captured during the test; however there are some distinct differences in the FE simulations. The windshield behaviour was not realistic; the modeling of the steering wheel needs to be improved to capture the failure in the steering column during the impact. The region around the welded zone looked similar to the test vehicle; the fender region in the top view of the impact shows deformation not consistent with the test. It was concluded based on visual comparison that the material modeling of plastic parts and windshield needs closer investigation to improve the behaviour during high speed impacts.

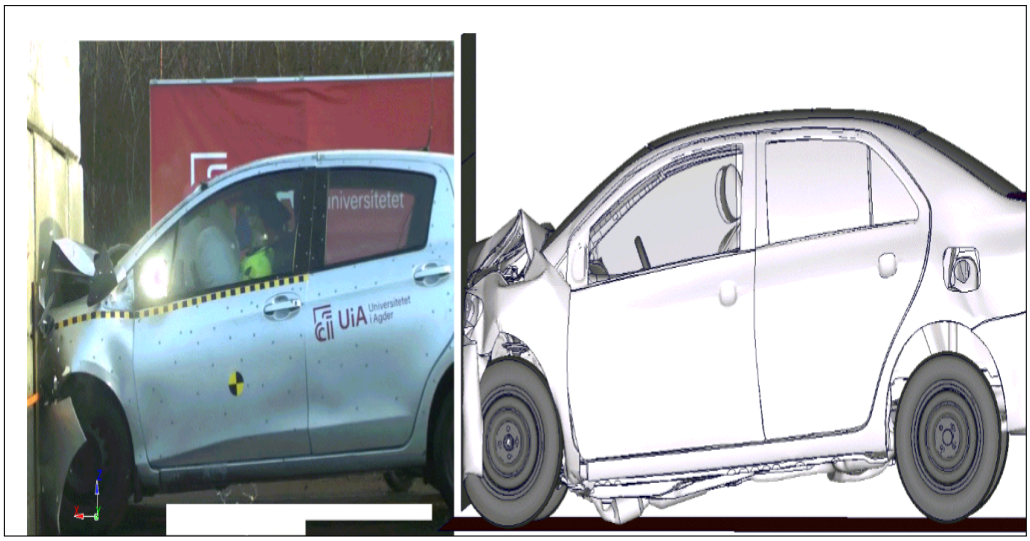

Figure G.21: Physical Test vs FE comparison for full scale test in side view

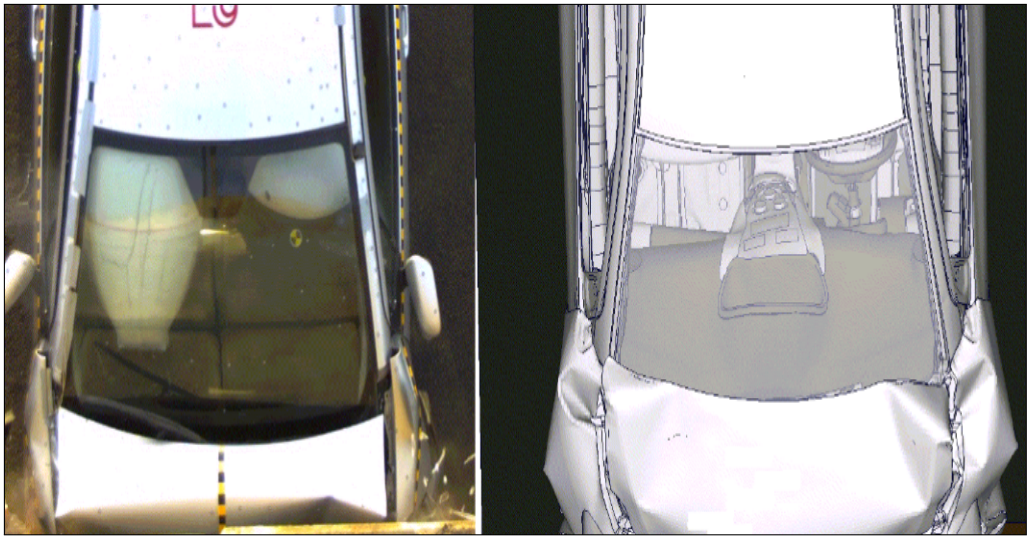

Figure G.22: Physical Test vs FE comparison for full scale test in top view

The FE validation model was also updated to include the accelerometers mounted on the test vehicle; the 6 accelerometers with the exception of the rear mounted one were compared with data acquired from the DAS. The curves are plotted in Figure G.23; the FE model follows the trend in most mounting locations capturing the maximum acceleration values with a small deviation. The curves have been filtered with a butterworth CFC-60 filter to compare the data; this filter uses a cut off frequency of 100 Hz.The deviation with test data is significantly higher in case of the 3D accelerometers; this can be attributed to the absence of steel mounting brackets in the FE model replicating the impact. The steel brackets supporting the 3D accelerometers were not modeled in the simulation which could be contributing to the deviation in the results. Figure G.24 also compares the velocity of the test vehicle

against the simulation curves showing close correlation and a maximum velocity of ≈ 54 km/hr.

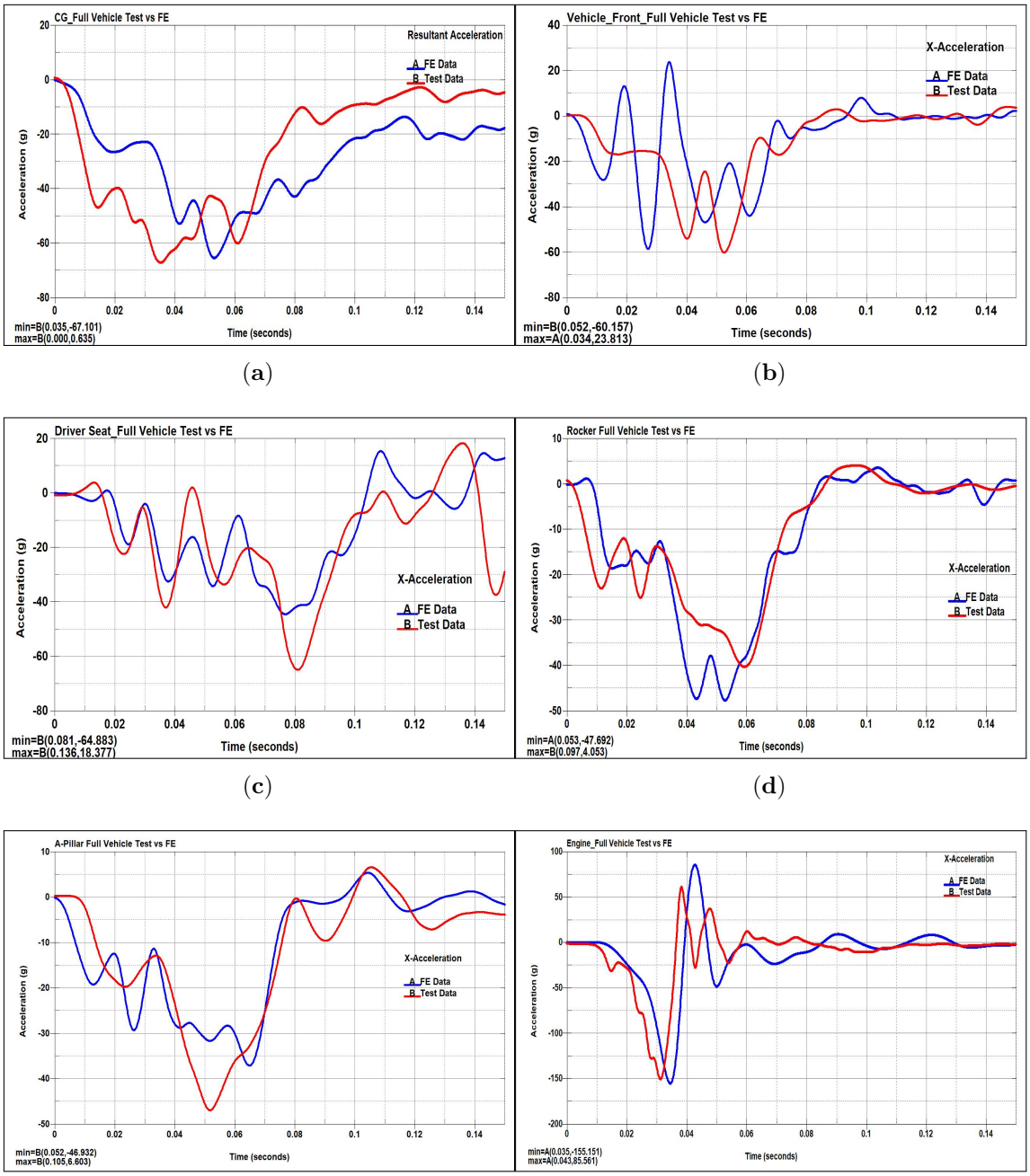

Figure G.23: (a) Comparison of FE vs Test curves - CG, (b) Comparison of FE vs Test curves - Front,
(c) Comparison of FE vs Test curves - Driver Seat, (d) Comparison of FE vs Test curves - Rocker
(e) Comparison of FE vs Test curves - A-Pillar, (f) Comparison of FE vs Test curves - Engine
Acceleration plots to compare test vs FE data

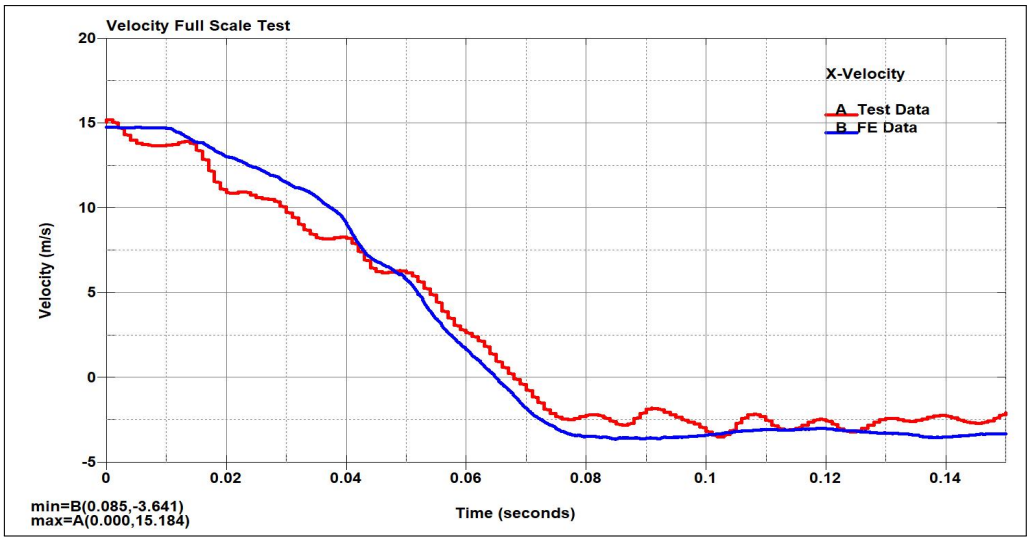

Figure G.24: Comparison of FE vs Test curves - Velocity

Pitching is an important parameter contributing to head and neck deflections in occupants during a crash event. The vertical displacement (z-axis) at the CG and the rear of the vehicle have been plotted to compare the rotation of the vehicle about the impact point. Figure G.25 shows the displacements indicating a close correlation between the curves. The curves deviate at the CG indicating the contribution of the mounting brackets on the simulation results along with the modeling methodology of the welds and the heat affected zone on the TRIP steel members.

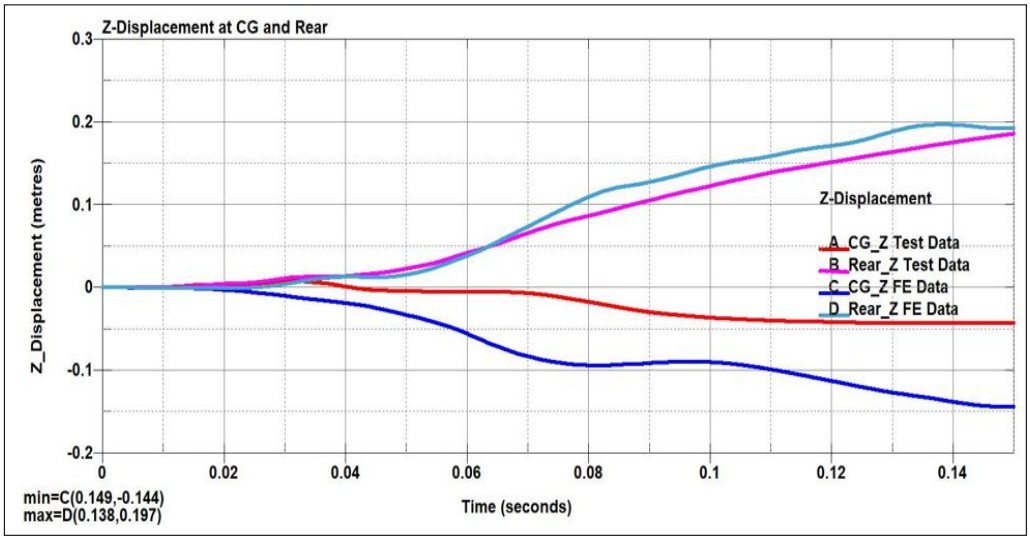

Figure G.25: Comparison of Physical Test vs FE in Z-Displacement

G.4 Conclusion and Next Steps

Literature review has concluded that welding and heat treatment of TRIP steels affects the ultimate and yield strength of samples; consequently vehicle manufacturers

recommend to follow the repair manual strictly on parts using TRIP steel in the vehicle structure. This paper presents the test results conducted to determine the behaviour of welded and heat treated TRIP steel on an improperly repaired vehicle undergoing full frontal impact. The preparation of the vehicle to undergo the full scale impact conducted during this research has been described along with observations made post-test. The description of the instrumentation and cameras used during this test will provide a knowledge base for academicians planning similar tests in the future. Besides, the test data has been compared with baseline crashworthiness impact performance for the same vehicle to draw conclusions around the changes in impact response for the vehicle. It was concluded that the welding and heat-treatment of structural TRIP steel members leads to modification in the air-bag timing in the vehicle. This could potentially change the EURONCAP safety rating of the vehicle and other regulatory tests indicating reduced safety performance in crashworthiness loadcases.

The crash test has been replicated on an FE model modified to include the welds in the TRIP steel members along with a HAZ in the A-Pillar and Rocker parts. The simulation has been compared to the test data generated in the test; the possible reasons for deviation in the performance has been discussed in the paper. The modeling methodology of welds adopted in this study is a starting point for more research to be conducted in this field.

The next steps for this research are outlined below:

- The full vehicle test was conducted with a rigid barrier at 0% offset; however it will be interesting to include other crash scenarios where unprofessional repairs could influence the performance of the vehicle; the test can also be run at different speeds.

- The intrusions in the driver compartment due to the crash needs to be investigated and the compared to the baseline performance without repairs.

- The welded and heat treated members should be investigated to check for microstructual changes with microscopic analysis to determine the change in material behaviour.

- Occupant protection was kept out of scope in this study; however the modeling of dummies and airbags in the FE model would provide better understanding of the crash performance.

G.5 Acknowledgement

The authors would like to thank the engineers at the Mechatronics Lab at University of Agder and the Mechatronics Innovation lab for their constant support and guidance in conducting this research. We also greatly acknowledge the support of Sam Eyde videregående skole (Arendal) for their support in conducting repairs on the vehicle. The crash test was conducted at Lista (Norway) and we thank Farsund Airport Authorities for access to the facility for this research.

References – Paper G

[1] I. Tamura. Deformation-induced martensitic transformation and transformation-induced plasticity in steels. *http://dx.doi.org/10.1179/030634582790427316*, 16 (5):245–253, 5 2013. ISSN 03063453. doi: 10.1179/030634582790427316. URL https://www.tandfonline.com/doi/abs/10.1179/030634582790427316.

[2] Maryam Soleimani, Alireza Kalhor, and Hamed Mirzadeh. Transformation-induced plasticity (TRIP) in advanced steels: A review. *Materials Science and Engineering: A*, 795:140023, 9 2020. ISSN 0921-5093. doi: 10.1016/J.MSEA.2020.140023.

[3] Daniel Krizan. TRIP STEELS: ADVANCED HIGH STRENGTH MULTIPHASE STEELS FOR AUTOMOTIVE APPLICATIONS. In *Proc. Int. Conf. on 'COM-MATTECH', Trnava, Slovakia*, pages 659–668, 2006. URL https://www.researchgate.net/publication/322664721_TRIP_STEELS_ADVANCED_HIGH_STRENGTH_MULTIPHASE_STEELS_FOR_AUTOMOTIVE_APPLICATIONS.

[4] Jean Hubert Schmitt and Thierry Iung. New developments of advanced high-strength steels for automotive applications. *Comptes Rendus Physique*, 19(8): 641–656, 12 2018. ISSN 1631-0705. doi: 10.1016/J.CRHY.2018.11.004.

[5] Günter Wassermann. Untersuchungen an einer Eisen-Nickel-Legierung über die Verformbarkeit während der γ-α-Umwandlung. *undefined*, 10(7):321–325, 1 1937. doi: 10.1002/SRIN.193700538.

[6] ZACKAY V F, PARKER E R, FAHR D, and BUSCH R. The enhancement of ductility in high-strength steels. *Trans Am Soc Met*, 60: 252–259, 1967. URL https://jglobal.jst.go.jp/en/detail?JGLOBAL_ID=201602018455359736.

[7] Gulshan Noorsumar, Dmitry Vysochinskiy, Even Englund, Kjell G. Robbersmyr, and Svitlana Rogovchenko. Effect of welding and heat treatment on the properties of UHSS used in automotive industry. *EPJ Web of Conferences*, 250:05015, 2021. ISSN 2100-014X. doi: 10.1051/EPJCONF/202125005015.

URL https://www.epj-conferences.org/articles/epjconf/abs/2021/04/epjconf_dymat2021_05015/epjconf_dymat2021_05015.html.

[8] Gulshan Noorsumar, Kjell Robbersmyr, Svitlana Rogovchenko, and Dmitry Vysochinskiy. Crash Response of a Repaired Vehicle - Influence of Welding UHSS Members. *SAE Technical Papers*, 2020-April(April), 4 2020. ISSN 0148-7191. doi: 10.4271/2020-01-0197. URL https://www.sae.org/publications/technical-papers/content/2020-01-0197/.

[9] Mei ZHANG, Lin LI, Ren yu FU, Ji cheng ZHANG, and Zi WAN. Weldability of Low Carbon Transformation Induced Plasticity Steel. *Journal of Iron and Steel Research, International*, 15(5):61–87, 9 2008. ISSN 1006-706X. doi: 10.1016/S1006-706X(08)60250-2.

[10] M. Amirthalingam, M. Hermans, and I. Richardson. Microstructural development during welding of siliconand aluminum-based transformation-induced plasticity steels-inclusion and elemental partitioning analysis. *Metallurgical and Materials Transactions A: Physical Metallurgy and Materials Science*, 40(4): 901–909, 2009. ISSN 10735623. doi: 10.1007/S11661-008-9761-5.

[11] Schmortte Uwe. Crash-Test Results to Analyse the Impact of Non-Professional Repair on the Performance of Side Structure of a Car. In *22nd Enhanced Safety of Vehicles Conference (ESV 2011)*, Washington, DC, USA, 2011.

[12] Jaroslav Mackerle. Finite Element Crash Simulations and Impact-Induced Injuries. *Shock and Vibration*, 6(5-6):321–334, 1999. ISSN 1070-9622. doi: 10.1155/1999/802580. URL https://www.hindawi.com/journals/sv/1999/802580/.

[13] Philipp Spethmann, Stefan H. Thomke, and Cornelius Herstatt. The impact of crash simulation on productivity and problem-solving in automotive R&D. 2006. URL https://www.econstor.eu/handle/10419/55496.

[14] Kjell G. Robbersmyr. Calibration test of a standard Ford Fiesta 1.1 l, model year 1987, according to NS-EN 12767. Technical report, Agder University College, Grimstad, 2004.

[15] EUROPEAN NEW CAR ASSESSMENT PROGRAMME (Euro NCAP) FULL WIDTH FRONTAL IMPACT TESTING PROTOCOL. Technical report, 2015.

[16] SIRIUS Technical Specifications | Dewesoft, . URL https://dewesoft.com/products/daq-systems/sirius/tech-specs.

[17] Piezoresistive accelerometer - Model 701AH - 701FH, . URL https://endevco.com/contentstore/mktg/downloads/edv-ds-701ah-701fh_lowres.pdf.

[18] Triaxial piezoresistive accelerometer Model 713-713F. . URL www.endevco.com.

[19] Crash Simulation Vehicle Models | NHTSA, . URL https://www.nhtsa.gov/crash-simulation-vehicle-models.

Paper H

Modeling of modified vehicle crashworthiness using a double compound pendulum

Gulshan Noorsumar, Svitlana Rogovchenko, Dmitry Vyscochinskiy and Kjell G. Robbersmyr

This paper has been published as:

Gulshan Noorsumar, Svitlana Rogovchenko, Dmitry Vyscochinskiy and Kjell G. Robbersmyr. Modeling of modified vehicle crashworthiness using a double compound pendulum. *12th International Conference on Simulation and Modeling Methodologies, Technologies and Applications - SIMULTECH 2022*, ISBN 978-989-758-578-4; ISSN 2184-2841, pages 102-111, doi: 10.5220/0011306100003274.

Modeling of modified vehicle crashworthiness using a double compound pendulum

Gulshan Noorsumar, Svitlana Rogovchenko, Dmitry Vyscochinskiy and Kjell G. Robbersmyr
Department of Engineering Sciences
University of Agder
4879 Grimstad, Norway

Abstract **Vehicle crash modeling has been a challenge for researchers for several decades. Occupant injury prevention and prediction is a critical area within vehicle safety design. The modeling of material failure in structural members during a full frontal crash has been presented in this paper. This study presents a Lumped Parameter Model (LPM) with an elastic double compound pendulum replicating the impact kinematics. The model defined using Lagrangian formulation; presents a novel methodology to represent material fracture caused due to heat affected zones or welding in Ultra High Strength Steels (UHSS) in a non-linear crash event. The material fracture leads to rotation of the vehicle; presented in the form of torsional springs in the LPM developed in this study. The Simulink model has been validated with a finite element simulation and shows good correlation to predict parameters crucial to design for occupant protection in a vehicle crash.**

H.1 Introduction

Traffic accidents lead to many fatalities on the roads worldwide. It is one of the major global problems which demands attention. With an increasing global population, transportation demands have increased leading to more cars on roads and appropriate efforts to reduce traffic related injuries should be taken. Automakers and researchers strive to achieve stringent safety regulations improving the safety of occupants and road users in a crash [1]. Real-time crash impacts had been the preferred mode of safety testing for new cars for decades; the emergence of mathematical models have reduced physical testing during the development process. There is still a need to further decrease the dependence on physical tests for crashworthiness assessment of vehicles.

Noorsumar et al. [1] have reviewed the mathematical models used in the industry and academia to replicate vehicle impacts. Finite Element Methods (FEM) have found applications in several areas of safety research; one of the early contributions

to the theory and applications of FEM in dynamic crush modeling was made in [2]. The increasing use of FEM in modeling vehicle and occupant models in the automotive industry is reported in [3].

Lumped Parameter Models (LPM) are often applied in crash modeling due to their low computational requirements and faster results but they produce lower accuracy as compared to FE Models. Kamal presented an LPM for vehicle impact in 1970 [4]. His work paved the way for several studies targeting parameter identification in impact loadcases [5], [6]. Elkady et al. have developed models to explore the effects of Vehicle Dynamics Control Systems (VDCS) on the crash mitigation for an impact with a rigid barrier [7],[8]. These models use non-linear springs to represent the front-end deformation; the studies show good correlation with the tests. LPMs have been used to represent flexible bodies in different applications where modeling of joints is crucial to replicate the system [9]. Occupant modeling for vehicle crashworthiness has been studied by several researchers using LPMs; Ionut et al. present a 2-dimensional model with 2 vehicles and 2 occupants using Lagrangian mechanics [10].

Deceleration of large vehicles along with rotation of the vehicle in different axes is the leading cause of head and chest injuries [11]. More recently, the Lagrangian formulation in an LPM employing a novel two-phase technique for the complex non-linear impact scenario was suggested [12]. The obtained results reinforce the conclusions that occupant's contact with a headliner during the vehicle pitch and drop lead to more serious head and neck injuries ([11], [13]). Good correlation with pitching data from validation tests is demonstrated. There is, however, a need to improve prediction models for better safety for unbelted occupants in crashes. The complexity of the model further increases if we want to incorporate material failure in the LPM. There are several manufacturing and joining processes involved in producing and repairing the parts of the vehicle which may result in reduced crashworthiness. Several papers investigate the weldability and heat treatment of Ultra High Strength Steels (UHSS) and the material changes due to the exposure of the workpiece to thermal changes [14], [15], [16]. Amirthalingam studied the change in material behavior due to welding and heat treatment of dog-bone samples [17]. Capturing these material behaviour changes in an LPM is a difficulty yet to be addressed by researchers in the industry and the academia. This challenge has also posed a limitation to use of LPMs in the automotive industry. Pavlov used an inverted pendulum to represent a vehicle undergoing pitching [18]. Occupant kinematics using a pendulum was presented in [19]. Double pendulum models have been used to define impact with a rough surface in ([20], [21]). In this paper, we study the crash impact of a modified vehicle with welds on the UHSS members against a rigid non-deformable barrier. We a compound double pendulum model with polar coordinates to define the system. In our model,the vehicle impacts the

barrier at 0% offset at 56 kmph and the body acts like a compound elastic double pendulum in motion.

H.2 Methodology

Our model represents a vehicle with welds and a heat affected zone (HAZ) leading to failures in the structural members during a full frontal impact. A double pendulum has been employed to replicate the scenario in the LPM; it includes two mass components representing the compartment before and after the welded zone. The weld is represented by a torsional joint in the model allowing the rotation of the body about the joint by a small angle θ_2. The assumptions in the model include [12]:

- A full frontal impact generally leads to rotation about the y-axis, hence only vehicle rotations about the y-axis (pitching) were considered in the model.
- Energy losses like friction and heat losses were neglected.
- It was assumed that the front-end spring and damper characteristics are piecewise linear with four breakpoints, even though the system behaves non-linearly in a crash.
- The welds are assumed to fail during the impact due to the behaviour of UHSS members affected by previous welding and heat treatment.
- A dimensionless torsional spring represents the weld and failure of the model occurs along the y axis.

The motion of a double pendulum is described as follows: the pendulum swings back and forth about the pivot point as shown in Figure H.1. Under impact, the vehicle behaves like a pendulum rotating around the pivot point, that is, an impact point in this case, thus, causing the pitching. As a result of the ground acting as a constraint, the vehicle cannot sway back and forth. The deformable front end crumple zone is represented with a spring and damper system for the pendulum; the suspensions acting as a constraint to prevent the pendulum to rotate beyond a certain angle. The 3 Degrees of Freedom (DOF) LPM is defined to determine the governing equations of motion; the system is simplified by converting the cartesian coordinates to polar coordinates.

Figure H.2 shows the model of the vehicle impacting a rigid barrier. The front end deformation is represented by the elastic pendulum; the spring and damper coefficients are defined using a piecewise linear function with five breakpoints. The torsional spring connects the mass components before and after the welded zone.The

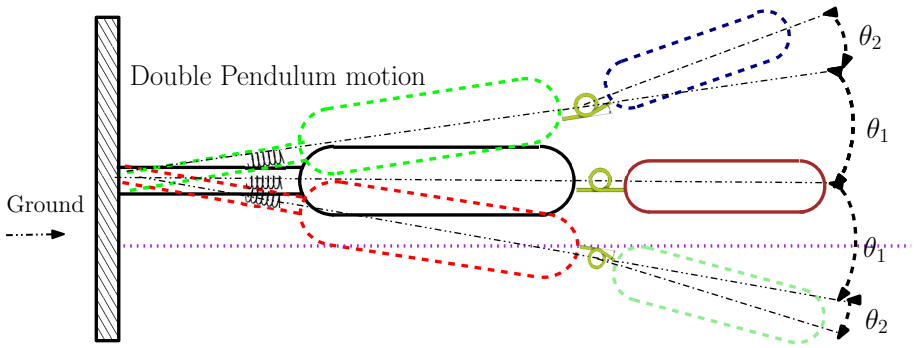

Figure H.1: Vehicle body rotating like a pendulum about the impact point.

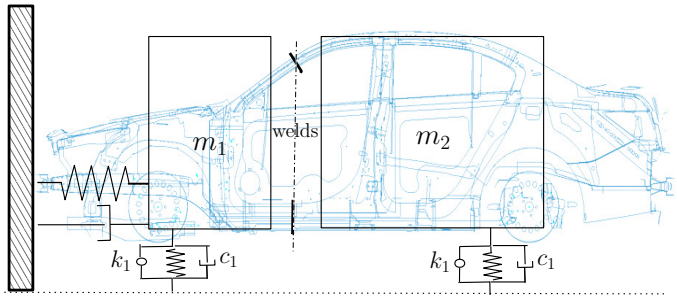

Figure H.2: Vehicle body with welds and the occupant compartments divided into lumped mass systems

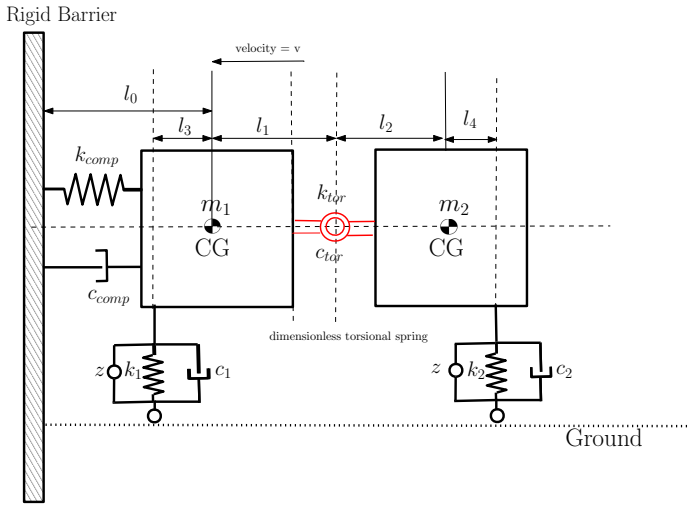

Figure H.3: LPM of the vehicle impacting the rigid barrier at time $t = 0$.

LPM containing two mass components along with the constraints is presented in Figure H.3

The event has been divided into three phases:

- Deformation of the front end leading to energy absorption modeled as an elastic spring.
- Rotation of the vehicle body about the impact point with an angle θ_1.
- Failure of the welds leading to rotation of the vehicle about the torsional joint

with an angle θ_2.

The double pendulum model replicating the vehicle rotating about the torsional spring with an angle θ_2 is shown in Figure H.4.

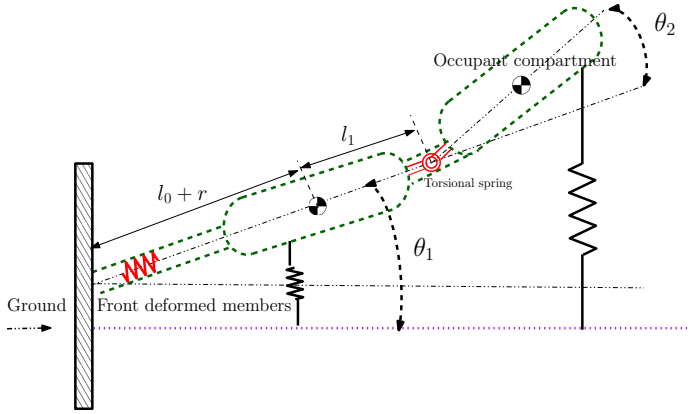

Figure H.4: Vehicle body rotating about the impact point after front-end deformation.

H.2.1 Parameter identification for front end spring and damper characteristics

The front end spring damper characteristics were defined using an algorithm developed by the authors [12]. The gradient descent optimization algorithm has been modified to fit the force-deformation curve for the entire dynamic event.

The spring and damper coefficients derived from the algorithm are presented in the next section. The non-linear force deformation curve have been approximated to represent the front end system in the LPM. The stiffness k and spring force F_k are related by the equation (H.1). Similarly, the damper coefficient c is related to the damping force F_c by the equation (H.2) ([8], [12]).

$$F_k = k(x) \cdot x, \tag{H.1}$$

$$F_c = c(\dot{x}) \cdot \dot{x}, \tag{H.2}$$

where

$$k(x) = \begin{cases} \frac{(k_2-k_1)\cdot|\hat{x}|}{x_1} + k_1, & \text{for } |\hat{x}| \le x_1, \\ \frac{(k_3-k_2)\cdot(|\hat{x}|-x_1)}{(x_2-x_1)} + k_2, & \text{for } x_1 \le |\hat{x}| \le x_2, \\ \frac{(k_4-k_3)\cdot(|\hat{x}|-x_2)}{(x_3-x_2)} + k_3, & \text{for } x_2 \le |\hat{x}| \le x_3, \\ \frac{(k_5-k_4)\cdot(|\hat{x}|-x_3)}{(x_4-x_3)} + k_4, & \text{for } x_3 \le |\hat{x}| \le x_4, \\ \frac{(k_6-k_5)\cdot(|\hat{x}|-x_4)}{(x_5-x_4)} + k_5, & \text{for } x_4 \le |\hat{x}| \le x_5, \\ \frac{(k_7-k_6)\cdot(|\hat{x}|-x_5)}{(C-x_5)} + k_6, & \text{for } x_5 \le |\hat{x}| \le C. \end{cases}$$

The damper characteristics are defined similarly to the spring characteristics in the model:

$$c(\dot{x}) = \begin{cases} \frac{(c_2-c_1)\cdot|\hat{\dot{x}}|}{\dot{x}_1} + c_1, & \text{for } |\hat{\dot{x}}| \le \dot{x}_1, \\ \frac{(c_3-c_2)\cdot(|\hat{\dot{x}}|-\dot{x}_1)}{(\dot{x}_2-\dot{x}_1)} + c_2, & \text{for } \dot{x}_1 \le |\hat{\dot{x}}| \le \dot{x}_2, \\ \frac{(c_4-c_3)\cdot(|\hat{\dot{x}}|-\dot{x}_2)}{(\dot{x}_3-\dot{x}_2)} + c_3, & \text{for } \dot{x}_2 \le |\hat{\dot{x}}| \le \dot{x}_3, \\ \frac{(c_5-c_4)\cdot(|\hat{\dot{x}}|-\dot{x}_3)}{(\dot{x}_4-\dot{x}_3)} + c_4, & \text{for } \dot{x}_3 \le |\hat{\dot{x}}| \le \dot{x}_4, \\ \frac{(c_6-c_5)\cdot(|\hat{\dot{x}}|-\dot{x}_4)}{(\dot{x}_5-\dot{x}_4)} + c_5, & \text{for } \dot{x}_4 \le |\hat{\dot{x}}| \le \dot{x}_5, \\ \frac{(c_7-c_6)\cdot(|\hat{\dot{x}}|-\dot{x}_5)}{(v_0-\dot{x}_5)} + c_6, & \text{for } \dot{x}_5 \le |\hat{\dot{x}}| \le v_0, \end{cases}$$

where k is the front end spring coefficient, c is the front end damper coefficient, $\hat{x}$ is the computed vehicle deformation, $\dot{x}$ is the vehicle velocity, $\hat{\dot{x}}$ is the computed vehicle velocity, C is the maximum dynamic crush, v_0 is the velocity at the time of maximum dynamic crush. The optimization algorithm which minimizes the error between the test and computed values has been used to determine the acceleration, velocity and deformation of the vehicle [12].

H.2.2 Defining the equations of motion

The governing equations of motion have been modeled using the relativistic Lagrangian formulation [22].

$$\frac{d}{dt}\frac{\partial L}{\partial \dot{q}_i} - \frac{\partial L}{\partial q_i} + \frac{\partial D}{\partial q_i} = Q_i,$$

where, in general case, $L = T - V$, T is the total kinetic energy of the system equal to the sum of the kinetic energies of the particles, $q_i, i = 1, ..., n$ are generalized coordinates and V is the potential energy of the system. Here D is the dissipation function and Q_i is the external force acting on the system; in this case it is the vertical component of the force experienced by the vehicle at the time of maximum dynamic crush [1].

The cartesian system is converted to polar coordinates; the horizontal and vertical coordinates for the two mass system (x_1,y_1) and (x_2,y_2) and the rotations (θ_1 and θ_2) about the y-axis have been represented in (H.3)-(H.6):

$$x_1 = [l_0 + r(t)]\cos\theta_1(t), \tag{H.3}$$

$$z_1 = [l_0 + r(t)]\sin\theta_1(t), \tag{H.4}$$

$$\begin{aligned} x_2 =& [l_0 + r(t)]\cos\theta_1(t) + l_1\cos\theta_1(t) \\ &+ l_2\cos\theta_2(t), \end{aligned} \tag{H.5}$$

$$\begin{aligned} z_2 =& [l_0 + r(t)]\sin\theta_1(t) + l_1\sin\theta_1(t) \\ &+ l_2\sin\theta_2(t), \end{aligned} \tag{H.6}$$

where l_0 is the distance from the center of gravity (CG) of mass m_1 to the point of impact of the vehicle in the rest position, l_1 is the distance from the CG_{m1} to the front suspension, l_2 is the distance from the CG_{m2} to the rear suspension, $r(t)$ is the displacement along the polar radius of the elastic pendulum spring, t is the time, and r, θ_1 and θ_2 are the radius and angles in polar coordinates respectively. Taking the derivatives with respect to time of x_1, x_2 and z_1, z_2 we obtain (H.7)-(H.10):

$$\dot{x_1} = \dot{r}\cos\theta_1 - (l_0 + r)\sin\theta_1 \cdot \dot{\theta_1}, \tag{H.7}$$

$$\dot{z_1} = \dot{r}\sin\theta_1 + (l_0 + r)\cos\theta_1 \cdot \dot{\theta_1}, \tag{H.8}$$

$$\begin{aligned}\dot{x_2} =&\dot{r}\cos\theta_1 - (l_0+r)\sin\theta_1\cdot\dot{\theta}_1\\ &- l_1\dot{\theta_1}\sin\theta_1 - l_2\dot{\theta_2}\sin\theta_2,\end{aligned} \tag{H.9}$$

$$\begin{aligned}\dot{z_2} =&\dot{r}\sin\theta_1 + (l_0+r)\cos\theta_1\cdot\dot{\theta}_1\\ &- l_1\dot{\theta_1}\sin\theta_1 - l_2\dot{\theta_2}\sin\theta_2,\end{aligned} \tag{H.10}$$

where $\dot{x_1}$, $\dot{x_2}$, $\dot{z_1}$ and $\dot{z_2}$ represent the velocity of the mass components in horizontal and vertical directions. Squaring both sides of the equations gives

$$\begin{aligned}\dot{x_1}^2 =&\dot{r}^2\cos^2\theta_1 + (l_0+r)^2\sin^2\theta_1\cdot\dot{\theta_1}^2\\ &- 2\dot{r}\cos\theta_1\cdot(l_0+r)\sin\theta_1\cdot\dot{\theta}_1,\end{aligned} \tag{H.11}$$

$$\begin{aligned}\dot{z_1}^2 =&\dot{r}^2\sin^2\theta_1 + (l_0+r)^2\cos^2\theta_1\cdot\dot{\theta_1}^2\\ &+ 2\dot{r}\cos\theta_1\cdot(l_0+r)\sin\theta_1\cdot\dot{\theta}_1,\end{aligned} \tag{H.12}$$

$$\begin{aligned}\dot{x_2}^2 =&\dot{x_1}^2 + l_1^2\dot{\theta_1}^2\sin{\theta_1}^2 + l_2^2\dot{\theta_2}^2\sin{\theta_2}^2\\ &- 2\dot{x_1}l_1\dot{\theta_1}\sin\theta_1 + 2l_1l_2\dot{\theta_1}\dot{\theta_2}\sin\theta_1\sin\theta_2\\ &- 2\dot{x_1}l_2\dot{\theta_2}\sin\theta_2,\end{aligned} \tag{H.13}$$

$$\begin{aligned}\dot{z_2}^2 =&\dot{z_1}^2 + l_1^2\dot{\theta_1}^2\cos^2\theta_1 + l_2^2\dot{\theta_2}^2\cos^2\theta_2\\ &+ 2l_1l_2\dot{\theta_1}\dot{\theta_2}\cos\theta_1\cos\theta_2 + 2\dot{z_1}l_1\dot{\theta_1}\cos\theta_1\\ &+ 2\dot{z_2}l_2\dot{\theta_2}\cos\theta_2.\end{aligned} \tag{H.14}$$

Adding the terms we have:

$$\begin{aligned}\dot{x_1}^2 + \dot{z_1}^2 =&\dot{r}^2(\cos^2\theta_1 + \sin^2\theta_1)\\ &+ (l_0+r)^2\cdot\dot{\theta_1}^2(\cos^2\theta_1 + \sin^2\theta_1),\end{aligned} \tag{H.15}$$

$$\begin{aligned}\dot{x_2}^2 + \dot{z_2}^2 =&x_1^2 + x_2^2 + l_1^2\dot{\theta_1}^2 + l_2^2\dot{\theta_2}^2 - 2\dot{x_1}l_1\dot{\theta_1}\sin\theta_1\\ &+ 2l_1l_2\dot{\theta_1}\dot{\theta_2}\sin\theta_1\sin\theta_2 - 2\dot{x_1}l_2\dot{\theta_2}\sin\theta_2\\ &+ 2\dot{z_1}l_1\dot{\theta_1}\cos\theta_1 + 2l_1l_2\dot{\theta_1}\dot{\theta_2}\cos\theta_1\cos\theta_2\\ &+ 2\dot{z_1}l_1\dot{\theta_1}\cos\theta_1 + 2\dot{z_1}l_2\dot{\theta_2}\cos\theta_2.\end{aligned} \tag{H.16}$$

The kinetic energy of the system is given by

$$T = \frac{1}{2}[m_1(\dot{x_1}^2 + \dot{z_1}^2) + m_2(\dot{x_2}^2 + \dot{z_2}^2)], \tag{H.17}$$

or, in polar coordinates,

$$\begin{aligned} T =& \frac{1}{2} m_1 [\dot{r}^2 + (l_0 + r)^2 \dot{\theta_1}^2] \\ &+ \frac{1}{2} m_2 [[\dot{r}^2 + (l_0 + r)^2 \cdot \dot{\theta_1}^2 + l_1^2 \cdot \dot{\theta_1}^2 + l_2^2 \cdot \dot{\theta_1}^2] \\ &+ 2 l_1 l_2 \dot{\theta_1} \dot{\theta_2} \sin\theta_1 \sin\theta_2 \\ &- 2[\dot{r} \cos\theta_1 - (l_0 + r)\dot{\theta_1} \sin\theta_1] l_1 \dot{\theta_1} \sin\theta_1] \\ &- 2[\dot{r} \cos\theta_1 - (l_0 + r)\dot{\theta_1} \sin\theta_1] l_2 \dot{\theta_2} \sin\theta_2]. \end{aligned} \tag{H.18}$$

The potential energy of the system can be found as

$$\begin{aligned} V =& m_1 g (l_0 + r) \sin\theta_1 \\ &+ m_2 g [(l_0 + r) \sin\theta_1 + l_1 \sin\theta_1 + l_2 \sin\theta_2] \\ &+ \frac{1}{2} k_{comp} r_1^2 + \frac{1}{2} k_{tor} \theta_2^2 + \frac{1}{2} k_1 r^2 + \frac{1}{2} k_2 r_2^2 \end{aligned} \tag{H.19}$$

where r_1 and r_2 are expressed in terms of r, θ_1, θ_2, l_1, l_2, l_3 as follows:

$$r_1 = (l_0 + r - l_3)\theta_1, \tag{H.20}$$

$$r_2 = (l_0 + r + l_1)\theta_1 + l_2 \theta_2. \tag{H.21}$$

Here m_1 is the mass of the lumped body before the weld and HAZ, m_2 is the mass of the occupant compartment after the weld and HAZ, l_3 is the distance from the CG_{m1} to the front suspension, l_2 is the distance from the weld to the CG_{m2}. Simplifying the expression for potential energy in equation (H.19), we obtain:

$$\begin{aligned} V =& m_1 g (l_0 + r) \sin\theta_1 + m_2 g [(l_0 + r) \sin\theta_1 + l_1 \sin\theta_1 + l_2 \sin\theta_2] \\ &+ \frac{1}{2} k_1 (l_0 + r - l_3)^2 \theta^2 + \frac{1}{2} k_2 ((l_0 + r + l_1)\theta_1 + l_2 \theta_2)^2 \\ &+ \frac{1}{2} k_{comp} r_1^2 + \frac{1}{2} k_{tor} \theta_2^2. \end{aligned} \tag{H.22}$$

Here k_1 and k_2 are the suspension spring coefficients for the front and rear suspensions respectively. Using equations (H.18) and (H.22) and Lagrangian formulation, $L =$

$T - V$, we conclude that

$$\begin{aligned} L =& \frac{1}{2}m_1[\dot{r}^2 + (l_0+r)^2\dot{\theta_1}^2] + \frac{1}{2}m_2[\dot{r}^2 + (l_0+r)^2\dot{\theta_2}^2 \\ &+ l_1\dot{\theta_1}^2 + l_2\dot{\theta_2}^2 - 2\dot{r}\dot{\theta}_1 l_1\theta_1 \\ &+ 2(l_0+r)l_1\dot{\theta_1}^2\theta_1^2 + 2l_1l_2\dot{\theta}_1\dot{\theta}_2\theta_1\theta_2 \\ &- 2\dot{r}\dot{\theta}_2 l_2\theta_2 + 2l_2(l_0+r)\dot{\theta}_1\dot{\theta}_2\theta_1\theta_2] \\ &- m_1 g(l_0+r)\sin\theta_1 \\ &- m_2 g[(l_0+r)\sin\theta_1 + l_1\sin\theta_1 + l_2\sin\theta_2] \\ &- \frac{1}{2}k_{comp}r_1^2 - \frac{1}{2}k_{tor}\theta_2^2 - \frac{1}{2}k_1 r^2 - \frac{1}{2}k_2 r_2^2, \end{aligned} \tag{H.23}$$

The governing equations of motion are:

$$\begin{aligned} Q_r^{ext} =& m_1\ddot{r} + m_2\ddot{r} - m_2 l_1(\ddot{\theta}_1\theta_1 + 2\dot{\theta}_1) \\ &- m_2 l_2(\ddot{\theta}_2\theta_2 + 2\dot{\theta}_2) - m_1(l_0+r)\dot{\theta_1}^2 \\ &+ m_2(l_0+r)\dot{\theta_1}^2 + m_2 l_1\dot{\theta_1}^2\theta_1^2 + m_2 l_2\dot{\theta}_1\dot{\theta}_2\theta_1\theta_2 \\ &+ m_1 g\theta_1 + m_2 g\theta_2 + k_1(l_0+r-l_3)\theta_1^2 \\ &+ k_2[(l_0+r+l_1)\theta_1^2 + l_2\theta_1\theta_2] + k_{comp}r, \end{aligned} \tag{H.24}$$

$$\begin{aligned} Q_{\theta_1}^{ext} =& m_1(l_0+r)^2\ddot{\theta}_1 + 2m_1(l_0+r)\dot{r}\dot{\theta}_1 \\ &+ 2m_2(l_0+r)\dot{r}\dot{\theta}_1 + m_2 l_1^2\ddot{\theta}_1 - m_2 l_1\dot{\theta}_1\dot{r} \\ &- m_2 l_1\dot{\theta}_1\ddot{r} + 2m_2 l_1[\dot{r}\dot{\theta}_1\theta_1^2 + (l_0+r)\theta_1^2\ddot{\theta}_1] \\ &+ 2(l_0+r)l_1\dot{\theta_1}^2\theta_1 + m_2 l_1 l_2[\ddot{\theta}_2\ddot{\theta}_1\theta_2 + \dot{\theta}_2\dot{\theta}_1\theta_2] \\ &+ m_2 l_2[\dot{r}\dot{\theta}_2\theta_1\theta_2 + (l_0+r)\ddot{\theta}_2\theta_1\theta_2 \\ &+ (l_0+r)\dot{\theta}_2\dot{\theta}_1\theta_2] + m_2\dot{r}\dot{\theta}_1 l_1 - 2m_2(l_0+r)l_2\dot{\theta_1}^2\theta_1 \\ &- m_2 l_1 l_2\dot{\theta}_2\theta_1\theta_2 + m_2 l_2(l_0+r)\dot{\theta}_2\theta_1\theta_2 \\ &+ m_1 g(l_0+r) + m_2 g[(l_0+r) + l_1] \\ &- k_1[l_0+r-l_3]^2\theta_1 - k_2[l_0+r+l_1]^2\theta_1 \\ &- k_2[l_0+r+l_1]l_2\theta_2, \end{aligned} \tag{H.25}$$

$$\begin{aligned} Q_{\theta_2}^{ext} =& m_2 l_2^2\ddot{\theta}_2 + m_2 l_1 l_2[\ddot{\theta}_1\theta_1\theta_2 + \dot{\theta_1}^2\theta_2 + \dot{\theta}_1\theta_1\dot{\theta}_2] \\ &- m_2 l_2[\dot{r}\dot{\theta}_1\theta_1\theta_2 + (l_0+r)\ddot{\theta}_1\theta_1\theta_2 + (l_0+r)\dot{\theta_1}^2\theta_2] \\ &- m_2 l_1 l_2\dot{\theta}_1\dot{\theta}_2\theta_1 + m_2\dot{r}\dot{\theta}_2 l_2 - m_2 l_2(l_0+r)\dot{\theta}_1\dot{\theta}_2\theta_1 \\ &+ m_2 g l_2 + k_2[(l_0+r+l_1)l_2\theta_1 + l_2^2\theta_2] \\ &+ k_{tor}\theta_2 \end{aligned} \tag{H.26}$$

where Q_r^{ext}, $Q_{\theta_2}^{ext}$ and $Q_{\theta_2}^{ext}$ are the external forces acting on the vehicle. The non-

conservative forces in the system are included in the Lagrange's equation of motion in the form of generalized forces expressed with the formulation of virtual work δU [19]

$$\delta U = \sum_{j=1}^{m} F_j \cdot \delta r_j \tag{H.27}$$

where F_j are the force components, δr_j are the virtual displacements given by

$$\delta r_j = \sum_{i=1}^{N} \frac{\partial r_j}{\partial q_i} \delta q_i \tag{H.28}$$

for $j = 1, 2, 3, \ldots, m$. This yields the following equation for virtual work:

$$\begin{aligned} \delta U = F_1 \cdot \sum_{i=1}^{N} \frac{\partial r_j}{\partial q_i} \delta q_i + F_2 \cdot \sum_{i=1}^{N} \frac{\partial r_j}{\partial q_i} \delta q_i + \cdots \\ + F_m \cdot \sum_{i=1}^{N} \frac{\partial r_j}{\partial q_i} \delta q_i. \end{aligned} \tag{H.29}$$

Using equation (H.29), we compute the generalized forces acting the system:

$$\begin{aligned} \delta U = F_{x_1} \cdot \left(\frac{\partial x}{\partial r} \cdot \delta r + \frac{\partial x}{\partial \theta_1} \cdot \delta \theta_1 + \frac{\partial x}{\partial \theta_2} \cdot \delta \theta_2 \right) \\ + F_{x_2} \cdot \left(\frac{\partial x}{\partial r} \cdot \delta r + \frac{\partial x}{\partial \theta_1} \cdot \delta \theta_1 + \frac{\partial x}{\partial \theta_2} \cdot \delta \theta_2 \right) \\ + F_{z_1} \cdot \left(\frac{\partial z}{\partial r} \cdot \delta r + \frac{\partial z}{\partial \theta_1} \cdot \delta \theta_1 + \frac{\partial z}{\partial \theta_2} \cdot \delta \theta_2 \right) \\ + F_{z_2} \cdot \left(\frac{\partial z}{\partial r} \cdot \delta r + \frac{\partial z}{\partial \theta_1} \cdot \delta \theta_1 + \frac{\partial z}{\partial \theta_2} \cdot \delta \theta_2 \right). \end{aligned} \tag{H.30}$$

Substituting equations (H.3) and (H.4) in equation (H.30), we get

$$\begin{aligned} dU = F_{x_1} \cdot [(\cos(\theta_1)\delta r - (l_0 + r) \sin \theta_1 \delta \theta_1] \\ + F_{x_2} \cdot [(\cos(\theta_1)\delta r - (l_0 + r) \sin \theta_1 \delta \theta_1 - l_1 \sin \theta_1 \delta \theta_1 \\ - l_2 \sin \theta_2 \delta \theta_2] + F_{z_1} \cdot [(\sin(\theta_1)\delta r + (l_0 + r) \cos(\theta_1) \delta \theta_1] \\ + F_{z_2} \cdot [(\sin(\theta_1)\delta r + (l_0 + r) \cos(\theta_1) \delta \theta_1 + l_1 \cos \theta_1 \delta \theta_1 \\ + l_2 \cos \theta_2 \delta \theta_2]. \end{aligned} \tag{H.31}$$

The external forces included in this LPM are barrier forces, damper forces including front end spring damper system and suspension damper system forces. The

corresponding equations are:

$$Q_r^{ext} = Q_r^{bar} + Q_r^{damp}, \tag{H.32}$$

$$Q_{\theta_1}^{ext} = Q_{\theta_1}^{bar} + Q_{\theta_1}^{damp}, \tag{H.33}$$

$$Q_{\theta_2}^{ext} = Q_{\theta_2}^{bar} + Q_{\theta_2}^{damp}. \tag{H.34}$$

Here F_x and F_z are the horizontal and vertical force components acting on the vehicle; Q_r^{bar}, $Q_{\theta_1}^{damp}$ and $Q_{\theta_2}^{damp}$ are the non-conservative barrier and damper forces acting on the system.
Then δU assumes the form

$$\begin{aligned}\delta U = Q_r^{damp} \cdot \delta r + Q_{\theta_1}^{damp} \cdot \delta\theta_1 + Q_{\theta_2}^{damp} \cdot \delta\theta_2 \\ + Q_r^{bar} \cdot \delta r + Q_{\theta_1}^{bar} \cdot \delta\theta_1 + Q_{\theta_2}^{bar} \cdot \delta\theta_2\end{aligned} \tag{H.35}$$

where

$$\begin{aligned}Q_r^{bar} =& F_{bx_1} \cos\theta_1 + F_{bz_1} \sin\theta_1 \\ &+ F_{bx_2} \cos\theta_1 + F_{bz_2} \sin\theta_1,\end{aligned} \tag{H.36}$$

$$\begin{aligned}Q_{\theta_1}^{bar} =& - F_{bx_1}(l_0 + r)\sin\theta_1 + F_{bz_1}(l_0 + r)\cos\theta_1 \\ &- F_{bx_2}[(l_0 + r)\sin\theta_1 + l_1 \sin\theta_1] \\ &+ F_{bz_2}[(l_0 + r)\cos\theta_1 + l_1 \cos\theta_1],\end{aligned} \tag{H.37}$$

$$Q_{\theta_2}^{bar} = -F_{bx_2} l_2 \sin\theta_2 + F_{bz_2} l_2 \cos\theta_2 \tag{H.38}$$

where F_{bx} and F_{bz} are the barrier forces acting on the vehicle in the horizontal and vertical directions. These values are included from the FE simulation data. The derivative of the dissipation energy D and the damper forces are given by the equations

$$\begin{aligned}D =& \frac{1}{2} c_{comp} \dot{r}^2 + \frac{1}{2} c_1 [(l_0 + r - l_3)\dot{\theta}_1 + \dot{r}\theta_1]^2 \\ &+ \frac{1}{2} c_2 [(l_0 + r + l_1)\dot{\theta}_1 + \dot{r}\theta_1 + l_2\theta_2]^2 \\ &+ \frac{1}{2} c_{tor} \dot{\theta}_2,\end{aligned} \tag{H.39}$$

$$\begin{aligned}Q_r^{damp} =& F_{bx_1} \cos\theta_1 + F_{bz_1} \sin\theta_1 \\ &+ F_{bx_2} \cos\theta_1 + F_{bz_2} \sin\theta_1,\end{aligned} \tag{H.40}$$

$$\begin{aligned}Q_{\theta_1}^{damp} =& - F_{bx_1}(l_0 + r)\sin\theta_1 + F_{bz_1}(l_0 + r)\cos\theta_1 \\ &- F_{bx_2}[(l_0 + r)\sin\theta_1 + l_1 \sin\theta_1] \\ &+ F_{bz_2}[(l_0 + r)\cos\theta_1 + l_1 \cos\theta_1],\end{aligned} \tag{H.41}$$

$$Q_{\theta_2}^{damp} = -F_{bx_2} l_2 \sin\theta_2 + F_{bz_2} l_2 \cos\theta_2, \tag{H.42}$$

where c_1 and c_2 are the damper coefficients for the front and rear suspensions, c_{comp} and c_{tor} are the damper coefficients from the front end compression spring and the torsional spring respectively.

H.2.3 Validation with an FE model

The LPM is validated against a modified FEM developed by NHTSA [23] where the effect of welding and material behavioural changes in UHSS structural members is included by the authors. The crashworthiness response is affected by the changes in material behaviour which compromise the safety performance. The acceleration, velocity and displacement curves from the 2010 Toyota Yaris FE model for a full frontal impact were used to validate the LPM performance. The speed of the impact was 56 kmph and the barrier is a rigid non deformable barrier with 0% offset.

The baseline FE model developed by National Crash Analysis Center (NCAC) and National Highway Transport Safety Administration (NHTSA) [24], [23] was adopted to modify the structural members. The model is cut and welded to incorporate the repairs of UHSS material on load bearing structural members. The material and section properties of the weld were adopted from a similar FE developed in [15]. The weld zone and HAZ lead to reduced strength in the members and replicates the behaviour in a physical test. It will be interesting to use physical test data in a future study.

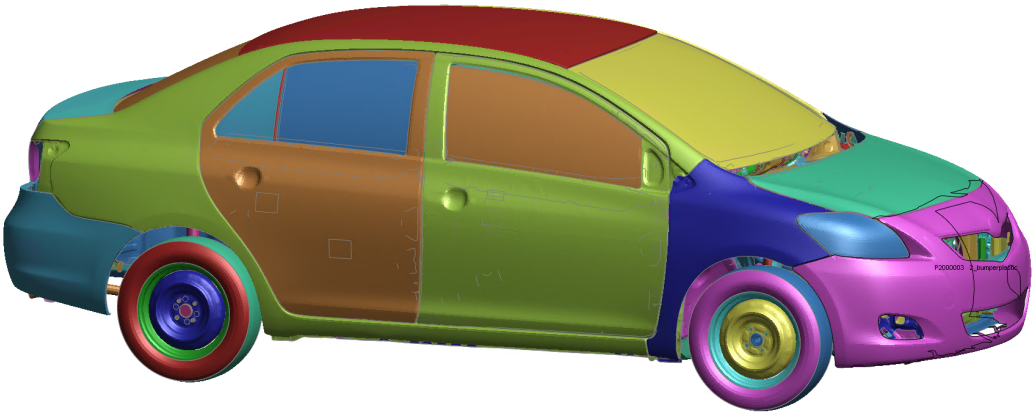

Figure H.5: Baseline 2010 Toyota Yaris FE Model

Figure H.5 shows the FE model developed by NHTSA which replicates a 2010 four-door passenger sedan consisting of 917 parts, 1,480,422 nodes and 1,514,068 elements. The FE model weighs 1,100 kg which is close to the physical test vehicle weighing 1,078 kg.The model was correlated with a number of crash loadcases confirming the reliability of the model representing the physical vehicle.

The next section highlights the results and discussion on the model simulations.

H.3 Results and Discussion

The LPM defined in the Section H.2 was simulated in MATLAB Simulink and the results were compared with the data generated from the LS Dyna FE model for a 2010 Toyota Yaris impacting a rigid barrier at 56 kmph. Prior to overlaying the LS Dyna curve outputs with the LPM results, the FE outputs were converted into polar coordinates to compare the results. The Simulink model was run with an ode45 (variable timestep) solver; it was observed that changing the solver parameters did not influence the results significantly. The maximum values of the pitching angles θ_1 and θ_2 are crucial to determine the occupant injury prediction during the vehicle development stage. The maximum crush of the vehicle and the velocity during energy absorption stage helps predict the vehicle crashworthiness performance in an impact. These parameters have been measured with the Simulink model developed in the study. The values of k_1, k_2, c_1, c_2 have been adopted from [25] and presented in Table H.1.

Table H.1: Automotive Parameters set

Symbol	Value	Unit	Meaning
M	400	kg	Sprung mass
m_{ij}	50	kg	Unsprung masses (i = front, rear and j = left, right)
I_x	250	kg.m^2	Roll inertia
I_y	1400	kg.m^2	Pitch inertia
t	1.4	m	Front and rear axle
l_f	1.4	m	COG-front distance
l_r	1	m	COG-rear distance
r	0.3	m	Nominal wheel radius
h	0.7	m	Chassis COG height
k_f	30,000	N/m	Front suspension linearized stiffness (left, right)
k_r	20,000	N/m	Rear suspension linearized stiffness (left, right)
c_f	1500	N/m/s	Front suspension linearized damping (left, right)
c_r	3000	N/m/s	Rear suspension linearized damping (left, right)
k_t	200,000	N/m	Tire stiffness (front, rear and left, right)
β	50	rad/s	Suspension actuator bandwidth

The front-end spring and damper coefficients (k_{comp} and c_{comp}) were determined from the optimization algorithm presented in Subsection H.2.1. The LPM was compared against the data from FE in the parameter identification code. The computed acceleration, velocity and displacement curves are shown in Figure H.6. The corresponding spring and damper coefficients are presented in Figure H.7.

The values of m_1, m_2, l_0,l_1, l_2, l_3, k_{tor}, c_{tor} along with external forces F_{bx_1}, F_{bz_1},

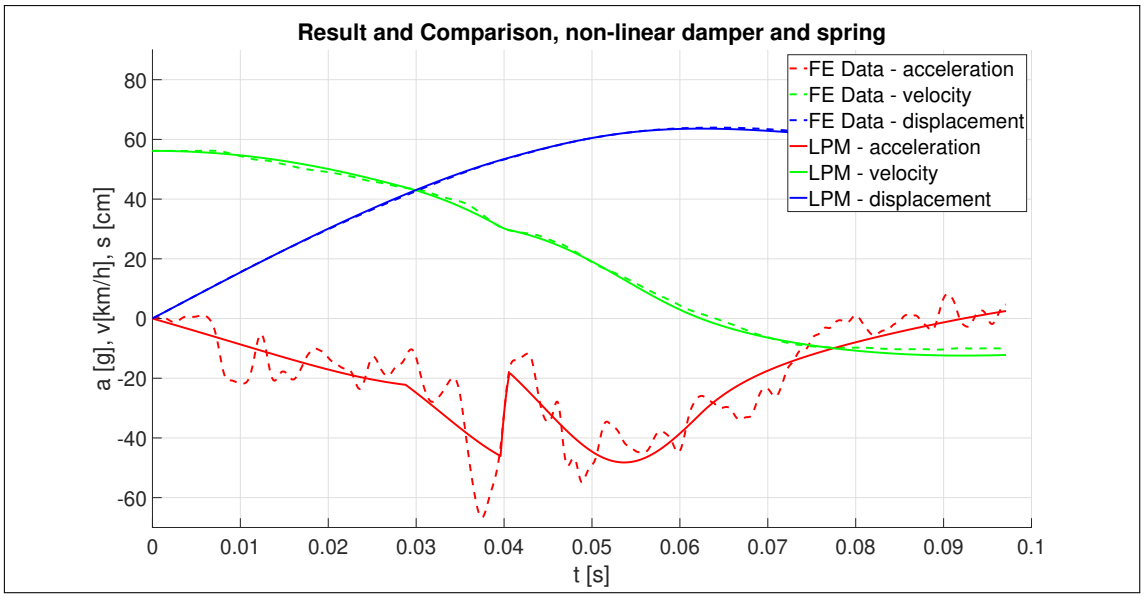

Figure H.6: Comparison of FE and LPM curves for parameter identification algorithm

F_{bx_2}, F_{bz_2} were calculated from the LS Dyna model and presented in Table H.2.

Table H.2: Model Parameters.

Mass Body 1 m_1	539 kg
Mass Body 2 m_1	629 kg
l_1	0.57 (metres)
l_2	1.3 (metres)
l_3	0.10 (metres)
l_0	0.91 (metres)
k_{tors}	Curves from LS Dyna model
c_{tors}	Curves from LS Dyna model

Figure H.8 shows the change in the velocity of the vehicle in m/s after the impact. The LPM was overlaid with the FE data curves and the plots show good correlation of the time when the vehicle attains zero velocity. The trend of the curves is similar indicating the impact kinematics has been replicated in the LPM. The maximum deformation experienced by the vehicle during the full frontal impact is shown in Figure H.9 and the maximum crush values are closely correlated, demonstrating a good prediction capability of the model.

Figure H.10 shows the plot of θ_1 which indicates the pitching of the vehicle about the point of impact. The curves for the LPM over-predict the maximum pitching angle; this could be attributed to the approximation of the model parameters like suspension spring and damper coefficients which were assumed to be constant throughout the simulation. It is however, crucial to predict the maximum pitching angle to design the restraint systems for occupants in the vehicle; the pitching angle θ_1 is closely correlated in the LPM developed in this study.

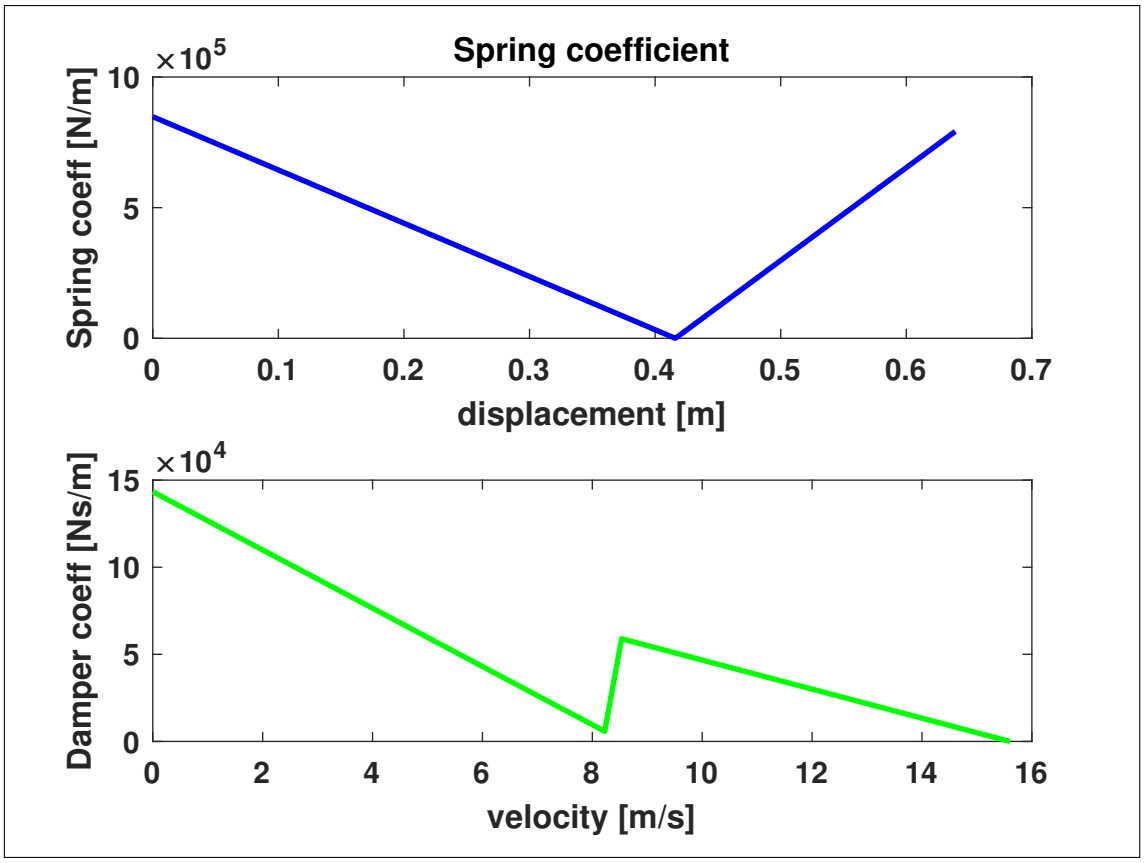

Figure H.7: Front-end Spring and Damper coefficients for Toyota Yaris

As explained in Section H.2, the model uses a torsional spring to represent fractures in the structural members due to HAZ (from welding or heat treatment processes); leading to an angle θ_2 in the vehicle pitching. The plot for θ_2 is shown in Figure H.11; the stiffness of the spring is approximated from the weld failure data used in the FE model. It is observed that the predicted angle from the LPM is close to the maximum value from the FE model, however, the model can be further improved.

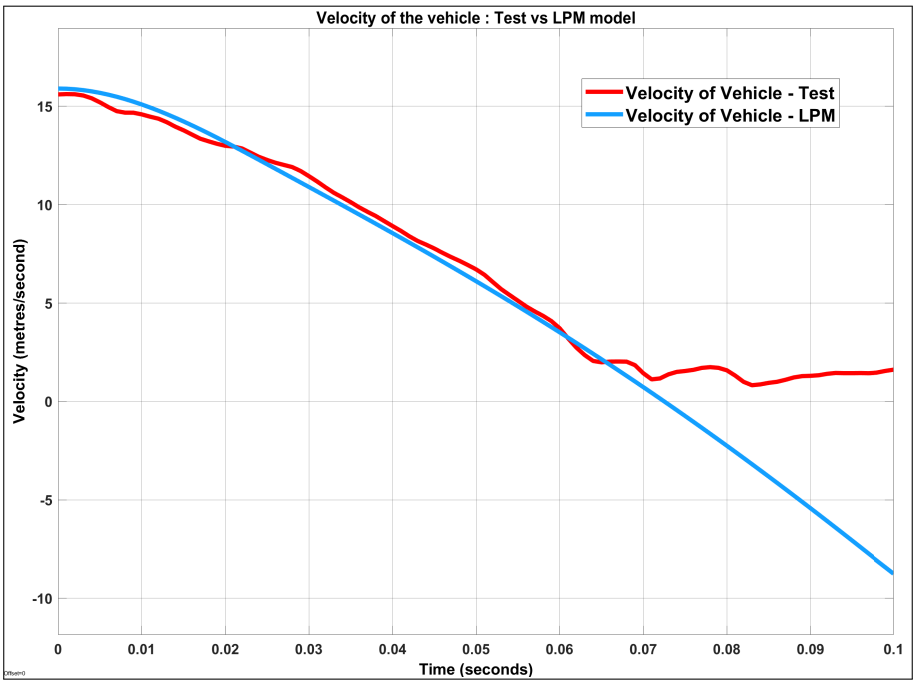

Figure H.8: Velocity of the vehicle - curves comparison for LPM vs FE model

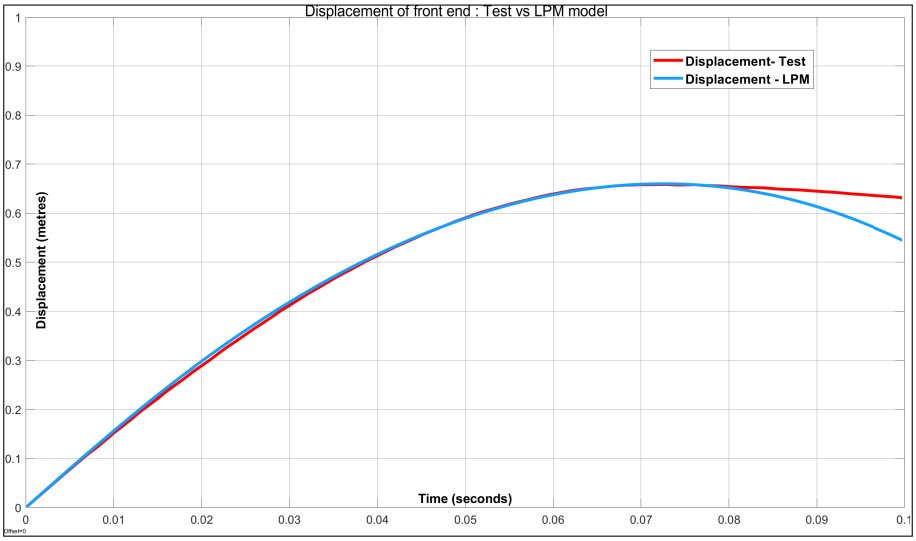

Figure H.9: Displacement of the vehicle front-end - curves comparison for LPM vs FE model

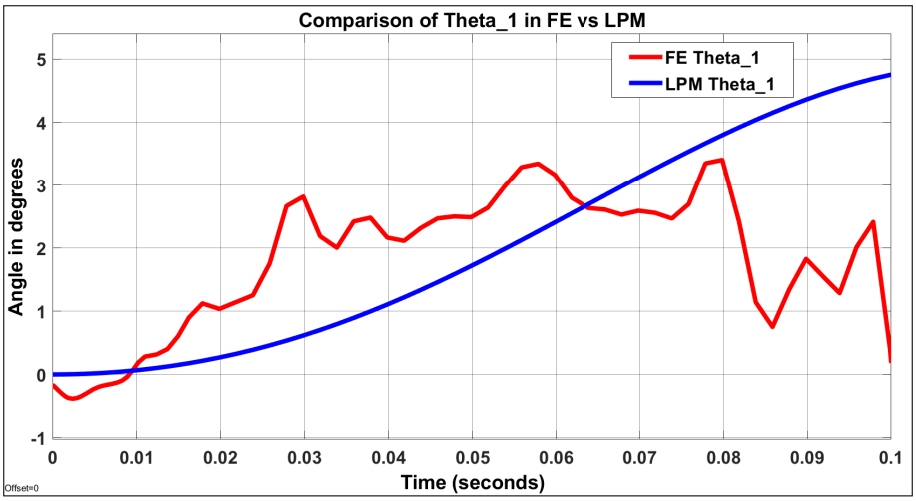

Figure H.10: θ_1 curve comparison for LPM vs FE model

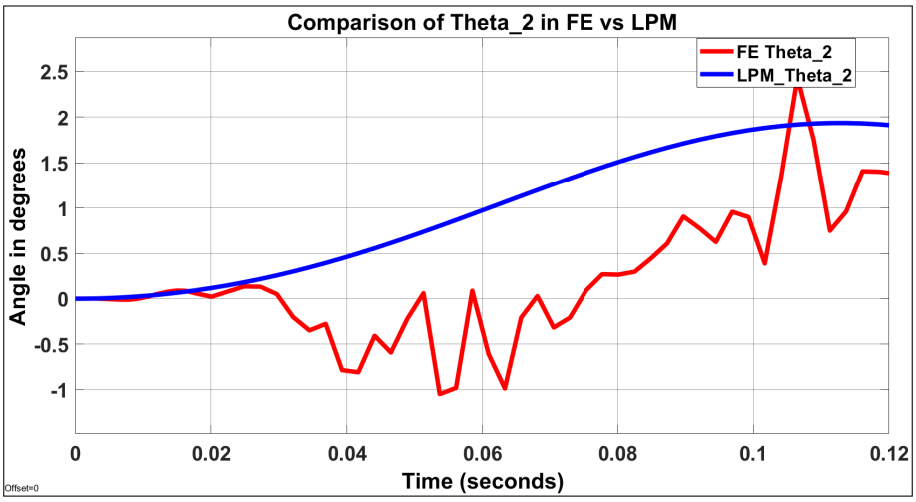

Figure H.11: θ_2 curve comparison for LPM vs FE model

H.4 Conclusions

The reliability of mathematical modeling to replicate and predict vehicle crashworthiness response has increased during the last decade. These models are slowly replacing physical tests; LPMs provide results with low computational time and fewer vehicle parameters. LPMs can be used during the initial stages of the vehicle development process when full scale CAD models are not available. The literature review indicated little research in the area of representing welds and material failure in LPMs. Our 3 DOF LPM predicts the following vehicle parameters in a full frontal impact:

- Maximum vehicle crush during an impact.
- Time for the vehicle to reach zero velocity from the start of the event.
- Vehicle pitching angle about the point of impact.
- Failure of the structural members leading to higher pitching angle in a modified vehicle.

The model uses an elastic double compound pendulum replicating the event kinematics to capture the front-end deformation and the rotation of the vehicle; first around the point of impact and then around the failure of the material due to welding or heat treatment. The LPM employs Lagrangian formulation to define the equations of motion and is presented in polar coordinates to simplify the system. The model correlates well with the FE data for a 2010 Toyota Yaris; the deformation, velocity and pitching angle are predicted well for a full frontal impact at 56 kmph. The failure of the structural members is simulated in the model with a torsional spring. The angle of rotation of the vehicle θ_2 due to material behavioural changes is close to the maximum values in the validation data. The novel methodology presented in this study can be further enhanced with real-time weld fracture data from physical tests. The model predictability can be further improved by replacing the piece-wise linear approximation for the vehicle parameter values with non-linear functions for stiffness and damping coefficients.

References – Paper H

[1] G. Noorsumar, S. Rogovchenko, K.G. Robbersmyr, and D. Vysochinskiy. Mathematical models for assessment of vehicle crashworthiness: a review. *International Journal of Crashworthiness*, 2021. ISSN 17542111. doi: 10.1080/13588265.2021.1929760.

[2] A.B. Pifko and R. Winter. *Theory and Application of Finite Element Analysis To Structural Crash Simulation*, volume 13. Pergamon Press Ltd, 1981. doi: 10.1016/b978-0-08-027299-3.50036-4. URL `http://dx.doi.org/10.1016/B978-0-08-027299-3.50036-4`.

[3] C S Böttcher, S Frik, and B Gosolits. 20 years of crash simulation at Opel-experiences for future challenges. *4th LS-DYNA Anwenderforum*, pages 79–86, 2005.

[4] M. M. Kamal. Analysis and simulation of vehicle to barrier impact. *SAE Technical Papers*, pages 1498–1503, 1970. ISSN 26883627. doi: 10.4271/700414.

[5] D.J. Benson, J.O. Hallquist, M. Igarashi, K. Shimomaki, and M. Mizuno. Application of DYNA3D in large scale crashworthiness calculations, 1986. URL `http://inis.iaea.org/Search/search.aspx?orig_q=RN:17073039`.

[6] Stuart G. Mentzer, Randa A. Radwan, and William T. Hollowell. The SISAME methodology for extraction of optimal lumped parameter structural crash models. *SAE Technical Papers*, 1992. ISSN 26883627. doi: 10.4271/920358.

[7] Mustafa Elkady, Ahmed Elmarakbi, and John Macintyre. Enhancement of vehicle safety and improving vehicle yaw behaviour due to offset collision using vehicle dynamics. *International Journal of Vehicle Safety*, 6(2):110–133, 2012. ISSN 14793113. doi: 10.1504/IJVS.2012.049011.

[8] Mustafa Elkady and Ahmed Elmarakbi. Modelling and analysis of vehicle crash system integrated with different VDCS under high speed impacts. *Central European Journal of Engineering*, 2(4):585–602, 2012. doi: 10.2478/S13531-012-0035-Z.

[9] Dipendra Subedi, Ilya Tyapin, and Geir Hovland. Modeling and Analysis of Flexible Bodies Using Lumped Parameter Method. In *Proceedings of 2020 IEEE 11th International Conference on Mechanical and Intelligent Manufacturing Technologies, ICMIMT 2020*, pages 161–166. Institute of Electrical and Electronics Engineers Inc., 1 2020. ISBN 9781728153322. doi: 10.1109/ICMIMT49010.2020.9041188.

[10] Radu Alexandru Ionut, Cofaru Corneliu, and Tolea Bogdan. Mathematical model validated by a crash test for studying the occupant's kinematics and dynamics in a cars' frontal collision. *International Journal of Automotive Technology 2017 18:6*, 18(6):1017–1025, 8 2017. ISSN 1976-3832. doi: 10.1007/S12239-017-0099-0. URL https://link.springer.com/article/10.1007/s12239-017-0099-0.

[11] J. Michael Chang, Miinshiou Huang, Tau Tyan, G. Li, and L. Gu. Structural optimization for vehicle pitch and drop. In *SAE Technical Papers*. SAE International, 4 2006. doi: 10.4271/2006-01-0316. URL https://www.sae.org/publications/technical-papers/content/2006-01-0316/.

[12] G. Noorsumar, S. Rogovchenko, K.G. Robbersmyr, D. Vysochinskiy, and A. Klausen. A novel technique for modeling vehicle crash using lumped parameter models. In *Proceedings of the 11th International Conference on Simulation and Modeling Methodologies, Technologies and Applications, SIMULTECH 2021*, 2021. ISBN 9789897585289. doi: 10.5220/0010529200620070.

[13] J. Michael Chang, Mohammad Ali, Ryan Craig, Tau Tyan, Marwan El-Bkaily, and James Cheng. Important modeling practices in CAE simulation for vehicle pitch and drop. In *SAE Technical Papers*. SAE International, 4 2006. doi: 10.4271/2006-01-0124. URL https://www.sae.org/publications/technical-papers/content/2006-01-0124/https://www.sae.org/publications/technical-papers/content/2006-01-0124/?PC=DL2BUY.

[14] Gulshan Noorsumar, Dmitry Vysochinskiy, Even Englund, Kjell G. Robbersmyr, and Svitlana Rogovchenko. Effect of welding and heat treatment on the properties of UHSS used in automotive industry. *EPJ Web of Conferences*, 250:05015, 9 2021. ISSN 2100-014X. doi: 10.1051/EPJCONF/202125005015. URL https://www.epj-conferences.org/articles/epjconf/abs/2021/04/epjconf_dymat2021_05015/epjconf_dymat2021_05015.html.

[15] Gulshan Noorsumar, Kjell Robbersmyr, Svitlana Rogovchenko, and Dmitry Vysochinskiy. Crash Response of a Repaired Vehicle - Influence of Welding UHSS Members. In *WCX SAE World Congress Experience*. SAE International,

3 2020. doi: https://doi.org/10.4271/2020-01-0197. URL https://doi.org/10.4271/2020-01-0197.

[16] Mei Zhang, Lin Li, Ren yu Fu, Ji cheng Zhang, and Zi Wan. Weldability of Low Carbon Transformation Induced Plasticity Steel. *Journal of Iron and Steel Research, International*, 15(5):61–87, 9 2008. ISSN 1006-706X. doi: 10.1016/S1006-706X(08)60250-2.

[17] M. Amirthalingam, M. Hermans, and I. Richardson. Microstructural development during welding of siliconand aluminum-based transformation-induced plasticity steels-inclusion and elemental partitioning analysis. *Metallurgical and Materials Transactions A: Physical Metallurgy and Materials Science*, 40(4): 901–909, 2009. ISSN 10735623. doi: 10.1007/S11661-008-9761-5.

[18] Nikolay Pavlov. Study the vehicle pitch motion by spring inverted pendulum model. (February), 2019.

[19] Oscar Cyrén and Sofia Johansson. Modeling of Occupant Kinematic Response in Pre-crash Maneuvers A simplified human 3D-model for simulation of occupant kinematics in maneuvers, 2018.

[20] Grażyna Sypniewska-Kamińska, Roman Starosta, and Jan Awrejcewicz. Motion of double pendulum colliding with an obstacle of rough surface. *Arch Appl Mech*, 87:841–852, 2017. doi: 10.1007/s00419-017-1230-4.

[21] Grażyna Sypniewska-Kamińska, Roman Starosta, and Jan Awrejcewicz. Double pendulum colliding with a rough obstacle. In *Dynamical Systems - Mechatronics and Life Sciences*. Instytut Mechaniki Stosowanej, Wydział Budowy Maszyn i Zarządzania, Politechnika Poznańska, 2016.

[22] Herbert Goldstein, Charles Poole, John Safko, and Stephen R. Addison. Classical Mechanics, 3rd ed. *American Journal of Physics*, 70(7):782–783, 7 2002. ISSN 0002-9505. doi: 10.1119/1.1484149. URL http://aapt.scitation.org/doi/10.1119/1.1484149.

[23] Crash Simulation Vehicle Models | NHTSA. URL https://www.nhtsa.gov/crash-simulation-vehicle-models.

[24] D Marzougui, D Brown, H K Park, C D Kan, and K S Opiela. 3 th International LS-DYNA Users Conference Session: Automotive Development & Validation of a Finite Element Model for a Mid-Sized Passenger Sedan. 2011.

[25] Sergio Savaresi, Charles Poussot-Vassal, Cristiano Spelta, Olivier Sename, and Luc Dugard. *Semi-Active Suspension Control Design for Vehicles*. Elsevier Ltd, 2010. doi: 10.1016/C2009-0-63839-3.